Tropospheric Photochemistry of Ozone, its Precursors and the Hydroxyl Radical: A 3D-Modeling Study Considering Non-Methane Hydrocarbons

Dissertation
zur Erlangung des Grades
„Doktor der Naturwissenschaften"

am Fachbereich Physik der
Johannes Gutenberg-Universität
in Mainz

Rolf von Kuhlmann

geboren in Bielefeld

Mainz, 2001

Jahr der mündlichen Prüfung: 2001

Für meine Mutter

Prediction is very difficult,
especially about the future.

Niels Bohr

Abstract

A 3-dimensional global model of the lower atmosphere was used to study the chemistry of ozone (O_3), the hydroxyl radical (OH) and other related species, such as reactive nitrogen compounds and hydrocarbons. For this purpose the treatment of non-methane hydrocarbons (NMHC) has been added to the model, including the development of a simplified representation of their photochemistry and the implementation of deposition processes and emissions. For the solution of the coupled system of stiff ordinary differential equations of the chemistry a fast Rosenbrock method has been adopted and implemented giving the possibility to easily change the chemical reactions in future studies with the model.

To assess the quality of the model predictions an extensive comparison of model results with surface, air-, and space-borne observations of ozone and related species has been carried out. The model was found to be able to reproduce a large part of the behavior of the main species in terms of magnitude and seasonal cycles. However, a number of deviations were also found which can help to improve emission fields or model dynamics and give indications on missing chemistry in the model.

In order to investigate further the role of different groups of species to the model results, 3 simulations with chemical schemes of different complexity were analyzed. It was found that the inclusion of NMHCs significantly changes the distribution of several species, including an increase in O_3 concentrations. The biogenically produced compound isoprene was found to cause about half of the total effects of NMHCs (more in the tropics, less elsewhere).

In a sensitivity study the uncertainties in modeling isoprene have been examined. It was found that uncertainties in physical parameterization (deposition, heterogeneous processes) can be as large as the uncertainty in the gas-phase chemistry, which could lead to globally relevant deviations. The local differences were even larger.

It can be concluded that the numerical studies performed in this work gave new insights into important aspects of the photochemistry of the troposphere and led to recommendations for future studies to reduce the key uncertainties found.

Zusammenfassung

Ein 3-dimensionales globales Modell der unteren Atmosphäre wurde für die Untersuchung der Ozonchemie, sowie der Chemie des Hydroxylradikals (OH) und wichtiger Vorläufersubstanzen, wie reaktiver Stickstoffverbindungen und Kohlenwasserstoffe, verwendet. Hierfür wurde die Behandlung von Nicht-Methan-Kohlenwasserstoffen (NMKW) hinzugefügt, was auch die Entwicklung einer vereinfachten Beschreibung ihrer Chemie, sowie die Erfassung von Depositionsprozessen und Emissionen erforderte. Zur Lösung der steifen gewöhnlichen Differentialgleichungen der Chemie wurde eine schnelles Rosenbrock-Verfahren eingesetzt, das so implementiert wurde, dass die Modell-Chemie für zukünftige Studien leicht abgeändert werden kann.

Zur Evaluierung des Modells wurde ein umfangreicher Vergleich der Modellergebnisse mit Bodenmessungen, sowie Flugzeug-, Sonden- und Satelliten-Daten durchgeführt. Das Modell kann viele Aspekte der Beobachtungen der verschieden Substanzen realistisch wiedergeben. Es wurden jedoch auch einige Diskrepanzen festgestellt, die Hinweise auf fehlerhafte Emissionsfelder oder auf die Modell-Dynamik und auch auf fehlende Modell-Chemie liefern.

Zur weiteren Untersuchung des Einflusses verschiedener Stoffgruppen wurden drei Läufe mit unterschiedlich komplexer Chemie analysiert. Durch das Berücksichtigen der NMKW wird die Verteilung mehrerer wichtiger Substanzen signifikant beeinflusst, darunter z.B. ein Anstieg des globalen Ozons. Es wurde gezeigt, dass die biogene Substanz Isopren etwa die Hälfte des Gesamteffekts der NMKW ausmachte (mehr in den Tropen, weniger anderswo).

In einer Sensitivitätsstudie wurden die Unsicherheiten bei der Modellierung von Isopren weitergehend untersucht. Dabei konnte gezeigt werden, dass die Unsicherheit bei physikalischen Aspekten (Deposition und heterogene Prozesse) ebenso groß sein kann, wie die aus dem chemischen Gasphasen-Mechanismus stammende, welche zu global bedeutsamen Abweichungen führte. Lokal können sich noch größere Abweichungen ergeben.

Zusammenfassend kann gesagt werden, dass die numerischen Studien dieser Arbeit neue Einblicke in wichtige Aspekte der Photochemie der Troposphäre ergaben und in Vorschläge für weiter Studien mündeten, die die wichtigsten gefundenen Unsicherheiten weiter verringern könnten.

Contents

Chapter 1

Introduction

During the last decades expressions from the atmospheric vocabulary such as "climate change", "global warming", "ozone hole", "acid rain", and "photochemical smog" have become household words. Their notoriety is evidence for the growing concern about the human impacts on climate, the earth's atmospheric chemical composition and possible health effects resulting from the observed and future changes. Studying the complex climate system is often interdisciplinary, owing to the multitude of aspects and processes taking place in its main components: the atmosphere, the oceans, and the biosphere.

The changing composition of the atmosphere is of particular interest since some of the minor constituents (trace gases) of air can affect the earth's energy balance. The so-called greenhouse gases absorb infrared radiation and can therefore "trap" the outgoing long wave radiation leading to changes in the climate system (e.g. increasing the temperature near the surface, changing the hydrological cycle through increased evaporation etc.). Several greenhouse gases have increased significantly (or even emerged) since preindustrial times which is believed to cause the (direct) anthropogenic greenhouse effect (e.g. *Harries et al.* (2001)). Apart from the prominent gas carbon dioxide (CO_2), which is estimated to account for the largest portion of this additional greenhouse effect, methane (CH_4) and ozone (O_3) are also important contributors (IPCC, 2001).

Methane concentrations have increased by more than five-fold since the last glacial maximum about 18,000 years ago (*Stauffer et al.* (1988); *Raynaud et al.* (1988)) and are still increasing. Its lifetime in the atmosphere depends on the oxidizing efficiency of the atmosphere, which is also believed to be strongly affected by anthropogenic emissions.

Before the 1970s it was commonly believed that tropospheric ozone was basically transported downward from the stratosphere and eventually destroyed at the earth's surface (e.g. *Regener* (1957); *Junge* (1962)), although some ozone production in heavily polluted summer "smog" episodes was recognized (e.g. *Haagen-Smit* (1952); *Leighton* (1961)). In the 1970s it was discovered that ozone is produced and destroyed in the troposphere during the oxidation of methane and carbon monoxide (CO) catalyzed by free radicals and nitrogen oxides (NO_x=NO+NO_2) (*Crutzen* (1972, 1973, 1974); *Chameides and Walker* (1973)). Radical chemistry, formerly only considered to be important in the stratosphere, was found to be strongly involved in tropospheric chemistry as well, and ozone was identified as the main precursor of the important hydroxyl radical (OH) (*Levy* (1971, 1972, 1973)). OH is the dominant sink for methane, carbon monoxide and many other organic substances in the atmosphere and is therefore often called the "detergent of the atmosphere".

Thus, the role of ozone in the atmosphere is manifold: It is an effective greenhouse gas, and

largely controls the oxidizing power of the atmosphere. Additionally, ozone is a toxic gas which can have detrimental effects on human health and crops (e.g. *McKee* (1993)). The controlling factor in determining ozone production or loss in large parts of the troposphere is the abundance of NO_x, which is largely emitted by human activity. It has been estimated with 3D global models that ozone concentrations may have more than doubled over large parts of the Northern Hemisphere (NH) since preindustrial times (e.g. *Crutzen and Zimmermann* (1991); *Lelieveld and Dentener* (2000)), which is also supported by measurements (*Volz and Kley* (1988)).

Other volatile organic compounds (VOC) than methane and CO can produce O_3 in the atmosphere. Emission from the biosphere is believed to be the dominant contributor to this group of compounds, but anthropogenic emissions are also considerable. The global emission strength from biogenic and anthropogenic sources is estimated to be about 1100 and 180 Tg(Carbon)/yr $(Tg(C)/yr)^1$, respectively (*Guenther et al.* (1995); *Olivier et al.* (1996)), although large uncertainties exist, especially for the biogenic emissions. This may be compared to the emission strength of the most abundant hydrocarbon in the atmosphere, methane, which is about 500 $Tg(CH_4)/yr$ (*Houweling et al.* (1999)).

Biogenic emissions are also of special interest because they could change in the future due to a shifting climate, and thus, through their photochemical impact on ozone and OH, could provide a positive feedback loop. This mechanism has been suggested for the single most important biogenic hydrocarbon isoprene (*Shallcross and Monks* (2000)), whose emissions are known to depend mainly on temperature and solar irradiance, but can also be extended to other compounds and a more general view on biosphere-atmosphere feedbacks (*Fuentes et al.* (2001)). Much more research is needed to better understand the effects of environmental conditions on VOC emissions and the effects of VOCs on the atmosphere.

Numerical models in combination with field measurements have proven to be useful tools in studying the complex interactions of chemical species and meteorology in the atmosphere. However, a few things have to be kept in mind when interpreting such model calculations. Due to the enormous complexity of the system as we currently understand it, often strong simplifications have to be introduced in order to have a computationally manageable model. Further assumptions are made to treat the mathematical equations that express the physical understanding. Additionally, many parameters, e.g. reaction rate constants, cross sections etc., go into the model, each of them adding some uncertainty to the model results. It is apparent that a classical error analysis, where every single error is considered and combined to give the overall uncertainty of the model results, is not feasible at present. Therefore, the interpretation of the model results and explanation of discrepancies must to some degree rely on scientific arguments and the intuition of the researcher, so that indications instead of proofs are to be expected as results of such numerical studies.

The complexity and non-linearity of the system also brings about the possibility that the model "knows" more than the scientist, meaning for example that a certain behavior observed in nature can be reproduced by the model, but it is not apparent why. This can either be because the reason behind the observed behavior is non-intuitive, or because several model biases are canceling each other. Therefore, two methods are employed in this study to help elucidate the way the input into the model and its different components (processes) influence the model results: sensitivity studies and budgeting.

Sensitivity studies can help us to understand the influence of a particular aspect in the

---

[1] Tg = teragrams or 10^{12} g.

coupled model and potentially identify single processes which are critical for the modeled result and therefore presumably also represent an important process in the atmosphere. An important result can thus be a recommendation for future laboratory or field studies. Budgeting can be seen as a numerical trick that facilitates learning about how a modeled result was produced, e.g. the ozone concentration at a specific point in space and time. Ideally, full information on each process involved at each place in time and space should be made available. However, due to storage limitations this is not possible and therefore averaged budget information is mostly used.

This study mainly employs a three-dimensional global scale meteorology-chemistry model to study the photochemistry of the troposphere, especially considering the effects of non-methane hydrocarbon chemistry (NMHC). In the following sections of this chapter a brief overview on the most important photochemical reactions and concepts for the troposphere is given. In Chapter 2 the 3D-model is presented focusing on new or extended model components. Mainly, this is the inclusion and development of a representation of NMHC chemistry for the global scale, implemented with a new technique which allows flexibly changing the model chemistry in the future. The uncertainty associated with some assumptions is discussed as well. Further details and tests of purely numerical aspects are supplied in the appendix.

In Chapter 3 model results from 16-month simulations using two different resolutions with the full chemistry are presented and extensively compared with available observations of ozone and its precursors. The observations include surface measurements, ozone soundings, airborne, shipborne and space-borne (satellite) measurements from various campaigns. Along with the comparison several pieces of information about the species' budgets are given. This chapter serves to give a picture of the model's strengths and weaknesses which are important to know for the sensitivity studies in the following chapters. Sensitivity studies only make sense when the model base simulation compares reasonably well with reality, or at least its deficiencies are known.

A first step to analyze the effects of different compound groups in the model is made in Chapter 4 in analyzing a series of three runs with stepwise increasing complexity. By this procedure the effects of non-methane hydrocarbons and particularly of one biogenic hydrocarbon compound with the highest global emissions (isoprene) can be separated to some degree, giving indications about their relative importance on several trace gas budgets. Chapter 5 addresses various uncertainties in the chemistry of isoprene by shorter sensitivity simulations further helping to explain the discrepancies shown in Chapter 3 and to point out critical assumptions which require more laboratory and/or modeling efforts. These tests include pure chemical aspects (the oxidation scheme) as well as the more meteorological/physical aspects of wet and dry deposition of intermediates in the oxidation of isoprene.

In the final Chapter the main results of this thesis are summarized and recommendations for future studies are given.
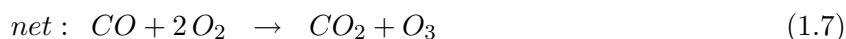
1.1   Background Tropospheric Chemistry

The oxidation of many compounds in the atmosphere is controlled by the hydroxyl radical (OH). Its primary source in the atmosphere is the photolysis of ozone at wavelengths shorter than 411 nm followed by reaction with water vapor:

$$O_3 + h\nu \;\; \rightarrow \;\; O(^1D) \tag{1.1}$$

$$O(^1D) + H_2O \quad \rightarrow \quad 2\,OH. \tag{1.2}$$

Note that only a small portion (about 1-10%) of the exited oxygen $O(^1D)$ reacts with water vapor. The rest is quenched by an unreactive air molecule (M, generally either N_2, O_2, or Argon) to its ground state which, in the troposphere, quickly recombines with molecular oxygen (O_2) to form ozone, thus resulting in no net effect on ozone.

In the presence of nitrogen oxides ($NO+NO_2$) the oxidation of hydrocarbons in the atmosphere can lead to ozone production. The simplest such reaction sequence which is nevertheless sufficient to explain some of the important principles in atmospheric chemistry, is the oxidation of carbon monoxide (CO) (the effect of hydrocarbons is further discussed in Section 1.2):

$$CO + OH\,(+O_2) \quad \rightarrow \quad CO_2 + HO_2 \tag{1.3}$$
$$HO_2 + NO \quad \rightarrow \quad OH + NO_2 \tag{1.4}$$
$$NO_2 + h\nu \quad \rightarrow \quad NO + O \tag{1.5}$$
$$O + O_2 + M \quad \rightarrow \quad O_3 + M \tag{1.6}$$

$$net: \quad CO + 2\,O_2 \quad \rightarrow \quad CO_2 + O_3 \tag{1.7}$$
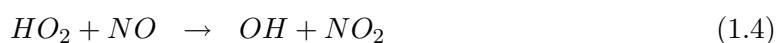
It can be seen that the radicals OH and HO_2 as well as the oxides of nitrogen NO and NO_2 are not affected by this reaction sequence. Such catalytic cycles are characteristic of atmospheric chemistry. It is advantageous to introduce two conceptual families here, $\mathbf{HO}_x$=OH+HO_2, and $\mathbf{NO}_x$=NO+NO_2. Grouping into such families reflects that the lifetime of an individual compound is very short, whereas the lifetime of the family is much longer because most reactions only convert the species into a different family member. The number of times that the reaction sequence 1.3-1.6 is repeated (the so-called chain length) depends on reactions that remove either HO_x or NO_x. The main terminating reaction for NO_x is:

$$OH + NO_2\,(+M) \rightarrow HNO_3 + M\,. \tag{1.8}$$
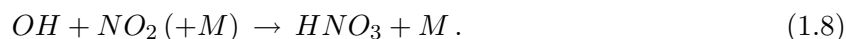
Nitric acid (HNO_3) is a very soluble substance and is only moderately reactive, so that it has a high chance of depositing and being lost from the atmosphere before it can release back the NO_2. HO_x radicals can also directly react with ozone:

$$HO_2 + O_3 \quad \rightarrow \quad OH + 2\,O_2 \tag{1.9}$$
$$OH + O_3 \quad \rightarrow \quad HO_2 + O_2. \tag{1.10}$$

Reaction 1.9 competes with 1.4, and it can thus be seen that the availability of NO_x is an important factor in determining whether net production or destruction (basically through reactions 1.2, 1.9 and 1.10) prevails.

Most NO_2 is not produced from reaction 1.4 but by

$$NO + O_3 \rightarrow NO_2 + O_2\,. \tag{1.11}$$

Together with 1.5 and 1.6 this represents a null cycle for ozone. Thus, also considering the large fraction of $O(^1D)$ from reaction 1.1 that reforms ozone, another conceptional family called the odd oxygen family $O_x = O_3 + O(^1D) + NO_2$ can be formed. Since the O_3 is by far the most

abundant species in the O_x family in the background atmosphere, the two are often treated as synonyms.

The main effects of the oxidation of methane is in principle similar to that of the reaction sequence 1.3-1.6 and the reaction sequence under high NO_x conditions is (see e.g. *Crutzen* (1972, 1973, 1974)):

$$CH_4 + OH \rightarrow CH_3 + H_2O \qquad (1.12)$$
$$CH_3 + O_2 + M \rightarrow CH_3O_2 + M \qquad (1.13)$$
$$CH_3O_2 + NO \rightarrow CH_3O + NO_2 \qquad (1.14)$$
$$CH_3O + O_2 \rightarrow HCHO + HO_2 \qquad (1.15)$$
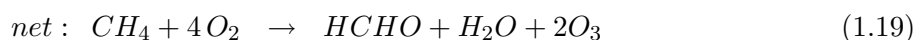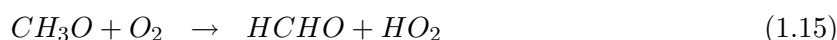$$HO_2 + NO \rightarrow OH + NO_2 \qquad (1.16)$$
$$2(NO_2 + h\nu \rightarrow NO + O) \qquad (1.17)$$
$$2(O + O_2 + M \rightarrow O_3 + M) \qquad (1.18)$$

$$net: \quad CH_4 + 4O_2 \rightarrow HCHO + H_2O + 2O_3 \qquad (1.19)$$
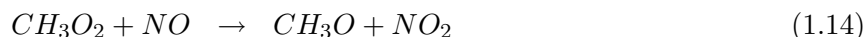
This net reaction is again catalyzed by HO_x and NO_x. The reactions of the intermediates CH_3 and CH_3O with oxygen (as well as reaction 1.6) are so fast that they are usually assumed to be immediate. The gas phase oxidation of formaldehyde (HCHO or CH_2O) to CO can occur through photolysis or reaction with OH leading to production of two HO_x molecules or one conversion of OH to HO_2, respectively. Under NO_x-bereft conditions reaction of the methyl peroxy radical (CH_3O_2) with HO_2 can compete with reaction 1.14

$$CH_3O_2 + HO_2 \rightarrow CH_3O_2H + O_2 \qquad (1.20)$$
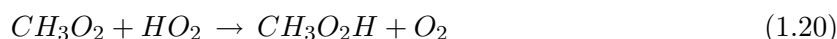
forming the simplest hydroperoxide CH_3O_2H which again can photolyze or react with OH ($CH_3O_2H + OH \rightarrow CH_3O_2 + H_2O$). These reactions tend to destroy HO_x which will thus be lower under low NO_x conditions. The intermediates HCHO and CH_3O_2H may also be deposited and HCHO can react in cloud droplets (e.g. *Lelieveld and Crutzen* (1991)).

Further NO_x reactions include reaction of NO_2 with O_3 to form the nitrate radical NO_3 which can also act as an oxidant in the atmosphere. Reaction with another NO_2 molecule leads to the formation of N_2O_5 which is of importance because it can react with water on aerosol surfaces or cloud droplets to form HNO_3. This represents a significant loss mechanism of NO_x in the atmosphere (*Dentener and Crutzen* (1993)). NO_3 and N_2O_5 quickly photolyze so that these reactions are mainly of importance during night. These reactions are depicted in Figure 1.1. NO_2 can also react with HO_2 to form per-nitric acid (HNO_4), a significant reservoir species in the upper troposphere. Under warm conditions and higher pressures HNO_4 is very short lived and decomposes back to NO_2 and HO_2. In the upper troposphere its lifetime is also limited by photolysis and reaction with OH.

1.2 NMVOC Chemistry in the Troposphere

Since CH_4 and CO are readily available even in remote parts of the atmosphere, ozone production from these hydrocarbons is largely limited by the availability of NO_x. Near the main source
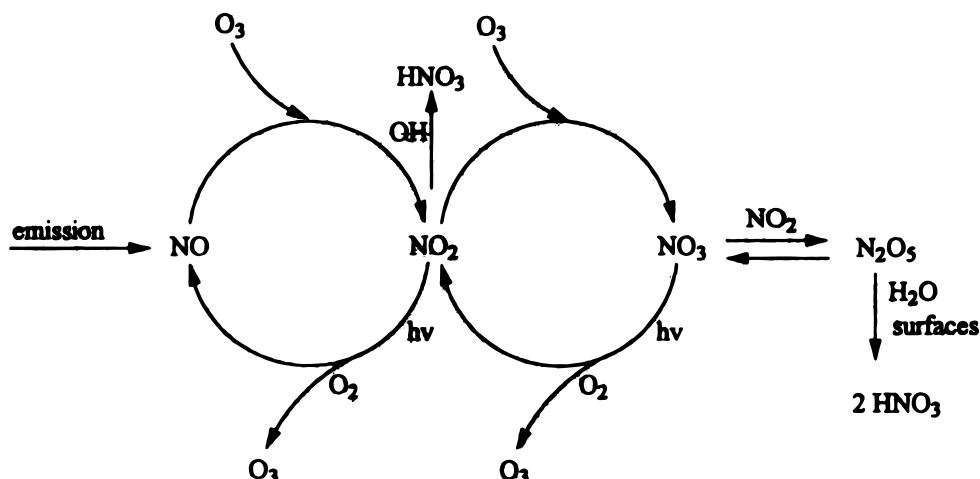
Figure 1.1: Scheme illustrating the main nitrogen reactions in the troposphere (from *Atkinson* (2000), reprinted with permission from Elsevier Science).

regions, where sufficient NO_x is available, the ozone production may actually also depend on the production rate of the peroxy radicals (HO_2 or CH_3O_2) which in this case originated from the oxidation of methane and carbon monoxide. In polluted regions therefore the oxidation of other (mostly shorter lived) volatile hydrocarbons, collectively called Non-Methane Volatile Organic Compounds (**NMVOC**, also NMOC) is also of importance. The aforementioned regime is referred to as the VOC limited regime. The term **NMHC** (Non-Methane Hydrocarbons) is introduced when partially oxidized species are excluded. However, the use of these terms varies and they are sometimes used as synonyms. In this thesis the term NMHC will be used mostly to indicate unoxidized species, such as alkanes and alkenes; otherwise the term NMVOC is used.

A Generalized Degradation Sequence of VOCs

A general discussion of all VOC groups and reactions cannot be given here. The following discussion is intended to point out a few key aspects of the complex interplay of VOC and NO_x in the atmosphere. For more details the reader is referred to the reviews of *Jenkin and Clemitshaw* (2000) and *Atkinson* (2000), upon which this discussion is largely based.

Many features are very similar among the various hydrocarbons. A generalized oxidation scheme which is applicable to most VOCs is given in Figure 1.2. The initial reaction with OH or NO_3, or photolysis leads to alkyl radicals ($R\cdot$) which quickly combine with oxygen to form peroxy radicals (RO_2). Peroxy radicals can react with HO_2, other RO_2 or NO (depending on the NO_x concentration). The HO_2 reaction yields a hydroperoxide (ROOH), whereas the RO_2+RO_2 products are usually carbonyls[2] (e.g. ketones or aldehydes) or alcohols (ROH). A small fraction of the reaction of RO_2 with NO can yield alkyl-nitrates ($RONO_2$) and the remaining fraction forms alkoxy radicals ($RO\cdot$), which can react via isomerization, decomposition or with O_2. The degree to which each occurs is a function of the specific molecular structure. This also holds for the nitrate yield which tends to increase with increasing chain length, e.g. methyl nitrate:

---

[2]The carbonyl group is $\overset{\overset{\textstyle O}{\|}}{\diagup C \diagdown}$. Ketones have one C-atoms on each side of the carbonyl group. Aldehydes have one hydrogen (H) and one C attached to the carbonyl-C (written as R-CHO).

<0.1%, ethyl nitrate: <1.4%, propyl nitrate: ≈4%. Peroxy nitrates ($ROONO_2$) may also be formed, but they are thermally unstable except in the tropical upper troposphere. The reaction of the alkoxy radical (RO·) is usually quite fast so that often only the final products are treated explicitly in chemical mechanisms.
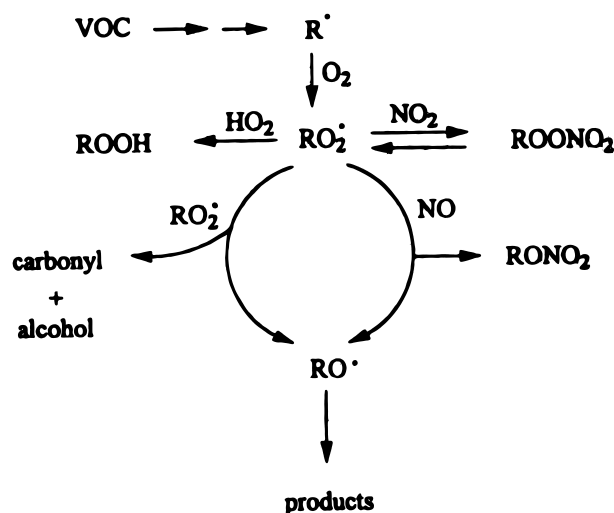
Figure 1.2: Generalized degradation scheme for VOC (from *Atkinson* (2000), reprinted with permission from Elsevier Science).

Several examples of this basic structure of the degradation of VOC can be found in the chemical scheme listed Table A.1 in Appendix A.

Effects of NMVOC on Atmospheric Chemistry

From the multitude of ways in which NMVOC affect atmospheric chemistry, five main aspects will be discussed as follows:

1. Formation of peroxy radicals, which can convert NO to NO_2 and thus produce ozone.

2. Sequestering reactive nitrogen in less reactive forms.

3. Long range transport of these odd nitrogen reservoirs.

4. Providing a sink for HO_x.

5. Providing additional sources of HO_x especially in the Upper Troposphere (UT).

The most direct effect is that NMVOC provide additional peroxy radicals and thus contribute to ozone production similarly to reactions 1.14 or 1.16, when HO_2 or CH_3O_2 is replaced by RO_2. Anthropogenic NMVOC is mostly emitted into a high NO_x atmosphere so that the additional peroxy radicals can significantly contribute to local ozone production. If the meteorological situation is such that little exchange of air (and pollutants) with cleaner air masses exists, the photochemical smog often result.

The peroxy radicals produced in the oxidation of NMVOC can also sequester NO_x in an inactive form which can be transported away from the NO_x source region and finally release

back NO_2 (see Figure 1.2). A special group of peroxy radicals, the peroxy acyl radicals, which are formed from aldehydes upon reaction with OH, can also react with NO_2 resulting in stable peroxy acyl nitrates. The most abundant of these is peroxy acetyl nitrate (PAN) formed from the peroxy acetyl radical $CH_3C(=O)O_2$ (shortened as CH_3CO_3):

$$CH_3CO_3 + NO_2 + M \rightarrow PAN + M \,.$$
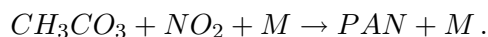
At room temperature and surface pressure the reverse decomposition reaction is relatively fast (the lifetime τ against decomposition is about 50 minutes) so that a low equilibrium concentration is present. However, with decreasing temperature and pressure, as prevalent in the upper troposphere the lifetime quickly exceeds one year. Concentrations of PAN have been measured to exceed those of the NO_x species (e.g. *Singh et al.* (1992)) in the upper troposphere. The second most abundant PAN analogue, peroxy propionyl nitrate (PPN), is typically only about 1/10 as abundant as PAN (e.g. *Williams et al.* (1997)). The subsequent down-mixing of PAN (and potentially its higher analogues) can thus act as a significant NO_x source to remote regions (*Crutzen* (1979); *Singh and Hanst* (1981); *Singh et al.* (1985); *Moxim et al.* (1996)).

A third influence of hydrocarbons on atmospheric chemistry is thus exerted by reducing NO_x concentrations near the sources by transferring NO_x into more inactive forms. The effect can be expected to be especially large where VOC levels are high and NO_x levels low.

Point four is quite apparent: If sufficiently large amounts of a reactive hydrocarbon are present the primary oxidant OH can be substantially reduced. But some partially oxidized species which may be directly emitted or produced in the oxidation of NMHCs can actually produce additional HO_x. These additional HO_x source are especially important in the upper troposphere where the primary production of OH via Reaction 1.2 is less efficient since less water vapor is available. *Jaeglé et al.* (2001) calculated that with water vapor mixing ratios of less that 100 nmol/mol other HO_x sources become important. HO_x is produced through photolysis of acetone (CH_3COCH_3), hydroperoxides (ROOH) and aldehydes. The relative contributions among these potential candidates is still a matter of debate (e.g. *Chatfield and Crutzen* (1990); *Prather and Jacob* (1997); *Jaeglé et al.* (1997, 2000); *Collins et al.* (1997); *Müller and Brasseur* (1999)). It is noted that many of these compound are actually not produced in the upper troposphere but pumped up by deep convection which therefore is an important process in atmospheric chemistry. Since convective injection of HO_x precursors and NO_x occurs often simultaneously ozone can be produced efficiently.

Alkenes[3] can also react directly with ozone. The reaction mechanism is quite complex and as pointed out by *Neeb and Moortgat* (1999) laboratory data are always obtained under NO_x-free conditions so that an extrapolation of the laboratory behavior to the atmosphere is difficult. In large scale models therefore only a simple "one step" reaction is often included which does not treat all intermediate species. The reaction of alkenes with ozone also produces some HO_x which might be important under polluted northern hemispheric winter conditions when other HO_x sources are weak (e.g. *Ariya et al.* (2000)).

---

[3]Acyclic hydrocarbons containing one or more double bonds (C_nH_{2n}), as opposed to **alkanes** which are saturated acyclic hydrocarbons (C_nH_{2n+2}).

Chemistry of Isoprene

Isoprene (2-methyl-1,3-butadiene or $CH_2=C(CH_3)CH=CH_2$ or [structure] or C_5H_8) is probably the most important alkene in the atmosphere and the compound with the largest biogenic emissions, which are of about the same magnitude as methane emissions ($\approx$400-500 Tg(C)/yr). Therefore special attention is given to this compound in this thesis (see Chapter 5).

The oxidation of isoprene involves many thousands of reactions (*Carter and Atkinson* (1996); *Poisson* (1997); *Saunders et al.* (1997b)). Most of them have not been measured, but are inferred from analogy assumptions and rate constants are often estimated using the structure-reactivity relationship (SAR) method (*Kwok and Atkinson* (1995); *Neeb* (2000)). Nevertheless the chemistry of isoprene must be considered well known compared to most other biogenic hydrocarbons (e.g. terpenes, see *Fuentes et al.* (2000)). In order to get an overview of the most important reaction pathways only a reduced isoprene oxidation scheme will be briefly presented here. The scheme, known as the Mainz Isoprene Mechanism (**MIM**), was developed (including contributions from the author of this thesis) for 3D applications, and was found in numerous box model tests to closely agree with an extensive scheme containing about 2000 isoprene related reactions (*Pöschl et al.* (2000b)) in the prediction of key species such as O_3, OH, CO, CH_3OOH, and PAN. Figure 1.3 sketches the main degradation pathways initiated by OH. As in the generalized reaction scheme in Figure 1.2 peroxy radicals are formed. In the case of isoprene there are six different possible isomers, which are lumped into the representative species ISO_2 in MIM. In each stage of the degradation only a few species are used to represent the main oxidation products and to cover the reaction pathways dominating under high and low NO_x conditions. The scheme also includes four nitrates (ISON, MPAN, NALD and PAN) with different reactivities. It is interesting to note that species on the right side (i.e. hydroxyperoxides from isoprene, peracetic acid) as well as the lumped species for multi-functional C_5-nitrates ISON can generally be lost by dry and wet deposition, because they are probably quite soluble. This issue is further discussed in Chapter 5.

Isoprene can also react with ozone, with the main stable products being methacrolein ($CH_2C(CH_3)CHO$) and methyl vinyl ketone ($CH_3C(O)CHCH_2$, MVK) and formaldehyde HCHO. The first two C_4-compounds are lumped into one species (MACR) in MIM. Isoprene can furthermore react with the nitrate radical NO_3 by addition to a double bond, but the chemical behavior of the products is highly uncertain (*Carter and Atkinson* (1996)), so that in MIM they were simply lumped with the other C_5-nitrates (ISON) (whose fates are likewise uncertain). The uncertainty in the treatment of these nitrates will be addressed in Chapter 5.

1.3   The concept of ozone production efficiency (OPE)

On the basis of the simple reaction sequences given so far it is possible to introduce another important concept in atmospheric chemistry first discussed by *Liu et al.* (1987): One can look at different chemical regimes in terms of their ozone production efficiency (**OPE**) as a function of NO_x. More precisely the OPE is defined as the net production of O_3 per NO_x molecule lost. Obviously the OPE will depend on ambient conditions such as UV radiation, VOC mixture, and NO_x concentrations. It has been calculated that the OPE is zero at very low NO_x concentrations when net ozone loss prevails then increase to a maximum and decrease again with increasing NO_x
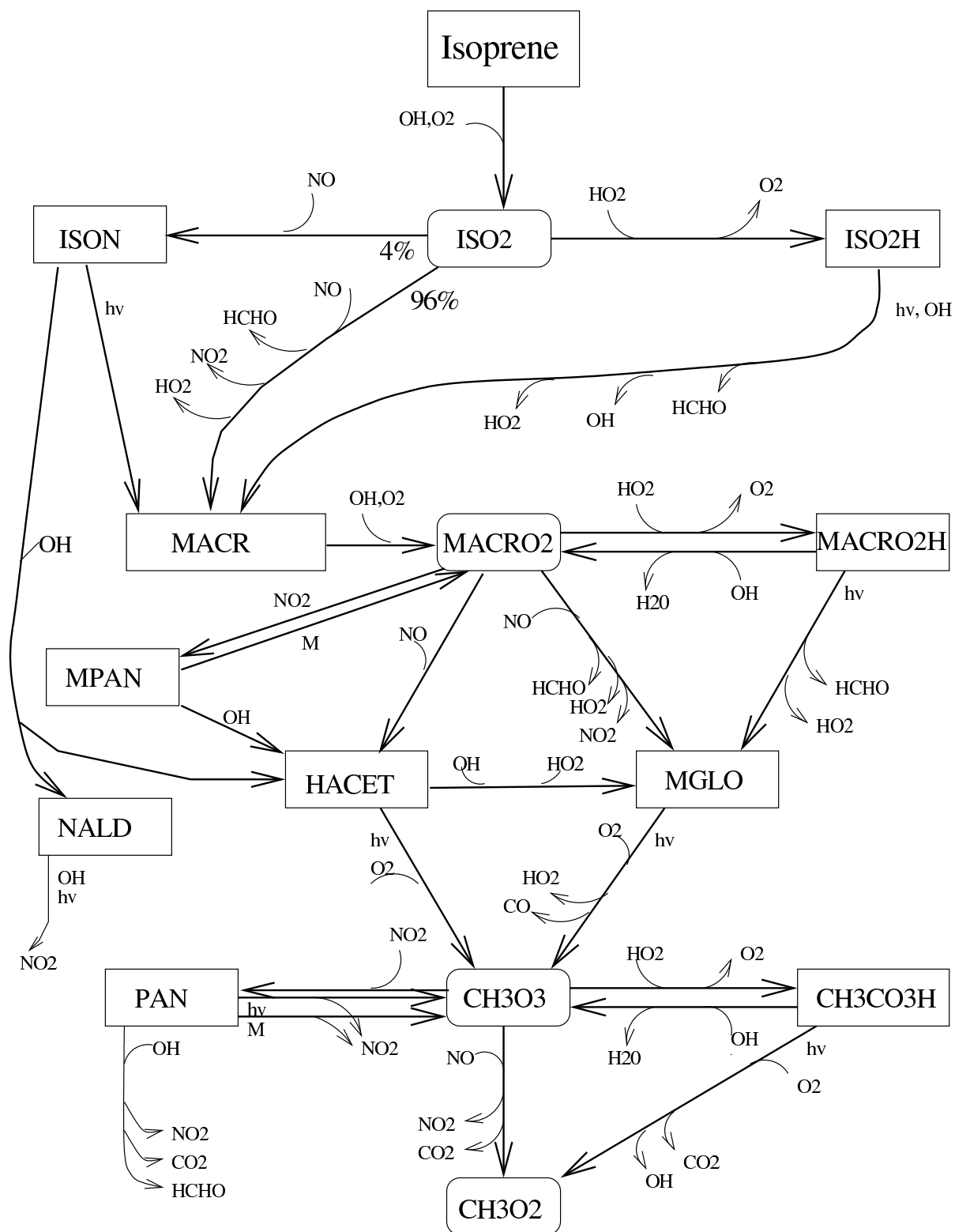
Figure 1.3: Main reaction pathways in the oxidation of isoprene initiated by OH as represented in the strongly simplified Mainz Isoprene Mechanism (MIM).

concentration when NO_x mixing ratios exceed a few hundred pmol/mol.[4] Observations are consistent with values of 1-5 under polluted boundary layer conditions (see *Jenkin and Clemitshaw* (2000) and references therein) and calculations indicate that the OPE can increase with decreasing NO_x up to 20-100 (*Lin et al.* (1988)). The highest values are reached for very high VOC/NO_x ratios. The decrease in efficiency with higher NO_x conditions can be explained by Reaction 1.8 which gets more efficient in terminating the catalytic cycles of VOC oxidation, similar to the methane oxidation sequence show above.

This non-linearity of ozone production has some important consequences for photochemical modeling, which need to be mentioned. *Kanakidou and Crutzen* (1993) have found that using a three-dimensional model of tropospheric chemistry resulted in up to 20% lower zonal mean ozone concentration than using zonal mean fields (thus mimicking a 2D model). This is because in the 2D simulation polluted and pristine conditions are averaged and result in NO_x concentration which are more effective in producing ozone. The problem, however, also exists in 3D simulation through the sub-grid mixing which is assumed to be instantaneous, i.e. each grid box is generally considered to be well mixed. With the resolution of global models still being 200-1000 km, mixing of "point" sources like power plants, cities or forest fires is too efficient. *Sillman et al.* (1990) found with a regional (single layer) model that the morning to afternoon buildup of ozone was over-predicted by 35% when using a resolution of $400{\times}480$ km^2 compared to a $20{\times}20$ km^2 resolution run, when both results where averaged over the model domain. A recent study basically confirmed these results using a pair of mixing box models (*Liang and Jacobson* (2000)) for various initial conditions and dilution factors, which express the rate at which the polluted parcel mixes air with the background parcel. However, *Liang and Jacobson* (2000) also indicated that the overall net ozone production could be either under- or overestimated by a coarse resolution model depending on the ambient conditions.

An assessment of these sub-grid errors in a global model has not been attempted to date (to the best of the author's knowledge), but would be a rewarding (and demanding) research task.

---

[4]Note that alternatively the OPE is sometimes defined as the production (not the *net* production) of ozone per NO_x molecule lost (e.g. *Crutzen* (1995)), which increases monotonically with decreasing NO_x.

Chapter 2

The 3D Global Chemistry-Meteorology Model MATCH-MPIC

In this chapter the main tool used in this study, the **M**odel of **A**tmospheric **T**ransport and **CH**emistry – Max-Planck-Institute for Chemistry Version (MATCH–MPIC) is described. For brevity hereafter it will be referred to simply as MATCH. The model can be structured into two main parts: the meteorological module and the photochemical module, which will be presented in subsections 2.2 and 2.3, respectively. In short, the model as described in *Lawrence et al.* (1999b) is applied here with a new flexible chemical integration method, extended chemical schemes, expanded photolysis rate calculations, modified and extended budgeting capabilities, updated and expanded emission inventories, and a new dry deposition scheme.

2.1   General Aspects

MATCH is an "offline" model: It needs basic meteorological data as input, namely, temperature, zonal and meridional wind, surface pressure, latent and sensible heat fluxes, and surface wind stresses, and calculates from these fields the remaining parameters to describe the redistribution and transformation of chemical tracers (e.g. vertical velocity, convective mass fluxes, cloud fraction, vertical turbulence).

In this study two different input datasets were used:

1. Analyzed data from the NCEP/NCAR reanalysis project (*Kalnay et al.* (1996))

2. Output from the NCAR - Community Climate Model (CCM, *Kiehl et al.* (1998)) middle atmosphere version (MACCM).

The NCEP data is used at a resolution of approximately $1.9° \times 1.9°$ (about 210 km$\times$210 km near the equator). Due to computational limitations[1] for most of the sensitivity calculations a three times lower horizontal resolution ($5.6° \times 5.6°$) is used. In analogy to the triangular truncation of higher wave numbers in spectral models, these resolutions will be subsequently referred to as the

---

[1]One model year at this resolution, which encompasses about 500,000 gridboxes, can take over a week of CPU time on a NEC SX-5 supercomputer.

T63 and **T21** resolution, respectively. The CCM meteorological data is only applied here to test the sensitivity of the model results, particularly the stratosphere-troposphere exchange of ozone (Section 3.7), to the meteorological dataset. The MACCM data, provided at T42 resolution, were only used at T21 resolution. The vertical grid in MATCH is usually taken from the meteorological input fields. The NCEP data are provided on 28 pure sigma levels (i.e. $\sigma = p/p_{surf}$ is the vertical coordinate) extending from the surface to about 2.7 hPa, with 18 levels below 200 hPa. The first 5 layers near the surface have approximate thicknesses of 90, 140, 180, 220, and 280 m (for tropical conditions) and increase to 1–1.5 km near the tropopause. From the 52 levels of the MACCM data (extending up to 0.006 hPa) only the lowest 36 (up to 2.6 hPa) are used for better comparison to the NCEP data. The resolution near the tropopause is about twice that of the NCEP data.

The time step used in this study is 30 minutes. The meteorological input data are archived every 6 hours and linearly interpolated to the beginning of each time step. Driving an offline model with fields sampled at this frequency has been found by *Rasch et al.* (1997) to introduce only small errors compared to an online calculation. These authors also state that this interval is sufficient to drive parameterizations in the offline model, when not all necessary parameters (such as convective fluxes, etc.) are supplied in the driving dataset.

For lower resolutions the model all meteorological parameters, such as the convective fluxes and cloud cover are pre-calculated from a high resolution run and then averaged to the coarser grid. The lower resolution run is the driven by these archived data ("archived mode"). The reason is that the convective and cloud physics parameterizations predict much less convective clouds, when the averaged input data is used, since they mainly depend on a critical value of relative humidity, which is less often exceeded in the averaged datasets. An exception to this is the sensitivity simulation employing the CCM data, where convection was also diagnosed at the lower resolution of $5.6° \times 5.6°$. It is noted, however, that the archived convective fluxes were calculated with the previous version of MATCH (*Lawrence et al.* (1999b)) which particularly did not include the mass-wind consistency fixer described in Section 2.2.1. The T63 and T21 runs presented in Chapter 3 are therefore not completely comparable and have to be seen as independent model versions.

A clear advantage of offline calculations is that they are computationally much less expensive (about a factor of 4, *Rasch et al.* (1997)) than online calculations with a climate model. Thus, chemical processes can be treated in more detail at the same computational burden. The major disadvantage may be that some feedbacks between chemistry and the energy equation cannot be taken into account. On the other hand this could also be seen as an advantage, since complex coupled processes can often be understood more easily, when distinct components are looked at separately and in more detail.

The main equation solved in MATCH including parameterized processes can be written as:

$$\frac{\partial}{\partial t}\rho + \nabla \cdot (\rho \overrightarrow{v}) = P_{turb} + P_{conv} + P_{wet} + P_{em} + P_{chem} + P_{dry}, \qquad (2.1)$$

where ρ is a tracer density, the second term on the left hand side is advection and the different P-terms represent other processes taken into account: vertical turbulent diffusion, convective redistribution, wet scavenging, emissions, chemical transformations and dry deposition, respectively. This coupled system of differential equations (note that the equations for each chemical species are coupled through the term P_{chem}) is solved in MATCH using "1st-order splitting". This

means the individual processes are treated sequentially and the result from the prior process is used as input to the next process. The order of treatment used in MATCH is as in Equation 2.1. The method is standard in atmospheric sciences since the work of *McRae et al.* (1982). However, an error is obviously introduced (the "splitting error"), which is generally assumed to be small compared to other model uncertainties. Several more complex methods of splitting have been proposed (for an extensive review see *Verwer et al.* (1998)), but all have one major drawback: the scientific interpretation of model results becomes more difficult, because the processes are coupled at the algebraic level of the splitting technique, whereas the 1st-order method allows straightforward budgeting of each process separately (see Section 2.3.7). In the current implementation convection and wet scavenging, as well as emissions and chemistry are actually coupled to a certain degree. Quantification of the operator splitting error is very difficult in a 3D model and is not attempted here. The study of *Berkvens et al.* (2000), however, who compared 3 different splitting methods in a 1-D model, concluded that at a 30 minutes time step all methods performed well, with maximal errors of a few percent of the daily variations for some short lived species. It is also noted that information on the splitting technique is hardly found in the literature on global chemistry models. Better documentation on this issue is strongly recommended, since it would clearly increase the transparency of scientific results.

2.2 Meteorological Parameterizations

The meteorological component is historically based on the climate model CCM2 (Community Climate Model – Version 2) of the National Center for Atmospheric Research (NCAR)(*Hack et al.* (1993)). The dynamical parts of the model have been described and evaluated in *Rasch et al.* (1997); *Mahowald* (1996) and *Mahowald et al.* (1997a,b). Therefore, these components will be only briefly discussed here, except for a new procedure used to ensure mass conservation in the advection algorithm, which has not been published.

2.2.1 Advection Scheme and Mass Conservation

Horizontal and vertical transport of chemical tracers with the mean wind components is calculated in MATCH using the algorithm described in *Rasch and Lawrence* (1998). The scheme called SPITFIRE (Split Implementation of Transport Using Flux Integral Representation) is a flux-form scheme, which means that tracer fluxes are actually calculated at the cell walls. Each spatial direction is treated separately. The flux through a cell wall is estimated from evaluating the mass integral

$$\psi(a) = \int_0^a q(a')da' \quad \text{(with } a \text{ being the } x, y \text{ or } z \text{ coordinate, } q \text{ the tracer density)}$$

at the cell walls and at the respective departure points of the cell wall locations. The departure points are not necessarily at the model grid points, and thus an interpolation is required to calculate the mass integral, which is done using a 4th order accurate cubic interpolator. Due to the involved calculation of a departure point the scheme could be more accurately classified as a flux-form semi-Lagrangian (FFSL) scheme (*Lin and Rood* (1996)).

The SPITFIRE scheme is inherently mass conserving, but only on its own implied grid. This aspect has been described in detail by *Jöckel et al.* (2001). The issue is that tracer densities are

actually advected[2], and thus, conversion from mixing ratios to densities and back again is needed before and after the advection step. This involves multiplication with the air density. In an offline model the surface pressure is prescribed from the meteorological input dataset. Furthermore, the integral of the airmass in a column determines the surface pressure. Since the air mass change in a model column implied by the advection scheme is not necessarily consistent with the surface pressure change, the tracer mass is not generally conserved when the updated air masses are used for the conversion.

As pointed out by *Jöckel et al.* (2001) the mass conservation can even be violated when the surface pressures do match. This happens when the airmass transported into a single grid cell is not consistent with the amount of air in that cell which is implied through the updated surface pressure and the discrete vertical level boundaries ("mass/wind inconsistency"). Since the surface pressure fully defines the vertical grid boundaries in the model, the problem can also be seen as an inconsistency between the updated model grid and the grid implied by the advection scheme (*Jöckel et al.* (2001)). This inconsistency can occur for various reasons: It can be caused by the use of a different advection algorithm in the model that calculated the meteorological input fields, or through the interpolation between the 6 hourly input intervals, or through the conversion to a different horizontal grid.

In order to assure accurate tracer mass conservation, with a minimum of artificial transport, it is thus necessary to either map the results from the implied grid to the grid of the new time step, or to correct the winds to match the new surface pressure and the mass in each grid box before applying the advection algorithm (*Jöckel et al.* (2001)). Since *Jöckel et al.* (2001) demonstrated problems with the mapping technique, the second method will be used in MATCH, although it has not yet been proven that either of the methods can be judged superior based on physical arguments. The re-mapping applied in *Jöckel et al.* (2001) resulted in an artificial vertical diffusion, and it is thus likely that a correction of the wind fields will imply a similar vertical redistribution (see below). The correction applied in MATCH is based on personal communication with *P. Rasch* (NCAR, 2000), and is only sketched here.

A two dimensional (vertically integrated) correction field C to the velocity field is introduced with the requirement that the vertically integrated divergence of the corrected velocity field match the surface pressure changes. It is specified as the gradient of a scalar field (ϕ) to ensure that it is irrotational. C can be obtained after solving for ϕ, which in turn requires solving a Helmholtz equation.

Partitioning of the vertically integrated correction flux into the model layers is arbitrary, but can significantly influence the vertical distribution of air and tracers. Here, an iterative procedure is applied that minimizes the difference between the a priori calculated and the fixed fluxes (weighted by the layer thickness). Already one (Picard-) iteration cycle is enough to reduce the remaining mass mismatch to an insignificant amount. Finally, the vertical velocity follows from the two horizontal components by continuity, thus ensuring that the correct amount of air enters each grid box.

The largest effects of this correction were found in the tropopause region for species with large gradients (O_3 and NO_y) and especially for the lower resolution runs. Ozone was reduced in the region directly below the tropopause by as much as 30-40%, giving better agreement with ozone soundings (see Chapter 3.1). These result show that the correction of the mass/wind

---

[2]In fact, the transported quantity in MATCH is the "pseudo density" $q\partial p/\partial\eta$, where q is the tracer mixing ratio, p is pressure and η is the vertical coordinate.

inconsistency has been a crucial improvement in the model dynamics.

It should be noted that this procedure will also be needed if another advection scheme that operates on tracer densities is implemented in MATCH (as opposed to semi-Lagrangian schemes, which use tracer mixing ratios, but are generally not mass conserving).

2.2.2   Cloud Parameterizations

In MATCH two schemes are used in tandem to parameterize convection. First, the penetrative deep convection scheme of *Zhang and McFarlane* (1995) is used to reduce any convective available potential energy (CAPE). It is based on a plume ensemble approach, where ensembles of up and down-drafts are assumed to exist, whenever the atmosphere is conditionally unstable. The updraft ensemble is treated as a collection of entraining[3] plumes, allowing entrainment throughout the convective column. Detrainment from the updraft on the other hand is confined to a thin layer near the cloud top and to the sub-cloud layer in the case of the associated downdraft.

Next, the local mixing scheme of *Hack* (1994) is applied to remove any local instabilities left by exchanging moisture, energy and tracers between neighboring layers. The Hack scheme is meant to deal with shallow- and mid-level convection not occurring in the boundary layer.

It was found (*Mahowald* (1996)) that before applying these schemes, the archived moisture and temperature profiles need to be destabilized in order to diagnose realistic amounts of convection in the model. This is achieved by applying the tendencies from advection and vertical diffusion also to the moisture and virtual temperature before diagnosing convection.

The cloud fractions are diagnosed using the parameterization of *Slingo* (1987), with some modifications described in *Kiehl et al.* (1998). Additional modifications were made by *Lawrence* (1996) so that the scheme diagnosed cloud fractions using the NCEP data are in close agreement with different cloud climatologies (see *Lawrence* (1996) and references therein). Four different types of clouds are treated: convective clouds, high-level clouds (cirrus), mid-level layered clouds and low-level stratus.

The cloud microphysics module of *Rasch and Kristjánsson* (1998), which is based on a bulk microphysical approach, is used to derive condensation and evaporation rates for the non-convective clouds, whereas precipitation and evaporation rates for convective clouds are calculated by the *Zhang/McFarlane* scheme. Four different kinds of condensates are considered: cloud water, cloud ice, rain and snow/graupel. However, only the total of the four is transported and the partitioning is reevaluated each time step. The diagnosed formation and evaporation rates of these condensates are subsequently used in the wet scavenging module and also for the redistribution of trace gases through settling of cloud particles (see Chapter 2.3.5).

2.2.3   Vertical Turbulent Diffusion

While horizontal diffusion is not accounted for, since it is believed to be small compared to horizontal advection or numerical diffusion, vertical sub-grid-scale turbulent transport is an important process in the atmosphere, not only for the redistribution of trace species, but also for momentum and energy exchange near the earth's surface. In MATCH vertical turbulent mixing is based on the scheme of *Holtslag and Boville* (1993). In addition to the typical down gradi-

---

[3]Entrainement here means the process of mixing in ambient air into the cloud. Detrainment is the opposite process.

ent diffusion based on local-K theory, the scheme also includes a non-local (sometimes called "counter-gradient") term to account for large-eddy motion in the convective boundary layer.

2.3   Chemical Module in MATCH-MPIC

In this section the treatment of chemical transformations and source and loss processes of chemical species in MATCH are described. Apart from chemical reactions, dry and wet deposition, emissions and the redistribution of trace gases through gravitational settling of non-precipitating cloud particles are considered.

2.3.1   Chemical Schemes

Several sets of reactions have been used in the course of this study, making use of the flexible integration procedure described in Section 2.3.3. In this section only the standard set of reactions is described.

The full scheme comprises 141 gas phase reactions, of which 33 are photolysis reactions and one heterogeneous process. It has been put together from several sources along with some additional assumption in order to keep it computationally manageable. All reactions are listed and referenced in Table A.1 in Appendix A and the 35 transported species and surrogate species are listed in Table 2.1. Two pairs of hydroperoxides, ISO_2H + $MACRO_2H$ and $C_4H_9O_2H$ + $MEKO_2H$, respectively, are lumped together during transport, since their behavior during deposition processes is assumed to be the same and their spatial distribution has similar gradients. Iso-propylnitrate, similarly, is transported together with the higher nitrates pool "ONIT". This reduces the computational burden, and does not change the model results significantly (generally $<1\%$ for the key species after several weeks). However, further grouping of hydroperoxides originating from different NMHCs led to larger errors, and was thus abandoned. The extended NO_x family (which is denoted as **NOX** throughout this thesis, see Table 2.1) is transported instead of transporting each member separately. This is also done in other 3D modeling studies (*Roelofs and Lelieveld* (1995); *Poisson et al.* (2000)) and can be justified with the fact that the adjustment time of the species in the NOX family is usually fast compared to the model time step for transport (30 minutes). Short lived species, such as O^1D, OH, HO_2 and peroxy radicals are not transported in the model. For non-transported species the values from the last time step are used at the beginning of the chemical integration routine. For species grouped for transport the ratios within the family are conserved during transport.

The scheme currently includes CH_4-CO-HO_x-NO_x "background" chemistry (reactions R1–R45) similar to *Lawrence et al.* (1999b), a representation of isoprene (2-methyl-1,3-butadiene) chemistry (about 30 reactions), a fairly explicit ethane (C_2H_6) chemistry (about 25 reactions), along with simple representations of propane (C_3H_8), ethylene (C_2H_4), propylene (C_3H_6) and n-butane (C_4H_{10}) chemistry. The latter is used as a surrogate for all higher alkanes.

Changes in the background tropospheric inorganic chemistry and methane oxidation compared to *Lawrence et al.* (1999b) are mainly (1) inclusion of O_2-photolysis (R5), which might be of importance in the upper tropical troposphere (*McLinden et al.* (2000)), (2) addition of the chemistry of methanol (R17+R45), a compound of increasing interest which has also been measured in several recent field campaigns (e.g. *Singh et al.* (1999, 2000)) and (3) addition of gas phase reaction of N_2O_5 with water vapor (R40) based on *Wahner et al.* (1998), although it is

Table 2.1: Transported species in MATCH.

	Species	Name/Group		Species	Name/Group
1	O_3	ozone	20	CH_3COOH	acetic acid
2	CO	carbon monoxide	21	HCOOH	formic acid
3	CH_4	methane	22	NALD	nitrooxyacetaldehyde
4	NOX	$= NO + NO_2 + NO_3 + 2 N_2O_5 + HNO_4$	23	C_2H_6	ethane
5	HNO_3	nitric acid	24	$C_2H_5O_2H$	ethyl-hydroperoxide
6	H_2O_2	hydrogen peroxide	25	CH_3CHO	acetaldehyde
7	CH_3O_2H	methyl-hydroperoxide	26	C_3H_8	propane
8	HCHO	formaldehyde	27	$C_3H_7O_2H$	secondary propyl-hydroperoxide
9	CH_3OH	methanol	28	$C_3H_7ONO_2$	iso-propyl nitrate
10	C_5H_8	isoprene (2-methyl-1,3-butadiene)	29	CH_3COCH_3	acetone
11	ISO_2H	C_5 β-hydroxyhydro-peroxides from C_5H_8+OH products (ISO_2)	30	$CH_3COCH_2O_2H$	acetonylhydroperoxide
12	ISON	C_5 β-hydroxyalkyl-nitrates from ISO_2 and $C_5H_8+NO_3$ products	31	C_3H_6	propene (=propylene)
13	MACR	methacrolein, methylvinylketone (MVK) and other C_4 carbonyls	32	$C_3H_6OHO_2H$	hydroxyhydroperoxide from C_3H_6
14	$MACRO_2H$	hydroperoxides from MACR	33	C_2H_4	ethene (=ethylene)
15	MPAN	peroxycryloyl nitrate and other higher perox-yacylnitrates	34	C_4H_{10}	n-butane, $\geq C_4$ alka-nes
16	HACET	hydroxyacetone and other C_3 ketones	35	$C_4H_9O_2H$	hydroperoxide from C_4H_{10}
17	MGLY (CH_3COCHO)	methylglyoxal and other C_3 aldehydes	36	MEK	methylethylketone and other $\geq C_4$ ketones
18	PAN	peroxyacetyl nitrate	37	$MEKO_2H$	hydroperoxides from MEK
19	CH_3CO_3H	peroxyacetic acid	38	ONIT	organic nitrates (other than from isoprene)

probably much slower than the heterogeneous conversion rates. The latter conversion on sulfate and sea salt aerosols is included using monthly archived pseudo-first order rate constants from *Dentener and Crutzen* (1993) and on cloud droplets based on the modeled liquid water content:

$$N_2O_5 \longrightarrow 2\,HNO_3\,.$$
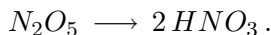
Thus, total and immediate release of HNO_3 to the gas phase is assumed. Heterogeneous uptake of NO_3 was not considered, but it is probably of minor importance (*Schultz et al.* (2000)) considering the low reaction probability of $\gamma = 0.01$ (upper limit, *Jacob* (2000)), in comparison to $\gamma = 0.1$ used for N_2O_5 by *Dentener and Crutzen* (1993).

Isoprene chemistry is represented by the Mainz Isoprene Mechanism (**MIM**, *Pöschl et al.* (2000b)), which has recently been developed to closely mimic the isoprene chemistry of the Master Chemical Mechanism (**MCM**, *Jenkin et al.* (1997); *Saunders et al.* (1997a,b)) of the University of Leeds. While the MCM includes about 2000 isoprene related reactions, the MIM has been condensed to only 44 reactions and 16 species including three nitrates. These numbers include some reactions involved in ethane oxidation, too. The reduction has been achieved by combining several reaction pathways, and introducing surrogate species that represent a class of several real species. For example the species ISO_2 actually represents six different peroxy radicals formed from the reaction of isoprene with OH (and subsequent addition of O_2). The nitrates from isoprene are not lumped with the nitrate pool (ONIT) from higher alkanes, since they are more reactive (due to the remaining double bond) and more soluble (due to the hydroxy-group).

In the same study 5 other isoprene oxidation schemes were intercompared with the MIM and the MCM, all of which have been used in other 3D large scale studies. Considerable differences in the predictions of O_3, OH and nitrogen containing compounds have been pointed out. The implication of these differences for the global scale will be addressed in Chapter 5.

Ethane oxidation is treated fairly completely. Ethanol formation from reaction R94 has been omitted, since it is fairly unreactive and much less abundant than methanol (e.g. *Singh et al.* (2000)). Ethyl as well as methyl nitrate formation have also been neglected due to the low reaction yields (<1.4% and <0.1% from reactions R15 and R96, respectively, *Tyndall et al.* (2001)). Peroxy-nitrates (RO_2NO_2) are generally considered to be too unstable throughout most of the troposphere. Thus formation of peroxy-nitrates via reactions of peroxy radicals with NO_2 is only considered in the case of HNO_4 (=HO_2NO_2). However, it should be noted that this assumption may not be valid under upper tropospheric and polar winter conditions.

In the oxidation of propane (C_3H_8) only the formation of the secondary peroxy radical (i.e. the radical resulting from H abstraction from the middle C atom) is treated explicitly. Based on kinetic data from *DeMore et al.* (1997) 81-83% of the reaction proceeds via this channel. Instead of the primary radical, the ethyl-peroxy-radical is formed, so that the formation of the higher PAN-analogue peroxypropionyl-nitrate (PPN) is parameterized as additional PAN formation and no radicals are lost in the mechanism. New data on the kinetics and products of the reaction of acetone with OH (*Wollenhaupt et al.* (2000); *Wollenhaupt and Crowley* (2000)) are also considered (R111+R112). Iso-propylnitrate is considered as an individual species, but it is transported with the higher nitrate pool ONIT.

Propene and ethene chemistry is treated only very crudely. The mechanism has been largely adopted from *Müller and Brasseur* (1995). Ethene chemistry after the first oxidation step with OH is parameterized into the propene oxidation chain. They are included here mainly to provide

peroxy radicals near the sources, which can significantly enhance local ozone production rates. The simple treatment of these alkenes may be justified by their relatively short atmospheric lifetime and their low organic nitrate formation yields, which likely limits their importance to strongly polluted regions.

The chemistry of n-butane (C_4H_{10}) has been added based on *Poisson et al.* (2000), representing all higher alkanes, which are mainly of anthropogenic origin. The main change made is that a higher average yield of alkyl nitrate formation of 16% has been used, based on *Zaveri and Peters* (1999). These authors estimated the average yield based on available kinetic data (*Carter and Atkinson* (1989)) and an alkane mixture from the National Acid Precipitation Assessment Program (NAPAP) anthropogenic alkane emissions inventory (*Middleton et al.* (1990)).

Non-photolytic reaction rates are generally taken from the most recent NASA or IUPAC[4] evaluations (*Sander et al.* (2000); *DeMore et al.* (1997); *Atkinson et al.* (1999, 1997)) with some updates from a recent review by *Tyndall et al.* (2001) and some more exceptions as listed in Table A.1 in Appendix A.

Omissions and Limitations

Although the scheme has been put together with the aim of representing the most important processes affecting ozone and the oxidizing capacity of the troposphere, it is important to see its limitations. While methane oxidation is fairly well known, some reaction rates and product yields of NMVOCs are not well established. Especially the formation yields and atmospheric lifetimes of nitrates from higher hydrocarbons are quite uncertain and errors are introduced using the lumped approach (e.g. for higher alkanes).

Some groups of NMVOCs are not considered in the current scheme. These include terpenes, higher ($> C_3$) alkenes, aromatics, halogens, sulfur-containing organics and some other compounds like higher alcohols, esters, ethers etc. The influence of some of these compounds of mainly industrial origin (e.g. aromatics, alkenes) is likely to be rather local, owing to their short atmospheric lifetimes.

Halogen chemistry is also not included, which is likely to affect the predictions of O_3 in the marine boundary layer (e.g. *Sander and Crutzen* (1996); *Dickerson et al.* (1999)). However, halogen activation would require the inclusion of aerosol processes and multi-phase chemistry, which has not been attempted in a global model to date.

Some heterogeneous processes have also been recommended by *Jacob* (2000) for inclusion into large scale O_3 models. The author states that there still is a large uncertainty associated with these processes, so that a reaction probability formulation, which express the heterogenous reaction as a first order rate constant process, with immediate release of the products to the atmosphere, which is very similar to the method of *Dentener and Crutzen* (1993). However due to the large uncertainty in these processes and the difficulty in obtaining reliable aerosol distributions, these processes are not included at present.

Aqueous phase chemistry in cloud droplets has also been neglected in this study, except for the hydrolysis reaction of N_2O_5. The studies of *Lelieveld and Crutzen* (1990, 1991) indicated that O_3, as well as a number of other trace gases, can be strongly affected through aqueous phase reactions. More recent studies that attempted global estimates of these effects arrived at moderate (*Dentener* (1993); *Jonson and Isaksen* (1993)) to small (*Liang and Jacob* (1997))

---

[4]International Union of Pure and Applied Chemistry; NASA: North American Space Association.

effects on global O_3 (less than 3% in the latter study).

Terpenes, which following isoprene are probably the second most important class of species of biogenic origin, are estimated to be emitted with rates of 125-147 Tg/yr (*Guenther et al.* (1995); *Müller* (1992)). These values may only be accurate to a factor 3, but indicate that the total terpene emissions are probably 3-5 times lower than those of isoprene. The emission strengths of the other compound groups are likely even much lower. Terpenes have recently gained more interest since they are known to condense and form aerosols (*Odum et al.* (1996); *Hoffmann et al.* (1997)), thus having potential impact on the radiation budget of the earth. This aspect is especially interesting, because the process of secondary organic aerosol (SOA) formation is possibly influenced by anthropogenic activities (*Kanakidou et al.* (2000)). Since a large spectrum of terpenes is emitted to the atmosphere (e.g. *Geron et al.* (2000)) and their oxidation mechanisms are still quite uncertain (*Jenkin and Clemitshaw* (2000)), they are not included in this work. However, they are a good target for future studies with MATCH, especially considering the flexible integration technique presented in Chapter 2.3.3.

At present some of the omitted NMVOCs are accounted for as additional emissions of CO, and in the case of the terpenes also of acetone (see Chapter 2.3.6). Possible effects of these omissions and/or simplifications will be discussed in the appropriate sections in Chapter 3, when model results are compared to observations.

2.3.2   Photolysis Rates

Photolysis rates in MATCH are computed online each time step using the scheme of *Landgraf and Crutzen* (1998). The method calculates actinic fluxes at eight "base" wavelengths for a purely absorbing atmosphere, using the model O_3 and O_2 distributions, and then introduces a correction to account for scattering by molecules, cloud particles, aerosols and the earth's surface. The contributions of eight wavelength bands, which are represented by the eight "base" wavelengths, is parameterized from the corrected actinic fluxes using lookup tables or polynomial expressions as a function of slant overhead ozone column. Clouds are accounted for using the modeled cloud fractions and cloud water and ice contents. Aerosols are only taken into account very rudimentarily, assuming an average of continental and marine aerosols optical properties in the lowest 5 model layers. More details on the method can be found in *Landgraf* (1998) and *Landgraf and Crutzen* (1998).

Since many new photolyzing species are now included in the chemical scheme compared to *Lawrence et al.* (1999b), which included most of the species covered by *Landgraf and Crutzen* (1998), the scheme needed to be extended. Instead of finding polynomial expressions for all new species a much simpler approach was attempted. Photolysis rates calculated with the 2-dimensional model of *Brühl and Crutzen* (1989), which employs the 2 stream radiative code of *Zdunkowski et al.* (1980), have been used to calculate correlation coefficients between various photolysis rates including those to be implemented and those already available from *Landgraf and Crutzen* (1998). A linear regression analysis (forced through zero) was performed on the data below 100 hPa at 11 o'clock and from 24 samples (twice-monthly output) covering one year.

Very high correlation coefficients were found for some pairs, which enables coupling of the new photolysis frequencies to existing ones. In Table 2.2 the best correlations to a preexisting photolysis rate are listed. Correlations with HNO_4 have not been used, since the cross section data of this species still rather uncertain (*Ch. Brühl*, personal communication, 1999). In Figure 2.1 the scatter plots for two species with very high ($r^2>0.99$) correlations and two with a somewhat

Table 2.2: Correlation coefficients of photolysis rates used in MATCH to calculate photolysis frequencies of new species in the chemical scheme. The resulting approximation then reads $J_{new} = m \cdot J_{Partner}$. References for all cross section data and, if available, quantum yields, are also given.

New Species	Partner	Slope m	r^2	References[a]
MVK[b]	CH_3COCHO	0.031	0.982	*Gierczak et al.* (1997)
Methacrolein[c]	$HCHO{\rightarrow}CO+H_2$	0.037	0.996	*Gierczak et al.* (1997)
i-$C_3H_7ONO_2$[d]	PAN	3.7	0.976	*Atkinson et al.* (1997)
CH_3CHO[e]	$HCHO{\rightarrow}HCO+H$	0.19	0.984	*Atkinson et al.* (1997)
HACET	$HCHO{\rightarrow}HCO+H$	0.11	0.996	*J. Crowley* (pers. comm., 1999)
CH_3CO_3H	$HCHO{\rightarrow}HCO+H$	0.025	0.997	*Giguère and Olmos* (1956)
MEK	$HCHO{\rightarrow}HCO+H$	0.42	0.983	*Martinez et al.* (1992)
PAN	N_2O_5	0.019	0.872	*DeMore et al.* (1997)
MGLY	$HCHO{\rightarrow}CO+H_2$	3.95	0.667	*Meller et al.* (1991); *Koch and Moortgat* (1998)
CH_3COCH_3	$HCHO{\rightarrow}HCO+H$	0.051	0.773	*Gierczak et al.* (1998); *McKeen et al.* (1997)

[a]When two references are given, the second is for quantum yields.
[b]Methylvinylketone, assumed to contribute 50% to the photolysis of MACR.
[c]Assumed to contribute 50% to the photolysis of MACR.
[d]This rate also used for photolysis of ISON and ONIT.
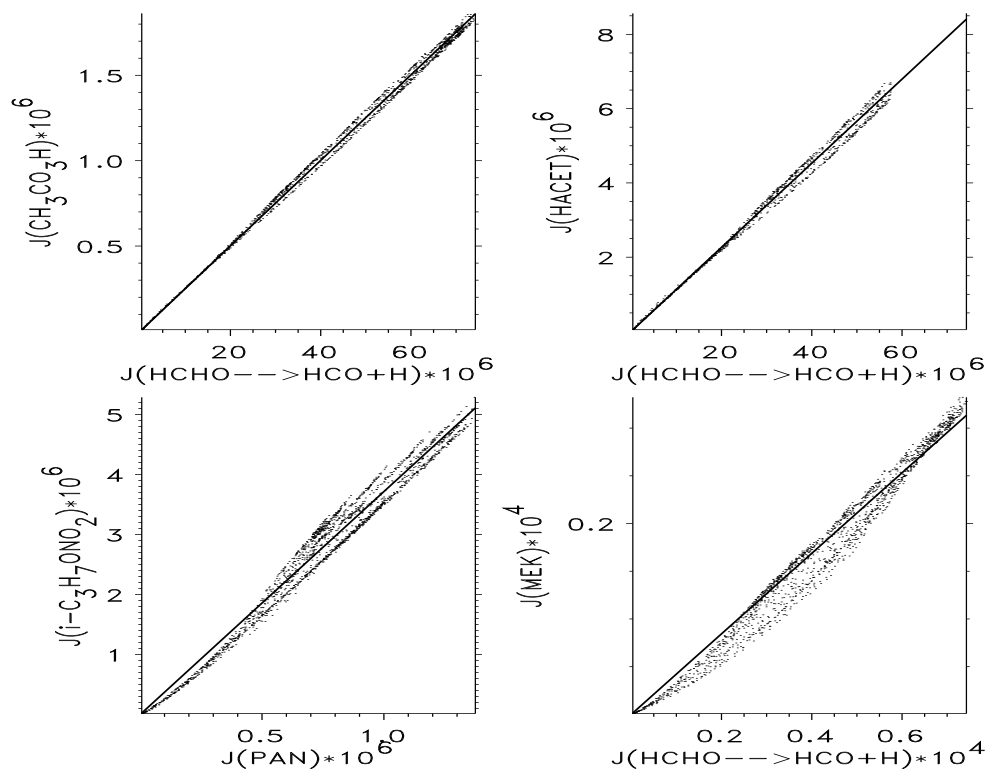[e]This rate also used for photolysis of NALD.

Figure 2.1: Scatter diagrams and linear regression line through zero for four of the new photolysis rates in MATCH. Units of all axis are sec^{-1}.

lower correlation are shown as examples. For the species where an error of up to 10% might be introduced by this method, other uncertainties exist or photolysis is not the dominant loss process in the atmosphere. Methylvinylketone and methacrolein photolysis is quite slow and reaction with OH is the dominant reaction pathway in the atmosphere (approximately 6% of the loss of MACR in the standard run proceeds via photolysis). MEK photolysis can only be regarded as an approximation, since this species also represent other ketones from higher alkanes.

For three species, PAN, acetone (CH_3COCH_3) and methylglyoxal (CH_3COCHO, MGLY) the best correlation was judged from scatter plots to be not sufficiently accurate, so that these species were parameterized using the method of *Landgraf and Crutzen* (1998). Additional polynomial fits were needed for these species to account for a temperature or pressure dependence of the cross section data (PAN) or the quantum yields (MGLY and CH_3COCH_3), which is probably the reason why no satisfactory "partner" species could be found for these three compounds. The parameterization has been tested with an accurate reference radiative transfer code (DISORT, see in *Landgraf* (1998)) for low solar zenith angle conditions and found to deviate less than 5% throughout the troposphere.

2.3.3   A flexible technique for time integration of chemical differential equations

Integrating the chemical equations forward in time involves the solution of a set of stiff differential equations. In 3D chemical modeling mainly two techniques are applied, the Quasi-Steady-State-Approximation (QSSA, *Hesstvedt et al.* (1978)) and the Euler Backward Iterative (EBI, *Hertel et al.* (1993)) method (see e.g. *Kanakidou et al.* (1998) for an overview), or a parameterization of the chemistry is used (*Wang et al.* (1998a); *Levy et al.* (1999)). However, all of these methods are heavily dependent on the problem to be solved. Although they have been proven to be fast enough for 3D applications (one of the strongest constraints on a numerical method in this field, especially as chemical schemes are becoming more and more complex), their implementation requires much error-prone manual coding and considerable experience. For good performance and stability, they need manual lumping of species into strongly interacting groups. Also, the methods are not generally mass conserving.

Since a goal of this thesis was to use different chemical schemes (see Chapter 5), a general solving method, which allows flexible changing of the chemical mechanism, is clearly advantageous. Therefore it was decided to use a new method based on a fast general differential equation solver and a preprocessor that provides the basic mathematical routines needed. The solver chosen is a linearly-implicit 2-stage Rosenbrock method called **ROS2** (*Verwer et al.* (1997, 1999)). Implicitness here means that the solution for the next time step (or approximations thereof) are involved in the algorithm, in this case in a linear way. For a general overview of time integration methods in air pollution modeling the reader is referred to *Verwer et al.* (1998). In an extensive intercomparison of numerical methods it was found by *Sandu et al.* (1997a,b) that Rosenbrock methods performed best for the low accuracies (2-3 digits) required in 3D chemistry modeling. It was even concluded that Rosenbrock methods are probably close to optimal for the atmospheric chemistry problem. ROS2 is the simplest and fastest of this group of methods and has been found to be a promising candidate for application in air quality models, since it exhibited a more stable behavior at large step sizes than the higher order Rosenbrock methods.

The procedure to calculate a new vector of concentrations $C_{t+\Delta t}$ over a time step Δt is as

follows:

$$C_{t+\Delta t} \;=\; C_t + \frac{3}{2}\Delta t\, k_1 + \frac{1}{2}\Delta t\, k_2\,, \tag{2.2}$$

$$(I - \gamma\Delta t A)\, k_1 \;=\; f(C_t)\,, \tag{2.3}$$

$$(I - \gamma\Delta t A)\, k_2 \;=\; f(C_t + \Delta t\, k_1) - 2k_1\,. \tag{2.4}$$

Here the function f is the sum of production and loss terms for each species, $A = f'$ is the Jacobian matrix of the system, I is the unitary matrix, and the parameter $\gamma = 1 + 1/\sqrt{2}$ follows from the theory of Rosenbrock methods and stability considerations. Thus, solving this system basically requires computing the Jacobian A and solving two linear systems. The latter involves a matrix factorization (LU decomposition) and two forward-backward substitutions (back-solves).

Code for these mathematical procedures, also exploiting the sparsity[5] of the Jacobian, is produced by a symbolic preprocessor **KPP** (Kinetic PreProcessor, *Damian-Iordache* (1996)) directly from specified reaction tables and a species list, resembling Tables 2.1 and A.1, but obeying a certain syntax. This is an enormous help in the implementation of new chemistry schemes. Furthermore, the LU decomposition, which requires a large part of the computer time, can be rewritten in a way that avoids indirect addressing to further speed up the calculations (*E. Spee*, pers. comm., 1998). Additional processing scripts have been written that practically automate the conversion from the reaction table all the way to the fully vectorizable[6] 3D implementation in MATCH.

These technical steps are mentioned here, because each of them (fast solver capable of large step sizes, sparse matrix treatment, direct addressing, vectorization) was an essential prerequisite to yield an acceptable computational efficiency of the method. A few more additions were necessary to ensure its accuracy, as discussed below. Each step was tested carefully, and some tests are discussed in Appendix B.

O^1D concentration are usually adjusted to photochemical equilibrium within less that a microsecond, and therefore this species is set to its steady state ($[O^1D] = k_1[O_3]/(k_2[O_2] + k_3[N_2] + k_4[H_2O])$, numbering as in Table A.1) prior to the integrations in order to remove some stiffness from the system of ordinary differential equations. ROS2 is absolutely mass conserving due to the use of the exact Jacobian. It is, however, not strictly positive and thus, when negatives are produced and are subsequently set back to zero, mass is produced. Testing in the 3D framework of MATCH revealed that using the full 30 minute model time step resulted in occasional negatives leading to an insufficient accuracy and sometimes instabilities.

Thus, an additional technique is applied with ROS2 in MATCH. The time steps are asymmetrically subdivided in sub-steps. Through testing it was found that the surface layer and the planetary boundary layer were the main origin of the inaccuracies, so that more sub-steps are required there. Through numerous box model tests and also some 3D tests (see Appendix B), but without a strict optimization procedure, suitable intervals were determined for 2 to 5 sub-steps and are listed in Table 2.3.

The idea behind the sub-steps is that through the operator splitting in MATCH at the beginning of the chemical integration stiff transients exist in the chemistry. Some strongly interacting

---

[5]Many elements in the Jacobian matrix are zero, since not all species react with each other. Thus, many operations can be avoided if this is taken into account. The technique employed here is described in *Sandu et al.* (1996).

[6]Vectorization is a technical feature of many current super-computers (vector computers, e.g. CRAY-C90, NEC-SX 4/5), by which computations of an inner loop are performed at a much higher speed.

species may be far from a more slowly changing state ("equilibrium"), which poses a difficulty for any general ordinary differential equation solver. The first small step is designed to deal with these initial transients and allows the faster reactions in the system to get closer to the chemical equilibrium. The solver is then able to take larger step sizes with sufficient accuracy. One can also regard the method of predefined sub-stepping as the substitute of an internal step size control, which many solvers include, but which are also much more computationally costly.

Table 2.3: Asymmetric sub-steps for use with ROS2 in the context of operator splitting.

No. of sub-steps	Fractions of the full time step
2	0.2, 0.8
3	0.04, 0.35, 0.61
4	0.03, 0.20, 0.35, 0.42
5	0.02, 0.12, 0.22, 0.30, 0.34

Since vectorization in MATCH is realized along the longitudes, it is easily possible to choose different numbers of sub-steps for each level and longitude. It was tested that 2,3, and 5 sub-steps for the free troposphere, PBL and the surface layer, respectively, result in deviations in all species of less than 0.5%, unless the concentration of the species are very low (e.g. OH in the polar night). A more thorough optimization of the sub-steps, e.g. based on NO_x levels and/or photolysis rates, is probably achievable, but has not been attempted. With these sub-steps it has been found that negatives occurred only occasionally; mostly within the NOX family, but with values less than 1% of the total NO_y. In order to ensure a strict conservation of NO_y the small mass difference caused by setting negatives to zero all NO_y are multiplied with a scaling factor (slightly smaller than one) after the chemical integration so that NO_y from before the chemistry is reproduced in each grid cell.

When a good approximation of the turnover of each reaction is also desired for the sake of a closed budget (see Chapter 2.3.7), more sub-steps are needed. Thus, in this study values of 3, 4, and 8 (=2×4) sub-steps were used for the three regimes, respectively. It should be noted that the situation can be different if new compound groups, e.g. halogens or aqueous phase chemistry, are introduced or the method is extended into the stratosphere. This would again require reevaluating the necessary number of sub-steps and full testing of the procedure.

All direct sources are treated as constant terms in the chemical integration within the ROS2 solver. This has the advantage of further reducing numerical instabilities at the beginning of the time step (see Appendix B). Another advantage is that species which are only transported in a family, like NO in the NOX-family, can be emitted as the individual species, whereas when emissions are treated in a separate operator, one then needs to emit the whole group, increasing each family member by the same percentage. Surface sources are usually emitted into the lowest grid box (with about 80m height), with the exception of isoprene which is emitted evenly within the PBL.

2.3.4   Dry Deposition

Dry deposition, i.e. the transport of trace gases and particles to the earth's surface, is an important loss process for many reactive and soluble trace gases. The flux of a gas to the surface is commonly expressed as the product of a deposition velocity and the concentration of the gas in

air[7]:

$$F = -V_d C_a \,.$$

In most global models dry deposition is calculated by specifying mean deposition velocities for each species and broad surface categories (e.g. land, ocean, ice). In MATCH a more elaborate approach is used. Previous versions of the model employed globally distributed values for O_3, HNO_3 and NO_x and constant land/sea velocities for the other species were used. This has now been replaced by an online computation.

The deposition velocity of a species i is calculated using an analogy to Ohm's law in electrical circuits:

$$V_d^i = (R_a + R_b^i + R_c^i)^{-1} \,, \tag{2.5}$$

where R_a is the aerodynamic resistance, which is the same for all gases, R_b^i is the quasi-laminar sub-layer resistance, and R_c^i is the total surface resistance of the gas. The latter resistance encompasses several separate deposition pathways, depending on the surface type. In MATCH we have adopted the formulation of such a resistance model by *Ganzeveld and Lelieveld* (1995) and *Ganzeveld et al.* (1998), along with formulas given by *Wesely* (1989) to calculate resistances for species other than O_3 and NO_x, based on their solubility (see Table 2.4) and a reactivity coefficient. Very little is known from direct measurement about the deposition process of species other than O_3, SO_2 and NO, so that the relations by *Wesely* (1989) are currently the only consistent way to parameterize the dry deposition of these species.

More details on the implementation of the dry deposition formulation can be found in Appendix A.2. They are probably not of immediate interest to the general reader, but nevertheless important to document. However, one point requires mentioning here: After completion of the high resolution run of this thesis (presented in Chapter 3) it has been noticed that a very high (>0.8) wet skin fraction[8] is calculated for the Amazon basin during the wet season (about December to May). This is probably due to an inconsistency of an input data field taken from the ECHAM model (namely the "skin reservoir content"), which is not calculated online in MATCH and the leaf area index (LAI) distribution assumed in the code to calculate the wet skin fraction from these fields (see *DKRZ* (1993)). The effect of the inconsistency is that the deposition of insoluble, but reactive gases (mainly O_3, but also PAN) can be significantly reduced over the wetted canopies. This is because it has been assumed by *Ganzeveld and Lelieveld* (1995) that stomatal uptake stops and cuticular uptake is that for a water surface in the wetted fraction of the canopy. The other runs in this thesis have been (re)done with the consistent LAI in this subroutine, which nevertheless results in wet skin fractions up to about 0.5. The effect of the error in the high resolution run can be estimated from a pair of lower resolution run and is discussed where appropriate in Chapter 3.

With the corrected parameters the maximum daytime deposition velocity of O_3 over the Amazon in January is about 2 cm/s and the diurnal average 1 cm/s. Since the uptake of O_3 on thin surface films can even be enhanced (*Wesely and Hicks* (2000) state a range from mild

---

[7]It should be noted that the use of a *transfer velocity*, which couples the flux of the gas to the concentration **difference** between the surface and the atmposphere, would be more valid. The concept of a deposition velocity basically assumes that the concentration within the surface is zero. This shows that the concept is questionable for substances that are emitted from the surface. However for a more accurate approach it would be necessary to couple emission and deposition – a complexity which cannot be justified in view of the current uncertainties of the emissions distributions and strengths.

[8]The fraction of vegetation or soil in a grid cell that is covered with water from rain, fog or dew.

Table 2.4: Annual average dry deposition rates in MATCH over land, ocean and sea ice in cm/s and solubility parameters used in the dry and wet deposition parameterization. Note that the land category includes land ice and snow covered regions.

Species	V_d [cm/s]		H_{298}[a]	$-\Delta H/R$	References
	Land	Ocean	[mol/l/atm]		
O_3	0.26	0.05	—	—	—
CO[b]	0.02	0.0	—	—	—
H_2O_2	0.9	1.0	$7.4 \cdot 10^4$	6615	*Lind and Kok* (1986)
NOX[c]	0.09	0.08	—	—	—
HNO_3[d]	2.0	1.0	$2.1 \cdot 10^5$	8700	*Schwartz and White* (1981)
CH_3O_2H	0.18	0.35	$3.1 \cdot 10^2$	5200	*O'Sullivan et al.* (1996)
$HCHO$	0.36	0.9	$3.2 \cdot 10^3$	6800	*Staudinger and Roberts* (1996)
CH_3OH	0.16	0.28	$2.2 \cdot 10^2$	5200	*Snider and Dawson* (1985)
ISO_2H[e]	1.6	1.0	$1.7 \cdot 10^6$	9700	*O'Sullivan et al.* (1996)
$MACR$	0.07	0.05	$2.3 \cdot 10^1$	6550	*Iraci et al.* (1999); *Allen et al.* (1998)[f]
CH_3COCHO	0.33	0.9	$3.7 \cdot 10^3$	7500	*Betterton and Hoffmann* (1988)
CH_3CO_3H[g]	0.64	1.0	$8.4 \cdot 10^2$	5300	*O'Sullivan et al.* (1996)
PAN, MPAN	0.10	0.02	—	—	—
$ISON$[h]	0.46	0.97	$1.7 \cdot 10^4$	9200	*Treves et al.* (2000); *Shepson et al.* (1996)
CH_3COOH[i]	1.1	1.02	$4.1 \cdot 10^3$	6300	*Johnson et al.* (1996)
HACET	0.12	0.22	$1.3 \cdot 10^2$	7200	*Snider and Dawson* (1985), as i-propanol
$HCOOH$[j]	2.0	1.0	$8.9 \cdot 10^3$	6100	*Johnson et al.* (1996)
NACA	0.1	0.05	$1.3 \cdot 10^1$	5700	as CH_3CHO
RO_2H[k]	0.14	0.4	$3.4 \cdot 10^2$	5700	*O'Sullivan et al.* (1996), as C_2H_5OOH
CH_3CHO	0.07	0.03	$1.3 \cdot 10^1$	5700	*Staudinger and Roberts* (1996)
CH_3COCH_3	0.08	0.05	$3.0 \cdot 10^1$	4600	*Staudinger and Roberts* (1996)
MEK	0.07	0.04	$2.1 \cdot 10^1$	5000	*Staudinger and Roberts* (1996)
ONIT	0.01	0.0	$1.0 \cdot 10^0$	5800	*Kames and Schurath* (1992), as 1-butylnitrate

[a] temperature dependence: $H(T) = H_{298}e^{-\Delta H/R(1/T - 1/298)}$

[b] Calculated from a soil resistance of 2000 s/m (see Appendix A.2)

[c] Numbers given are effective deposition velocities for the NOX-family (=$NO+NO_2+NO_3+2N_2O_5+HNO_4$).

[d] The effective Henry's Law constant is used: $H_{eff} = H + (1 + K_A/[H^+])$, $K_A = 15.1$, $[H^+] = 10^{-5}$ (i.e. pH=5).

[e] Assumed values for methylhydroxyhydroperoxide ($OHCH_2O_2H$). Same values assumed for $MACRO_2H$.

[f] An average value for methyl-vinyl-ketone and metacrolein of *Iraci et al.* (1999) is used with T-dependence of *Allen et al.* (1998).

[g] H_{eff} used, K_A assumed same as CH_3COOH.

[h] Used value for 5-nitroxy-2-butanol (*Treves et al.* (2000)) and T-dependence of 1-nitroxy-2-butanol (*Shepson et al.* (1996)).

[i] H_{eff} used, $K_A = 1.74 \cdot 10^{-5}$ (*Lide* (1999)).

[j] H_{eff} used; $K_A = 1.78 \cdot 10^{-4}$ (*Lide* (1999)).

[k] Same values used for all hydroperoxides except for the hydroxyhydroperoxides from isoprene (ISO_2H + $MACRO_2H$).

hindering to significant enhancement), it may be more valid to omit the effect of the wet skin fraction for this trace gas. If this is done the maximum and average values increase to 2.8 and 1.3 cm/s, respectively. *Fan et al.* (1990) found maximum dry deposition velocities of 2-2.5 cm/s during a relatively dry period in the wet season (April-May) in the Amazonas basin. Which assumption for the wet skin fraction is more representative cannot be decided based on these limited measurement.

It is noted that an error could already be introduced by the use of monthly mean fields as input parameters. When e.g. dew formation (predominantly during night) and efficient stomatal conductance (during day) are anti-correlated, this will result in an underestimation of the 24h-averaged dry deposition of ozone. The situation is further complicated since rain and dew actually appear to have different impacts on dry deposition of O_3 (*Wesely* (1989) and references therein), but are not separated in the current scheme. Further research is need to clarify these effects.

The annual average deposition velocities, calculated over land and ocean are listed in Table 2.4. There is reasonable agreement with the averages shown in *Lawrence et al.* (1999b), which where based on basically the same deposition scheme, but on monthly averaged deposition velocity fields from the ECHAM model (*Ganzeveld and Lelieveld* (1995)) or specified representative constants. Some deposition velocities over oceans are significantly higher than in *Lawrence et al.* (1999b) or other studies (e.g. *Brasseur et al.* (1998)). These values are strongly influenced by the southern high latitude oceanic regions, where strong wind speeds result in a high surface roughness and thus a low aerodynamic resistance, which combined with low temperatures and thus increased solubility result in a high deposition velocity. The correctness and extent of this behavior is not known; however, it is probably not of large importance for the overall model results.

2.3.5 Wet Deposition and Cloud Gravitational Settling

The method of calculating the uptake of soluble trace gases into water droplets and ice crystals in MATCH has been described by *Lawrence and Crutzen* (1998) and *Crutzen and Lawrence* (2000). The process can be subdivided into two aspects: 1) precipitation scavenging, i.e. uptake of gases in particles with large fall velocities ("precipitate") and 2) uptake and gravitational settling of smaller (non-precipitating) cloud particles, with subsequent evaporation in lower layers. If the precipitate reaches the ground, one usually refers to this process as "wet deposition".

For both aspects the partitioning of a species into the gas and condensed phase is calculated assuming equilibrium between the phases and applying Henry's Law. The Henry's law coefficients (H) used are listed in Table 2.4. For acidic substances the dissociation in the aqueous phase is taken into account using an effective Henry's law coefficient (see footnotes in Table 2.4). Wet deposition is only considered for species with a Henry's law constant larger than 10^2 mol/l/atm. *Crutzen and Lawrence* (2000) have calculated for test species with surface sources and $H=10^3, 10^4$ and 10^5 mol/l/atm, that wet deposition reduces the concentrations in the middle and upper troposphere by roughly 20%, 60% and 90%, respectively, compared to an insoluble tracer.

Although PAN itself is fairly insoluble (*Kames et al.* (1991)), observed reduction of PAN in a polluted fog episode off the coast of the North-Eastern United States has been tentatively attributed to hydrolysis of the peroxyacetyl radical CH_3CO_3 (PA), the precursor radical of PAN (*Roberts et al.* (1996); *Villalta et al.* (1996)). However, it was judged by *Jacob* (2000) that the 24-h averaged effect of this is probably negligible. Nevertheless, hydrolysis of PA might help to explain the relatively high dry deposition velocity (roughly one third that of O_3, see *Wesely and*

Hicks (2000) and references therein) inferred for PAN despite its insolubility.

Uptake on ice surfaces is more difficult to estimate, and laboratory studies have only been found for H_2O_2 and HNO_3. Therefore in this study only uptake of those two gases on ice crystals is considered. For H_2O_2, *Conklin et al.* (1993) found a relationship between uptake on ice and water, which is used here to express uptake on ice through Henry's law as well:

$$H_{ice,H_2O_2} \cong 0.002 \cdot H_{water,H_2O_2} \,. \tag{2.6}$$

Laboratory studies of HNO_3 uptake on ice have generally indicated efficient uptake of one monolayer (*Abbatt* (1997); *Zondlo et al.* (1997); *Arora et al.* (1999)), which is sufficient for complete transfer from the gas phase. Additionally, *Iribarne and Pyshnov* (1990) have concluded from laboratory experiments that no significant change in the concentration of HNO_3 and H_2O_2 occurred upon freezing of super-cooled droplets, implying that all the trace gas in the aqueous phase is retained in the ice. However, *Meilinger et al.* (1999) deduced from measurement taken at high latitude near the tropopause that HNO_3 uptake on cirrus particles was not very efficient (less than 1% of a monolayer), and that most HNO_3 likely existed in ternary solution droplets and the gas phase. Until a better understanding of these processes is achieved it has been chosen to use the same approach as for H_2O_2 (Equation 2.6), which basically means highly effective uptake of HNO_3 on ice particles.

In MATCH the trace gases in the particles, both precipitate and small cloud particles, are followed through the model column, and at each level the amounts of the trace gases released or taken up are computed from the cloud water content and the evaporation or formation rate of precipitation.

It is pointed out that the scavenging of highly soluble species (mainly HNO_3) in MATCH is probably an upper limit estimate for two reasons. Firstly, due to the assumption of phase equilibrium, which basically implies instantaneous uptake (or release) and neglects limitations due to turbulent and molecular diffusion to the surface of the particles and the details of the uptake kinetics at the gas-water interface. Secondly, the model cannot remember which part of a grid cell has been cloudy during the last time step and should thus contain a reduced concentration of the trace gas. The model spreads the remaining amount of the tracer evenly in each grid cell during a time step and thus assumes rapid exchange of air between cloud free and cloudy portions of the grid cells. The trace gas can then be efficiently removed from the cloudy fraction of the grid box during the next time step. This problem is, to the best of the authors knowledge, not dealt with in more detail in any global scale model so far. There are more details in the process of precipitation that are not easily parameterized in a global model (see e.g. *Wurzler* (1998); *Lawrence and Crutzen* (1998)). For now it has to be kept in mind that wet deposition of highly soluble trace gases is an uncertain factor in global scale modeling.

The second scavenging process, cloud gravitational settling, is neglected in most other global models so far, but was found by *Lawrence and Crutzen* (1998) to have significant impact on the key soluble trace gases HNO_3 and H_2O_2. Their standard case (STDFALL) is also used in this study, though a lower uptake of HNO_3 (based on Equation 2.6) is used here. The process is implemented in a mass conserving way and thus only redistributes the trace gases vertically. All substances are released back to the gas phase at the end of the time step and final removal from the atmosphere can only occur through wet and dry deposition or chemical reactions. Since wet deposition is, however, more efficient at lower altitudes, this downward redistribution leads to an

overall enhancement of wet deposition.

2.3.6   Emissions and Boundary Conditions

Emissions of 16 trace gases of anthropogenic and natural origin are presently taken into account in the model. The source distribution and annual totals are discussed in this section with special focus on new distributions compared to the work of *Lawrence et al.* (1999b). Also, some indication of the degree of uncertainty associated with the estimates will be given. The annual mean total NO_x emissions, which will be discussed first, are summarized in Table 2.5. Emissions of CO, CH_4, and other non-methane volatile organic compounds will be dealt with after that.

Table 2.5: Tropospheric sources of NO_x in MATCH and estimated range.

Source	Magnitude [Tg(N)/yr]	Range[a] [Tg(N)/yr]
Industrial	24.1^b	16–30
Biomass burning	7.8^c	4–16
Soils	5.5	1.2–10
Lightning	4.9	2–16
Aircraft	0.45	0.5–0.6
Stratosphere	0.1^d	0.08–1
NH_3 oxidation	—	$0.3–3^e$
Oceans	—	<1
Total	42.85	

[a] From *Bradshaw et al.* (2000).
[b] Including 2.6 Tg(N)/yr from ocean going ships; excluding biofuel burning and waste treatment.
[c] including biofuel burning and agricultural waste buring.
[d] Plus 0.3 Tg(N)/yr in the form of HNO_3.
[e] *Lee et al.* (1997) give a range of 0–1.6 Tg(N)/yr.

NO_x Emissions

Industrial NO_x Emissions   The predominant source of nitrogen oxides (NO_x) is from the combustion of fossil fuels. The industrial NO_x emissions are taken from the EDGAR database Version 2.0 (*Olivier et al.* (1996)), which are provided on a $1°×1°$ resolution. The categories "biofuel burning" and "waste treatment" are omitted from the EDGAR NO_x emissions, since these categories are instead included in the biomass burning dataset applied in this work (see below).

Recently emissions from ocean-going ships have gained increasing interest (*Corbett and Fischbeck* (1997); *Lawrence and Crutzen* (1999); *Corbett et al.* (1999); *Kasibhatla et al.* (2000)). The study of *Corbett et al.* (1999) indicated that the emissions from ships may have been underestimated in global models of tropospheric chemistry. However, evidence of elevated NO_x concentrations in the North Atlantic could not be found in two potentially influenced ocean regions (*Kasibhatla et al.* (2000)) and it is speculated that this may be caused by processes occurring in the ship plumes as they mix out in the background atmosphere. Here, we use the distribution from *Corbett et al.* (1999) scaled to a total emission strength of 2.6 Tg(N)/yr, which

is the revised total for 1990 of the EDGAR dataset (*J. Olivier*, as cited by *Lawrence and Crutzen* (1999)). The Corbett et al. *(1999)* data are based on reported ship positions aggregated on a $2° \times 2°$ grid. The annual total used in this work is slightly lower than the estimated range of 2.66–4.00 Tg(N)/yr in *Corbett et al.* (1999), but can still be justified considering the uncertainty in the associated effects of the emissions. Since the *Corbett et al.* (1999) distributions are based on actual ship positions they are more spread out than the corresponding EDGAR data, in which emission are extremely well confined to the main shipping routes (see *Lawrence and Crutzen* (1999)).

The resulting annual mean total NO_x source from industrial activities is shown in Figure 2.2a. Note that no seasonal or diurnal dependence is assumed for any of the industrial emissions, except for the ship emission data (updated monthly). However, the latter only show a slight variation with time.

Biomass Burning NO_x Emissions   Large amounts of NO_x are also produced from the burning of biomass (e.g. *Crutzen and Andreae* (1990); *Andreae* (1991)). While fires can be started through lightning discharges, today the dominant part of fires must be attributed to human activities (*Delmas et al.* (1997)), especially in tropical and subtropical regions. The biomass burning emissions have been updated from the *Hao et al.* (1990) and *Hao and Liu* (1994) data, used in previous studies with MATCH. The current temporal and spatial emissions pattern is based on the work of *Galanter et al.* (2000), who constructed updated NO_x and CO emission datasets by modifying preliminary unpublished compilations of *J. Logan* (see *Galanter et al.* (2000) and references therein). These authors partitioned the burning sources into six types of biomass (forest, savanna, fuelwood, agricultural residues, domestic crop residues and dried animal waste (dung)) and estimated the timing of the first three fire types for 20 different regions, whereas the latter three sources are constant throughout the year. The annual mean source strength is plotted in Figure 2.2b. The new dataset now also includes extratropical burning not covered by *Hao and Liu* (1994), mainly fires in North America and Asia in summer, but also in the part of South America south of 30°S and in Australia. The most notable difference to the *Hao and Liu* (1994) data is that the new dataset shows a much less pronounced burning activity in the peak burning season (August, September, and October) in South Africa and South America, with maximum emissions up to a factor of 4 lower than the old dataset. Another advantage of the new dataset is the availability of individual fuel types, which can be used to apply specific emission factors per fuel type for NMVOCs emitted from biomass burning (see below).

Biogenic Soil NO_x Emissions   Soil bacteria are a significant source of nitrogen oxides to the atmosphere. Although this is a natural process it should be noted that it is often manipulated by man through changes in land use and the use of fertilizer (e.g. *Sanhueza* (1997)). This emission source remained unchanged from the previous version of MATCH and the annual total and monthly updated distributions are taken from *Yienger and Levy* (1995) (obtained via the Global Emissions Inventory Activity (GEIA) database), whose emissions are, however, a factor of 2 lower than estimates from a recent review by *Davidson and Kingerlee* (1997). The annual mean distribution is shown in Figure 2.2c. Note that the so-called "*pulsing*" of emissions after wetting of a dry soil is not treated as a time resolved process, but included in the monthly mean emission rates. However, we believe that a larger uncertainty in modeling this process is due

to the assumed total strength of soil emissions and due to the recapture of nitrogen containing compounds within the plant canopy of vegetated areas (e.g. *Jacob and Wofsy* (1990)). This effect can occur though uptake of NO_2 through the leaf stomata[9] (e.g. *Hanson and Lindenberg* (1991)). NO_2 can be formed within the canopy from the reaction of freshly released NO with ozone, but also by reactions with peroxy radicals from the oxidation of hydrocarbons emitted by the plants. In the latter reactions soluble nitrates could also be formed (see Chapter 5), which are likely to deposit even more efficiently to the leaf surfaces than NO_2. Thus, canopy recapture is a critical issue for future research efforts in this field (*Matson* (1997)). *Yienger and Levy* (1995) do account for the canopy reduction effect, but do not include the influence of varying NO to NO_2 conversion rates due to varying amounts and composition of hydrocarbons. Deposition of nitrates is also not considered. A revised treatment of biogenic soil emissions in global models should couple in a multilayer canopy model to account for the chemical conversion and deposition processes within the plant foliage (e.g. *Ganzeveld* (2001)).
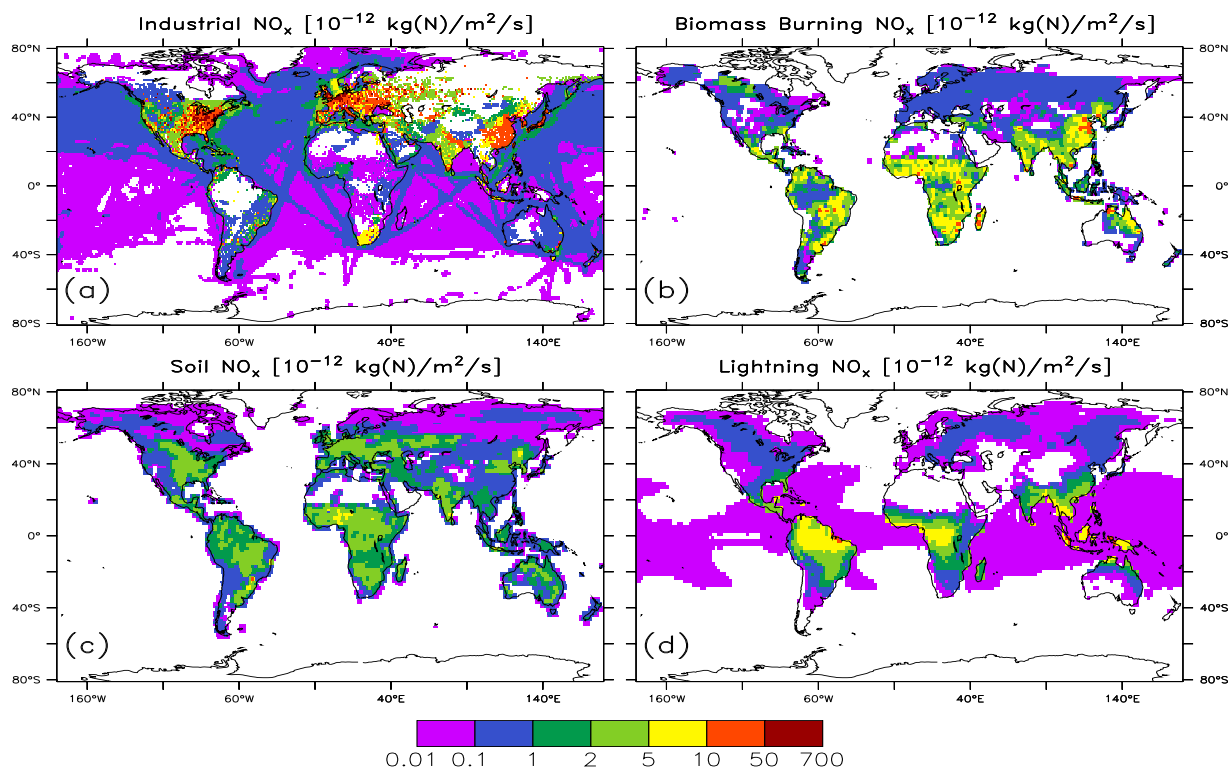
Figure 2.2: Annual mean NO_x emissions in units of 10^{12}kg(N)/m^2/s applied in MATCH from (a) industrial processes, (b) biomass burning, (c) soils, and (d) lightning.

Lightning NO_x NO formation from lightning discharges constitute a significant contribution to the NO_x budget of the free troposphere and is even a dominant source in parts of the tropics (*Kraus et al.* (1996); *Levy et al.* (1999)). It has also been suggested that lightning could mediate a positive climate feedback mechanism, potentially further increasing the climate forcing by influencing tropospheric ozone (*Toumi et al.* (1996); *Sinha and Toumi* (1997)). The estimated magnitude of the NO_x source from lightning is still fairly uncertain. The review based estimated

---

[9]The openings in the epidermis of a plant organ (such as a leaf) through which gaseous interchange takes place.
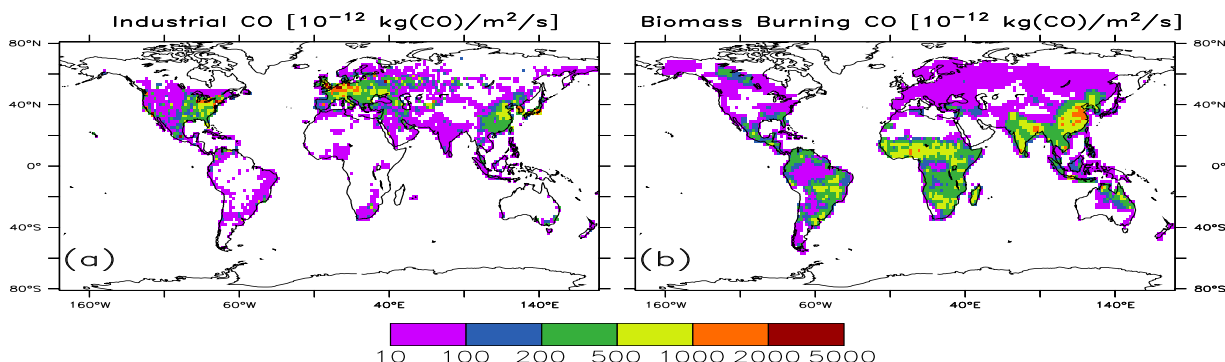
Figure 2.3: Annual mean CO emissions in units of 10^{12}kg(CO)/m^2/s in MATCH from (a) industrial processes, and (b) biomass burning.

range of $1 - 8$ Tg(N)/yr given by *Lawrence et al.* (1995) is still spanned by results from recent studies (*Nesbitt et al.* (2000): 0.9 Tg(N)/yr; *Price et al.* (1997a,b): 12 Tg(N)/yr). Here, a total figure of 5 Tg(N)/yr is used. The distribution of NO emitted is calculated each time step using the algorithm of *Price and Rind* (1992), along with corrections given in *Price and Rind* (1994). This algorithm couples the flash rate to the cloud top height diagnosed by the convection scheme, only differentiating between continental and marine thunderstorms. From the flash rates, which averages to about 60 flashes/s globally in the standard simulation, the amount of NO produced is calculated from a conversion factor of $1 \cdot 10^{26}$ molecules/flash. Note that no difference in this factor is made between cloud-to-ground and intra-cloud flashes at this point. The nitrogen emission is then emitted with a density weighted profile in the column below the cloud top (for more details see *Lawrence* (1996)). The annual mean distribution is depicted in Figure 2.5d, clearly showing the much lower emission rates over the oceans implied by the parameterization. Improvements on this simple parameterization can be expected when algorithms are developed that make use of recently available satellite data (e.g. *Nesbitt et al.* (2000)).

Other NO$_x$ Sources   Aircraft emissions of NO$_x$ are also included in MATCH. The distribution and annual total is taken from the Upper Atmospheric Database Project NASA study (*Baughcum et al.* (1994)). The distribution shows the strongest emissions over North America and Europe and in the connecting North Atlantic flight corridor maximizing in $10 - 12$ km altitude. Details can be found in *Lawrence* (1996). A small input of NO$_x$ into the troposphere is also through influx from the stratosphere, which is, however, significant to the upper troposphere (*Kraus et al.* (1996)).

Other possible sources of reactive nitrogen to the atmosphere could be through the oxidation of ammonia (NH$_3$; e.g. *Crutzen* (1974)) and through nitrite photolysis in seawater with subsequent release of NO to the atmosphere. However, these sources are still very uncertain and a net source term of zero is within the range of uncertainty. It has thus been omitted in the model (for a more detailed discussion see *Lee et al.* (1997); *Bradshaw et al.* (2000) and references therein). NO was also found to be emitted by several higher plants (*Wildt et al.* (1997)), but the global extrapolation results in only 0.23 Tg(NO)/yr. Recently, release of light alkyl nitrates (namely methyl and ethyl nitrate) from the southern arctic oceans has been discussed as a potential source of nitrogen to this region (*Jones et al.* (1999)); however, more evidence is needed to confirm these findings. The effect will also be very likely confined to this remote region, which is probably not

important to the average oxidation power of the global atmosphere.

Carbon Monoxide (CO) Emissions

Direct emissions of carbon monoxide by industrial processes, biomass burning and biogenic activity (both soils and oceans) are accounted for in the model, totaling to 1261 Tg(CO)/yr (summarized in Table 2.6). In addition to these primary sources roughly the same amount of CO comes from the oxidation of VOCs in the atmosphere. The total amount formed from CH_4 and NMVOCs in the standard run is about 1300 Tg(CO)/yr. More details on the calculated CO budget will be discussed in Chapter 4. All source magnitudes chosen for this study are within the range of values used in other global modeling studies, as reported by *Kanakidou et al.* (1999).

The distribution of technological sources is taken from the EDGAR database (*Olivier et al.* (1996, 1999)). The annual total is depicted in Figure 2.3a. The emissions from biofuel and waste burning are again excluded and taken from the biomass burning distribution instead. The total of 297 Tg(CO)/yr in the EDGAR data has been increased to 400 Tg(CO)/yr to get better agreement at several remote long term measuring stations in the northern hemisphere. A higher source in the Northern Hemisphere has also been suggested by *Bergamaschi et al.* (2000a,b), based on an inverse modeling study. It should also be noted that these extra emissions could also account for CO produced from the oxidation of some industrially emitted NMVOC not explicitly accounted for in our chemical scheme (e.g. higher alkenes, aromatic compounds, higher alcohols, esters).

The monthly distribution and total source strength of biomass burning is taken from *Galanter et al.* (2000). The annual mean distribution of the biomass burning CO source is shown in Figure 2.3b. The emissions are dominated by industrial processes in most of the Northern Hemisphere, whereas biomass burning dominates in the Southern Hemisphere. A notable exception is in East Asia where biomass burning is also a large source of CO.

Emissions from the ocean are based on the study of *Bates et al.* (1995), who derived CO fluxes to the atmosphere based on measurements of CO concentrations in sea water from several cruises in the Pacific Ocean, the temperature dependent solubility of CO, and surface wind speed data. Their estimates are given for four seasons and as zonal means, which we have interpolated to monthly mean values on the model grid. The extrapolated total source strength of 13 Tg(CO)/yr from *Bates et al.* (1995) is considerably lower than the estimates of *Erickson* (1989) (165±80 Tg/yr), but in agreement with the recent study of *Rhee* (2000) (14±10 Tg/yr), which is based on CO measurement in seawater of the Atlantic Ocean.

Another source of carbon monoxide is the terrestrial biosphere. *Schade and Crutzen* (1999) have estimated that 50–170 Tg/yr may result from photochemical degradation of plant matter. Direct biogenic emissions from soils and vegetation are also possible (e.g. *Kirchhoff and Marinho* (1990)), but a global quantification based on available studies is difficult. The total of 100 Tg/yr assumed in this thesis is meant to also account for some CO produced from the oxidation of other biogenic compounds currently not included in MATCH. Comparing this with the proposed emissions, this estimate is probably a lower limit to the actual amount emitted or produced. The distribution has been obtained by scaling the mean of the distributions for terpenes and "other volatile organic compounds" (OVOC) from *Guenther et al.* (1995) (depicted in Figure 2.4) to the desired total in Table 2.6.

Table 2.6: Global surface emission rates applied in MATCH. Units are Tg(Species)/yr and Tg(C)/yr for first and second value, respectively.

Species	Technological	Biomass Burning	Terrestrial Biogenic	Ocean	Total Tg/yr,Tg(C)/yr
CO	400/172	748/321	100/43	13/5.6	1261/541
CH_4					571/427
HCHO	1.2/0.5	7.8/3.1	—	—	9.0/3.6
CH_3OH	2.0/0.7	14.7/5.5	60.0/22.5	—	76.7/28.7
C_2H_6	5.7/4.6	6.5/5.2	—	0.5/0.4	12.8/10.2
C_3H_8	6.6/5.4	2.0/1.7	—	0.4/0.3	9.0/7.3
CH_3COCH_3	2.0/1.2	4.2/2.6	40.0/24.8	—	46.2/28.6
CH_3CHO	—	4.7/2.5	—	—	4.7/2.5
CH_3COOH	—	14.6/5.8	3.4/1.4	—	18.0/7.2
HCOOH	—	8.0/2.1	5.6/1.5	—	13.6/3.5
C_3H_6	2.7/2.3	5.1/4.4	2.2/1.8	1.3/1.1	11.2/9.6
C_2H_4	5.7/4.9	11.4/9.8	10.0/8.6	2.2/1.9	29.3/25.1
C_4H_{10}	45.9/37.9	2.6/2.1	—	0.4/0.3	48.9/40.4
MEK	2.7/1.8	9.9/6.6	—	—	12.6/8.4
Isoprene	—	—	397/350	—	397/350
total NMVOC (without Isoprene)	—/54	—/51	—/61	—/4	—/175

Emissions of Non-Methane Volatile Organic Compounds (NMVOC)

A wide variety of volatile organic compounds (VOC) are emitted to the atmosphere from industrial processes, biomass burning and biological activity. Emissions of 13 compounds are explicitly taken into account in MATCH at present. Other compounds are assumed to be lost from the atmosphere through physical processes or are accounted for as CO emissions. For monoterpenes, an additional amount of acetone, a known product from the oxidation of several monoterpenes (*Reissel et al.* (1999); *Orlando et al.* (2000)) is emitted instead.

Industrial emissions of NMVOC are taken from the EDGAR database, generally keeping the specified total source strength with the following exceptions. First, emissions from the use of biofuels are again excluded here. Methanol has been emitted with the distribution of the EDGAR species category "alcohols" using a source strength of 2 Tg/yr (*Singh et al.* (2000)). For acetone (CH_3COCH_3) the distribution of ketones was used, scaled to a total of 2 Tg/yr in agreement with *Singh et al.* (2000). The remaining amount in this group of compounds is emitted as methylethylketone (MEK). Presently, no industrial emissions of acetaldehyde or carboxylic acids are included; various studies (*Glasius et al.* (2000); *Bode et al.* (1997)) indicate that direct emissions or emissions of precursors from the biosphere together with biomass burning probably constitute the dominant source of these acids to the atmosphere.

Apart from CO and NO_x many other substances are released due to the incomplete combustion of biomass. Recently, *Andreae and Merlet* (2000) have reviewed the literature on emission factors for various trace gases and aerosols from biomass burning and proposed estimates where no data was found. These emission factors have been used in this study to calculate the corresponding emission ratio to carbon monoxide (ΔNMVOC/ΔCO) for each compound and each of
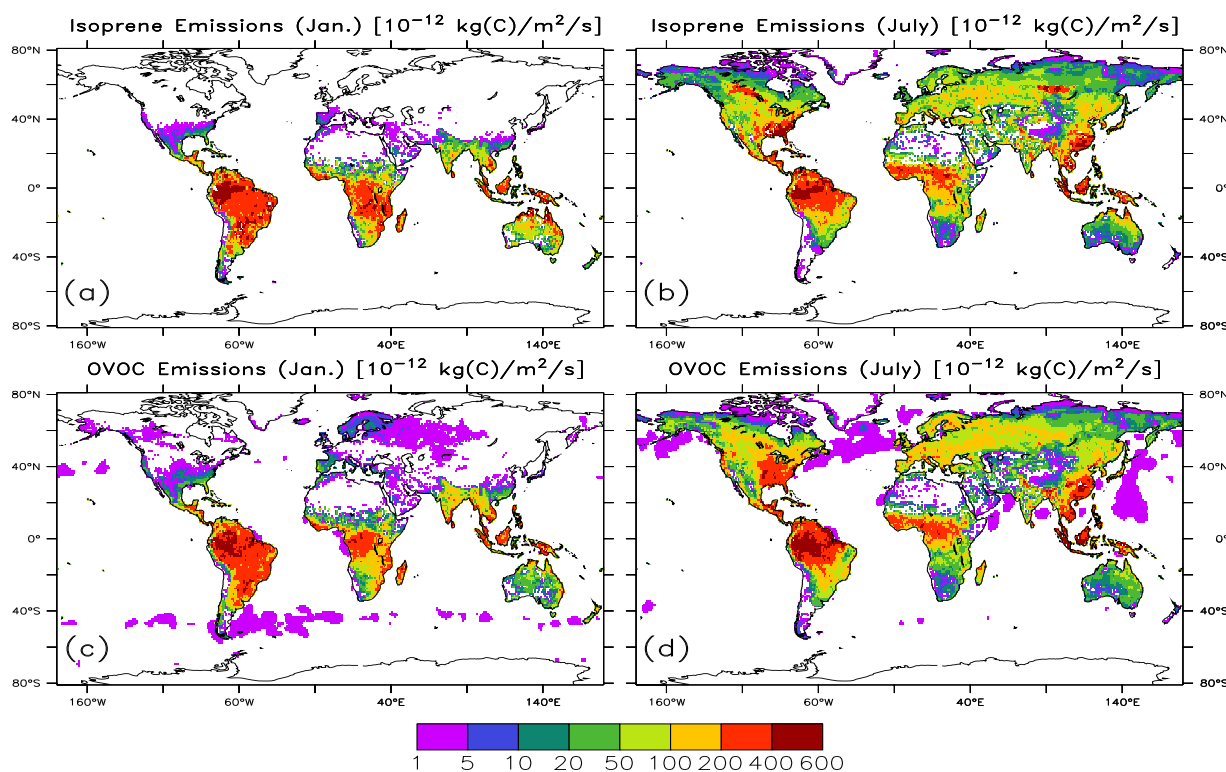
Figure 2.4: Emission distributions of isoprene and "other volatile organic compounds" (OVOC) for January and July (in 10^{12}kg(C)/m^2/s). The latter distribution is scaled to the same total as the isoprene emissions (350 Tg(C)/yr) for better comparability.

the fuel types differentiated by *Andreae and Merlet* (2000). The emission ratios were then used to convert the CO emission distribution of *Galanter et al.* (2000) to an emission distribution of the specific compound. Since *Galanter et al.* (2000) use slightly different nomenclature for fuel types, we made the following assignments: Forest poleward of 30° latitude was treated as extratropical forest, fuelwood and animal waste was assigned the emission ratios for "biofuel burning" and finally "domestic crop residues" was given the same emission ratio as for agricultural residues. Charcoal making and burning is not included in *Galanter et al.*'s data, but the emissions from this category are very small. The resulting total emission listed in Table 2.6 vary up to 30% from those calculated by *Andreae and Merlet* (2000) owing to the differences in the underlying estimates for the total biomass burned. The unpublished estimates of *J. Logan* as reported by *Lobert et al.* (1999), which are used in *Andreae and Merlet*'s study include 1970 Tg of dry matter burned from forests, whereas *Galanter et al.* (2000) use 2821 Tg. The total amount of biomass burned as biofuel is much higher (1950 Tg) in the former study, versus 838 Tg in the latter. These discrepancies may be taken as an indication of the degree of uncertainty associated with biomass burning estimates at present.

Biogenic NMVOC Emissions Knowledge of the global biogenic emissions of compounds (other than methane, isoprene, monoterpenes and dimethylsulfide) is fairly poor (*Fall* (1999)). Although emissions of many compounds have been measured for a series of plants (for a review see e.g. *Kesselmeier and Staudt* (1999)), a global extrapolation to determine a total emission strength remains highly uncertain and species-dependent emission distributions would be premature at

present. Therefore the generic distribution of *Guenther et al.* (1995) for "other volatile organic compounds" (OVOC; see Figure 2.4c and d) is used here for most compounds (not for isoprene), scaled to the specified total discussed below. Note that a small fraction ($\approx 1\%$) of the total emissions is over the oceans.

Isoprene Emissions   Isoprene (C_5H_8) is the emitted to the atmosphere in larger amounts than any other biogenic compound (e.g. *Fall* (1999); *Kesselmeier and Staudt* (1999)). From the large group of compounds that have been identified as being of biogenic origin, it is isoprene for which we probably have the best knowledge on formation mechanism within the plant, and thus the dependence of the emission on ambient conditions, for various plant species. Emission fluxes measured for isoprene are found to be mainly determined by light intensity and leaf tempera- ture, increasing with an increase of these parameters. While the dependence on light becomes saturated at higher light intensities, a decrease can be observed for leaf temperatures higher than about $40°C$ (*Guenther et al.* (1993)). Emission fluxes from plant species from a wide variety of ecosystems have been measured, but still extrapolation to all plant species and all ecosystems is associated with a large uncertainty, with potentially even larger errors for certain regions. A global inventory of emission from the biosphere has been developed by *Guenther et al.* (1995), arriving at a total of 503 Tg(C)/yr in the form of isoprene. These authors also state an uncer- tainty level of "a factor of 3 or higher" for this estimate. Their distribution, which was obtained as monthly averages from the GEIA database, is used in the model in conjunction with a sim- ple method to account for the light dependence of the emissions: Instead of incorporating the actual emission algorithm of *Guenther et al.* (1995), their monthly updated emission fluxes were scaled with the cosine of the solar zenith angle, assuming no emissions at night. This method roughly mimics the shape of the diurnal variation of isoprene emissions found in measurements (e.g. *Lamb et al.* (1996); *Guenther et al.* (1993)). The simple approach may be justified by the large uncertainty in the total emission strength. An explicit emission algorithm in future versions of the model will require the incorporation of a vegetation database.

Emission totals used in previous modeling studies range from 175 Tg(C)/yr by *Taylor et al.* (1990) to 597 Tg(C)/yr in the study of *Wang et al.* (1998a). A value of 350 Tg(C)/yr, 30% lower than the proposed total of *Guenther et al.* (1995), is used for our standard simulation. The reduction is based on the findings of *Houweling et al.* (1998) along with own test simulations with MATCH (see also Section 3.4.3), which indicated that computed isoprene concentrations using higher emissions (400 Tg(C)/yr and 500 Tg(C)/yr, respectively) were generally higher than observed values. However, as noted by *Granier et al.* (2000), reducing the emissions globally might not improve the agreement everywhere. It is thus probable that emissions from certain ecosystem will need to be reevaluated. The model sensitivity to changing the global source strength of isoprene will be discussed in Chapter 5. The mean distributions for January and July are depicted in Figure 2.4a and b. It can be seen that in January emissions from tropical forests and savanna are clearly dominating, while the emissions in the winter midlatitudes is at very low levels. In July emissions in the forested areas of the northern midlatitude also considerable.

Differently than other surface emissions, isoprene is emitted evenly below the boundary layer height, which is diagnosed online. The approach has been chosen in order to avoid an overly strong feedback cycle of isoprene and OH in the lowest model layer and potential splitting errors associated with splitting transport and chemistry of this reactive compound. The strong emission of isoprene into a layer of just 80 meters height causes OH to be depleted to very small values,

which in turn correspond to a very long lifetime (>5 h) of this otherwise shortlived compound.

Additionally, emissions from the forest are often encountered in short gusts caused by intermittent down-sweeps from large eddies in the PBL (*Raupach and Thom* (1981); *Fitzjarrald et al.* (1988)). These phenomena cannot be modeled using local K-theory and the included counter-gradient term in the boundary layer scheme (see Section 2.2.3) is probably still an oversimplification as it is applied more constantly over time. The temporal and spatial variability of trace gas concentrations is expected to result in different averaged chemical turnover rates than calculated using the averaged concentrations. The magnitude of this effect is expressed by the so-called intensity of segregation ($I_s = \frac{\overline{A'B'}}{\overline{A} \cdot \overline{B}}$, for a reaction $A + B \rightarrow C$). Using a Large Eddy Simulation (LES) *Patton et al.* (2001) have calculated that the maximal effect of 17% is found near the canopy top for an isoprene-like tracer.

The effect of the assumption to emitting isoprene in the whole PBL was only a 20% reduction in peak isoprene concentrations near the surface and the vertical gradient was still very steep. This test also indicates that a potential splitting error from separating vertical transport and chemistry of isoprene may be of the same magnitude.

Biogenic emissions of other NMVOCs Methanol (CH_3OH) emissions from plants have been measured in magnitudes sufficient to account for more than 100 Tg/yr globally (*Guenther et al.* (1995, 2000)). Additional sources are from decaying dead plant matter (*Warneke et al.* (1999)). However, as pointed out by *Singh et al.* (2000), these sources do not seem to be balanced by known removal processes in the atmosphere (removal by OH and deposition), so that we use the lower limits of the estimates by *Singh et al.* (2000) (i.e. 50+10 Tg/yr) here.

Alkane emissions from the terrestrial biosphere are believed to be small (*Kesselmeier and Staudt* (1999)). In the case of ethane (C_2H_6) *Rudolph* (1995) states that these sources will probably contribute less than 1 Tg/yr, but also concluded that the role of the biosphere in the budget of ethane is presently not understood. Emissions of alkanes from terrestrial biogenic sources are thus neglected in this version of MATCH.

Ethene (C_2H_4) is a known volatile plant hormone and is also emitted from soils (*Rudolph* (1997); *Fall* (1999)). Upon stress emission rates of ethene can increase severalfold for hours or days, making any global extrapolation highly uncertain. The total of 10 Tg/yr used in MATCH is assumed to constitute of 3 Tg/yr from soils (based on *Sawada and Tutsuka* (1986) and *Warneck* (1988)) and 7 Tg/yr from vegetation. The propene emission strength has been determined using the ethene/propene emission ratio measured over a midlatitude forest (*Goldstein et al.* (1996)) and by assuming a no-stress emission strength for ethene of 4 Tg/yr. Obviously, these estimates have to be regarded as being highly uncertain.

Sources of acetone (CH_3COCH_3) are believed to be dominated by the biosphere (*Singh et al.* (1994, 2000) and references therein). It is produced from decaying plant matter, directly emitted by plants and formed in the oxidation of several terpenes. The total in Table 2.4 is assumed to be comprised of these three sources. The total of 40 Tg/yr is somewhat higher that the best estimate of *Singh et al.* (2000), but within the range of uncertainty.

There is also growing evidence of direct emissions of aldehydes from vegetation (see *Kesselmeier and Staudt* (1999) and references therein). However, as also pointed out by *Kesselmeier and Staudt* (1999) this is often a bidirectional exchange. No global extrapolation has been attempted to date and for now it has been chosen to omit aldehyde emissions.

Emissions of formic acid (HCOOH) are included with a source strength of 5.6 Tg/yr. 4 Tg/yr

are assumed to stem from plants (*Bode et al.* (1997): 0.5-5.6) and 1.6 from savanna soils (*Helas and Kesselmeier* (1993)). The source magnitudes of acetic acid (CH_3COOH) is also taken from the same authors: 2+1.4 Tg/yr from vegetation and soils, respectively.

All oceanic sources taken into account are emitted with the distribution of CO of *Bates et al.* (1995). There is considerable disagreement in the proposed source strengths and a discrepancy appears to exist between flux estimates derived from measurements of concentrations in sea water and in surface air, as pointed out by *Donahue and Prinn* (1990). Based upon balance requirements of the oceanic source and photochemical sinks theses authors derived much higher fluxes than calculations with a standard diffusive layer model. However, their data were not sufficient to derive any reliable global estimate. While *Bonsang et al.* (1988) gave an order of magnitude estimate of 52 Tg(C)/yr of C_2-C_6-hydrocarbons from oceans (based on measurements solely taken in the Indian Ocean), more recent estimates come up with more moderate fluxes (*Plass-Dülmer et al.* (1995): 2.1, upper limit 5.5 Tg/yr, including 1 Tg/yr of butenes; *Guenther et al.* (1995): 5 Tg(C)/yr)). The 90% upper limit estimates of *Plass-Dülmer et al.* (1995) are used in this study as a compromise between the extremes.

Fixed Boundary Conditions

Since the model extends into the stratosphere, but no appropriate representation of stratospheric chemistry is included, some species concentrations need to be set to reasonable values. For ozone and water vapor monthly zonal mean values from the HALOE project (*Russel* (1993); *Harries et al.* (1996); *Brühl et al.* (1996); *Ch. Brühl and J. U. Grooß*, personal communication, 1999) are used to adjust the model calculated distribution above pressure levels (in hPa), defined by $P_{fix} = 200 - 165\cos^2\phi$ (where ϕ is the latitude). Although MATCH calculates almost the entire hydrological cycle in the troposphere, in the stratosphere the significant source from the oxidation of CH_4 is not included, which makes the correction of stratospheric water vapor necessary. While water vapor is fixed to the HALOE data, ozone is only nudged to match the zonal means, thereby keeping the longitudinal structure calculated by the model. Note that this can subsequently influence photolysis rates in the troposphere.

The magnitude of the net stratosphere-troposphere exchange (**STE**) of the affected substances is then calculated by the model dynamics. It has been found in two studies with a previous version of MATCH (*Crutzen et al.* (1999) and *Lawrence et al.* (1999b)) that using the SPITFIRE scheme for advection with the NCEP wind fields results in very high net ozone influx from the stratosphere (1440 and 1103 Tg(O_3)/yr in the two studies, respectively, depending on the model resolution). Comparison with ozone sonde data in *Lawrence et al.* (1999b) and this study (see Section 3.7.3) have shown that this STE flux is very likely too high, and in order to get a reasonable upper tropospheric ozone distribution it was chosen to reduce this flux artificially in this study. This was done by reducing the stratospheric O_3 values by 50% before the advection routine and setting then back after that. This procedure was favored over some others recently proposed in the literature (*McLinden et al.* (2000)) due to its simplicity. Although any 'tuning' of modeled processes is undesirable and should be avoided, the focus of this work is on the tropospheric distribution of trace gases and the procedure described above can be regarded as a boundary condition to the region of focus. More details on the ozone budget in various model configurations and its evaluation with measurements will be given in Chapter 3.7. The resulting net flux into the troposphere for the standard simulation is calculated to be 543 Tg(O_3)/yr.

The upper boundary of NO_y is obtained by scaling the concentrations of NOX and HNO_3 to

yield NO_y/O_3 ratios in agreement with the observations of *Murphy et al.* (1993). The adjustment is necessary, since photochemical sources of NO_x, mainly through the decomposition of nitrous oxide (N_2O) in the stratosphere, are not included in the model. For this procedure we used the reduced stratospheric O_3 mixing ratios (as described above) so that the stratospheric input of NO_y and O_3 are consistent. Other NO_y species are not changed since their precursors are hardly available in the stratosphere.

Finally, for methane upper and lower boundaries are specified. The surface concentration are set to the monthly zonal mean values from the study of *Fung et al.* (1991). These values are used relative to the mixing ratio at the South Pole, where an annual mean value of 1700 nmol/mol (as in *Lawrence et al.* (1999b)) is specified. The approach results in a methane source of 570 $Tg(CH_4)/yr$ in the standard simulation, which is within the range of a priori error estimates used in the inverse modeling study of *Houweling et al.* (1999) (528±90 Tg/yr), but significantly higher than their a posteriori values of 505±24 Tg/yr.

The stratospheric distribution of CH_4 is set to the rule of thumb $H_2O + 2 \cdot CH_4 \approx 7$ μmol/mol at the beginning of the run and is then nudged towards it with a relaxation time of 6 months. The relationship can be derived from the HALOE data (*Ch. Brühl*, personal communication, 2000). Methane is adjusted here to obtain reasonable stratospheric OH concentrations, which influence the speciation of NO_y in the stratosphere, and thus the speciation of the stratospheric input of NO_y into the troposphere.

2.3.7 Budget Calculations in MATCH

Budget calculations are straightforward in the context of the first-order operator splitting as used in MATCH. The total mass of a tracer is simply calculated in predefined model sub-domains before and after each of the operators (processes) and the difference can be attributed to the particular process.

Budgeting chemical reactions, especially with an implicit solver, is more difficult. Here, it was attempted to simply use the initial reaction tendencies to estimate the turnover of each reaction. It was found that also taking into account the information from the first stage solution in the ROS2 solver greatly improved the accuracy. This could be checked by adding all estimated losses and sources of a species and compare the result to the implicit calculation of the solver. The tendencies before the chemical integration and at the first stage solution (calculated from k_1 and k_2 in Equations 2.2 to 2.4) are each weighted by 50% to give the total estimated turnover. This factor is not obvious from the integration formula (Equation 2.2), but is easy to see from an alternative formulation of the method (e.g. *Berkvens et al.* (2000)). Since the loss and production terms need to be calculated for the time integration anyway, the additional computer load is minimal. From the closure of the chemical budget it is estimated that the error is less than 5-10%.

It should also be noted that when tropospheric budgets are presented, these refer to the region below the tropopause as defined by the *WMO* (1992), which is diagnosed online. South of 60°S, however, where the WMO definition yields much too low tropopause pressures (similar values to the tropics) a climatological formula as in *Lawrence et al.* (1999b) is used:

$$P_{trop} = 300 - 215 \cdot \cos^2 \phi \,,$$

where P_{trop} is the tropopause pressure in hPa and ϕ is the latitude.

Chapter 3

Description and Evaluation of the Standard Simulation

In this chapter simulations with the model as described in the previous chapter are presented and extensively compared to available observations. In order to avoid a lengthy description of the tracer distributions of MATCH without the link to reality, the presentation of model results is combined with the comparison to measurements. Also, the results of sensitivity simulations, performed to elucidate certain critical aspects of the model performance, are added where appropriate.

Obviously, with 12 monthly mean 3D-distributions of 35 transported species, only a small selection of results can be presented. Also, the observational data base has increased enormously during the late 90s and only selected results of the comparisons can be shown. The main purpose of this chapter is to test the model's ability to reproduce observations of ozone, its main precursors and OH in the troposphere, and to give indications of weaknesses and strengths of the model. Simulations at two different resolutions (T63 and T21) will be presented simultaneously. The high resolution run is used as a reference here to indicate whether the coarser resolution might be the cause for potential discrepancies of the T21 run compared to the observations or if other factors are dominating. As noted in the previous chapter, however, the two runs also need to be independently evaluated against observations, due to differences in meteorological parameters such as the convective fluxes, which were calculated with different model versions. Additionally, other phenomena might occur when the non-linear system of chemistry-transport is averaged in the horizontal direction, as done for the T21 simulation.

The interpretation of the comparison of measurements at a specific point in time and space with the monthly mean output of a global 3D model is not straight forward and several potential problems have to kept in mind. The model is driven by meteorology from the year 1998, which means that for multi-year datasets the inter-annual variability has to be taken into account. 1998 was an El-Niño year, which could lead to additional differences for some regions with campaigns in La-Niña or transition periods. Measurements in remote ocean regions and in the free troposphere are often only available from single measurement campaigns which are not necessarily representative of the mean state in that region. Furthermore, due to the coarse grid of global models some measurements near strong sources may not be well resolved even by the high resolution simulation. Last, measurements can also contain errors. These measurement uncertainties vary largely from species to species (and depending on the technique). Some cam-
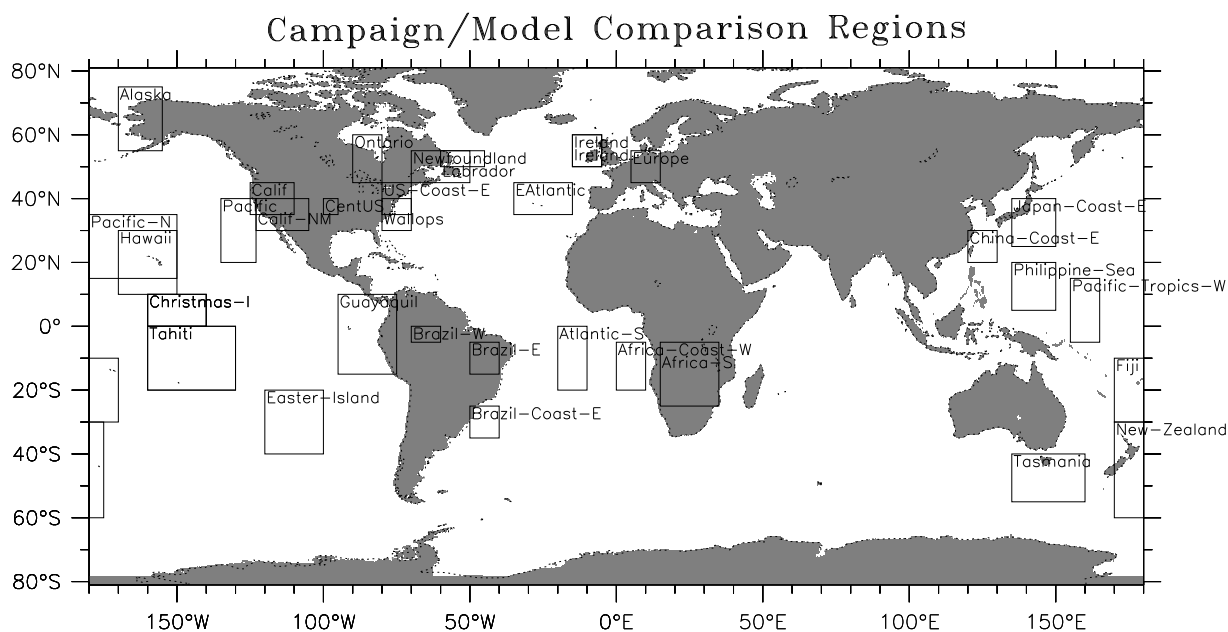
Figure 3.1: Model/observation comparison regions. Only selected regions are shown.

paigns were actually aimed at intercomparing different techniques (e.g. the CITE[1] campaigns) and some measurements judged to be too uncertain have been excluded from the comparison of airborne data (*Emmons et al.* (2000)). CO, NMHCs and O_3 are generally measured to an accuracy of a few percent. The other species shown subsequently are measured at an accuracy of roughly 10–30%, with the exception of nitric acid (HNO_3) which may be uncertain by up to 60%.

The campaign data are taken from the data collection of *Emmons et al.* (2000), who provided airborne observations aggregated over several regions to get meaningful vertical profiles. Comparisons have been made with all data included in the archive, which includes about 30 campaigns; however, only a selection of results can be shown here. Figure 3.1 shows the regions were comparisons with model output will be presented. It is striking that no campaigns over the Indian Ocean and East Asian continent are included. The recent INDOEX (Indian Ocean Experiment) campaign should provide valuable information on this relatively unexplored region. Studies with MATCH using the INDOEX data are ongoing projects (e.g. *Fischer et al.* (2001)) but are not included in this work. Additional to the campaigns included in the *Emmons et al.* (2000) data set (see also references therein), comparison with the SONEX campaign (*Singh et al.* (1999)), PEM-Tropics-B (*Raper et al.* (2001)) and LBA-CLAIRE (Surinam, *Crutzen et al.* (2000)) have been made.

In an extra section of this chapter results from three different model setups, which are not treated further in the following chapters are also discussed. In that part the exchange of the driving meteorological data set, less efficient uptake of HNO_3 on ice surfaces and a reduced reaction constant affecting the abundance of PAN is examined in an attempt to explain discrepancies during the first part of the chapter.

A synopsis of the results and findings from the comparisons are given at the end. A further analysis on the origin of ozone and other key species is given in the following Chapter, using

---

[1]Chemical Instrumentation Test and Evaluations

sensitivity runs with reduced chemical mechanisms.

3.1 Carbon Monoxide (CO)

Carbon monoxide provides the single most important sink for OH, accounting for about 40% of the OH loss in the troposphere (see Table 3.4). The ability of a model to reproduce the observed distribution of CO is therefore a critical test not only of the assumed emissions of CO but also of the calculated OH distribution. Due to the close link between CO and OH the CO emission totals are often adjusted within the range of uncertainty until reasonable agreement with long-term observations is found. In this study only mild adjustments have been made to the CO emission strengths of the original publications (see Section 2.3.6).

The budget of CO as calculated from the high resolution run is summarized in Table 3.1. The values for the lower resolution run, which is further evaluated in the next chapter, can differ by up to 10% from those in Table 3.1. Direct surface emissions constitute about half of the total source of CO. 75% of the direct emissions are in the NH. Also, the photochemical turnover is larger in the NH: approximately 57% of the photochemical production and 61% of the oxidation of CO by OH takes place north of the equator. The mean lifetime of close to 2 months is very similar in both hemispheres. The total source of 2560 Tg(CO)/yr is about 10% lower than estimated by *Bergamaschi et al.* (2000a,b) based on an inversion study, but well within the range of other studies (2090–2742 Tg/yr, *Kanakidou et al.* (1999)).

Table 3.1: Annual mean budget of CO in the Troposphere (T63 run). Units are Tg(CO)/yr.

	Global[a]	NH	SH
Surface Emissions	1260	930	330
Photochemical production[b]	1300	745	555
Total source	*2560*	*1675*	*885*
Photochemical destruction (CO+OH)	−2370	−1450	−920
Dry deposition	−150	−105	−45
Total sink	*−2520*	*−1555*	*−965*
Burden (Tg-CO)	361	223	138
Mean photochemical lifetime (days)[c]	56	57	55

[a]Note that all "tropospheric" budgets given in this chapter are based on the tropopause according to the WMO definition (temperature lapse rate) calculated online during the runs.

[b]From CH_4 and other VOCs.

[c]The mean lifetime τ of a compound with respect to a certain loss process or the sum of all loss processes in a certain region is defined here as $\tau = M/L$, with M the mean mass of the compound and L the mean loss rate, each integrated over the same region. Sometime this quantity is also referred to as the turnover time.

The distribution of CO is depicted in Figure 3.2 for the months of January and September. In January high mixing ratios of 150–300 nmol/mol are calculated over large parts of the northern hemisphere. A strong interhemispheric gradient is seen during the NH winter, which is not predicted for summer (not shown) or fall. This reflects the long lifetime of CO during darker periods due to low OH concentrations and the stronger sources of CO in the NH. In September during the dry season in southern Brazil and South Africa strongly enhanced concentrations are predicted due to biomass burning, which result in a more even distribution of CO among the

two hemispheres. The biomass burning emissions are transported upward into higher levels of the troposphere by convection and transported over large distances. The SH background mixing ratio is about 60 nmol/mol.

A comparison of longterm measurements of CO from the NOAA/CMDL[2] air sampling network (*Novelli et al.* (1998)) with the model simulations is presented in Figure 3.3. The stations are ordered from north to south. The data records are at least 2 years long, at most stations 4-7 years. Data until the end of 1996 are taken into account. It is noted that these measurements are selected to represent "background" conditions. Four sites are above the boundary layer (Niwot Ridge, Izaña, Mauna Loa and Qinghai Province). At these stations the model has been sampled at a higher level depending on the resolved orography of the region (indicated by the mean surface pressure in the model).
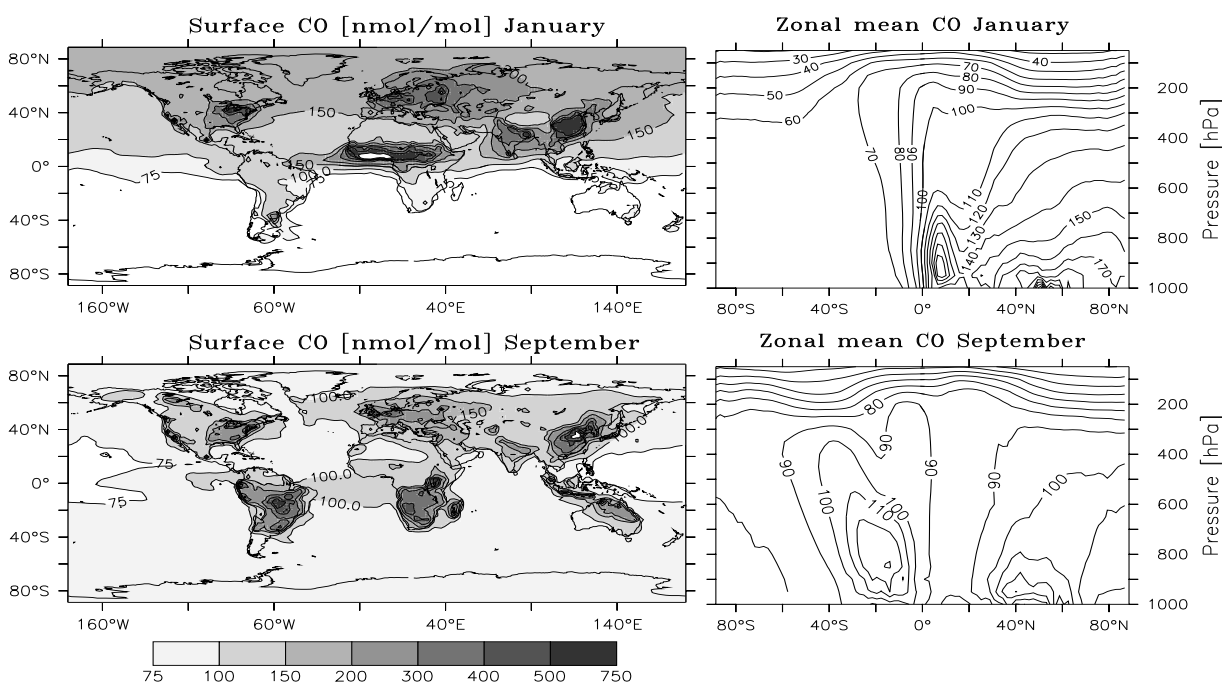
Figure 3.2: Distribution of carbon monoxide (CO) in the T63 run for January and September.

The magnitude and seasonal cycle of CO is generally well reproduced by the model. Some deviations of the lower resolution run from both the T63 run and the observations are likely due to the proximity of these stations to strong sources (e.g. Ulaan Uul is only about 1-2 grid cells away from the Peking region at T21 resolution, Key Biscayne is close to Miami). At all remote stations the two simulations yield very similar results. At high northern latitudes a slight underestimate of CO (e.g. at Barrow) appears to exist, but the amplitude of the seasonal cycle is consistent with the observations. The maximum in late winter at these stations is connected to the accumulation of CO during the dark winter period, when the lifetime of CO is long.

Comparing these results with those of previous studies with MATCH and to other studies can provide additional information on CO or OH. *Lawrence* (1996) (which will be referred to as MATCH-1.2 hereafter), who employed higher industrial CO emissions but also calculated higher OH concentrations, showed too large an amplitude of the seasonal CO cycle at the northern

---

[2]National Oceanic and Atmospheric Administration / Climate Monitoring and Diagnostics Laboratory.

arctic stations, with even lower mixing ratios in summer. This indicates that the lower industrial emissions used in this study are more realistic and OH levels were probably too high in MATCH-1.2 (see also methane lifetimes and methylchloroform-test in Sections 3.2 and 3.3.2). *Holloway et al.* (2000) concluded from comparing their modeled CO with the NOAA/CMDL stations that their industrial source of 300 Tg(CO)/yr is probably too low, which is consistent with the good agreement found in this study using 400 Tg/yr. This source strength appears to be significantly lower than estimated from inverse modeling of CO and its isotopes by *Bergamaschi et al.* (2000a,b) (about 600–800 Tg/yr). However, a large part of the difference is simply due to different nomenclature: While biofuel burning in is included in the "technological sources" category in *Bergamaschi et al.* (2000a,b), it is counted as biomass burning in this thesis. In the EDGAR emission data used in the study of *Bergamaschi et al.* (2000a,b) for biofuel burning this category amounts to 38% or 181 Tg/yr of the total "technological sources". Reducing the best estimate value of *Bergamaschi et al.* (2000a) (641 Tg/yr, scenario S2) by 38% yields a similar value than assumed in MATCH.

Both model versions overestimate CO at the Korean station "Tae-ahn Peninsula". This over-estimate was not observed in the MATCH-2.0 version (*Lawrence et al.* (1999b)) and inspection of the emission fields reveals that it appears to be connected with strong biomass burning in that region in the new biomass burning data set. The station is located at the east coast of South Korea only about 500 km (2-3 grid cells at T63 resolution) away from strong source areas in China. Therefore, it cannot be ruled out that the transport is not well enough resolved, especially by the coarse model grid, or the 1998 winds are not representative for the longer term average. The proximity to strong sources is also indicated by the large variability of the measurements, which is also reproduced by the model.

The strongest improvement over previous model versions is found at two stations with biomass burning influence. At Ascension Island, which is approximately downwind of the large savanna burning regions in South Africa during September and October, the September maximum of 280 nmol/mol CO shown in *Lawrence et al.* (1999b) is reduced to about 140 nmol/mol in this study. Although this is in much better agreement with the observations, an overestimation during the biomass burning season still remains. It is noted that vertical mixing of the elevated CO levels in the middle troposphere down into the marine boundary layer of the Atlantic ocean is probably also a critical parameter at this station (see vertical profile comparison below). At the Cuiaba Station in Brazil a strong seasonal influence of local biomass fires can be seen in the observations (taken from *Kirchhoff et al.* (1989)). Its timing and magnitude are well reproduced by the model. The previous versions of MATCH overestimated the peak in the biomass burning season by more than a factor of three at this station.

The improvement at these two stations must be attributed to the new biomass burning source of *Galanter et al.* (2000) which predicts much weaker peak emissions in Brazil and South Africa in September-October that appear to be more realistic.

At all southern hemispheric extra-tropical stations the CO mixing ratios are significantly higher in the model, by about 30–40% or 20 nmol/mol. While the amplitude of the seasonal cycle is approximately correct in the model, the SH summer minimum is too late by 1–2 months. *Holloway et al.* (2000) have calculated that about 25 nmol/mol of CO at low southern latitudes is from the oxidation of methane and that the seasonal cycle is the combined effect of biomass burning emissions and CO from the oxidation of biogenic hydrocarbons. An increase of OH levels by 1% would result in less than a 1% reduction of CO because the increased loss rate of CO is in
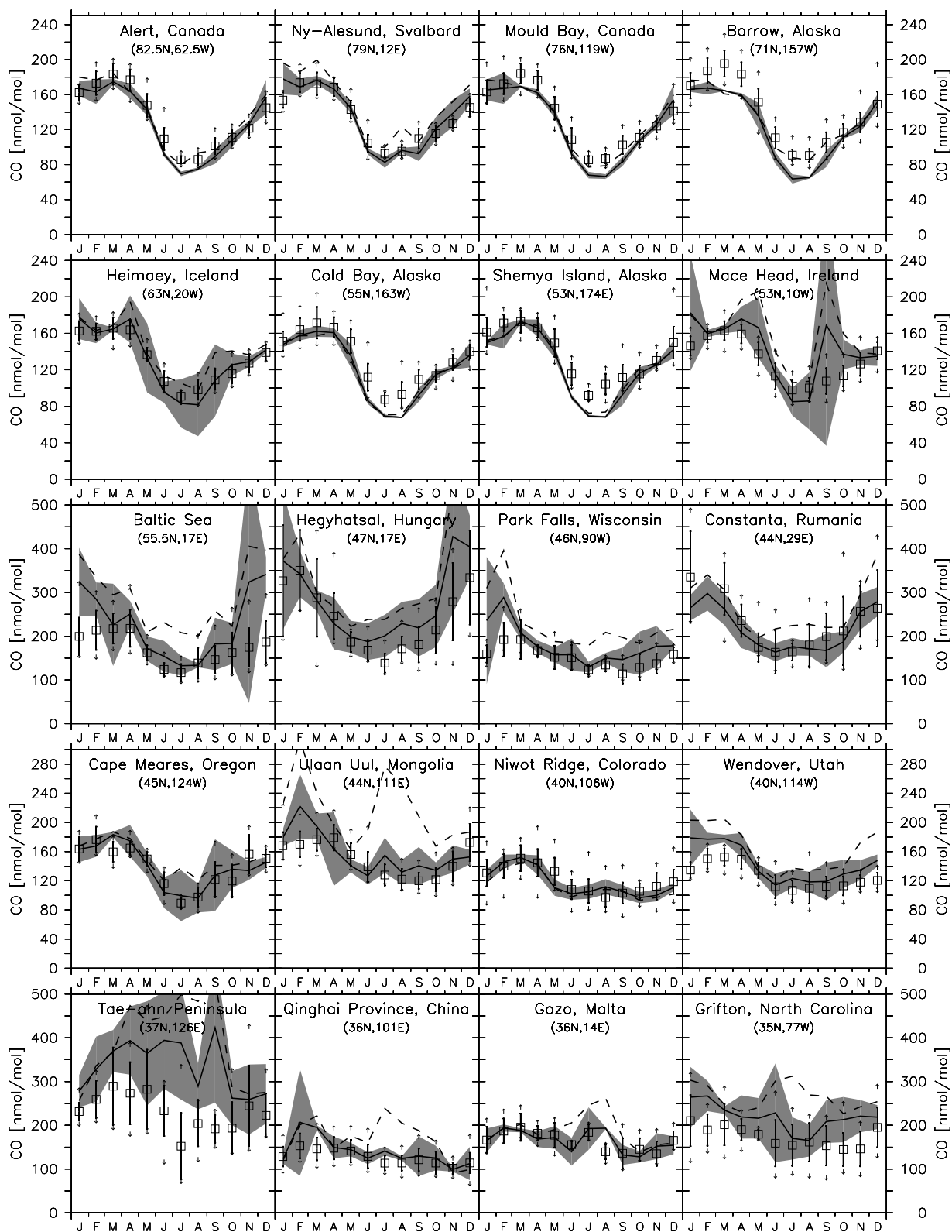
Figure 3.3: Comparison of CO measurements from the NOAA/CMDL network stations (*Novelli et al.* (1998)) and simulations with the T63 and T21 resolution version of MATCH (solid and dashed line, respectively). The shaded area indicates ±1 standard deviation of the T63 run. Vertical bars and arrows indicate the standard deviations and extreme values of the observations. Data for Cuiaba are taken from *Kirchhoff et al.* (1989) and Amsterdam Island from *Gros et al.* (1999). The approximate coordinates of the stations is also given.
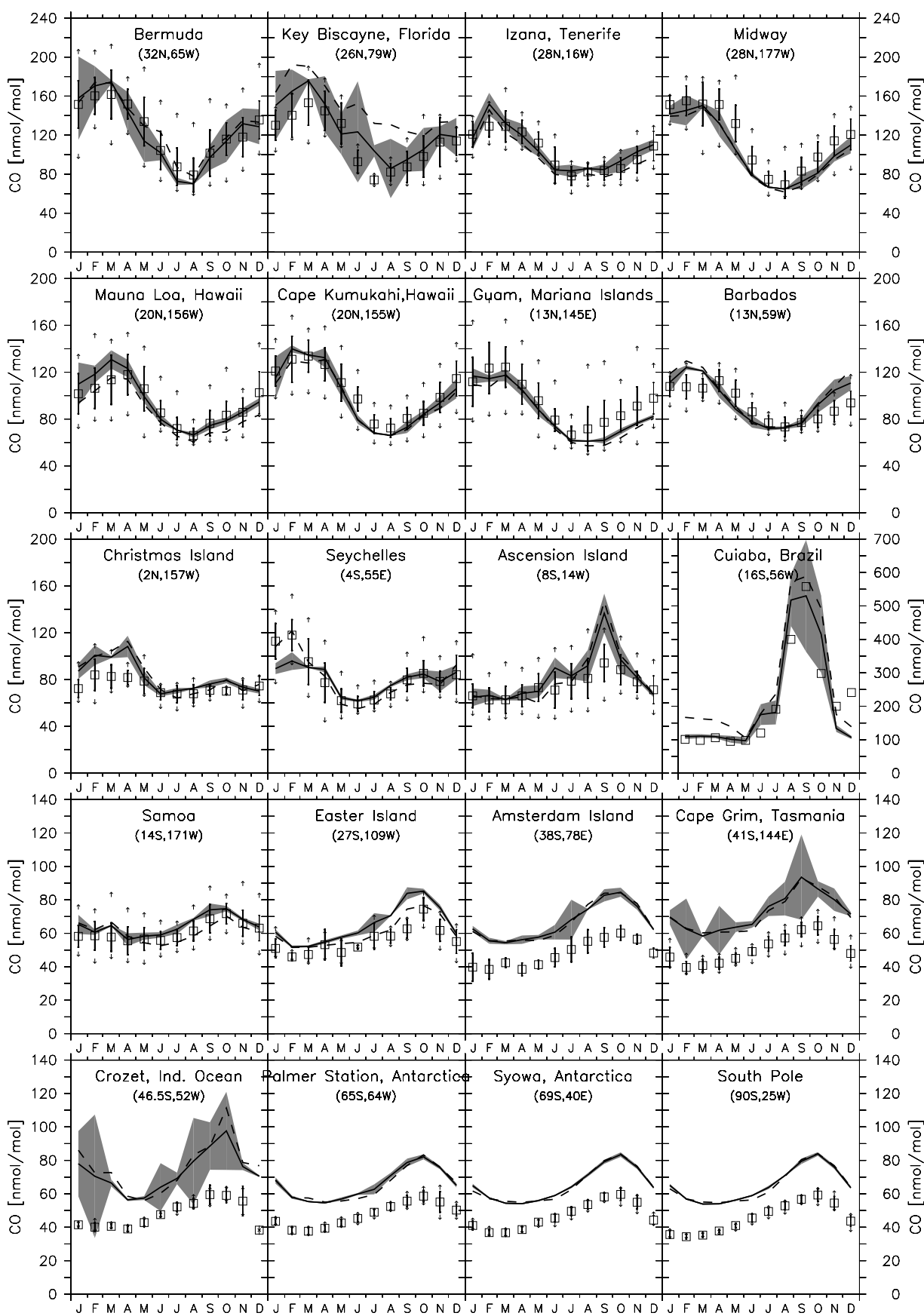
Figure 3.3: *(continued)* Note the special scale at Cuiaba, Brazil.
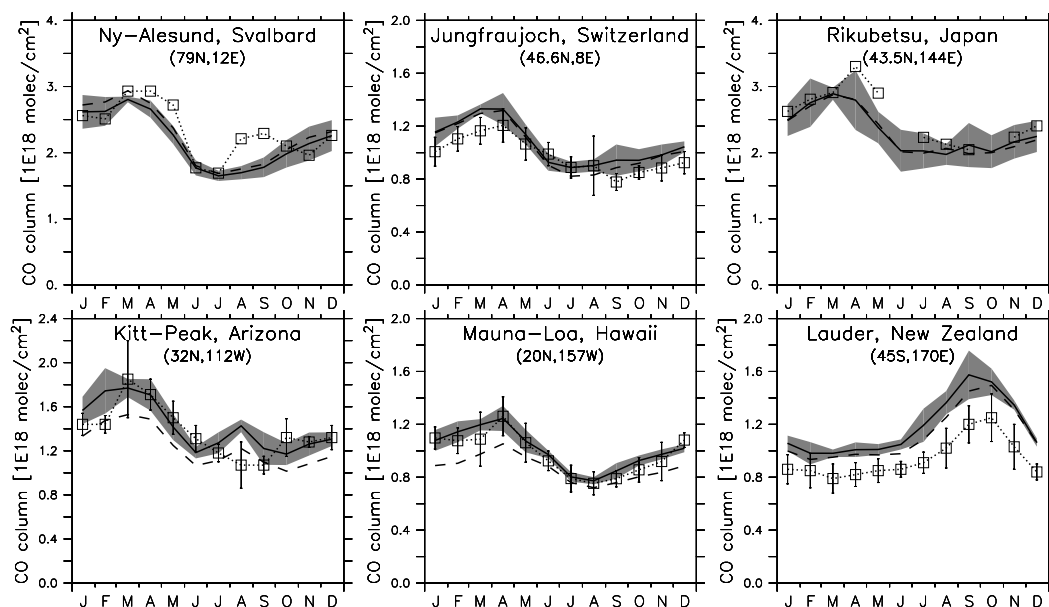
Figure 3.4: Comparison of CO column measurements with model simulation. Lines and symbols same as in Figure 3.3. Data are taken from *Notholt et al.* (1997); *Rinsland et al.* (1998, 1999, 2000) and *Zhao et al.* (1997). The accuracy of the technique was estimated to be better than 10% (*Rinsland et al.* (1999)).

part compensated by an increase in production from the oxidation of methane (e.g. *Kanakidou and Crutzen* (1999)). Considering that about half of the CO is from methane, a substantially higher mean OH concentration would thus be needed in order to explain the overestimate of CO. Therefore, other factors are likely involved as well. These could be too high emissions of CO from biomass burning, too high biogenic NMVOC emissions, too high a CO yield from these hydrocarbons or from methane.

A comparison with column integrated measurements of CO based on infrared solar (and lunar) spectroscopy can in combination with the surface stations provide information on the abundance of CO in the PBL as compared to the rest of the atmosphere. Figure 3.4 shows that the model is consistent with observations at the five northern hemispheric stations. Data from Rikubetsu are only from a single year, whereas the other monthly means are from longer data records. The comparison at Lauder (New Zealand) indicates an overestimation of the column CO abundance at the low southern latitudes consistent with the previous findings from surface observations. The surface measurements and column data at Ny Ålesund indicate that the abundance of this species in the boundary layer in relation to the rest of the troposphere is realistically simulated (i.e. not too much of the total CO column is in the PBL).

Finally, a comparison with measurements from airborne campaigns is presented in Figure 3.5. These observations, however, are made at a specific location and time so that deviations can occur when the meteorology during the campaign was not representative of the mean state in that area. More reliable information on persistent over- or underestimations of the model are obtained from the long-term observations. The aircraft data are therefore only used here to examine the vertical profiles of CO. Out of over 100 comparison regions only a small selection is shown, but more general statements are derived from all regions. Mostly regions which are strongly influenced by nearby sources have been selected to give indications of the source strength
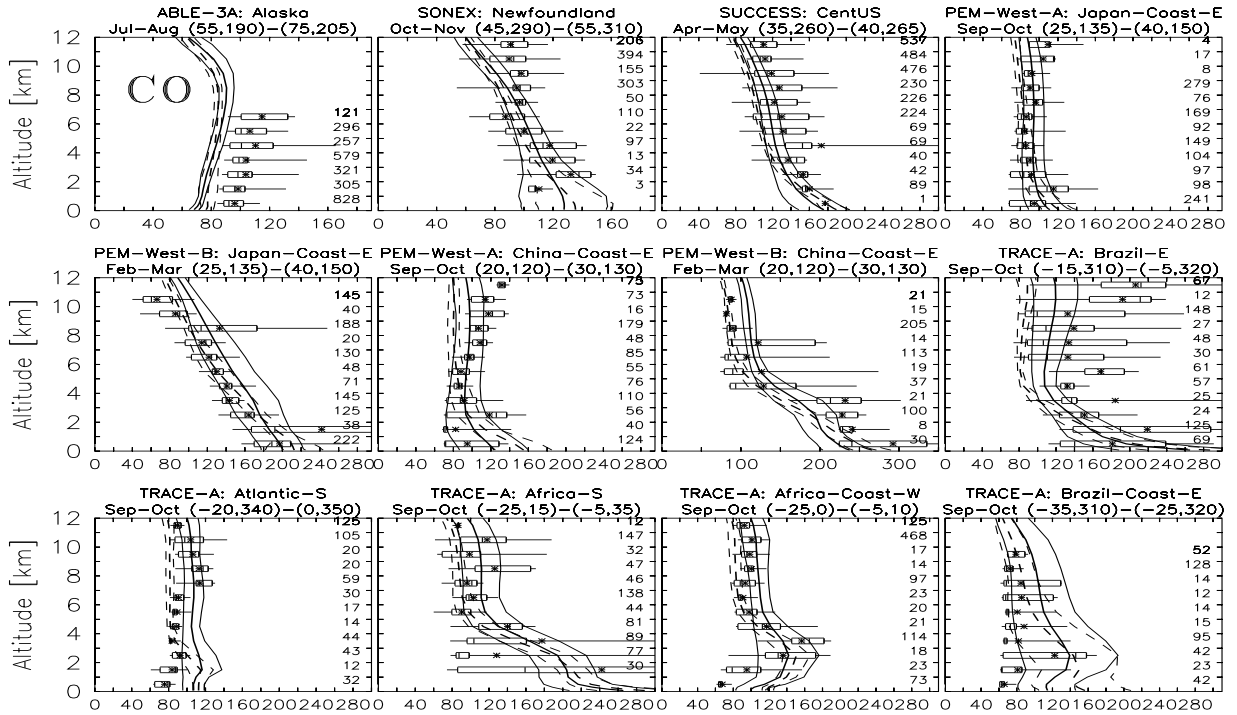
Figure 3.5: Comparison of CO simulations with airborne measurements (in nmol/mol) taken from the data collection by *Emmons et al.* (2000). Boxes and whiskers indicate the central 50% and 90% of the observations. Median and mean are marked by a vertical bar and a star. The number of observations at each altitude is given to the right. Model results with standard deviations are show as one thick and two thin lines (T63: solid, T21: dashed). The name of the campaign, the months during which the campaign took place and coordinates of the region are also given. For a map of regions see Figure 3.1.

and vertical mixing in the model.

The vertical gradient observed during various campaigns in the northern latitudes is mostly reproduced by the model, although it appears to be somewhat weaker in the observations at Newfoundland and "CentUS". Comparing to the ABLE–3A measurements in Alaska CO mixing ratios are underestimated by the model. The phases A and B of the PEM-West campaign took place during two different flow regimes: While during phase A the flow was mainly from the ocean onto Asia, during phase B outflow towards the ocean was predominant (*Hoell et al.* (1996, 1997)). The difference can be seen in Figure 3.5 in the different vertical gradients and the lower tropospheric concentrations of CO in the "Japan-Coast-E" and "China-Coast-E" regions, which are reasonably reproduced by the model.

The Trace A campaign took place during the SH dry season and some flights were influenced by biomass burning. Here, the agreement could be improved from the old model version, likely due to updating the biomass burning emissions from *Hao and Liu* (1994) to *Galanter et al.* (2000). The MATCH 1.2 and 2.0 versions strongly overestimated the bulge observed at 2-4 km altitude in the "Africa-Coast-W" region calculating a maximum of about 400 nmol/mol (not shown) compared to 160 nmol/mol in the measurements (Figure 3.5, 3rd panel in last row). However, the model still overestimates CO below 2 km. Despite the agreement in the lowest kilometer in the "Brazil-E" region during TRACE-A the upper tropospheric observations are underestimated

by a factor of 2–3, which suggests that convection is too weak in the model. However, *Pickering et al.* (1996) noted that the frequency of deep convection during the campaign was unusually high. Also, one of the two flights the data-merge consists of was actually devoted to sampling the outflow from convective systems, which thus makes the data unrepresentative in the upper troposphere. This comparison also reveals that vertical transport is more efficient in the high resolution run than in the T21 simulation, as indicated by the "Brazil-E" profiles and also observed for other tracers in the following sections.

3.2   Methane (CH_4)

Methane is the most abundant hydrocarbon in the atmosphere. Its photochemical degradation in the troposphere is almost exclusively via reaction with OH. The reaction with O^1D is only important in the stratosphere and is neglected here. Selected budgets of methane are listed in Table 3.2. The global tropospheric lifetime of methane against oxidation of OH (τ_{CH_4}) is often used as a measure of the oxidizing power of the troposphere. The tropospheric mean lifetimes of CH_4 of 8.8 and 9.1 years in the high and low resolution run, respectively, are compared with four recent studies as summarized in Table 3.3. Unfortunately, slightly different averaging domains are used. For a better comparability, the corresponding numbers from the MATCH (T21) simulation are also given. Both, lower and higher lifetimes of methane are calculated by the different studies, suggesting that the MATCH results are within the range of uncertainty.

Table 3.2: Calculated annual mean tropospheric budgets of methane. Units are $Tg(CH_4)/yr$ if not specified otherwise.

Resolution	T63	T21	T21	T21
Region	Global troposphere	Global trop.	Tropics[a]	UT ($\sigma<0.535$)
Tropospheric burden	4088 Tg	4058 Tg	1670 Tg	1783 Tg
Photochemical loss	-476	-445	-277	-92
Net transport	-103	-61	78	99
Quasi-source	571	508	201	—
Net tendency	0.3	2.0	-2.6	3.6
Mean lifetime	8.7 yr	9.1 yr	6.0 yr	19.4 yr

[a]Here defined as 20°S to 20°N.

The reason for the low methane lifetime in the study of *Krol et al.* (1998) is probably that the OH distribution used for the ensemble runs is strongly weighted towards low altitudes e.g. compared to the distribution of *Spivakovsky et al.* (2000). Due to the strong decrease of the reaction rate between CH_4 and OH with temperature, and thus with altitude this results in a relatively low methane lifetime, whereas other integral quantities such as the mass-weighted average OH concentrations are less affected (see also *Lawrence et al.* (2001) for a more thorough discussion).

This also brings out an important point in comparing global mean derived quantities from different studies. The uncertainty in quantities, which are not directly retrieved by the particular method will generally be higher than for the primarily obtained quantity (e.g. the CH_3CCl_3-loss-weighted global mean OH is usually derived in methyl-chloroform (MCF-) studies). Thus, the

Table 3.3: Comparison of the tropospheric methane lifetime $\tau_{\mathbf{CH_4}}$ against oxidation by OH calculated in this study with some recent studies direcly using observations.

Reference[a]	Method[a]	Region	$\tau_{\mathbf{CH_4}}$	MATCH[b]
Spivakovsky et al. (2000)	Box model constaint by observations of precursors	32°S-32°N:>100 hPa elsewhere:>200 hPa	9.6[c]	9.1
Prinn et al. (1995)	12-boxmodel optimized with CH$_3$CCl$_3$ (MCF) data 1978-1994	below 200hPa[d]	$8.9^{+1.6}_{-0.8}$[e]	8.8 (9.0)[f]
Prinn et al. (2001)	Like *Prinn et al.* (1995), but 1978-2000 data	below 200 hPa[c]	$10.12^{+1.68}_{-1.17}$	8.8 (9.0)
Krol et al. (1998)	3D model ensemble (Monte-Carlo) runs with fixed OH distribution, scaling factor for OH optimized using MCF data	below 100 hPa	$8.6^{+1.6}_{-0.8}$ (1993)	9.5

[a]For more information see Section 3.3.2 and 3.3.3 and the original literature.

[b]Averaged over the same region as in the corresponding study.

[c]This value is calculated from the methylchloroform lifetime of 5.7 yr and the rescaling method given in that study. However, *Lawrence et al.* (2001) calculate 8.23 using their monthly mean distribution and a tropopause defined by $p = 300 - 215 \cdot \cos^2(\phi)$ [hPa].

[d]With grid boundaries in the vertical only at 500 and 200 hPa it may be that the "troposphere" (below the tropopause) is the actual meaning of this compartment. See footnote [e].

[e]In *Prinn et al.* (1995) a value of 8.9±0.6 yr was given for the region including the stratosphere, but was changed in *Prinn et al.* (2001) to this figure for the region below 200 hPa, with a larger uncertainty now also including errors from the rate constant.

[f]Value in brackets is for region below the tropopause. The slight difference to the value in Table 3.2 is from the use of the monthly mean tropopause here.

methane lifetime calculated in MCF studies will be more uncertain than the MCF lifetime, because usually a OH distribution is assumed, which can have different effects on MCF than on methane due the different temperature dependences of the rate constants. In fact, *Lawrence et al.* (2001) show that this error is usually not very large, but the conversion into a mass-weighed global mean OH value is found to be more uncertain (10-20%).
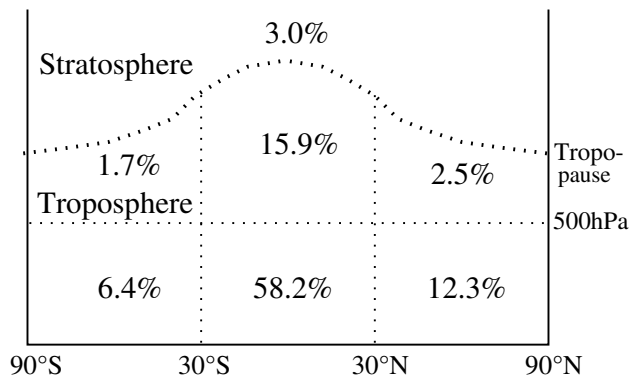
Figure 3.6: Percentage of photochemical loss of methane through reaction with OH per region. Results are from the T21 run.

Only about 20% of the tropospheric photochemical loss of methane is calculated to occur above about 500 hPa (σ < 0.535, see Table 3.2). The relative contribution of specific regions in the atmosphere to the oxidation of methane is depicted in Figure 3.6. The contribution from the tropical region (30S-30N), especially below 500 hPa, is clearly dominating. This also implies that the global tropospheric mean methane lifetime is not very sensitive to OH concentrations in the upper troposphere (UT) and in the extra-tropical regions. Further evaluations of the global mean OH and its distribution are performed in Sections 3.3.2 and 3.3.3. The use of uniform definitions of the

troposphere would clearly increase the comparability of the different studies.

The procedure to set the methane concentration in the lowest model layer to specified zonal means (see Section 2.3.6) makes a comparison with measurements not very meaningful. It is nevertheless noted that inspection of the airborne CH_4 measurements made during the STRATOZ III campaign (*Marenco et al.* (1989)) revealed similar vertical profiles and only small differences ($<4\%$) in the absolute concentrations compared to the model predictions.

3.3   The Hydroxyl Radical (OH)

As discussed before, OH is the dominant oxidant for most VOCs (among them methane) in the atmosphere. Its mixing ratios are very low, near surface during daytime on the order of 0.1 pmol/mol, but can vary by more than an order of magnitude. The abundance of OH is more commonly expressed as concentrations in units of molecules/cm^3. In this section the simulated global OH distribution and derived mean quantities are evaluated based on a simulation of methylchloroform (CH_3CCl_3 or MCF) and comparison with an extensively evaluated climatological OH distribution. First, the simulated distribution and more integral quantities are presented.

3.3.1   Global simulated OH

Figure 3.7 depicts the zonal mean distribution of OH for four months. A maximum at about 700 hPa is calculated for January and October, while it is smeared out towards the surface during the other two months shown. The maximum is mainly the result of two competing effects: increasing photolysis of O_3 to form O^1D, but decreasing abundance of water vapor available to react with O^1D to form OH. The largest concentrations of OH are calculated for the NH summer industrialized regions near the ground (about $5 \cdot 10^6$ molec/cm^3). Very low concentrations ($< 10^5$ molec/cm^3) are calculated poleward of about $50°$ in the winter hemisphere. The horizontal distribution and its change induced by the inclusion of NMHCs are presented in the next chapter.

The main sources and losses of OH are listed in Table 3.4. Globally averaged, photolysis of O_3 followed by reaction of O^1D with water vapor is the single dominant source for OH. In upper troposphere (UT) other sources can be important as well (e.g. *Jaeglé et al.* (1997, 2001)). However, as shown above, this region is not very effective in removing the greenhouse gas methane. But, since HO_x acts as a catalyst in the production of ozone, additional HO_x production can contribute to ozone levels at these altitudes. In Section 3.7 it will be shown that the height of the tropopause (or more precisely the ozonopause) is not always correctly modeled. Calculated ozone concentrations a these high altitudes are thus very uncertain, likely due to dynamical (linked to convection) or numerical problems (strong vertical gradients). A further analysis of upper tropospheric HO_x sources with MATCH therefore does not appear to be rewarding before these problems are resolved and is not attempted in this study.

Other integral indicators of global OH than the methane lifetime such as the mass weighted average concentration[3] or the volume weighted average[4] are also often given and are reported here for comparison. The tropospheric mass weighted mean concentration is about the same in

---

[3]This quantity would be a measure for the lifetime of a hypothetical atmospheric tracer which is evenly distributed and has a temperature-independent reaction constant for the oxidation with OH.

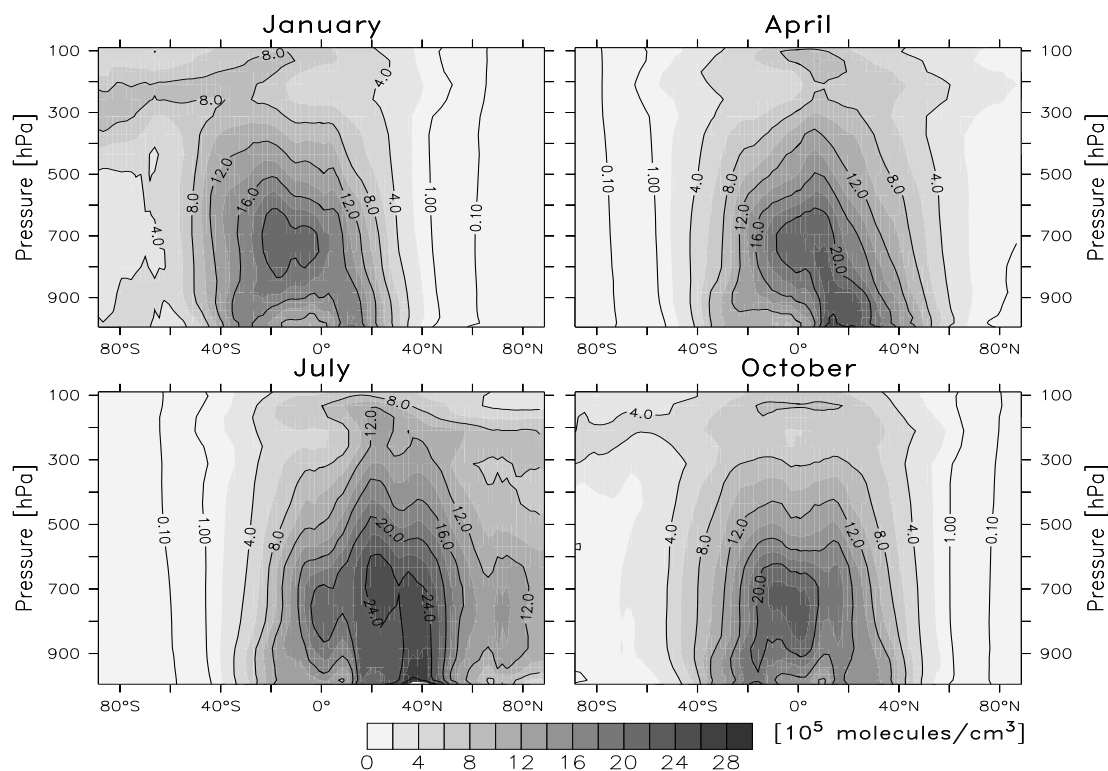[4]This quantity has, however, no direct physical meaning.

Figure 3.7: Zonal mean 24-hour average OH distribution in 10^5 molecules/cm^3 from the T63 simulation for January, April, July, and October.

Table 3.4: Main source and loss reaction of OH in the troposphere as calculated with MATCH (T63) in percent of the total mean rate of $7.7 \cdot 10^{11}$ molecules/cm^2/s. Minor reactions ($\leq 1\%$) are not listed.

	Reaction	Percent
Sources	$O^1D + H_2O \rightarrow 2\ OH$	47.8 %
	$NO + HO_2 \rightarrow NO_2 + OH$	28.6 %
	$O_3 + HO_2 \rightarrow OH$	11.9 %
	$H_2O_2 + h\nu \rightarrow 2\ OH$	9.2 %
	$CH_3OOH + h\nu \rightarrow HCHO + HO_2 + OH$	1.9 %
Sinks	$OH + CO \rightarrow HO_2 + CO_2$	41.2 %
	$CH_4 + OH \rightarrow CH_3O_2 + H_2O$	14.2 %
	$HCHO + OH \rightarrow CO + HO_2 + H_2O$	6.6 %
	$CH_3OOH + OH \rightarrow 0.7\ CH_3O_2 + \ldots$	6.5 %
	$O_3 + OH \rightarrow HO_2$	4.9 %
	$HO_2 + OH \rightarrow H_2O$	4.9 %
	$OH + H_2O_2 \rightarrow HO_2$	4.5 %
	$H_2 + OH \rightarrow HO_2 + H_2O$	4.4 %
	$ISOP + OH \rightarrow ISO_2$	2.4 %
	$MACR + OH \rightarrow MACRO_2$	1.9 %
	$MACROOH + OH \rightarrow MACRO_2$	1.5 %
	$CH_3CO_3H + OH \rightarrow CH_3O_3$	1.1 %

the two simulations: $9.85 \cdot 10^5$ and $9.60 \cdot 10^5$ molecules/cm^3 in the T63 and T21 run, respectively. The volume weighted averaged tropospheric OH is about 5% lower.

3.3.2   Evaluation with Methylchloroform

The short lifetime of OH (on the order of seconds) makes it impossible to determine the global OH distribution by in-situ measurements. Therefore, knowledge of the global OH distribution is mainly obtained from complex 3D models (such as MATCH). However, some constraints can be put on the average OH abundance by use of long-lived tracer with known sources. Methylchloroform (hereafter denoted as MCF) is the most prominent tracer used for this purpose, having well constrained solely anthropogenic sources. The uncertainty in the emission strength and regional attribution was stated to be about±3% (*Midgley and McCulloch* (1995)). Its only sinks in the atmosphere are the reaction with OH (lifetime about 5 years), slow uptake by to the ocean with an associated lifetime of about 80 years (25–134 yr), and photolysis in the stratosphere (50±25 years). Since OH is thus the dominant sink for MCF, with a relatively well constrained rate constant (±10%, *DeMore et al.* (1997)) it has been attempted to use MCF observations to constrain the global mean OH concentration (e.g. *Prinn et al.* (1992, 1995, 2001); *Krol et al.* (1998)). Precisely, the term "mean" here refers to the MCF-loss weighted average OH concentration.

As pointed out by *Jöckel* (2000) gaining information on scales smaller than global (e.g. hemispheric) is hampered by uncertainties in the dynamic part of the model (e.g. inter-hemispheric exchange rate). *Jöckel* (2000) also showed that different model configurations (i.e. different advection or convection parameterization) resulted in deviations comparable to using different OH distributions. It must also be noted that some of these results are obscured by problems associated with the mass/wind inconsistency problem (Section 2.2.1) which was either not corrected, or a global rescaling resulting in artificial diffusion was applied in the runs.

A simulation of MCF was performed over the time period of 1969 - 1993. The model setup is the same as in *Jöckel* (2000), where further details can be found. The simulation is initialized with a previous run, which started in 1950 and used the model version and OH distribution from *Lawrence* (1996). After this long spin-up the results should be insensitive to the initial conditions. For the further integration the version of *Lawrence et al.* (1999b) (MATCH-2.0) but employing the advection algorithm from MATCH-1.2 is used. This semi-Lagrangian advection scheme (*Williamson and Rasch* (1989); *Rasch and Williamson* (1990)) is faster, but more diffusive than the SPITFIRE scheme currently used. However, this should not have a large effect on the distribution of a tracer with weak gradients, such as MCF. The low resolution (T21) dynamics were used, but the OH distribution from the high resolution run averaged to the T21 grid is applied. *Krol et al.* (1998) derived a trend in global OH of 0.46±0.6% yr^{-1} between 1978 and 1993, which appears to be slow (and uncertain) enough to justify the use of a constant OH field in this test. Nevertheless, if the OH trend proves to be on the high side of this estimate, an additional error is introduced.

The results of the MCF test are shown in Figure 3.8, along with the result of the OH distributions from previous studies with MATCH (*Lawrence* (1996); *Lawrence et al.* (1999b), MATCH 1.2 and 2.0). The results obtained with the OH field from this study lie between the two previous versions, which is consistent with the intermediate methane lifetime calculated in this study (8.7 years, compared to 7.9 and 10.1 yr, in the other studies). Assuming that MCF concentrations scale linearly with the OH abundance and other errors are negligible, one could derive an underestimation of about 30%, 20%, 15%, 10%, and 10% from the overestimated trend at the five
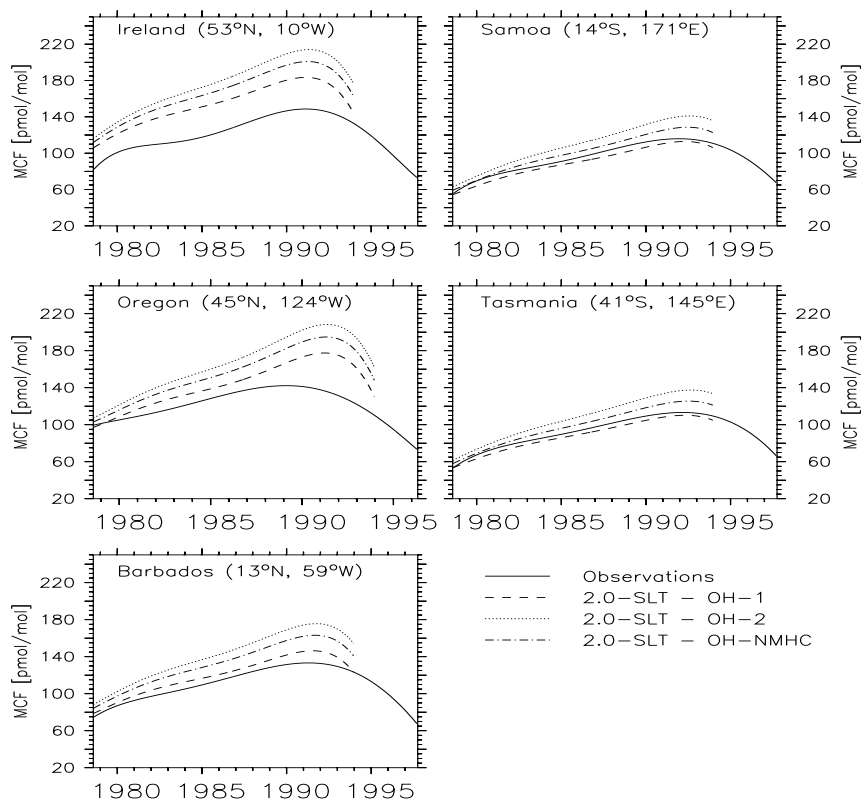
Figure 3.8: Comparison of the MCF time series and model simulations. Observations and model results are fitted by a series of Legendre polynomials (*Jöckel* (2000)) to eliminated the seasonal cycle and inter-annual variability. OH–1 and OH–2 denote OH fields from previous studies with MATCH (*Lawrence* (1996); *Lawrence et al.* (1999b), MATCH 1.2 and 2.0). OH-NMHC is calculated with OH from this study.

stations (respectively, from north to south). It is noted that the maximum at the Oregon station is not well constrained since no data are available between 1989 and 1995.

An interesting result seen in Figure 3.8 is the strong decrease in MCF in all model versions at the northern hemispheric stations, but especially at the Ireland and Oregon stations, after 1991. The strong decrease is certainly not consistent with the underestimate of OH derived from the long-term MCF trends, which points towards a dynamical rather than a photochemical explanation. The Ireland and Oregon station data are collected close to considerable MCF sources, and the measurements are filtered for local pollution; this is not done in the model. A possible explanation would therefore be too strong an influence in the model by local sources. However, sampling the model 20° west of the station coordinates, thus about 4 grid boxes upwind in the dominant wind direction, only shows small changes (< 3%) in the MCF concentrations. Thus, another explanation is needed. Possible issues are vertical mixing and potential inaccuracies in the true decrease of the emissions after 1990. The problem cannot be solved here, but it indicates that the strong decline of MCF contains additional information to that in the long-term increase, as also suggested by *Montzka et al.* (2000).

If the five stations are taken to be representative for their respective latitudes an overestimated North-South gradient in MCF can be diagnosed for all OH fields shown. Without further independent information it cannot be discerned whether this is due to erroneous NH-SH asym-

metry in the OH distribution or due to too weak interhemispheric exchange or both.

The interhemispheric exchange and vertical mixing in MATCH has been tested by *Jöckel* (2000) using the long-lived tracer SF$_6$. It was found that the interhemispheric exchange time of the configuration used here in the MCF simulation was higher than the tested configurations using SPITFIRE and that all MATCH-configurations tended to have rather weak vertical mixing and a slow interhemispheric exchange rate compared to 11 tracer models tested in an intercomparison exercise (*Denning et al.* (1999)). Modifying the dynamics in MATCH to better agree with SF$_6$ measurements would therefore also improve the agreement to the MCF measurements.

Denning et al. (1999) also found indications that vertical mixing is actually a strong factor in determining the meridional gradient of tracer concentrations near the surface. *Jöckel* (2000) could also show that the simulations with two model setups, which practically only differ by the convection scheme employed, result in differences at the two northern mid-latitude stations of about 5% in the MCF concentrations. The older version was found to be closer to the observed trend in MCF.

Finally, the uncertainty in the other two loss processes of MCF (photolysis at higher altitude and ocean uptake) can affect the results of the MCF test. *Krol et al.* (1998) found that their optimized global OH abundance was sensitive to these sinks and lead to their estimated range of uncertainty of about 10-15% in the global mean[5] concentrations of $1.07^{+0.09}_{-0.17} \cdot 10^6$ molecules/cm^3 below 100 hPa in 1993. The effect of mixing (vertical or interhemispheric), however, was not addressed in that study.

The situation is further complicated by recent findings that MCF may be emitted from forest soils (*Hoekstra et al.* (2001)), but also reemission of MCF that has previously deposited is a possible explanation of these findings. In this study also strong deposition of chlorinated solvents has been observed, indicating that the role of the terrestrial biosphere as a source or sink for MCF may not be negligible. However, further studies are needed to clarify these issues.

It is difficult to draw quantitative conclusions from the MCF comparison in view of the different factors that have an influence on the results besides the OH distribution. In summary, these uncertainties (potential effect on MCF concentrations in brackets) are: source strength (3%), measurement calibration (5%, *Prinn et al.* (1995, 2001)), reaction rate (10%, *DeMore et al.* (1997)), vertical mixing ($\approx$5%, based on *Jöckel* (2000)), interhemispheric exchange rate (5%-10%), and other loss processes (10%, *Krol et al.* (1998)). Although the combined uncertainty of these effects cannot be easily judged, it appears that the overall uncertainty of a such derived "mean" OH concentration is probably more than the 10% (*Krol et al.* (1998)) based on uncertainty in the ocean and stratospheric sinks alone. An uncertainty of $\pm$20% in the global MCF-loss weighed mean OH concentration is probably a more realistic estimate. Other integral quantities can only be derived from these measurements by assuming a distribution of OH in the troposphere, which introduces additional uncertainties in those derived quantities (*Lawrence et al.* (2001)). It is therefore judged that the accuracy of MCF as a means to constrain tropospheric OH was probably seen too optimistically in previous studies.

Considering the tendency of MATCH to have too weak vertical mixing and too weak interhemispheric exchange, it is judged that the MCF-loss weighted mean tropospheric OH concentration in this study is probably on the low side, but within the range of uncertainty of the MCF-test. It is also well within the range obtained by previous studies (e.g. *Lawrence* (1996); *Lawrence et al.* (1999b) bracketing the results from this study in Figure 3.8).

---

[5]Volume weighted (*M. Krol,* personal communication, 2001).

3.3.3 Comparison with the climatology of *Spivakovsky et al.* (2000)

In a recent study *Spivakovsky et al.* (2000) used global observation of various species affecting OH to derive a climatological distribution. Observations of O_3, H_2O, NO, CO, hydrocarbons, temperature and cloud optical depth were used to constrain a photochemical box-model to a periodic solution (24h period) to obtain a three dimensional monthly varying distribution of OH. This distribution was extensively evaluated using long-term trends and diurnal variations of a suite of tracers. They state that the distribution is "consistent within a few percent" of the budgets of MCF and another long-lived tracer (HCFC-22). The mass weighted mean (integrated below 100 hPa between 32°S and 32°N and below 200 hPa elsewhere) is $1.16{\cdot}10^6$ molec/cm^3 and the mean methane lifetime in that region (with respect to oxidation in the troposphere) can be calculated to be 9.6 years for their distribution. A recent study by *Prinn et al.* (2001) derived an optimal mass weighted average average concentration of $9.4{\pm}1.3 \cdot 10^5$ molec/cm^3 (below 200 hPa), but this values are derived using a recursive weighted least squares (Kalman) filter with a 2D model consisting of only 8 tropospheric and 4 stratospheric boxes. *Krol et al.* (1998) found $1.00\,^{+0.09}_{-0.15}{\cdot}10^6$ molec/cm^3 (below 100 hPa).

In order to make use of these findings, the OH from this study is compared to their distribution. However, the OH field from *Spivakovsky et al.* (2000) should not be regarded as a true reference, since uncertainties are clearly introduced when extrapolating the sparse available measurements of species affecting OH (e.g. of NO_x) in the troposphere to get a 3-dimensional seasonally varying distribution of these species.
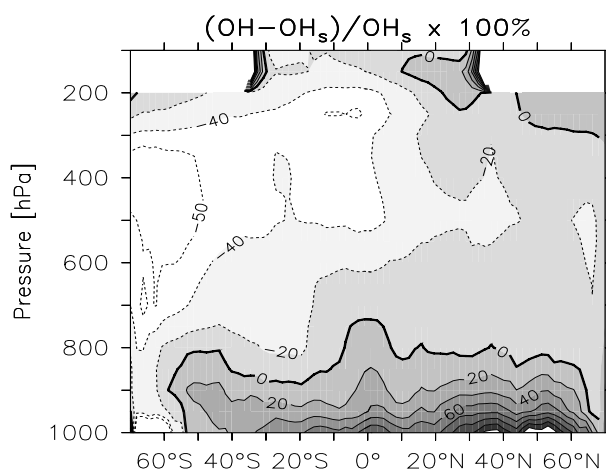

Figure 3.9: Relative difference of the annual mean distributions of the T63 run compared to the distribution of *Spivakovsky et al.* (2000)

In Figure 3.9 the relative difference of the OH from the high resolution run and the *Spivakovsky et al.* (2000) OH distribution (denoted OH_s) is shown. It can be seen that they differ by up to a factor of 2 with OH from MATCH being higher below about 800 hPa and lower in the upper troposphere especially in the SH. This discrepancy spans the full range of uncertainties for the local OH abundance (factor 2) given in *Spivakovsky et al.* (2000). The different vertical distribution can explain why the methane lifetime calculated in this study (8.4 years below 200 hPa, 9.5 years below 300 hPa) is higher. As shown in Figure 3.6 methane oxidation is strongly weighted towards low altitudes where more OH resides in the MATCH distribution.

MCF oxidation is also weighted toward the lower troposphere, although not as strongly

because the temperature dependence is weaker ($k_{CH_4} = 2.45 \cdot 10^{-12} e^{(-1775/T)}$ versus $k_{MCF} = 1.8 \cdot 10^{-12} e^{(-1550/T)}$). This means that at 220K the rate constant of the CH$_4$+OH reaction drops to 12% of its value at 298K. For MCF the corresponding fraction is 16%. Additionally, due to the longer lifetime of methane and relatively more emissions in the SH (about 30% and <1% of the total emission of CH$_4$ and MCF are in the SH; *Houweling et al.* (1999); *Midgley and McCulloch* (1995)) one would expect a relatively larger fraction of methane to reside in the SH. With this in mind it is hard to understand why the MCF test suggests too low OH concentrations while the methane lifetime is shorter in this study than that of *Spivakovsky et al.* (2000). This further indicates that other factors than the "test quantity" OH are significantly influencing the results of the MCF simulation. However, it cannot be ruled out that the lower OH concentrations already above 800 hPa together with the different temperature dependence is sufficient to explain the results.

The low southern hemispheric OH in the MATCH simulation is consistent with the overestimate of CO at these latitudes, although it is unclear whether one is causing the other (and which is causing which) or if another factor is involved. The NO$_x$ concentrations are certainly an important factor in determining the OH concentration in the low southern latitudes where NO$_x$ is generally quite low. Some assumptions made by *Spivakovsky et al.* (2000) to constrain the NO$_x$ distribution in this region can explain part of the difference seen in Figure 3.9. Measurements of NO during the PEM-Tropics A and TROPOZ II campaigns show lower NO concentrations than those used by *Spivakovsky et al.* (2000).

These authors also used the relative amplitude in the annual cycle of MCF and another tracer (CH$_2$Cl$_2$) at Tasmania to further constrain southern hemispheric OH and conclude from the two tracers that their OH distribution is probably 15-25% or 30-50% (from the two tracer, respectively) too high in the SH, but also state that the uncertainty in this estimate from dynamical parts of the model used to transport these tracer is about ±25%. Overall, this would bring the distribution of *Spivakovsky et al.* (2000) in better agreement with the MATCH results.

Finally, it is noted that the OH distribution from the T21 run is up to 40% higher in the tropical upper troposphere above about 400 hPa and differences are small in the lower troposphere. Although this may be explained by the stronger convection of CO and hydrocarbons (e.g. isoprene and its oxidation products) in the high resolution run, the magnitude of the difference is surprisingly large. Above 300 hPa HO$_x$ (OH+HO$_2$) is actually larger in the T63 runs, which confirms the view that the higher abundance of VOCs in the UT basically shifts the OH/HO$_2$ ratio towards HO$_2$. The calculated OH from the T21 runs is thus in better agreement with the distribution of *Spivakovsky et al.* (2000) in the UT.

3.4   NMHCs (Alkanes, Alkenes, Isoprene)

As mentioned in Section 1.2 the oxidation of non-methane hydrocarbons can participate in the production of ozone in the presence of sufficient NO$_x$ levels. Ethane (C$_2$H$_6$) is also a precursor for PAN (peroxyacetyl nitrate), which is important for long-range transport of NO$_x$. Propane (C$_3$H$_8$) is a precursor for acetone (CH$_3$COCH$_3$) and PAN. Acetone has gained more interest in the recent past as it produces HO$_x$ in the upper troposphere upon photolysis. Butane (C$_4$H$_{10}$) is only used here as a pool for all higher alkanes and its distribution will not be evaluated.

Alkenes are very short lived species and their importance is probably only local in these simulations, though propene can contribute to PAN formation. Also, changes in local chemistry

(e.g. of HO_x) can alter the partitioning of nitrogen reservoir species and thereby have an indirect long-range effect. Isoprene (a diene) is due to its emission strength of large importance. Especially for isoprene, but also for the other alkenes, however, a direct comparison of model results to point measurements is problematic. Due to their short lifetimes horizontal and temporal gradients can be quite large and the representativeness of the measurement site for the large grid-box in the global model is often not fulfilled. A discussion of some results is nevertheless attempted in Section 3.4.2.
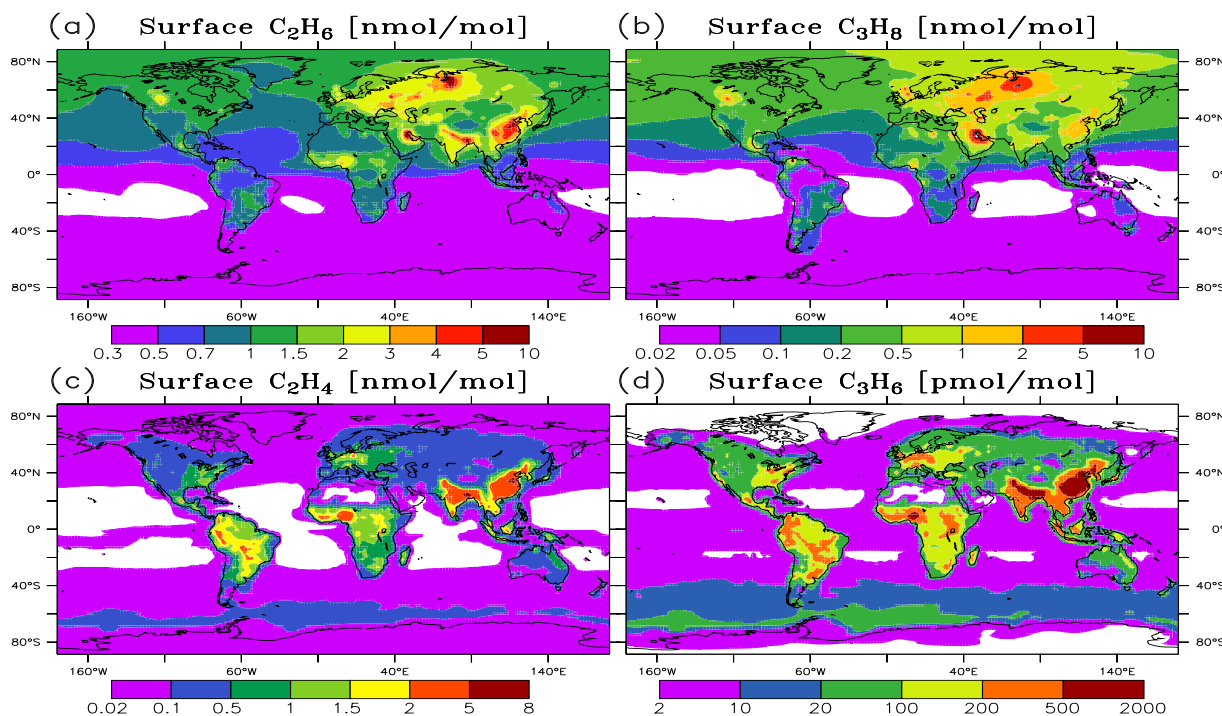

Figure 3.10: Annual mean surface distribution of C_2H_6 and C_3H_8 from the T63 simulation.

3.4.1 Ethane and Propane

The annual mean surface distributions of ethane and propane are shown Figure 3.10a and b. The distributions reflect the source distributions, with strong sources from fossil fuel exploitation (e.g. North Siberia, Persian Gulf, North Sea), and the different lifetimes of these compounds. The calculated mean tropospheric lifetime of ethane and propane are about 2.7 months and 28 days, respectively. The effects of biomass burning emissions are also visible in Figure 3.10. The vertical gradient of ethane is therefore similar to that of CO and propane displays a somewhat larger decrease with altitude.

The comparison of calculated ethane distribution with surface and column measurements compiled from the literature is presented in Figure 3.11. The simulations and measurements are in quite good agreement for the European stations, although the buildup during winter appears to be underestimated. However, at most North American stations (e.g. Fraserdale, Harvard Forest) the model significantly underestimates ethane mixing ratios, especially in winter. This indicates that the emissions from this region might be underestimated in the EDGAR database, or other sources not accounted for in this study (e.g. biogenic) significantly contribute to the ethane

budget at these locations. The free tropospheric stations Izaña and Mauna Loa are both also higher than simulated mixing ratios, whereas the southern hemispheric stations are fairly well reproduced. This indicates that the biomass burning source of ethane used here (5.2 Tg(C)/yr) is a reasonable estimate, provided that OH concentrations are not too low (see above). This finding is in agreement with the study of *Wang et al.* (1998c) which found better agreement with a biomass burning source of 6 Tg(C)/yr than with 2.5 Tg(C)/yr. At Scott Base the seasonal cycle appears to be shifted, with a delay of 1–2 months in the model. A similar deviation was found for CO and could thus point toward a problem with the meridional transport between 50°S and 70°S. Miscalculated abundance and/or seasonal cycle of OH or wrong seasonality in the sources, however, could also play a role.

Comparison of the simulations with ethane column abundances (last 5 panels in Figure 3.11) shows that the model also tends to underestimate the total column abundance of ethane in the northern hemisphere. At Lauder (New Zealand), however, the model is on the high side of the measurements.

Surface measurements of propane are show in Figure 3.12 along with the model results. The general picture is quite similar to that found for ethane (reasonable agreement in Europe, underestimation in North America). The overestimation of the low resolution run at Birkenes is probably due to the proximity of the station to the Norwegian oil exploitation field in the north sea, where large emissions of alkanes are predicted by the EDGAR data base (see Figure 3.10). In the SH also an underestimate of a factor of two is visible. Especially interesting is the result at Amsterdam Island. The fact that ethane was well reproduced and propane is underestimated by a factor of two suggests that either the ratio of the emission factors (EF) of propane and ethane ($EF_{C_3H_8}/EF_{C_2H_6}$) from biomass burning (taken from *Andreae and Merlet* (2000)) is too low or that other existing sources with a higher ratio are not included in the model. In particular, oceanic emissions could significantly enhance the background mixing ratios of propane at low southern latitudes. Thus, it is also possible that the oceanic emissions are underestimated in this region.

The results from the comparison of these alkanes with airborne measurements gives a similar picture as for CO. Both compounds are shown in Figure 3.13 (ethane in the upper 3 rows, propane in the lower 3 rows). The vertical profiles of both compounds are mostly well simulated, but some differences are also seen. In some regions the observations (ABLE–3A, SONEX–Newfoundland) are underestimated by up to a factor of two (propane over Alaska in summer). The fact that all three longer lived species (CO, C_2H_6, C_3H_8) are similarly underestimated in the Alaska region (ABLE-3A) also suggests that the meteorology of 1998 was not representative for the state encountered during the measurements.

Unlike for CO the outflow from Asia during PEM-West-B in the "Japan-Coast-E" a significant underestimate is seen for propane and ethane. In the "Brazil-E" region during the TRACE-A campaigns the same picture is as for CO is observed: Too low mixing ratios in the upper and agreement in the lower troposphere. Again, the representativeness of these data is questionable due to sampling in convective outflows. Comparison of with PEM-Tropics A and B campaigns (not shown) which took place during September and March/April over the southern Pacific Ocean (40°S-0°) does not reveal a systematic over or underestimation of the model. It is interesting to note that over the Amazon basin during the ABLE–2A campaign (not shown) propane mixing ratios are underestimated by a factor of 3–7 (100–200 pmol/mol observed, versus about 30 pmol/mol calculated). The campaign took place at the beginning of the dry season and generally
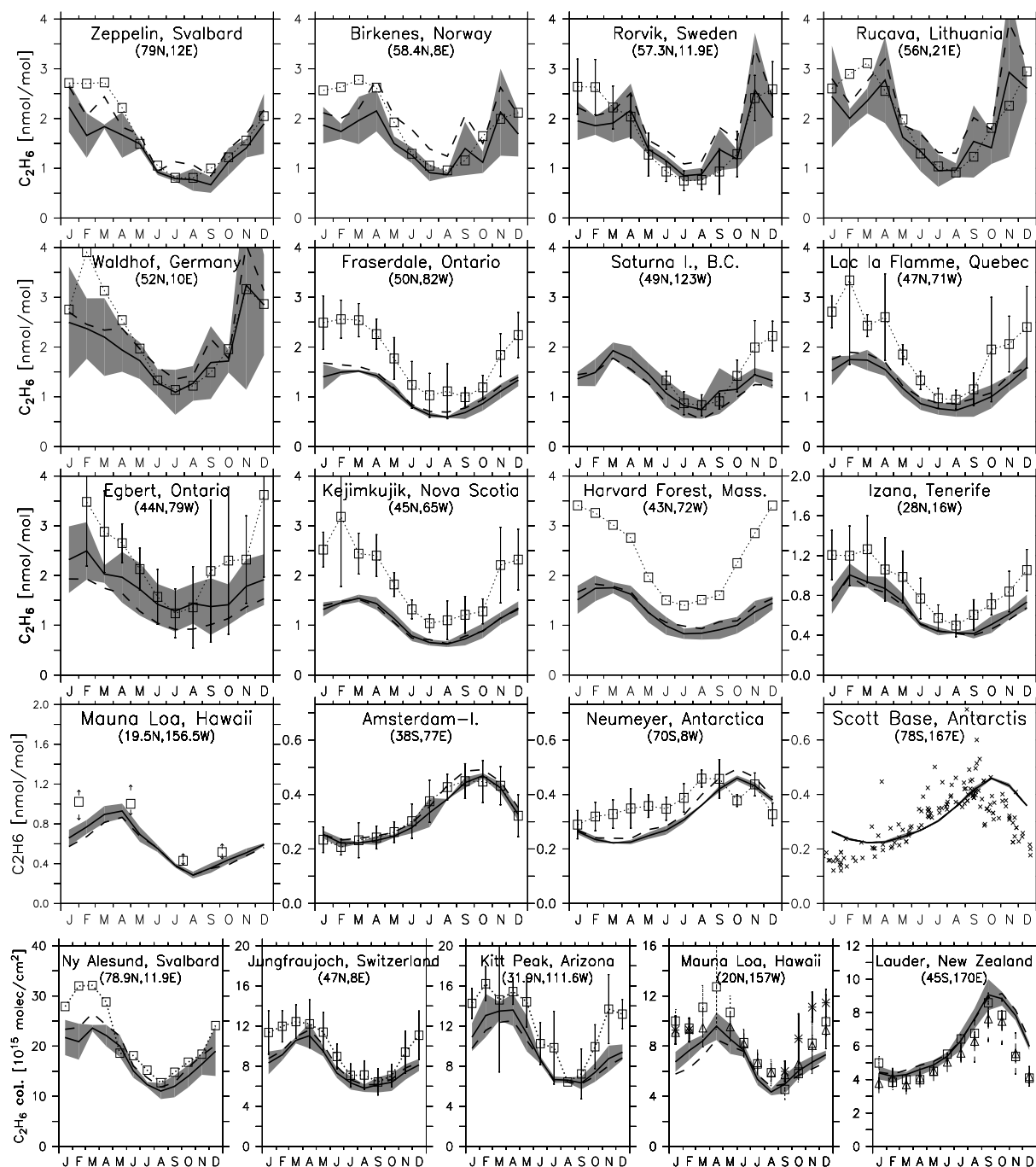
Figure 3.11: Measured and simulated ethane surface mixing ratios and column abundances (last row). Monthly mean measurements are shown as symbols and dotted lines. High and low resolution run are solid and dashed lines. Error bars and shaded areas indicate standard deviations of measurements and model, respectively. Surface data are from *Solberg et al.* (1996); *Lindskog and Moldanová* (1994); *Bottenheim and Shepherd* (1995); *Goldstein et al.* (1995); *Wang et al.* (1998c); *Greenberg et al.* (1996); *Touaty et al.* (1996); *Rudolph et al.* (1989); *Clarkson et al.* (1997) and column data from *Notholt et al.* (1997); *Rinsland et al.* (1998, 1999, 2000). At Scott Base individual measurements are marked by crosses. Arrows at Mauna Loa indicate 25th and 75th-percentiles. Different years of column measurements over Mauna Loa and Lauder are shown with different symbols.
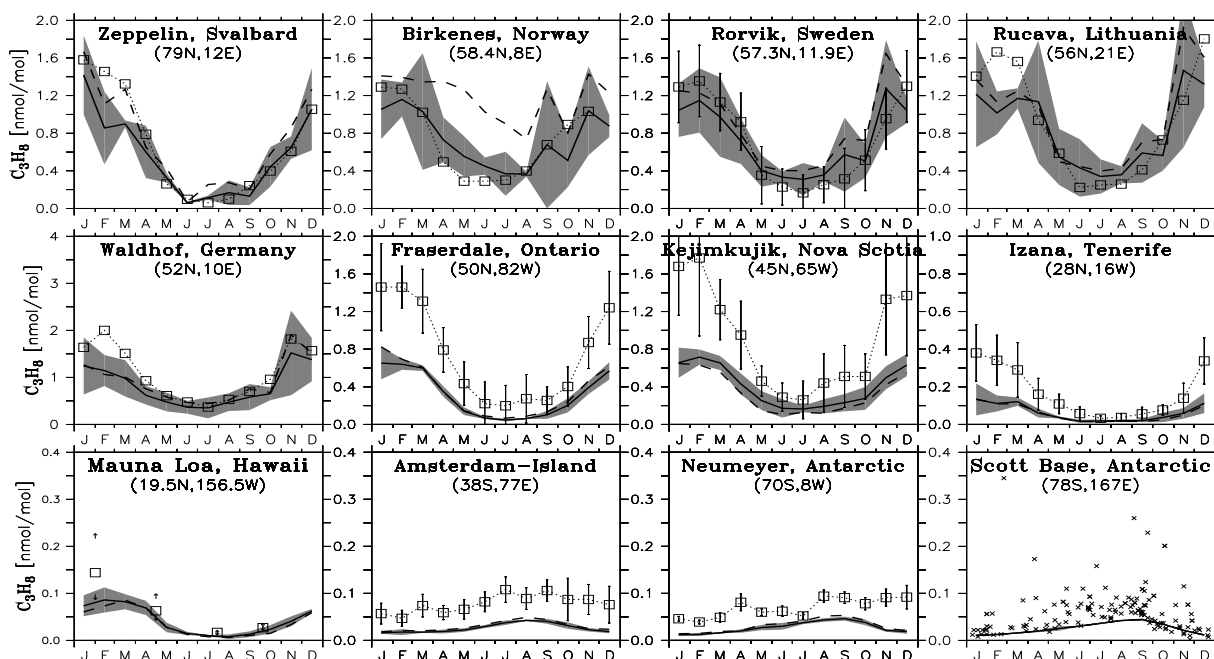
Figure 3.12: Measured and simulated propane surface mixing ratios. Like Figure 3.11.

sampled air not directly affected by biomass burning (*Torres and Buchan* (1988), see also NO and PAN measurements presented in Section 3.5) so that these high levels of propane are suggestive of direct biogenic emissions from the rain forest ecosystem.

3.4.2   Ethene (C_2H_4) and Propene (C_3H_6)

Alkenes are known to contribute to ozone production in polluted environments. Only a simple representation of the two smallest alkenes, ethene (or ethylene) and propene (or propylene), has been included to account for this local effect. The distributions of these two compounds are shown in Figure 3.10 c and d. The calculated mean lifetimes are 2.2 days and 16 hours, respectively. Thus, the distribution mainly reflects the assumed source distributions. It can be seen that biogenic sources (e.g. in Amazonia or South-East U.S.) and biomass burning (Brazil, Africa) are strong contributors to the abundance of these alkenes. At low southern latitudes oceanic influence is also visible, which is in part due to the low OH abundances, but is mainly because the ocean emissions used in this study (*Bates et al.* (1995)) are largest at these latitudes.

A comparison with surface measurements for ethene and propene is presented in Figure 3.14. A seasonal cycle driven by OH with lowest values in summer is seen at most stations. The seasonal cycle in the biogenic emission cannot compensate for the decreased lifetime in summer. As mentioned before comparison of station measurements with short-lived substances is not straightforward. Considering the high degree of variablity, model and observations are judged to be consistent with only a few exceptions. At the remote arctic and free tropospheric stations Zeppelin (near Ny Ålesund) and Izaña both compounds are strongly underestimated. For the Zeppelin measurement, *Solberg et al.* (1996) argued that local biogenic source are the most likely cause for the relatively high values at such a remote site. At some Canadian stations a secondary late summer maximum of ethene can be seen in the model, but not in the observations. This is likely due to the assumed biogenic ethene emissions of 10 Tg/yr. The estimate is highly uncertain
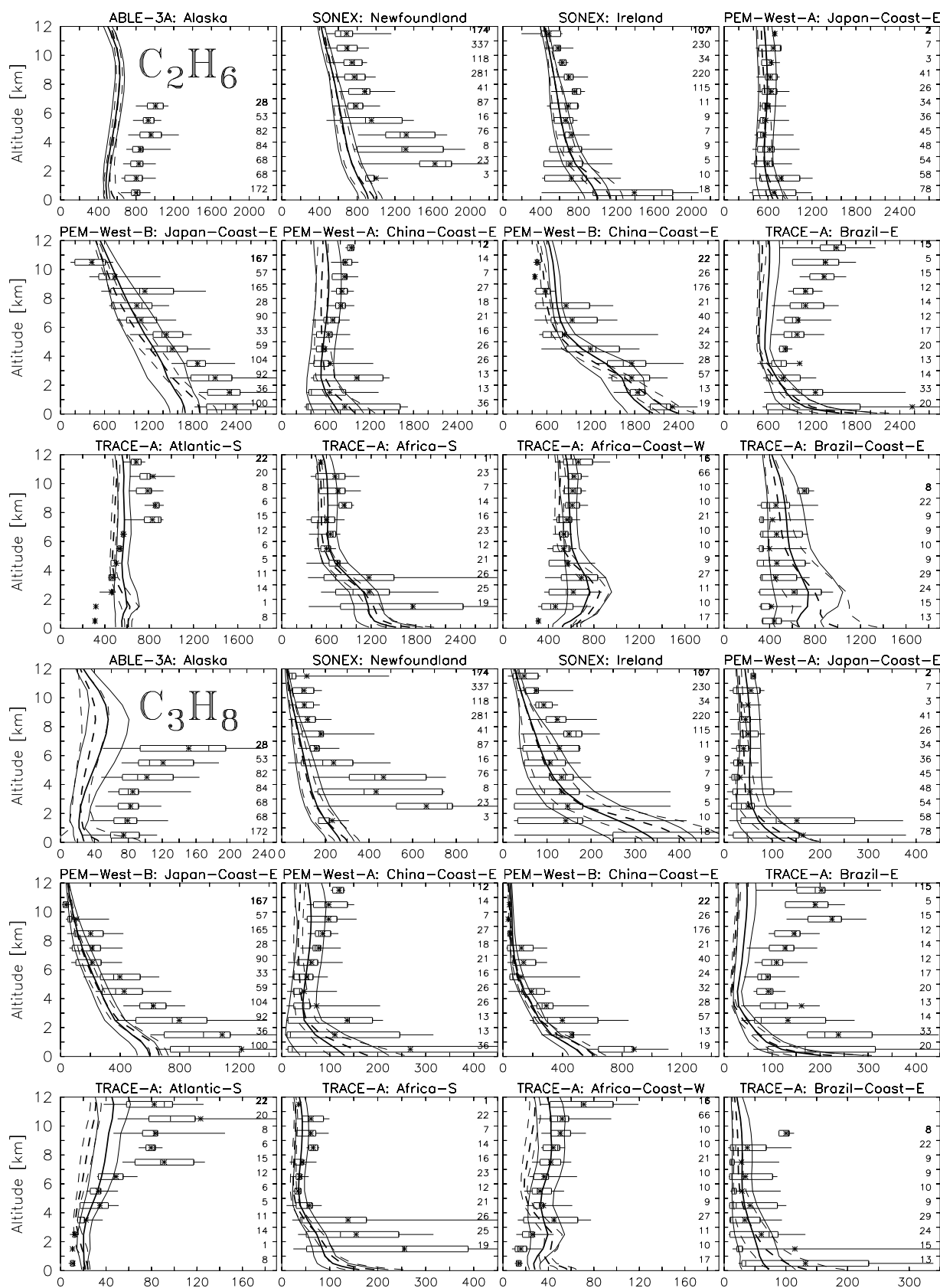
Figure 3.13: Airborne observations of ethane (first three rows) and propane (last three rows) in units of pmol/mol compared to model simulations, as in Figure 3.5.

especially considering the stress induced emissions, and it appears to be too large for the northern American region. On the other hand, the model is consistent with the few measurements made in South America at strongly biogenically-influenced sites. In the Amazon basin the model predicts about 1.3 nmol/mol of ethene and 0.2 nmol/mol of propene, in agreement with the observations (*Greenberg and Zimmerman* (1984); *Zimmerman et al.* (1988)). Compared to measurements in Venezuela (*Donoso et al.* (1996)) C_2H_4 is slightly overestimated at some stations or seasons (e.g. Buja: 0.9 nmol/mol simulated versus 0.6±0.3 observed), but too low at others (e.g. Calabozo in September: 0.8 versus 1.5 nmol/mol). Simulated propene appears to be mostly lower than the observations. However, due to problematic representativeness of these stations and too coarse model resolution no firm conclusions can be made at this point.

There are also measurements of alkenes from ship cruises (e.g. *Bonsang and Boissard* (1999) and references therein), but *Donahue and Prinn* (1993) suspect that many observation using canister samples, which yielded significantly higher values than in situ measurement techniques, suffer from systematic problems. Even only comparing to in situ observation (e.g. *Donahue and Prinn* (1993), during the SAGA 3 campaign) shows that the model is usually lower than observations by more than a factor of 2. The typical ranges found by *Donahue and Prinn* (1993) over the Pacific near the equator for ethene and propene were 30–100 pmol/mol and 20–80 pmol/mol, respectively, whereas the model shows only 10–20 pmol/mol and 2-6 pmol/mol. Thus, even the 90% upper limit of the emission estimate of *Plass-Dülmer et al.* (1995) applied in MATCH appears to be too low, or the latitudinal distribution assumed in this study is too much weighted toward the southern low latitudes.

Airborne measurements have also been made during several campaigns. The problem of representativeness is even more severe for these measurement. Therefore only the general picture obtained by the comparison is discussed here.

The ethene observations during ABLE-3B over Canada, PEM-West A+B and TRACE-A are reasonably well reproduced (not shown). This is especially interesting for the biomass burning regions in Brazil and South Africa and supports the emission ratios used for the alkenes, which were taken from *Andreae and Merlet* (2000). The vertical profile is more sensitive to the different vertical transport characteristics of the two resolutions and upper tropospheric concentrations of ethene over the biomass burning regions are overestimated by the high resolution run, whereas the low resolution run is in agreement with the observations.

Measured mixing ratios of propene in the free troposphere are very low (<10 pmol/mol, probably close to the detection limit). The model produces a pronounced C-shaped profile over source regions whereas the measurement appear to be more uniform. This could indicate too weak mixing in the updraft calculated by the convection scheme. When larger amounts are seen in the measurements the magnitude is correctly simulated by the model.

3.4.3 Isoprene

The important role of isoprene in atmospheric chemistry was already introduced in Section 1.2. Its source strength exceeds those of any other biogenically emitted compound known so far. The most important sink of isoprene is reaction with OH (85%), but reactions with ozone (11%) and NO_3 (4%) are also non-negligible. It is also noted, that biologically mediated loss of isoprene to different types of soil was also observed (*Cleveland and Yavitt* (1997)), but a first extrapolation to the global scale resulted in only about 20 Tg/yr compared to 300-500 Tg/yr of direct emissions. Recently, *Sanhueza et al.* (2001) could infer from surface measurements
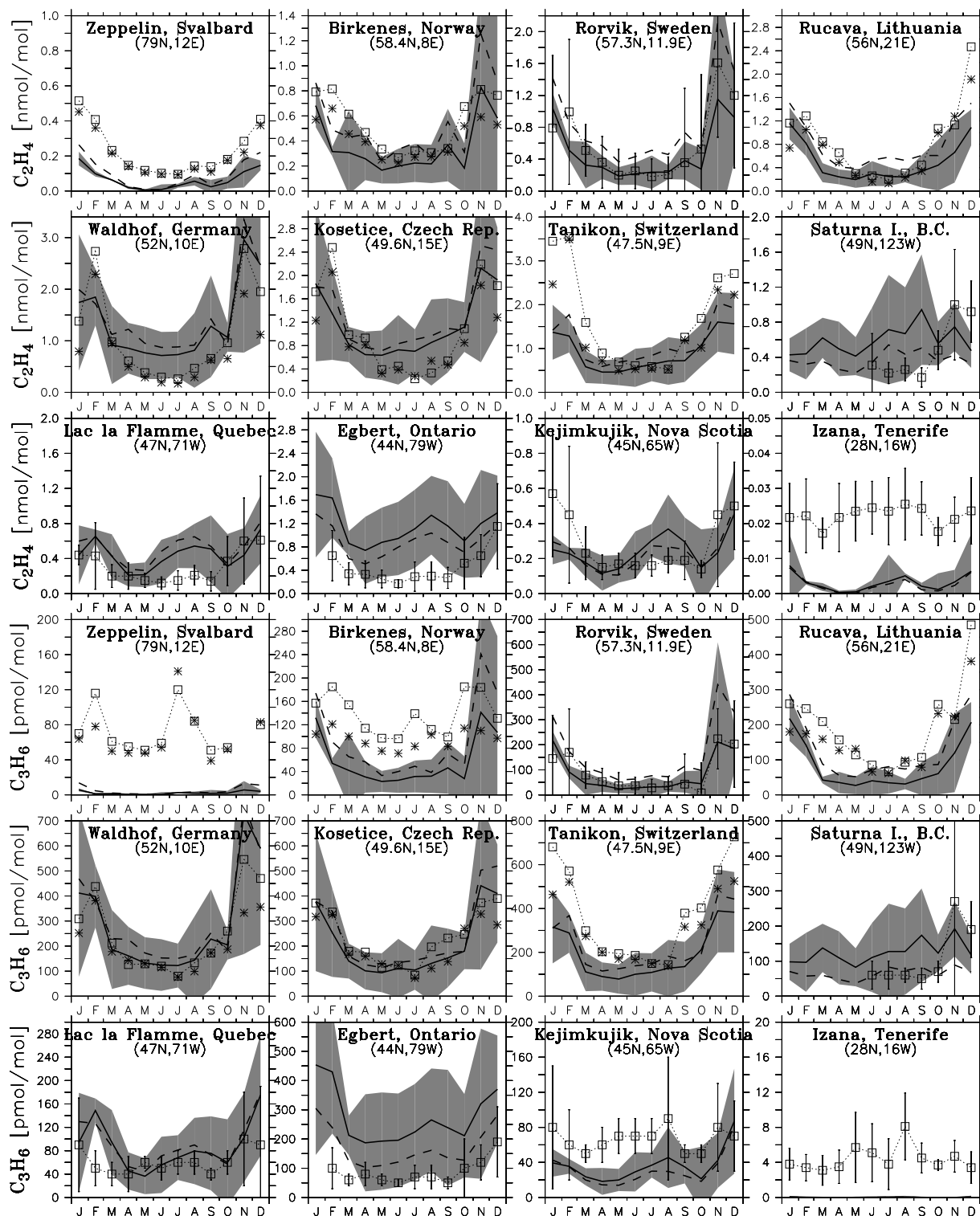
Figure 3.14: Measured and simulated ethene (C$_2$H$_4$, first three rows) and propene (C$_3$H$_6$, last three rows) Symbols and lines like in Figure 3.11. Additionally to means (square), also median value (star) is shown for some stations.

made at a savanna site in Venezuela and box model calculations that deposition of isoprene and its oxidation products methyl-vinyl-ketone and/or methacrolein, not accounted for in present models, must be a significant loss process for these compounds at this site.

The monthly (24h-averaged) surface distribution of isoprene is shown in Figure 3.15 for January and July. Due to its short lifetime of a few hours the distribution closely follows the emissions shown in Figure 2.4. Maximum values of 13 nmol/mol are shown in the central Amazon basin. Even higher maximum values of up to 27 nmol/mol are found in both runs for other months. It is noted that these results are obtained with a reduced source strength of isoprene of 350 Tg(C)/yr compared to *Guenther et al.* (1995) (500 Tg(C)/yr) and the procedure to emit isoprene with an even mixing ratio over the PBL height.

Even more so than for the other alkenes, comparison of measurements of isoprene at single locations is problematic due to the coarse model grid and small scale horizontal variations in its concentration. Nevertheless, the ensemble of model/measurement comparisons can give indications on general tendencies of the model to over or under-predict concentrations in certain ecosystems. A compilation of available surface measurements along with model predictions is listed in Table 3.5. It is noted that the model values are 24h averages, whereas the measurements are usually made during daytime. From box-model simulation one can estimate that the 24-average value is about 50-75% of mid-day concentrations.
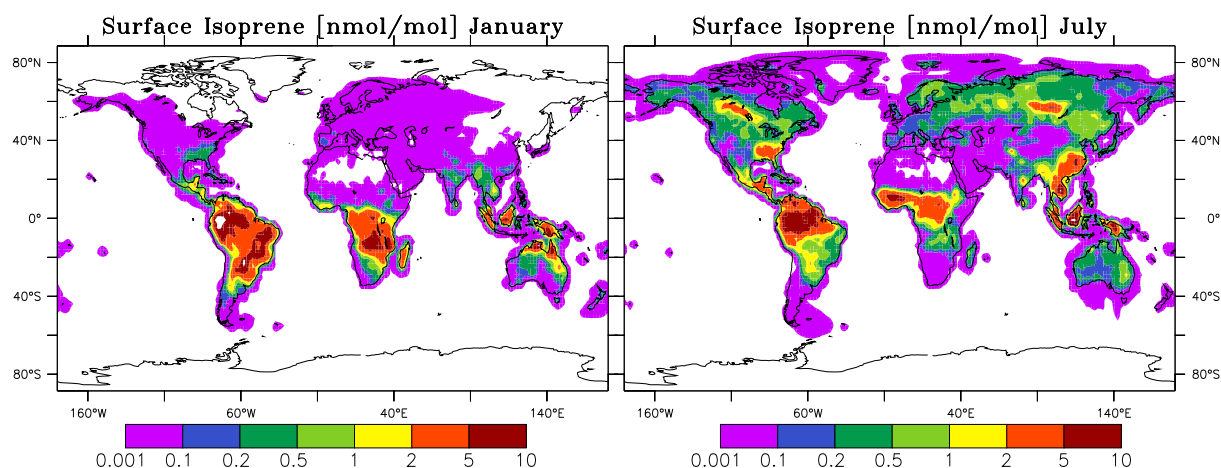

Figure 3.15: Mean (24h-averaged) isoprene surface mixing ratios for January and July. White spots over Amazonia are values above 10 nmol/mol.

The model appears to be in basic agreement with measurements made in North America. Measurements in Japan are expected to be higher, since the model grid-cells actually also contain an oceanic fraction. The values in the Georgian Republic are obtained in a coniferous forest on the southern slopes of the Caucasus Mountains, which might not be representative of the larger area. The model significantly overestimates mixing ratios found in the central Amazon region, sometimes by a factor of 3 or more. The Amazonia sites are probably quite representative of the region, since no major inhomogeneities in the vegetation are expected. The situation is different for the Peru site. It is located in a region where a strong horizontal gradient in isoprene is calculated by the model with mixing ratios below 1 nmol/mol to the west to more than 10 nmol/mol east of the site (within 2-3 grid cells even at the higher resolution). If the model value is obtained from interpolation of adjacent grids to the exact position of the site a

Table 3.5: Comparison of observed isoprene mixing ratios (in nmol/mol) with model calculations. 24-hour means are marked with "24h", otherwise daytime values are reported. Model values are monthly (24 hour) averages. In brackets maximum and minimum of single measurements.

Location	Time	Lat.	Lon.	Observations	T63	T21	Reference
Canada, Egbert	July	44	-79	0.5	0.3	0.4	Bottenheim and Shepherd (1995)
, Kejimkujik	July	45	-65	2.0	0.2	0.3	Bottenheim and Shepherd (1995)
, Fraserdale	Jul.-Aug.	50	-82	0.5-5	0.5	0.4	Jobson et al. (1994)
Niwot Ridge	Aug.-Sept.	40	-105	0.6 (0.2-1.8)	0.2	0.1	Greenberg and Zimmerman (1984)
	Nov.	40	-105	0.1(0.03-0.2)	0.04	0.04	Greenberg and Zimmerman (1984)
Georgian Rep.	Summer	42	43	1.4 (max. 6)	0.2	0.2	Shaw et al. (1983)
Japan	July, 24h	38	140	0.3	0.2	0.1	Yokouchi (1994)
	Nov, 24h	38	140	0.2	0.02	0.01	Yokouchi (1994)
Alabama	Jun.-Jul., 24h	32	-88	3.8 (1-7)	2.9	2.4	Montzka et al. (1993)
Amazonia	Jul.	2	-60	2.2 (1.2-3.2)	6.7	11.0	Rasmussen and Khalil (1988)
Amazonia	year-round	2	-60	2.4 (1.0-5.2)	6.1	9.0	Greenberg and Zimmerman (1984)
Amazonia	Jul.-Aug.	-2	-60	2 (1.1-2.7)	6.4	14.5	Zimmerman et al. (1988)
Peru	July	-5	-77	3.3	10.3	15.6	Helmig et al. (1998a)
Venezuela, Buja	Sept.	9	-62	3.3	3.8	3.0	Donoso et al. (1996)
, Auyantepuy	Apr., 24h	6	-62	1.6	1.9	3.1	Donoso et al. (1996)
, Calabozo	Sep.-Oct.,24h	9	-67	0.8 (0.2-3.1)	5.9	7.8	Sanhueza et al. (2001)
, Calabozo	Mar.-Apr.,24h	9	-67	0.5 (0.1-1)	0.5	0.5	Sanhueza et al. (2001)
, Parupa	Jan.-Feb.	6	-62	0.5 (0.1-1.2)	1.2	2.3	Sanhueza et al. (2001)
Surinam (PBL)	Mar.	2-7	-54-58	3.5 (0.5-7)	2.8	2.5	Warneke et al. (2001)

smaller value (5.7 and 5.2 nmol/mol for T63 and T21 run, respectively) is found than given in Table 3.5. Since the measurement site is well within the primary rain forest the value of the next grid cell to the east is used here instead. Both methods yield a significant overestimation compared to the daytime values of *Helmig et al.* (1998a).

Vertical profiles of isoprene have been reported by *Helmig et al.* (1998a); *Andronache et al.* (1994), and *Warneke et al.* (2001). The modeled steep gradient with values of less than 5% of the surface mixing ratio at 1.5 km altitude are consistent with the first two studies. Over Surinam (LBA-Claire campaign), however, the decrease in the model is much too fast and only about 100 pmol/mol are left at about 2.5 km, whereas the observations are still above 1 nmol/mol up to 4 km (*Warneke et al.* (2001) during the LBA-CLAIRE[6] campaign). These measurements, made with the PTR-MS[7] technique, however, only give information on the mass of the molecules. The mass signals then have to be attributed to molecules that can be expected under those condition (see e.g. *Williams et al.* (2001)). Although the full signal at mass 69 was assumed to be isoprene, other minor contributors may be possible. Therefore, an uncertainty of 0.5 nmol/mol has been assigned to these measurements (*Warneke et al.* (2001)). Even with this uncertainty, it appears that the shallow convection reaching up to about 4 km altitude often encountered during the campaign is not reproduced by the model, which can be seen in the stronger than observed decrease with height (not shown).

Mixing ratios of isoprene sometimes well above 1 nmol/mol have been observed during the LBA-Claire campaign at about 11 km altitude, provided no other substance is contributing significantly to mass 69. The model only reaches maximum mixing ratios of up to 120 pmol/mol over Surinam (at T63), but can reach nmol/mol levels over the central amazon basin. Note that the T21 run produces much smaller isoprene mixing ratios in the upper troposphere (about 100-300 pmol/mol over the same region) due to the difference in convective pumping between the two runs.

Despite the problems mentioned with the comparison of such a short lived compounds, we conclude that calculated isoprene mixing ratios are too high over the rain forest regions of South America. More vigorous vertical mixing in the boundary layer could help to reduce the discrepancy but it would probably also produce even higher concentrations in the upper troposphere, which appear to be unrealistic, at least for the high resolution run. Especially considering that *Jacob and Wofsy* (1990) assumed an uptake of isoprene through the leaf stomata, but no experimental confirmation of this is available.

The overestimated isoprene concentrations over the Amazon region has also been found in other studies (*Houweling et al.* (1998); *Granier et al.* (2000)) and appears to be an unsolved problem in current research of biosphere-atmosphere interactions. The uncertainties regarding this compound are still very large and more observations are clearly needed to resolve the problem.

---

[6]Cooperative LBA Airborne Regional Experiment (LBA: Large-scale Biosphere-Atmosphere experiment).
[7]Proton-Transfer-Reaction Mass Spectrometer

3.5 Nitrogen-Species

Nitrogen oxides ($NO_x=NO+NO_2$) play a central role in atmospheric chemistry (see Chapter 1) in controlling destruction and production of ozone and influencing OH. Their abundance in the atmosphere is also linked to a number of temporary reservoir species (e.g. PAN, HNO_3 or other organic nitrates). Accurate understanding and simulation of the distribution of these reactive nitrogen species ($NO_y = NO_x + NO_3 + 2 \cdot N_2O_5 + HNO_4 + PAN$ + other organic nitrates) is therefore a key to understanding present and future impacts of human activities on the atmosphere. This is also underlined by the fact that responses of ozone production to changes in NO_x are highly non-linear (e.g. *Liu et al.* (1987); *Lin et al.* (1988)).

The basic chemistry of nitrogen compounds was reviewed in Sections 1.1 and 1.2. In order to get a better overview on the dominant processes, some budgets and the distribution of the most important compounds are presented next, before an extensive comparison to observations is shown in the subsequent subsections.

3.5.1 The Distribution and Budget of Nitrogen Species

Table 3.6 shows the annual mean tropospheric burden of all nitrogen containing compounds included in the chemical mechanism. Results from a sensitivity simulation with an increased rate of the dissociation reaction of PAN are also included and will be discussed further in Section 3.5.4. Clearly, in all simulations PAN is the largest reservoir species for NO_y, followed by NOX (the extended NO_x-family: $NOX = NO_x + NO_3 + 2 \cdot N_2O_5 + HNO_4$) and HNO_3. In the NOX-family NO_2 is the largest contributor (62%), followed by NO (18%) and HNO_4 (17%). ONIT, the organic nitrate pool from higher alkanes is also a significant reservoir. The large difference between the T63 and T21 in MPAN, a PAN–analog from the oxidation of isoprene, is due to stronger convection in the T63 run (see below). The other nitrates from isoprene oxidation are only small contributors to the mean tropospheric NO_y budget, owing to their short photochemical lifetimes (21 and 10 hours for ISON and NACA[8], respectively). For the smaller nitrate NACA (nitrooxy-acetaldehyde), which is formed from ISON upon reaction with OH, the reactivity and photolysis rates are assumed to be the same as for acetaldehyde (CH_3CHO). With this assumption, which also implies a low solubility[9], only 2% of the NACA produced is lost through dry deposition, with the rest releasing back NO_2. Omission of this nitrate would therefore only mildly affect the results, and, considering uncertainty in the chemistry, the loss or fixation of nitrogen by this compound is probably sufficiently represented by ISON alone.

Table 3.6: Tropospheric burden of nitrogen-containing compounds in MATCH (in Gg(N) = 10^9g). "T21-LOWPAN" denotes a run with PAN dissociation reaction increased to the upper limit of the range of uncertainty (see text).

Species	Run	PAN	NOX	HNO_3	ONIT	MPAN	ISON	NACA	NO_y
Burden	T63	257	154	95	33	23	7	3	572
in [Gg(N)]	T21	204	125	81	32	9	6	3	460
	T21-LOWPAN	144	122	80	33	6	6	3	394

---

[8]See Table 2.1 for the list of species.

[9]Assumed equal to that of acetaldehyde.

Table 3.7: Global annual mean tropospheric budget of NO_y and HNO_3. All terms are in Tg(N)/yr.

NO_y		T63	T21	HNO_3		T63	T21
Emissions	NO	43	43	Sources	Transport	0.3	0.4
Wet Deposition	HNO_3	21.4	23.4		NO_2+OH+M	21.8	18.9
	ISON	0.9	1.5		N_2O_5 heterogeneous	13.2	16.7
	total	22.3	24.9		N_2O_5+H_2O (homogen.)	3.7	1.7
Dry Deposition	HNO_3	16.0	13.1		CH_3CHO+NO_3	0.25	0.20
	NOX	3.1	3.7		HCHO+NO_3	0.33	0.24
	PAN	0.6	0.8	Sinks	Dry Deposition	16.0	13.1
	ISON	0.8	0.6		Wet Dep. - Large Scale	19.2	19.3
	MPAN	0.2	0.3		Wet Dep. - Convective	2.2	4.0
	total	20.7	18.6		HNO_3+OH	1.4	1.3
Lifetime (days)	NO_y	4.9 d	3.9 d		HNO_3+hν	1.0	1.0

The lower resolution run predicts less PAN, which is understandable since less convection will lead to less PAN in the UT, where its lifetime is longest. The lower NO_x abundance in the T21 runs is in part also an effect of the corrected wet skin fraction in the T21 simulation, which leads to more efficient dry deposition of NO_2 over the affected regions. A run with the same wet skin fractions as the T63 simulation results in 144 Gg(N) of NOX; the other totals are only slightly affected. The mean tropospheric lifetime of NO_y is higher in the high-resolutions run (about 5 days) than in the lower resolution run, reflecting the tendency in the T63 simulation to store more nitrogen in the long lived PAN.

In order to examine possible reasons for an overestimation of PAN found in comparison with observations (see below) a sensitivity simulation has been performed ("LOWPAN"), in which a two times faster decomposition rate[10] of PAN is used in accordance with the range of uncertainty given in *DeMore et al.* (1997) and *Tyndall et al.* (2001). Although the resulting burden of PAN is reduced by about 30% compared to the corresponding standard simulation it is still the most abundant nitrogen-species in the troposphere. NOX and HNO_3 are only slightly affected.

The loss pathways for NO_y from the atmosphere are listed in Table 3.7. Here, HNO_3 plays the key role, with a calculated 85% of the total loss occurring via deposition of this compound. This number, however, also includes a fraction of loss occurring through deposition of aerosols. For the hydrolysis reaction of N_2O_5 on sulfate aerosols it was assumed that the HNO_3 is released back to the gas phase. In reality also a fraction of the aerosols could deposit directly before re-releasing HNO_3. Also, it has been argued in Section 2.3.5 that the estimate of wet deposition of highly soluble species such as HNO_3 is likely on the high side, so that the fraction given above can be regarded as an upper limit.

Due to its importance in removing reactive nitrogen from the atmosphere a more detailed budget of nitric acid is also shown in Table 3.7. Gas phase production via reaction of NO_2 with OH and the heterogeneous pathway are dominating the production terms. However, homogeneous production (recently found to occur by *Wahner et al.* (1998)) is also a non-negligible term, being larger than each of the two photochemical loss terms (via OH and photolysis). These terms may also be compared with the much faster exchange rates within the NO_x-family (NO→NO_2,

---

[10]For reaction R87 in Table A.1 k_{87} = k_{79} / $4.5 \cdot 10^{-29}$exp(-14000/T) was used.

$NO_2 \rightarrow NO$) which are globally averaged (in the troposphere) about 5000 Tg(N)/yr in both directions. The budget of HNO_3 also implies that the annual global mean lifetime of nitric acid against photochemical oxidation is about 14 days, whereas its lifetime against dry and wet deposition is only about 2.5 days. In the tropics the lifetime of HNO_3 against rainout can even be below one day (see e.g. *Brasseur et al.* (1998)). It is interesting to note that globally averaged large scale precipitation is the dominating pathway of nitric acid wet deposition (90%). In the tropics (20°S–20°N) convective core precipitation[11] has a larger contribution to total wet scavenging (18%).

The production and loss terms of PAN (not listed) are dominated by the fast equilibrium between the PA-radical (peroxy-acetyl radical, CH_3CO_3) and PAN (about 150 Tg-N/yr in each direction). Photolysis and reaction with OH have only 1% and 0.1% of this turnover. However, in the upper troposphere above 340 hPa ($\sigma < 0.341$) photolysis is the dominant pathway (93%) and reaction with OH (5%) and thermal decomposition (2%) account for the rest.

It is also interesting to determine the fraction of NO_y which is exported out of the main source region. For the T21 run it is calculated that only about 19% of the emissions into the continental PBL ($\sigma > 0.778$, continents defined by the model's land/sea mask) are exported out of this region and the rest is lost from the atmosphere via the pathways described above. Note that the net export is put in relation to the emission strength, which means that some import is not accounted for in the estimate. The fraction is not very different when calculated for the continental troposphere (16%) or the continental boundary layer of the U.S. (17%). The latter value is in good agreement with a corresponding total of 16.2% obtained by *Horowitz et al.* (1998) in a regional modeling study.

The distribution of NO_x for two months is shown in Figure 3.16. The largest concentrations are simulated during winter in the industrialized regions of the NH. The impact of biomass burning is also visible in both months in Africa. Enhanced mixing ratios in the north Atlantic and Pacific are due to ship emissions. In other regions of the oceans mixing ratios of NO_x are very low (few tens of pmol/mol or lower). While the zonal mean mixing ratio of PAN usually increases with height, NO_x concentrations mostly show a "C"-shaped profile. This can be explained by surface emissions that are efficiently converted into PAN and also to other nitrogen-reservoirs (e.g. HNO_3, HNO_4, ONIT) moving to higher altitudes and by stratospheric influx, and lightning NO_x and a longer lifetime of NO_x in the upper troposphere. Especially during winter (NH) in the middle and upper troposphere nearly all reactive nitrogen is in the reservoirs as opposed to summer when higher NO_x concentrations are seen. Lightning, which more intense during the summer season also helps maintaining this seasonal cycle.

The zonal mean distribution of PAN depicted in Figure 3.17 mainly reflects its increasing lifetime with altitude and the distribution of its precursors. The low resolution run differs significantly from that distribution. Surface PAN mixing ratios are higher in the regions where the maxima are seen in Figure 3.17, but less PAN is found in the UT: about 270 pmol/mol in the zonal mean compared to about 400 pmol/mol in the T63 run in July. The effects from smoothing of the non-linear chemistry in the T21 run should actually lead to higher PAN production, since the precursors (NO_x and hydrocarbons) are more efficiently mixed. The higher PAN concentrations in the UT at T63 resolution are therefore most likely due to more efficient vertical transport. In turn this indicates that a realistic representation of vertical transport is an important factor in calculating upper tropospheric PAN concentrations.

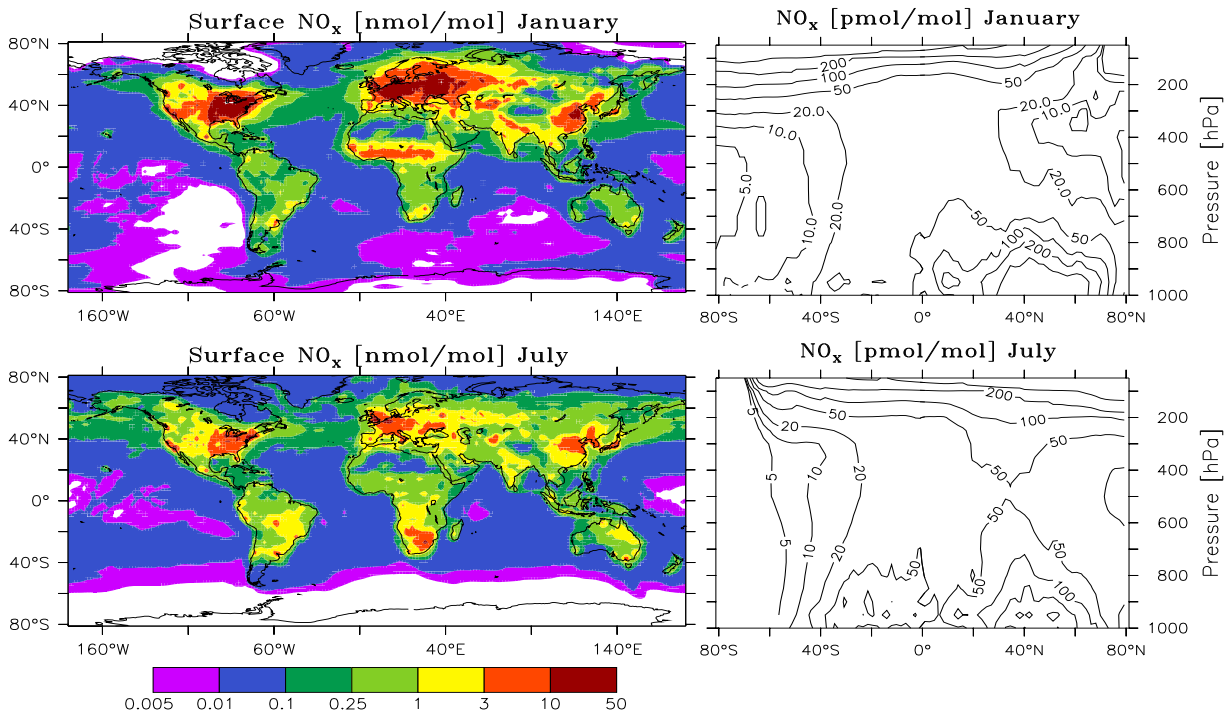[11]Note that precipitation from convective anvils is actually counted as "large scale" precipitation.

Figure 3.16: The simulated surface (left) and zonal mean (right) distribution of NO_x (from the T63 run) for January and July.
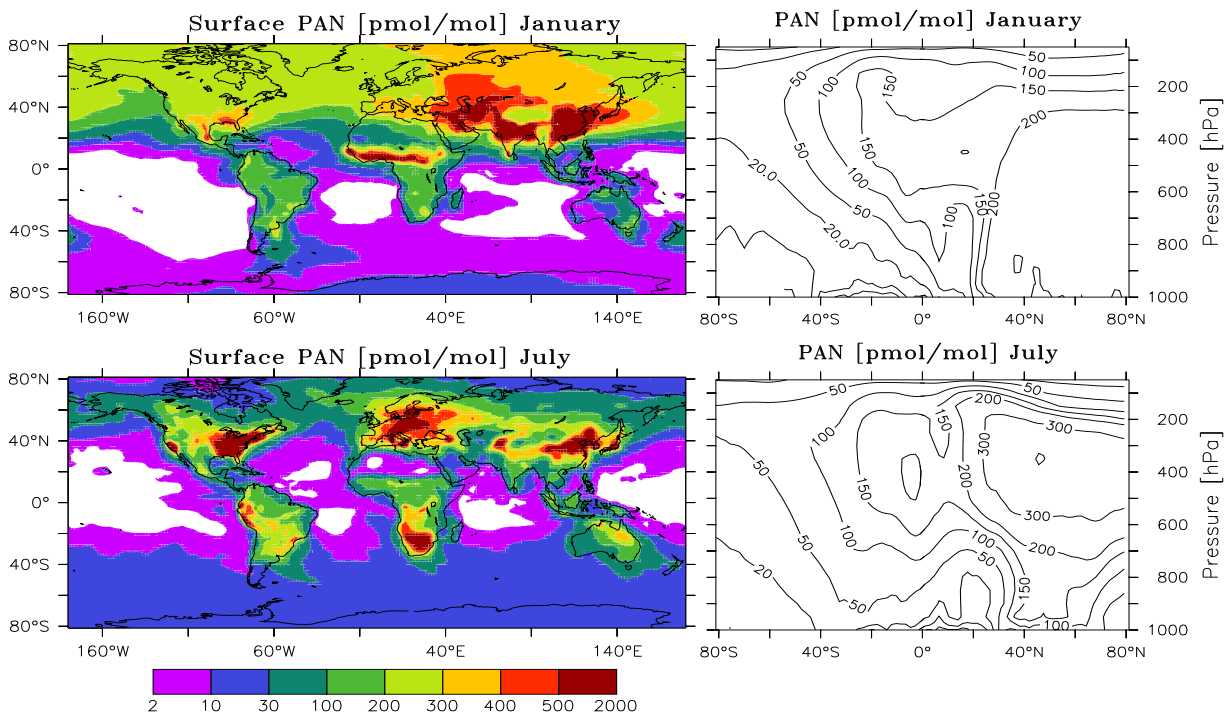

Figure 3.17: The simulated surface (left) and zonal mean (right) distribution of PAN (from the T63 run) for January and July.
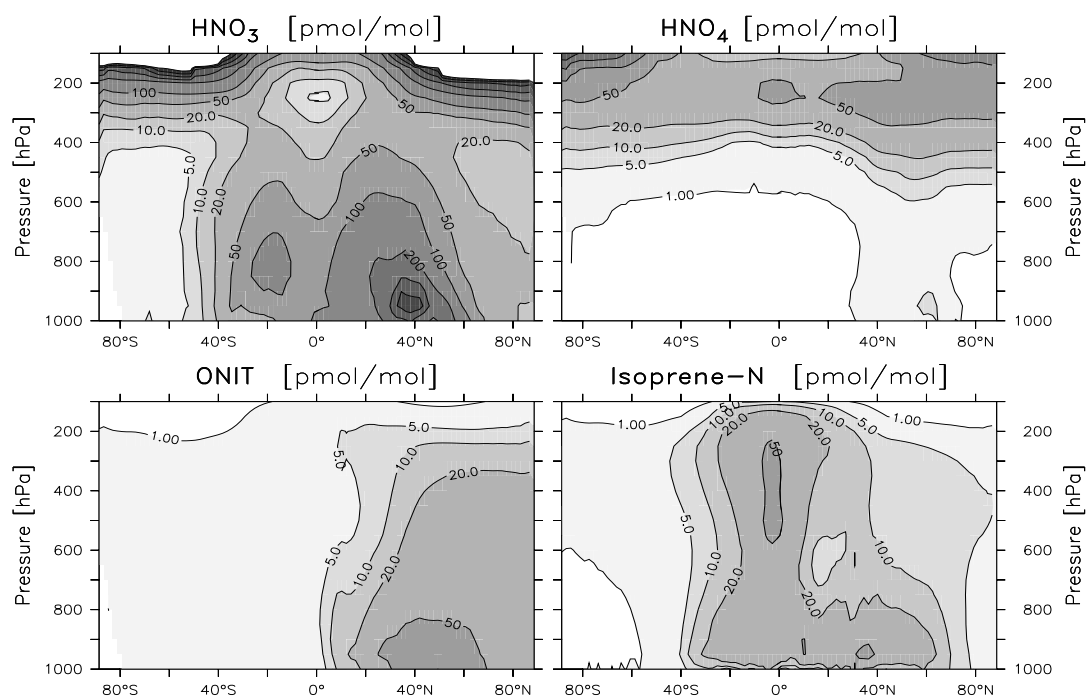
Figure 3.18: The annual zonal mean distribution of other nitrogen containing compounds. Isoprene-N denotes the sum of the compounds ISON, MPAN and NACA.

For the other nitrogen containing compounds only the annual zonal mean is shown in Figure 3.18. The distribution of HNO_3 displays a minimum in the upper tropical troposphere of only 5 pmol/mol. As will be shown in Section 3.5.5 these extremely low concentrations are mainly caused by the scavenging of nitric acid on ice particles in combination with gravitational settling or rainout. Pernitric acid (HNO_4) is transported with the NOX-family and not assumed to be washed out by precipitation. It is thermally quite unstable in the lower troposphere, and therefore appreciable amounts are only calculated in the UT. The alkyl-nitrates, represented by the species ONIT, are mainly formed from the higher-alkanes surrogate C_4H_{10} in the chemical mechanism. ONIT is therefore only found in larger amounts in the northern hemisphere industrialized regions, where these species are mainly emitted. Nitrates from isoprene (ISON, MPAN and NACA) are most abundant where isoprene emissions coincide with sufficient NO_x. Through convection in the tropics more than 50 pmol/mol of these compounds are calculate in the high resolution run. In the T21 run the isoprene-related nitrates only reach about 15 pmol/mol in the zonal mean in the UT, but higher mixing ratios (50 pmol/mol) near the surface. This is another clear sign for the weaker convection in that run and shows the strong implications this can have on the vertical distributions of some species.

3.5.2   Comparison of NO_2 with GOME-Satellite Column Retrievals

Satellite observations of tropospheric constituents are much more difficult than for the stratosphere due to interferences with clouds and aerosols, inhomogeneities in the ground albedo and the stratospheric contributions. While the retrieval of height resolving information on the tropospheric composition will only be available in the near future (see e.g. *Singh and Jacob* (2000)), column integrated abundances of a few species (O_3 NO_2, HCHO, SO_2, BrO) have been retrieved

from the Global Ozone Monitoring Experiment (GOME), and retrieval algorithms are continuing to be improved. A first broad comparison of NO_2 column data provided by *A. Richter* (*Richter and Burrows* (2001)) with MATCH results is presented in this section. The comparison in this study is merely aimed at getting an overview on strong and weak points of the NO_x emissions distributions and their seasonality applied in this study.

The GOME Retrieval and Error Estimate

GOME is installed on the ERS-2 satellite, which is in a sun-synchronous polar orbit that crosses the equator at 10:30 local time. Measurements in middle and low latitudes are therefore always taken in the late morning. Details on the retrieval can be found in *Richter* (1997) and *Richter and Burrows* (2001), and the procedure is only briefly sketched here.

The slant column retrieval uses the Differential Optical Absorption Spectroscopy (DOAS) technique in the wavelength interval 425-450 nm. The stratospheric NO_2 content is removed simply by subtracting the NO_2 slant column calculated for the 180-190° longitude sector, which is assumed to be essentially free of tropospheric NO_2. Another assumption implied by this approach is a zonally symmetric distribution of NO_2 in the stratosphere, which can be problematic near the edges of the polar vortex, especially over the northern high latitudes in winter and spring.

The slant columns then need to be converted to vertical column abundances. The two quantities are linked through the so called air-mass factor (AMF). Its calculation involves several parameters (solar zenith angel, cloud cover, vertical NO_2 profile, aerosol loading and properties and the surface albedo) and further assumptions have to be made in order to constrain them. *Richter and Burrows* (2001) used clear sky conditions, maritime aerosol, a constant surface albedo of 0.05 and a constant mixing ratio of NO_2 within the lowest 1.5 km (zero NO_2 above) to calculate the AMF. If substantial amounts of NO_2 are present in the upper troposphere, the retrieval algorithm would overestimate its contributions (*A. Richter*, private communication, 2001). Only pixels with a cloud cover below 0.1 are used in the data merges provided on a 0.5°×0.5° grid. The error from the slant columns calculation is about $1 \cdot 10^{15}$ molecules/cm^2. The error in the calculation of the air-mass factor calculation is estimated to be up to a factor of 2 for clear sky conditions and most NO_2 residing in the lowermost troposphere (*Richter and Burrows* (2001)), but can easily exceed a factor of 2 when large amounts are present in the upper troposphere (*A. Richter*, personal communication, 2001).

Examples of the GOME NO_2 data are shown in Figure 3.19 for two months. Enhanced column abundances over industrialized regions and typical biomass burning regions are clearly visible. The high values over high latitudes in Siberia in January are probably affected by snow cover, which drastically changes the surface albedo and makes the assumptions for the AMF calculations invalid. Enhanced values south of 40°S in September are probably due to an asymmetry in the polar vortex. The monthly mean data from the period January 1996 – August 2000 are averaged per month in the following comparison in an attempt to smooth the effect of inter-annual variability in biomass burning. Using only the year 1998 (corresponding to the meteorological input data used for the model) was also tested, but the main conclusions remained the same.

MATCH data are only available as monthly means (i.e. day-and-night averages), which means that a "sampling error" needs to be considered when comparing this to the late morning NO_2 values seen by GOME. The factor to correct for this effect, hereafter referred to as the "sampling correction factor" (SCF), depends on several parameters:

1. Length of the day: The shorter the day, the higher the SCF, since all NO_x is in the form of NO_2 during night.

2. Ozone concentration: The more ozone, the lower the SCF. The reaction of O_3 with NO is the dominant pathway for conversion of NO to NO_2 and thus affects the NO/NO_2 ratio during the day.

3. Solar insulation: The more UV radiation, the higher the SCF. Photolysis of NO_2 is the most important process for the conversion of NO_2 to NO and thus also influences the NO/NO_2 ratio. This parameter is also dependent on surface albedo, cloudiness and the solar zenith angle.

4. Vertical distribution of NO_x: The more NO_x resides in the upper troposphere, the higher the SCF. This is because the NO_2/NO_x ratio during day decreases with altitude due to the higher photolysis rate of NO_2 and the negative temperature dependence of the $NO+O_3$ reaction. This results in a lower column integrated value found for NO_2 at 10:30, if large amounts of NO_x are in the upper troposphere (e.g. from lightning).

The combined effects of these parameters is not easy to judge; thus, a globally constant SCF is used here. Through test simulations with MATCH over a few days in January, July, and September with output every hour it was calculated that the SCF can range from 0.4 to 1 for regions with a tropospheric NO_2 column abundance greater than $1 \cdot 10^{15}$ molec./cm^2. In most cases values where about 0.6-0.8. A constant SCF of 0.7 is used in the following comparison, but an uncertainty of about 20-30% cannot be avoided by this procedure. A further problem with determining the SCF is that it is not likely representative for the "clear sky" selection in the GOME data, because under these conditions a smaller NO_2/NO_x ratio would be expected due to a higher photolysis rate of NO_2. A globally averaged "clear sky SCF" is therefore likely lower than the value 0.7 applied here.

Comparison by Region

In Figure 3.20 the ratio of GOME-NO_2 and the model results are plotted for 6 months. The tropospheric column is separated in the model using the same "clean sector" technique as for the GOME data and a correction factor of 0.7 is applied globally. In view of the systematic error in the GOME data only areas are plotted where either GOME or MATCH tropospheric NO_2 columns reached values higher than $1 \cdot 10^{15}$ molec./cm^2. The green colors mark regions where the agreement is within a factor of 2 and thus model and GOME NO_2 are considered to be consistent (see error estimate above). Additionally, the seasonal cycle is depicted at selected coordinates in Figure 3.21 in order to facilitate the discussion. The focus of this discussion is on regions where discrepancies between model and satellite data are seen, and it is attempted to identify the most likely source category of NO_x by inspection of the emission fields.

It is also noted that the results are very similar for the low resolution run, but some results seen in the comparison with the high resolution run are not found in the T21 runs because they are too small to be resolved on the coarser grid.

Europe   While in central Europe the model is only slightly higher than the GOME values, especially in winter, a significant overestimation can be seen over parts of north-eastern Europe.
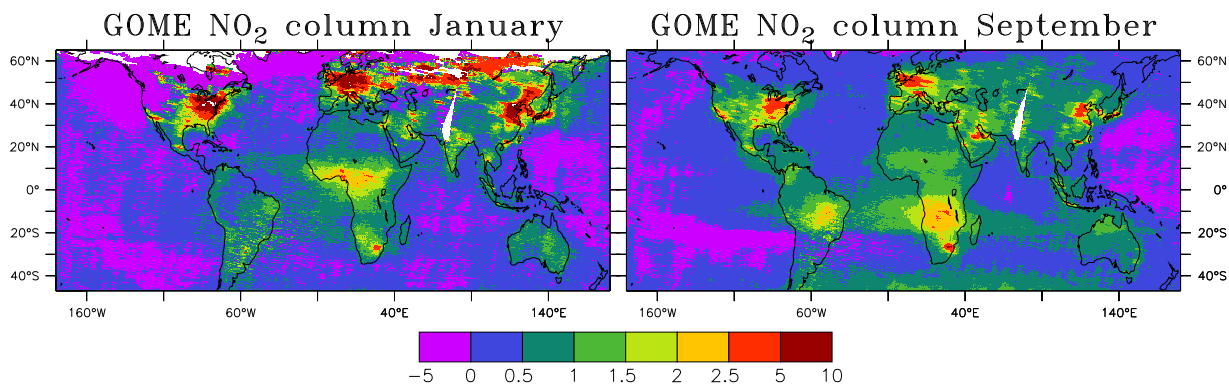
Figure 3.19: GOME tropospheric NO_2 column abundances (in 10^{15}molecules/cm^2). Averages of monthly means from the period January 1996 to August 2000 are shown (January 1998 missing).
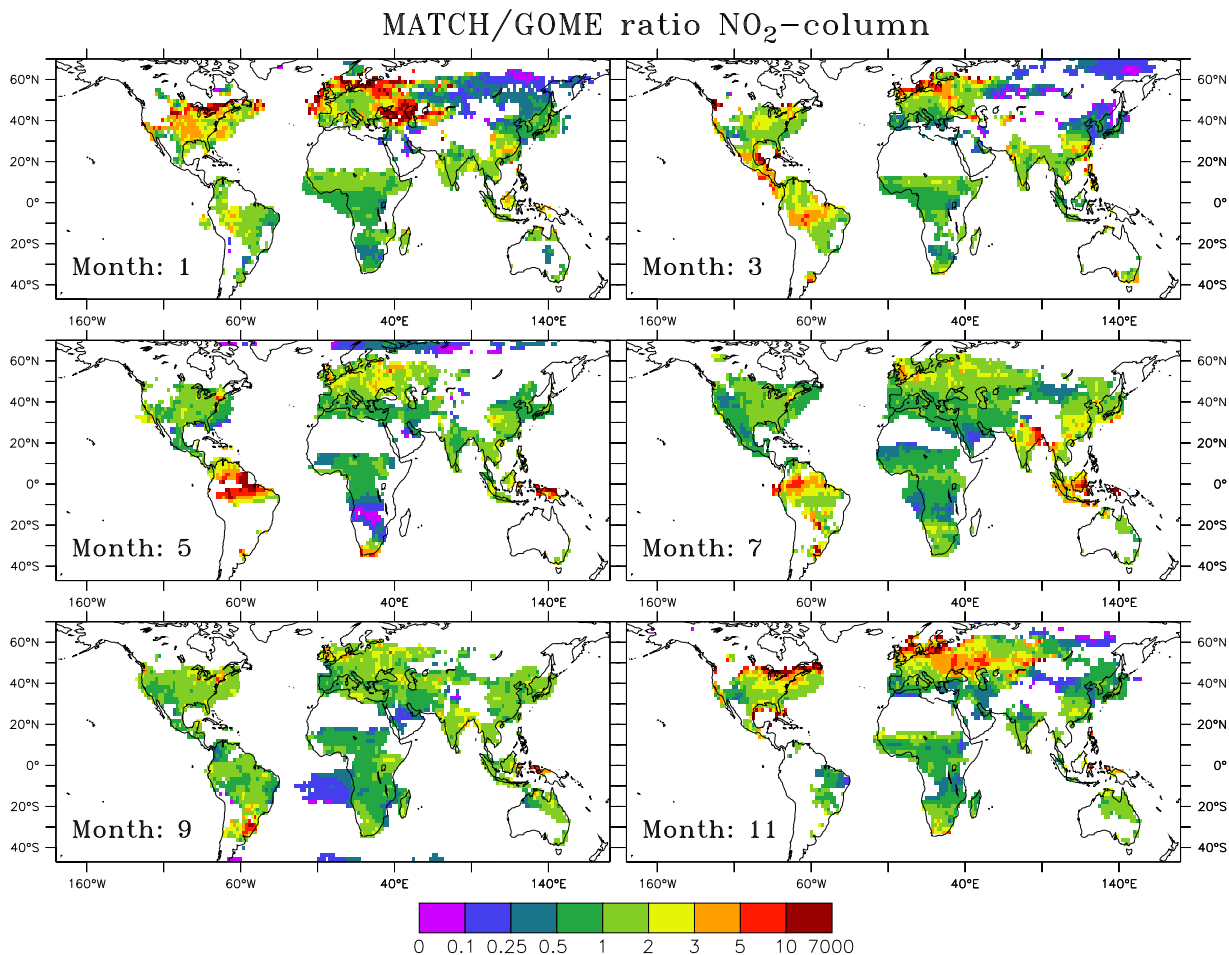

Figure 3.20: Ratio of tropospheric column NO_2 (MATCH/GOME) for January , March, May, July, September, and November. GOME data are means of monthly means from 1996-2000 (January 1998 missing). Only regions are plotted where either GOME or MATCH values are above $1 \cdot 10^{15}$ molec./cm^2.

The emission data for industrial NO_x, taken from the EDGAR database are for the year 1990. It seems that the strong decrease in industrial activities in the former "Eastern Bloc" countries during the 90s are therefore not included in the dataset and lead to this overestimation. The seasonal cycle of NO_x, which in the model is mainly determined by the NO/NO_2 partitioning and the lifetime of NO_x (the industrial emission strength is constant over the year), is very similar to that seen by GOME (1st panel in Figure 3.21).

An interesting point is the strong overestimation (factor 3-10) of MATCH in January over the northern Atlantic west of France. Since westerly winds are dominating in the region, this must be attributed to a local source. Furthermore, a corridor of column NO_2 of more than $0.5 \cdot 10^{15}$ molec/cm^2 is calculated in January over the North Atlantic (at about 45°N-53°N, not shown), whereas GOME only sees background noise (Figure 3.19). The two possible sources are aircraft and ship emissions. Inspecting the source distributions of these sources[12] reveals that the band of enhanced NO_2 columns in the model is clearly caused by aircraft emissions in the North Atlantic flight corridor. Effects of aircraft NO_x emissions in other regions or season are not predicted by the model, probably because this is the region over ocean with the highest emission rate and during winter the lifetime of NO_x is longest. Over continents the effect is masked by other sources. The overestimation east of the Bay of Biscay cannot be unequivocally attributed to one source type, but at least in the southern-most part ship emissions are more likely. Lacking evidence for the effects of ship-NO_x was also suggested by a comparison of marine boundary layer measurements with similar model results (*Kasibhatla et al.* (2000)) and early plume processes not accounted for in large scale models were suspected as a possible explanation. Similar findings were made by *Meijer et al.* (1997), who studied the effect of nitrogen conversion in aircraft exhaust plumes. They came to the conclusion that the perturbation in NO_x can decrease by 15-55% when taking into account plume-processing. The disagreement found here lends support of the hypothesis that plume chemistry of nitrogen compounds can be important for aircraft and ship emissions. These results further underline that more research is needed on sub-grid chemical phenomena.

North and Middle America Like for the most polluted European regions, the seasonal cycle (2nd panel in Figure 3.21) is qualitatively reproduced, but the values obtained by MATCH are on the high side, especially in winter. In the mid-west of the U.S. concentrations are significantly overestimated by the model (about a factor 3).

The overestimated NO_2 columns over Middle America in March (and April, which is not shown) can be clearly attributed to the biomass burning data set, which predicts burning for these months and is the dominant source during this time of the year. Thus, either the total biomass burned is overestimated or the burning season is too short in the *Galanter et al.* (2000) emission data.

Asia Several discrepancies can be seen over eastern Asia. Where strong industrial emissions are found in the GOME data (mainly over north-eastern China), the model results are considerably lower, especially in winter. The bulge in the model calculation in summer correlates well with biomass burning assumed to occur during that time, but it does not show up in the satellite data. This suggests that the burning activity is too high in the *Galanter et al.* (2000) data set, which could also in part be responsible for the overestimated CO seen at the

---

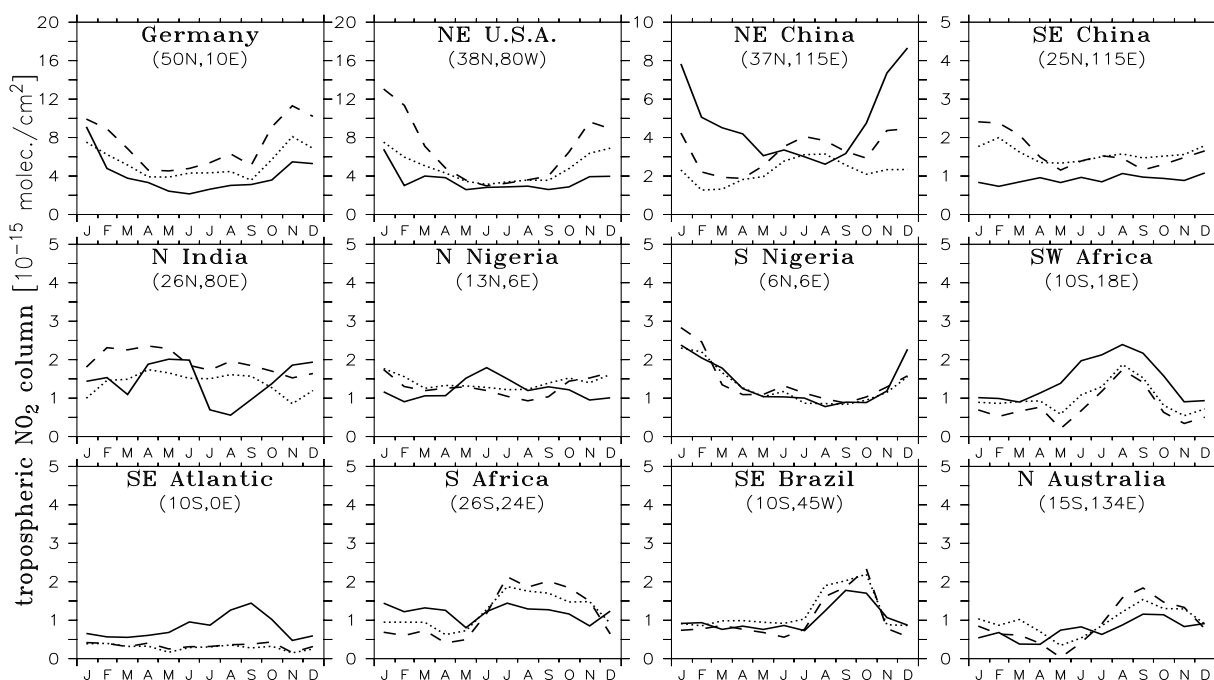[12]For the aircraft emissions see *Lawrence et al.* (1999b).

Figure 3.21: Seasonal variation of GOME tropospheric NO_2 column data (solid line) and model simulation (T63: dashed, T21: dotted line) for selected regions. The GOME values are obtained by averaging over the respective T63 grid cell.

Tae-ahn Peninsula station (Section 3.1, Figure 3.3). On the other hand, in south-eastern China the model overestimates and it appears from a comparison of the distribution of the NO_2-columns that emissions are too evenly distributed over east China in the EDGAR data (see Figure 2.2a). Further question which need to be addressed in this

Africa and South America   In Africa the seasonality and magnitude of the NO_2 columns are in good agreement with the satellite data for most regions. This is a significant improvement over the previously used data set of *Hao and Liu* (1994). In the results from MATCH-2.0 (*Lawrence et al.* (1999b)), which applied the datasets from *Hao and Liu* (1994) much too sharp and too strong maximum columns are found in southern and south-western Africa, the Sahel and also in south-eastern Brazil (not shown). The seasonality of the Hao and Liu *(1994)* data is also not consistent with GOME data, being to late in SW Africa and too early in SE Brazil by about 1 month, respectively. However, some discrepancies are also seen with the emission data from *Galanter et al.* (2000). The burning in the Sahel region during November to February appears to be too high and the underestimate in May in SW Africa (at about 15°S) suggests that the burning season may already start in this month. Lightning, as an alternative explanation, is not seen by the Lightning Imaging Sensor (LIS, *Christian et al.* (1999)) in this region in May.

A very interesting feature in the GOME data is the plume of NO_2 spreading from SW Africa over the Atlantic and, somewhat weaker, also over the Indian Ocean. This plume is not reproduced by the model indicating that the NO_x lifetime is much too short in the model or that a mechanism to convert the main reservoir species HNO_3 and/or PAN back to NO_x is missing. There have been indications of such a mechanism from other measurements (*Chatfield* (1994); *Fan et al.* (1994); *Hauglustaine et al.* (1996); *Jacob et al.* (1996), see also discussion in next

section). *Jacob et al.* (1996) actually conclude based on the TRACE-A measurements in this region during the burning season that a HNO_3 to NO_x conversion in the upper troposphere ($>$ 8 km altitude) on a time scale of 1 day must be present. The model deficiency is especially interesting, because in the same region also enhanced ozone concentrations have been observed (e.g. *Fishman et al.* (1990, 1991, 1996)) which are underestimated by the model (see Section 3.7). Since NO_x and ozone production are closely linked, it is suggestive that the problems encountered are also connected. However, it is also possible that the retrieval algorithm calculates too high column abundances, because a substantial fraction of NO_x was found above 8 km during TRACE-A in that region (see Figure 3.24, 4th row). This is distinctly different from what was assumed for the calculation of the air-mass factor.

A significant overestimation is seen over the Amazon basin from January to August, especially between March and June. During this time only lightning and soil emissions contribute significantly to the NO_x budget in that region, the vertically integrated lightning being more than 2 times higher than the soil biogenic emissions. Inspection of the spatial pattern of the area of enhanced NO_2 columns and these two emission fields suggests that both emission fields, but more clearly the lightning source, contribute to the overestimate. For the anticipated vertical distribution of NO_x (high NO_x content in the upper troposphere from lightning and little NO below) a larger sampling correction than the factor 0.7 applied globally would be required. An SCF of 0.4 is calculated from the aforementioned test runs to be more appropriate in this case. Thus, an additional reduction is needed, which increases the degree of agreement, but still cannot account for the observed difference of a factor of 5 or more, especially considering that the procedure to convert slant columns to vertical columns used by *Richter and Burrows* (2001) should exaggerate the contribution of NO_2 from lightning. Either of the two mentioned sources (or both) must therefore be overestimated in this region. Comparing the MATCH-2.0 results, which applied a total source strength from lightning of only 2 Tg(N)/yr as opposed to the 5 Tg(N)/yr used here, indeed gives better agreement with the satellite data in this region. Comparing the annual lightning NO distribution calculated by MATCH with the annual mean flash density as seen by the OTD[13] sensor (*Christian et al.* (1989)) also reveals that lightning over South America (especially the northern part) is probably too intense compared to lightning over central Africa (*Labrador et al.* (2001)).

These findings clearly show that studying the distribution and source magnitude of lightning should be a rewarding field of research, and could significantly help to better constrain the distribution of NO_x, especially in the upper troposphere.

Indonesia and Australia   Further signs of too high a lightning source (or a too concentrated distribution) can be found over Indonesia when no biomass burning is expected (outside the months July to October). The overestimated grid cells over Borneo and western New Guinea match well with grid points where strong lightning activity is calculated. This holds also for parts of the overestimation over the northern-most tips of Australia. Although not significant (within a factor of 2), it seems from the seasonality in the NO_2 column over northern Australia that the biomass burning predicted mainly for August to October is probably overestimated (Figure 3.21, last panel).

---

[13]Optical Transient Detector

Suggestions for future comparisons with GOME

From the problems encountered during this comparison some suggestions on how to improve upon the significance of such a comparison can be made. On the model side it would be clearly advantageous to write out NO_2 data at the time of overpass of the GOME instrument in order to reduce the overall uncertainty in the comparison. Cloud fractions should also be written out to allow filtering as in the NO_2 data from GOME. Due to the strong implications that our findings could have regarding the African plume it is advisable to further test the effect of using different vertical profiles of NO_2 in the calculation of the AMF e.g. increasing monotonously with altitude or a mid-tropospheric bulge. More efforts are also needed in order to understand the potential bias introduced by the omission of cloudy pixels in the GOME data. Another issue that requires further research is the effect of heavy aerosol loadings on the GOME measurements. In order to investigate the distribution of lightning, GOME pixels with higher cloud fractions (as in *Richter and Burrows* (2001)) should also be used and compared to the lightning distribution in the model or other satellite products. The question of how much NO_2 resides above the clouds could also be addressed by comparing tropospheric NO_2 columns with very high cloud fractions versus the same quantity in the model. Another possibility should also be investigated: Instead of inverting the radiance arriving at the GOME instrument to NO_2 columns it might also be fruitful to calculate the radiative transfer within the model and get as a result the radiance GOME would see. However, much more development and testing would be required for this option.

3.5.3   Surface Measurements

MATCH calculates summer mixing ratios of NO_x over the eastern United States of about 3-10 nmol/mol, which appear to be higher than the range of observations (up to 1-4 nmol/mol, see *Emmons et al.* (1997); *Liang et al.* (1998) and references therein) and values calculated by other global three dimensional models (*Hauglustaine et al.* (1998); *Wang et al.* (1998c)). This could indicate insufficient sequestering of NO_x to reservoir species, e.g. nitrates not considered in the chemical scheme, too weak vertical mixing or too large emissions. A direct comparison with measurements near strong sources, however, is difficult for several reasons. Measurement sites are usually not representative for the area of a typical grid-cell, since cities and surrounding rural areas are not resolved in the model. Furthermore, in this study all industrial emissions are assumed to be constant throughout the day and the year. At least part of these emissions (e.g. from traffic) are expected to have diurnal variations with enhanced emissions during day. The neglect of this could result in an unrealistically strong accumulation of NO_x during night, when vertical mixing and the height of the boundary layer is low. The model indeed displays a very strong gradient in the first few model layers. Non-linear sub-grid chemistry, and potentially splitting errors, could also play a role in simulating mixing ratios of NO_y species near such strong sources. Thus, in light of the these additional uncertainties, neither the emission data set nor the boundary layer mixing can be falsified from such limited comparisons.

Comparison with observations at remote sites is more elucidating. The MLOPEX[14] measurements (*Atlas and Ridley* (1996)) represent a data set from the lower free troposphere with a total of 6 weeks of sampling during all 4 seasons, which should provide a good test of the calculated speciation of nitrogen compounds in the remote atmosphere. In Figure 3.22 a comparison with these measurements in the remote free troposphere at Mauna Loa, Hawaii (*Ridley et al.* (1998))

---

[14]Mauna Loa Observatory Photochemistry Experiment.

is shown. The model is sampled at sigma level $\sigma = 0.633$. The data-set was filtered to include only downslope conditions at Mauna Loa, which are believed to be representative of the free troposphere (*Atlas and Ridley* (1996)). The most obvious discrepancy is found for PAN, while for the other compounds no systematic over- or underestimation is apparent. The model shows a much more pronounced spring maximum for PAN than the observations, and overestimates the mixing ratios by about a factor of 2-3 throughout the year. Ozone during winter and spring is also too high at this site, despite the 50% reduction in the stratosphere-troposphere flux (STF) for O_3 applied in the simulation (see Section 2.3.6). It is thus possible, that part of the overestimate of PAN is due to too efficient downward transport of PAN-rich air from the upper troposphere during this time.

NO_x mixing ratios tend to be on the high side of observations. Unfortunately, the NO_y data may suffer from artifacts from unintentionally converted non-NO_y nitrogen (e.g. HCN, NH_3) to NO during the measurement process so that they have to be interpreted with caution.
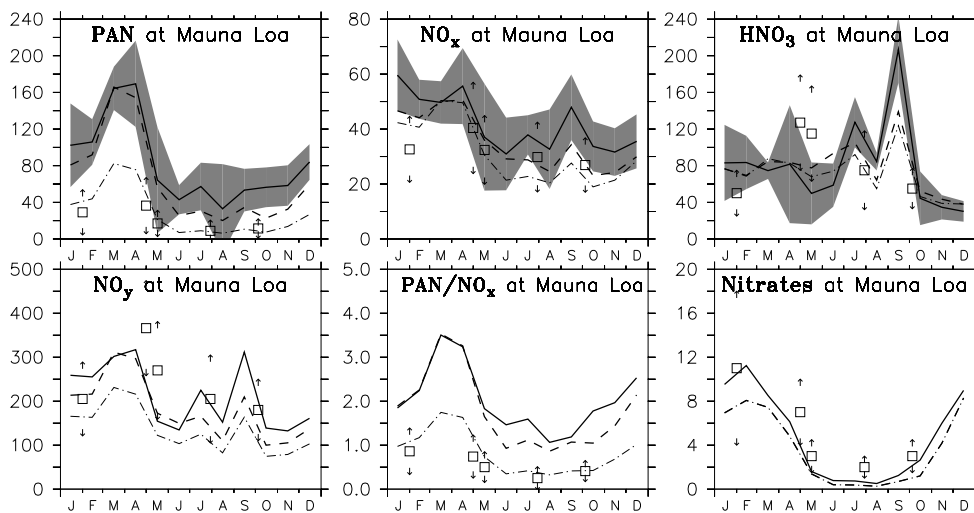

Figure 3.22: Model/measurement comparison of nitrogen speciation at Mauna Loa during MLOPEX 1+2 (*Ridley et al.* (1998)). Solid (shaded area: $\pm\sigma$) and dashed lines are the T63 and T21 standard simulations. Dotted line is simulation with a reduced PAN equilibrium constant (LOWPAN). All values are in pmol/mol.

The MATCH results are markedly different from those found by some previous comparisons with 3D-global simulations (*Kasibhatla et al.* (1993); *Müller and Brasseur* (1995); *Brasseur et al.* (1996); *Hauglustaine et al.* (1998)). While *Brasseur et al.* (1996) calculated too high HNO_3 mixing ratios, supposedly due to the omission of below-cloud scavenging, *Hauglustaine et al.* (1998) could reproduce the measured HNO_3 amounts with an updated version of the same model (MOZART, *Brasseur et al.* (1998)). PAN levels were correctly simulated, but NO_x levels were underestimated by about a factor of 2, and thus the HNO_3/NO_x ratio was strongly overestimated (factor 2-3) in both studies, which is similar to findings with other 3D-model studies (*Kasibhatla et al.* (1993); *Müller and Brasseur* (1995)). To explain the discrepancy additional mechanisms to convert HNO_3 back to NO_x were suspected (see Section 3.5.2). Contrary to this the HNO_3/NO_x ratio in the MATCH simulations is consistent with the observations at Mauna Loa, but PAN is significantly overestimated. The result from the LOWPAN run are in better agreement with the observations, but other problems occur: NO_x and NO_y tend to be too low in summer and

fall, while PAN is still on the high side in spring. Another possible explanation for the low PAN observations was pointed out by *Levy et al.* (1999): PAN mixing ratios at this altitude are strongly influenced by temperature and a local heating effect (the surface type near the station is black lava) might have biased the observations.

The reason for the different behavior of MATCH, especially with respect to the HNO_3/NO_x, which is in better agreement than other 3D global models, is difficult to assess, but differences in the wet deposition formulations, e.g., the coupling of convection and scavenging or uptake of HNO_3 on ice surfaces are the likeliest cause. One aspect of the HNO_3 deposition (the uptake on ice-particles) is further investigated in Section 3.5.5.
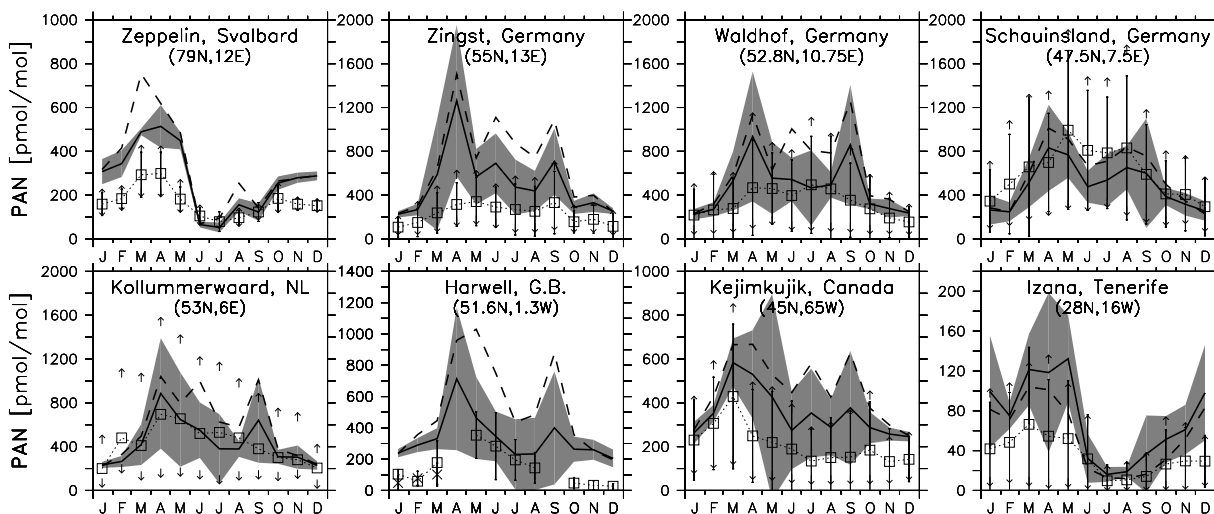

Figure 3.23: Comparison of surface measurements of PAN (squares) with model simulations (T63: solid line with shaded area indicating $\pm 1\sigma$; T21: dashed line, LOWPAN: dash-dotted line). Vertical bars and arrows are standard deviations and 10/90 percentiles of the measurements. At Kollummerwaard arrows are means from the cleanest and most polluted wind sectors. Data are from *Beine and Krognes* (2000); *Umweltbundesamt* (2000); *Roemer* (1996); *Penkett and Brice* (1986); *Bottenheim et al.* (1994) and *Schmitt and Volz-Thomas* (1997).

Comparison of PAN surface data compiled from various publications is presented in Figure 3.23. The seasonal behavior at all sites is reasonably reproduced by the model, but some discrepancies in the absolute mixing ratios are also apparent. The spring maximum at Zeppelin and the free tropospheric station Izaña are overestimated. This also holds for the LOWPAN simulation, which is otherwise in better agreement with the observations. The seasonal cycle of PAN in the high Arctic is likely the combined effect of a winter buildup and a maximum in downward transport in spring, as also seen in the simulation of ozone (Section 3.7). Thus, apart from too much photochemical production of PAN, too strong downward transport could also help to explain the overestimate at Zeppelin. As mentioned before, comparison near strong and inhomogeneous sources is difficult. The agreement found at the four West European stations (Zingst, Waldhof, Schauinsland, and Kollummerwaard) is therefore surprisingly good. Only the data from Zingst, located in a region in north-eastern Germany with relatively little local pollution are overestimated by the model. This can be easily explained by too large an influence of larger cities (e.g. Hamburg) on the model value in that grid cell. The European stations show a broad summer maximum, while the model tends to peak in late spring and late summer. The

model strongly overestimates the observations at Harwell (Great Britain) in wintertime. These measurements were rigorously filtered to represent background conditions (*Penkett and Brice* (1986)), which could explain part of the discrepancy. However, sampling the model at the same latitude but at 20°W over the Atlantic still results in winter mixing ratios which are about a factor of 2 higher than the measurements suggesting that the winter NH background concentrations are too high in the model or that there is a problem with the observations which are significantly lower than the European and Canadian wintertime values. PAN mixing ratios at Kejimkujik (Nova Scotia) are overestimated in summer. The outflow of pollution from the urban areas at the north-east coast of the U.S. (e.g. Boston, New York) mostly occurs only slightly south of Nova Scotia. Sampling the model 5° further north yields mixing ratios that are closer to the observations, but still on the high side.

3.5.4 Airborne Measurements

Airborne measurements of NO are available from a large number of campaigns. NO_2 was not always measured and sometimes appeared to be affected by an interferent (e.g. *Crawford et al.* (1996)), so that only NO measurements are used here in the direct comparison and NO_x from either measurements judged to be reliable (in *Emmons et al.* (2000)) or from box model calculation constrained by other measurements during the campaigns are used in the ratios HNO_3/NO_x and PAN/NO_x. The latter ratios are useful indicators of the processing of nitrogen species and are also included in the comparison. It is noted that the observed ratios are from simultaneous measurements, whereas in the model the ratio of the monthly means is used. In Figures 3.24 to 3.26 selected results of the measurements and the two model runs for three species (NO, HNO_3, PAN) and two ratios (HNO_3/NO_x, PAN/NO_x) in one region are plotted in one row. NO in the model is only available as 24h-averages, whereas the measurements are restricted to daytime. An average daytime NO from the model was calculated by assuming zero NO during night and constant NO during day. While the former assumption is a very good approximation, the latter is not exactly valid during dusk and dawn. In most cases the error is probably small; however, for data composites that contain a large portion of measurements during these times a bias could be introduced.

The magnitudes, vertical profiles and partitioning of NO_y species are well reproduced for the northern latitudes as observed during ABLE campaigns (Figure 3.24, rows 1 and 2). Good agreement for NO was mostly also found for other campaigns (OCTA-1 to 4, POLINAT, SUCCESS, SONEX, not shown) below about 8 km. During the SONEX and POLINAT campaigns measurements were also taken at higher altitude and the model tends to underestimate the observations of NO (see below).

Compared to the TRACE-A campaign the model strongly underestimates HNO_3 at most altitudes and NO at 10-12 km, while PAN shows no clear tendency to over or underestimate over the source regions. NO above 8 km in the outflow region "Africa-Coast-W" is distinctly underestimated, even more pronounced than directly above the biomass burning region ("Africa-S"). The strong underestimate off the coast of Africa has also been found by other 3D-models (*Thakur et al.* (1999); *Emmons et al.* (2000)) and an unexplained imbalance in the NO_x budget has been suggested based on box-model calculations by *Jacob et al.* (1996). On the other hand, the weak maximum at 3-4 km (better seen for NO_x) is well reproduced. This is the altitude where the strongest outflow of CO and NMHCs was observed (and reproduced, see Figures 3.5 and 3.13).
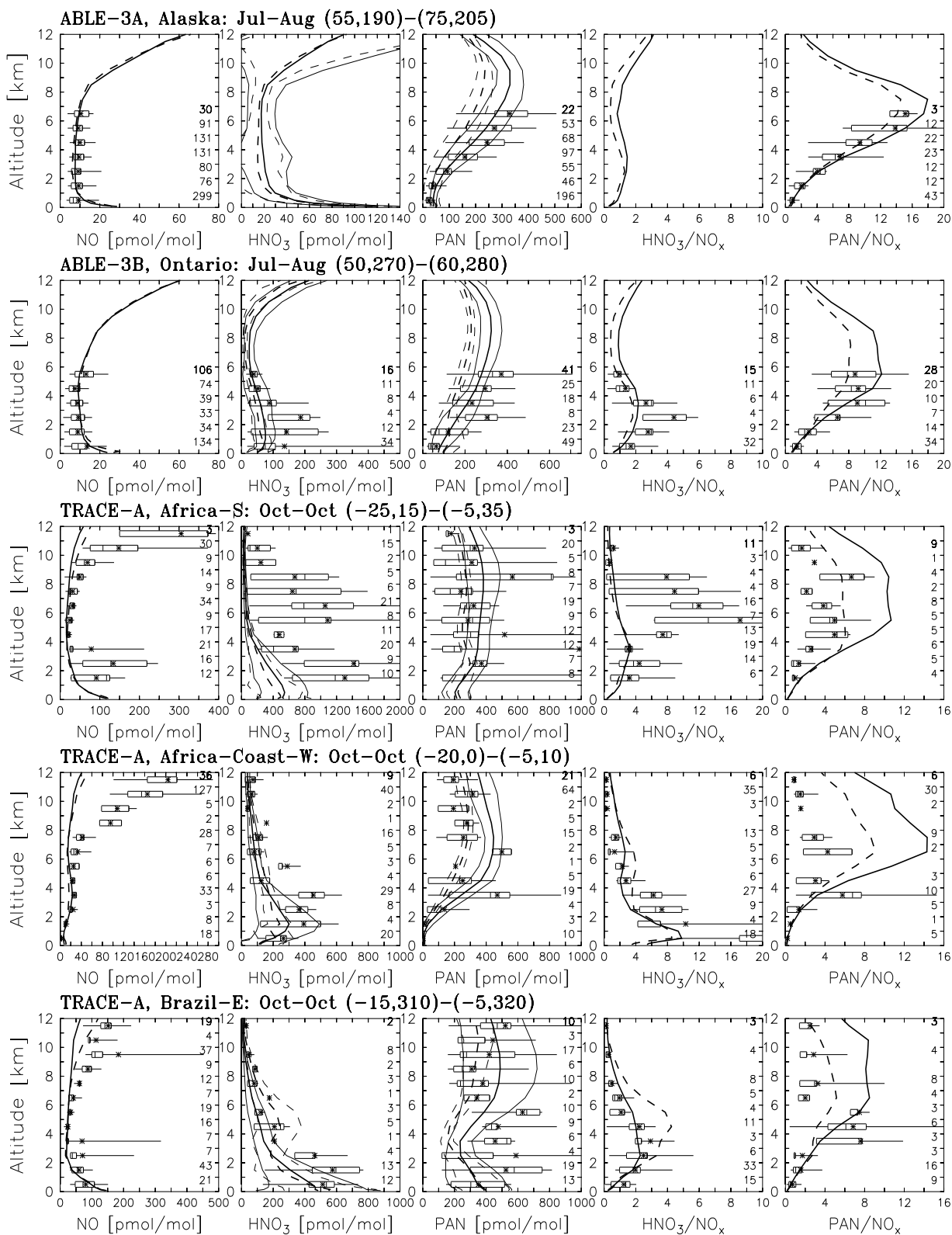
Figure 3.24: Comparison of airborne measurements of NO_y species with the model simulation. Lines and symbols are as in Figure 3.5. Result from the ABLE-3A and 3B and TRACE-A are shown.
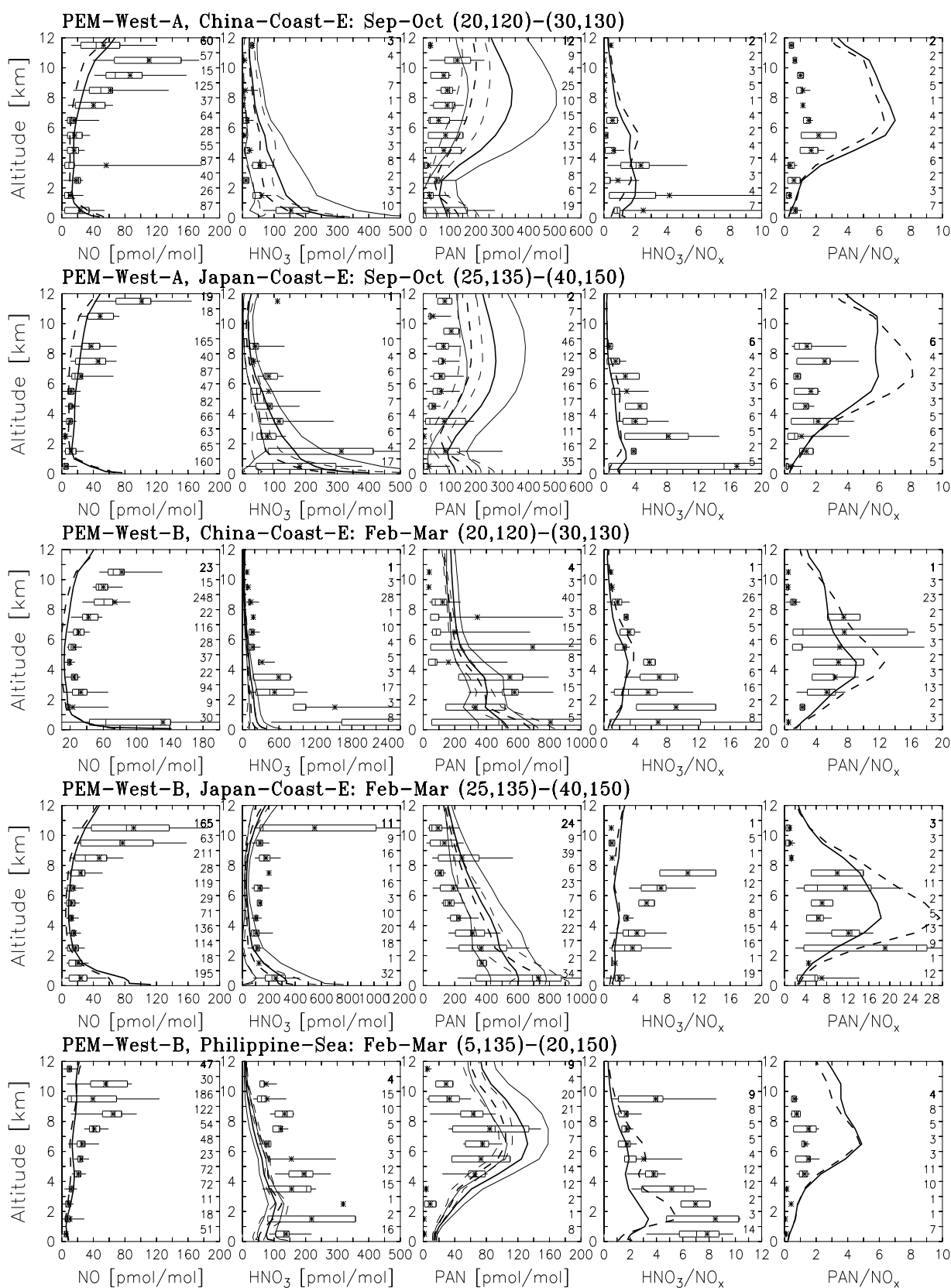
Figure 3.25: Same as Figure 3.24, but for the PEM-West-A and B campaigns.

A similar but less pronounced underestimation of NO at high altitudes is also found in the "Atlantic-S" region (not shown) and in "Brazil-E". HNO_3 on the other hand is well reproduced in these regions, though it is on the low side in "Atlantic-S" and "Brazil-E". Since HNO_3 is well reproduced in the upper troposphere an additional conversion of HNO_3 to NO_x, as suggested by *Jacob et al.* (1996) for this region, alone would therefore be at odds with the simulation of HNO_3. An additional channel for HNO_4 photolysis at long wavelengths (> 650 nm) has been suggested by *Zhang et al.* (2000) and *Salawitch et al.* (2001). In the model about 60 pmol/mol of HNO_4 are calculated at 10 km and the underestimate in NO is about 150 pmol/mol. If no significant non-chemical source of HNO_4 is present (e.g. by convection from the PBL), which is to be expected over the ocean regions, it is therefore unlikely that this can fully explain the underestimate in NO.

It is currently being investigated if PAN has a similar behavior at long wavelengths (*P. Wennberg*, private communication, 2001), but since at least the low resolution run (dashed lines) does not systematically overestimate PAN in the "Africa-Coast-W" region, this hypothesized explanation probably would cause problems with the model simulations as well. Along with the biomass burning, large amounts of fresh aerosols are also emitted and heterogeneous processes are another possible explanation. However, these aerosols mainly reside at about 4 km altitude (*Talbot et al.* (1996)) and thus, if processing of HNO_3 to NO_x would be mediated by aerosol surfaces, this should mainly be visible in that altitude range, which is not seen in the observations of NO_y species. The problem cannot be solved here, but suggests that there is a gap in the current understanding of NO_y chemistry. Another hypothesis, along with some more indications from a sensitivity run is discussed in Section 3.5.5.

In comparing with the PEM-West A and B campaigns very similar differences are seen (Figure 3.25): A tendency to underestimate upper tropospheric NO and HNO_3 at all altitudes and thus to underestimate the HNO_3/NO_x ratio in the middle troposphere. PAN and the PAN/NO_x ratio are always overestimated, with even higher values for PAN for the T63 run.

The results from the PEM-Tropics A and B campaigns (Figure 3.26) offer an opportunity to investigate the effect of biomass burning in September and October in the Southern Hemisphere on the NO_y species in the remote Pacific as compared to March/April when little burning activity is expected. An overestimation of PAN in remote regions (and also during the PEM-West-A campaign, when the main flow was from the Pacific onto Asia) clearly emerges as a persistent feature in both simulations, but especially in the high resolution run. Modeled NO in the MBL and middle troposphere is in good agreement for both seasons, but is underestimated at higher altitudes. Also, during PEM-Tropics-B an overestimation of NO (better seen in the comparison with NO_x) between about 2 and 6 km altitude is sometime visible (e.g. Fiji region). This is very likely caused from too much PAN transport. Most PAN decomposes in altitude range, as can be seen from the steep vertical gradient. In addition to the general overestimation of PAN the decrease often seen above about 6-7 km (e.g. Philippine-Sea, Fiji) appears to be more pronounced in the observations than in the model. This could indicate that convection in the model transports the boundary layer substances to too high altitudes. The above mentioned hypothetical PAN photolysis would also be a tempting explanation, but laboratory evidence is still lacking.

The cause for the general overestimation of PAN could be either too much availability of precursors of the PA-radical (CH_3CO_3), too high NO_x concentrations in the main source regions for PAN, or too strong convection. Neither indications for too high reaching nor for too strong

convection, however, have been seen so far in the other tracers (e.g. CO, NMHCs) or in studies with SF_6 by *Jöckel* (2000).

On the other hand, too high mixing ratios of isoprene in the Amazon region, which would mainly impact the South Pacific, have indeed been identified in Section 3.4.3. This might to a lesser extent also apply to NO_x concentrations: During the ABLE-2A and 2B campaigns very low mixing ratios of NO were measured between 1-4 km (not shown). About 20-30 pmol/mol were found in the dry season and around 10 pmol/mol in the wet season (*Torres and Buchan* (1988); *Torres and Hooks,* unpublished manuscript, 1989, as cited by *Jacob and Wofsy* (1990)), whereas the model calculates about 20-30 and 20 pmol/mol for the two seasons above 1 km. Taking into account the measurement uncertainty of 15% + 5 pmol/mol, model and observation are considered consistent for the dry season and the model tends to be somewhat too high in the wet season.

Measurements of PAN where only made during the wet season (*Singh et al.* (1990)) and the extremely low values of about 10-20 pmol/mol below 4 km are not reproduced by the model, which calculates 50-80 pmol/mol. The model is also on the high side (within a factor of 2) of surface measurements (at 39 m, above the canopy) of NO_y and NO (*Bakwin et al.* (1990b,a)). This is found by using the lowest model layer (at approximately 45m altitude), but it is noted that the gradient in NO and NO_y was found to be very steep over the first few tens of meters and a direct comparison might therefore be problematic.

Another possible reason for the overestimate in PAN, mentioned before, is the uncertain thermal equilibrium of PAN. This was tested in the LOWPAN run and the comparison with aircraft observations is summarized in the scatterplots in Figure 3.27. The T21 standard simulation is also plotted for comparison. A tendency to overestimate low mixing ratios, but also to underestimate high mixing ratios is visible. In the LOWPAN run the often severalfold underestimate especially in the upper troposphere (upright triangles) still remains, and the tendency to underestimate high values is more severe. In the remote regions where an strong overestimate was seen in the standard run (e.g. Philippine-Sea, Fiji) LOWPAN show only about 10-20% smaller mixing ratios and the vertical profile is not changed. Thus the decrease of PAN above 6-7 km us still too weak in these regions.

Overall, the agreement of the LOWPAN simulation with observations is not significantly improved over the standard run (see also the r^2 values), which suggests that other factors are mainly responsible for the general overestimate and the discrepancies in some vertical profiles.

Finally, it is mentioned, that sub-grid chemical effects could lead erroneous PAN formation rates. For example considering regions with scattered forest fires: In the model, biogenic VOC emissions and and the NO_x emissions from the fires would be instantaneously mixed likely resulting in conditions for efficient PAN formation. In reality, however, the biomass burning plumes and the biogenic emission are only mixed during the evolution of the plume with at a timescale hours to days. Furthermore, the direct emission of acetaldehyde (CH_3CHO) from biomass burning, which has been omitted in all other 3D-model studies so far (to the best of the authors knowledge), could contribute to the high PAN concentrations calculated here. Acetaldehyde produces PA-radicals upon reaction with OH or photolysis. Both processes, in turn might be hindered within a fresh biomass burning plume due to the reaction of $NO_2+OH \rightarrow HNO_3$ that depletes OH and aerosols that lower the photolysis frequencies (*J. Trentmann*, personal communication, 2001).

It is thus argued that errors in the conversion of NO_x in fresh biomass burning plumes into
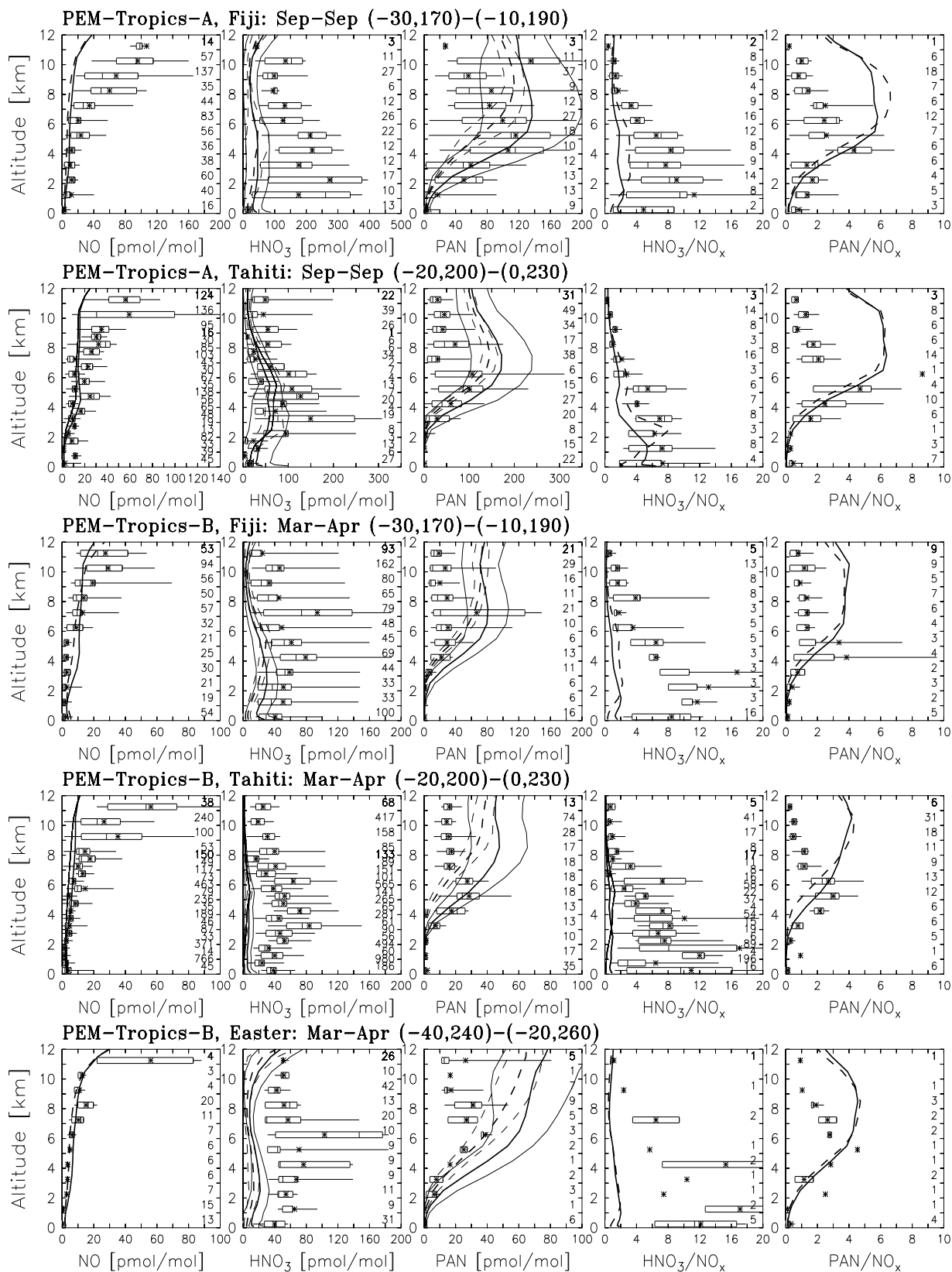
Figure 3.26: Same as Figure 3.24, but for the PEM-Tropics-A and B campaigns. In some regions the measurements are from two platforms and are placed in the upper (Lockheed P-3) and lower (McDonnell Douglas DC-8) part of the kilometer interval.
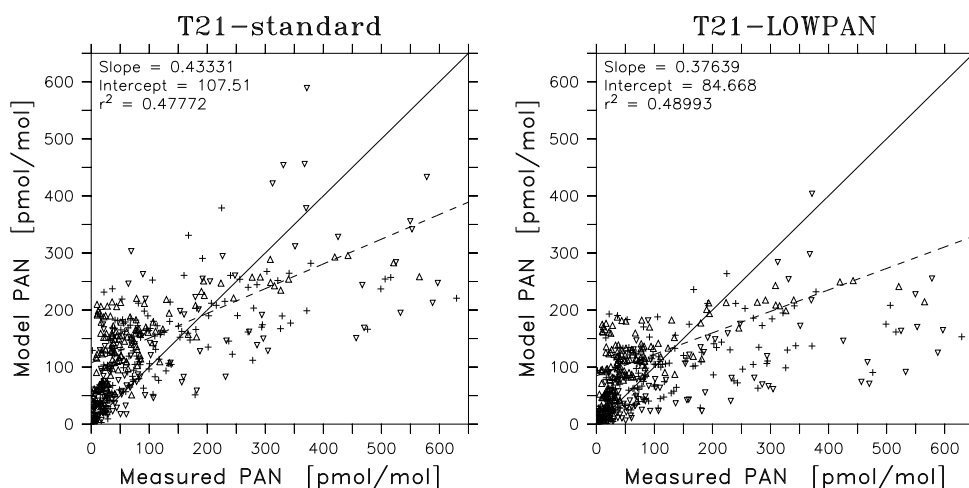
Figure 3.27: Scatter plot of modeled versus observed PAN for the T21 standard run (left) and the LOWPAN run (right). Each symbol is from one kilometer interval in a region-grid of *Emmons et al.* (2000). Triangles pointing up and downward are in the 8-12 km and 0-4 km range, respectively. Pluses are from 4-8 km altitude. Solid lines are the 1:1 comparisons, dashed lines are the linear regression lines.

the main reservoir species PAN and HNO$_3$ in coarse resolution models may be substantial. There have been a few studies on the effect of sub-grid segregation on local ozone production (*Sillman et al.* (1990); *Chatfield and Delany* (1990); *Poppe et al.* (1998); *Hilst* (1998); *Liang and Jacobson* (2000)), but none of them investigated the effect on the NO$_y$ partitioning, which could exert an important long-range effect. Clearly, more studies are needed to clarify these issues.

3.5.5   The effect of HNO$_3$-uptake on ice particles

In contrast to most other 3D-modeling studies HNO$_3$ was often underestimated. It would be thus valuable to find the controlling model assumption that led to these results. The assumption was made in this study that HNO$_3$ was efficiently taken up by ice surfaces. As discussed already in Section 2.3.5 the general validity of this assumption is still under dispute. The uncertainty arises mainly from the question if atmospheric ice particle behave like the ice surfaces examined in the laboratory.

In order to test the effects of this model assumption a model run ("NOICE") with no uptake of HNO$_3$ allowed on ice (H$_2$O$_2$ uptake is still allowed, based on *Conklin et al.* (1993)). A comparison of the T21 standard simulation and the NOICE run to observations in selected regions is shown in Figure 3.29. Omitting uptake on ice results in better agreement in some regions (e.g. Ireland, Japan during PEM-West-B), but lead to a larger discrepancy in others. In most cases, however, the NOICE simulation results in a change in the vertical gradient of HNO$_3$ in the middle troposphere which does not agree with the observations. The behavior during the two phases of the PEM-West campaigns can be largely explained by the different flow regimes during the two campaigns. During PEM-West-B the flow was from Asia towards the ocean. Thus, the pollution of the upper troposphere is probably quite fresh and thus, the model results are mostly determined by the efficiency of the wet scavenging parameterization, particularly its coupling to the convection in MATCH. The effect of ice particles is better seen, when the airmass
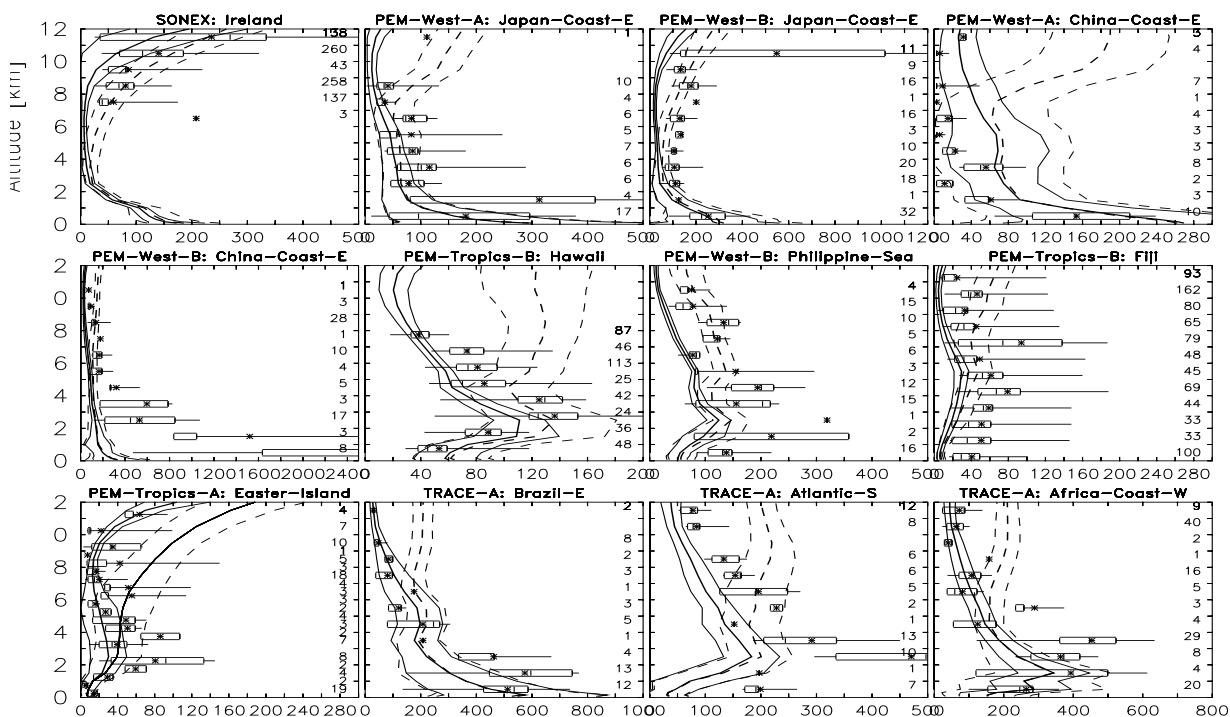
Figure 3.28: Comparison of modeled/observed vertical HNO$_3$ profiles. Solid line is the T21 standard simulation (thin lines are $\pm 1\sigma$) and dashed lines is the NOICE simulation. Symbols are as in Figure 3.5.
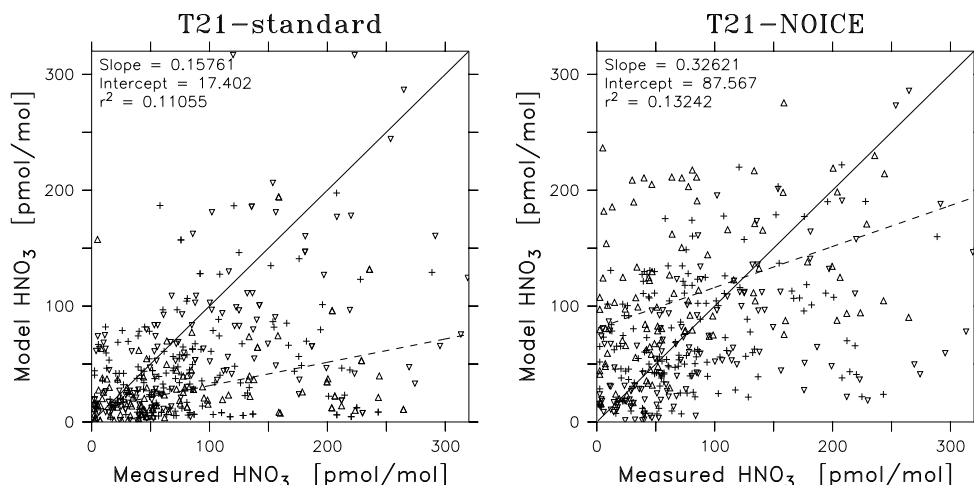

Figure 3.29: Scatter plot of modeled versus observed HNO$_3$ for the T21 standard run (left) and the NOICE run (right). Symbols and lines are as in Figure 3.27.

is more aged as e.g. during the PEM-West-A campaign.

A clearer picture is obtained by making a scatterplot of all airborne data from the *Emmons et al.* (2000) data set (Figure 3.29). It now becomes clearly visible that HNO_3 is often overestimated in the upper troposphere in the NOICE run (upright triangles in right panel), which was not the case in the standard simulation. This, strongly suggests that uptake of ice and subsequent removal of HNO_3 is occurring in at least certain regions of the upper troposphere. This is an important point because it also opens the door to potential processes occurring on ice particles in the atmosphere. It is known that photochemically mediated production of NO_x occurs in surface snow (*Honrath et al.* (1999, 2000a,b); *Jones et al.* (2000)). *Honrath et al.* (2000a) have recently proposed a mechanism of NO_x release from snow involving the photolysis of NO_3^- ions, which can be formed from HNO_3 in the aqueous phase. They suggest that this mechanism could also occur on cirrus particles. While loss of HNO_3 on ice particles often leads to better agreement with observations of HNO_3, this is not the case for NO in the upper troposphere, which is hardly affected and thus still underestimated considerably in some regions.

An especially tempting support is the comparison with the TRACE-A measurements. NO was underestimated in the upper troposphere especially over the Atlantic (see also *Jacob et al.* (1996)). From boxmodel calculations *Jacob et al.* (1996) concluded that an additional source of NO must be present in the upper troposphere. The altitude ranges where NO is underestimated (Figure 3.24) and where uptake on ice particles is effective (Figure 3.29) match well. It if argued here that this strongly indicates that conversion of HNO_3 to NO_x mediated by ultra-violet light and ice surfaces could occur in the upper troposphere. Only uptake and at least partial subsequent re-release of NO_x after conversion in or on the ice particle could help to improve the agreement at both species.

It is recognized that other proposed mechanisms could also play a role, such as reactions of HNO_3 on different types of aerosols (nitrate, sulfate, soot, mineral) (e.g. *Chatfield* (1994); *Iraci and Tolbert* (1997); *Rogaski et al.* (1997); *Tabazadeh et al.* (1998)). The issue cannot be resolved here, but the results encourage that the photochemistry of the nitrate ion in aqueous phase and on ice surfaces should be quantitatively investigated (especially the quantum yields). Also, further studies on the uptake of nitric acid onto ice surfaces under upper tropospheric conditions should be undertaken.

3.6 Oxygenates

Oxygenated substances are ubiquitous in the troposphere (e.g. *Singh et al.* (1994, 1995, 2000, 2001)). This group of compounds includes peroxides (H_2O_2, CH_3OOH and other ROOH), aldehydes (HCHO, CH_3CHO), ketones (acetone, methyl-ethyl ketone), alcohols (CH_3OH, C_2H_5OH) and carboxylic acids (HCOOH, CH_3COOH, PAA), as well as some multi-functional compounds such as methylglyoxal (CH_3COCHO), hydroxyacetone, methylvinylketone and methacrolein. While some of these compounds are formed in the oxidation of methane (H_2O_2, CH_3OOH, HCHO, CH_3OH) and are well known participants in atmospheric chemistry (with the exception of methanol, which is only beginning to draw some attention), the budget, distribution and importance of other compounds is only beginning to be understood and available observations are sometimes quite sparse.

Unlike NMHCs most oxygenates can photolyze and participate in HO_x formation. By providing the precursor radical for PAN (the PA-radical), acetone and acetaldehyde are intricately coupled to NO_x chemistry in the atmosphere. Thus, oxygenates can affect the production of

ozone by influencing atmospheric HO_x and NO_x levels. The annual zonal mean distributions of 9 oxygenates as calculated by MATCH are depicted in Figure 3.30 in order to provide an idea of their abundance in the atmosphere. In this section some available measurements are used to discuss potential shortcomings in the chemistry and/or emissions assumed in this work.

3.6.1 Hydroperoxides (H_2O_2, CH_3OOH, ROOH)

Hydrogen peroxide (H_2O_2) is almost solely formed from the self-reaction of HO_2 radicals[15] and can thus serve as sensitive indicator for HO_x chemistry in the atmosphere. Furthermore, it is an important oxidant of sulfur compounds in the aqueous phase. Due to its high solubility it can deposit efficiently, both wet (23%) and dry (16%), but also photolyze (31%), or react with OH (30%). The contribution of each pathway to the total sink in the troposphere as calculated by MATCH (T63) is given in brackets. It is noted, however, that the photochemical pathways can lead to substantial recycling to re-form H_2O_2 so that deposition has to be regarded as more important than suggested by these numbers. The tropospheric average photochemical lifetime of this compound is calculated to be 1.7 days; taking into account deposition processes it decreases to about a day.
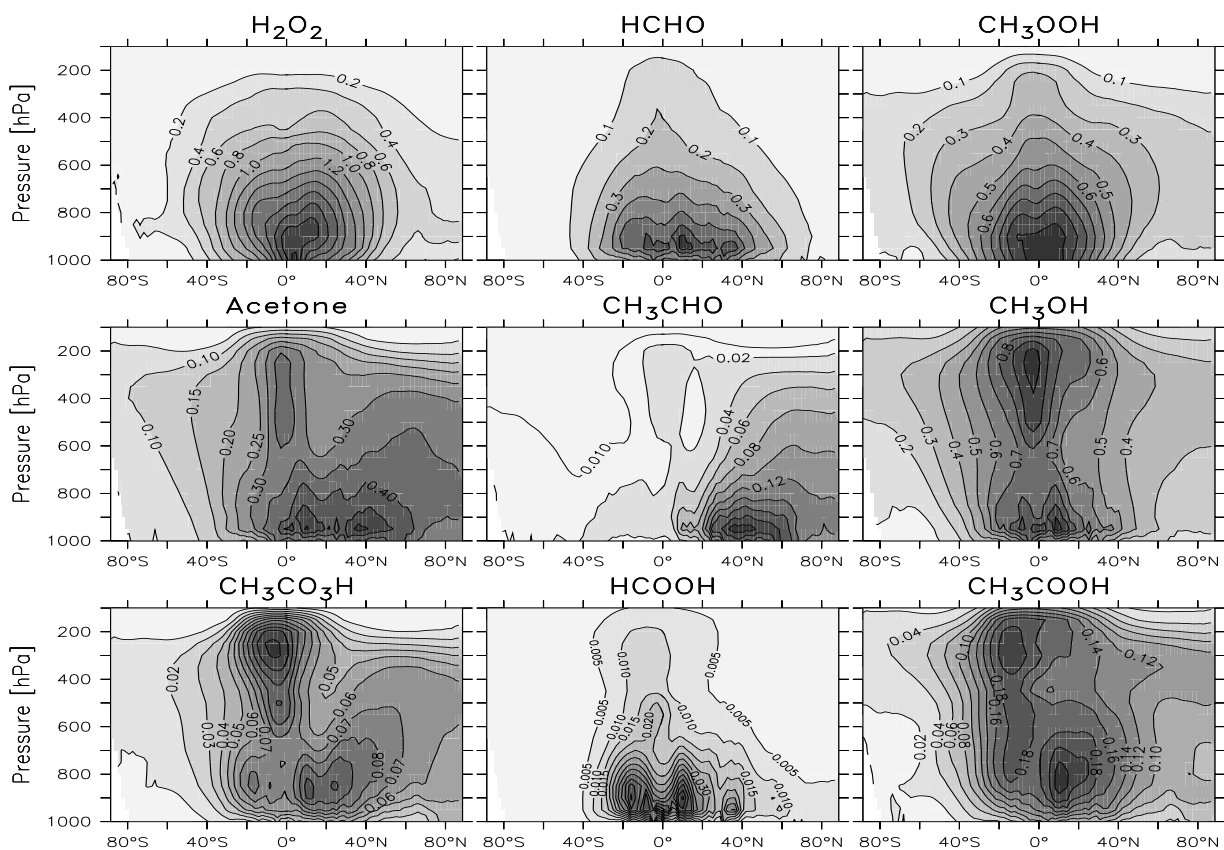

Figure 3.30: Calculated annual zonal mean distributions of some oxygenates (in nmol/mol). Results are from the T63 run.

Methyl hydroperoxide (MHP, CH_3OOH) is about 100 times less soluble than H_2O_2 and is

---

[15]Neglecting a small contribution from the ozonolysis of isoprene and potentially of terpenes (*Beker et al.* (1990, 1993)).

therefore more efficiently transported into the upper troposphere by convection. It has been suggested that photolysis of CH_3OOH injected into the upper troposphere by convection can provide a large source of HO_x radicals in this region (*Chatfield and Crutzen* (1990); *Prather and Jacob* (1997); *Jaeglé et al.* (1997)). The production rate strongly depends on NO_x concentrations, since the formation reaction $CH_3O_2 + HO_2$ is in competition with $CH_3O_2 + NO$. The average tropospheric lifetime of MHP is about one day (22h).

Higher hydroperoxides are also formed from other peroxy-radicals, but their chemistry (i.e. products of the OH or photolysis reaction) is only poorly known. Therefore, in most cases, the same reaction rates (for ROOH+OH and ROOH+$h\nu$) are assumed as for CH_3OOH. An interesting group of peroxides are the β-hydroxy-hydroperoxides[16] formed in the oxidation of isoprene under low-NO_x conditions. Due to the additional hydroxy-group they are much more soluble, and due to the remaining double bond also more reactive than other hydroperoxides, but considerable uncertainties are associated with these two properties. These hydroperoxides could provide an efficient loss of carbon in the oxidation chain of isoprene (see Chapter 5).
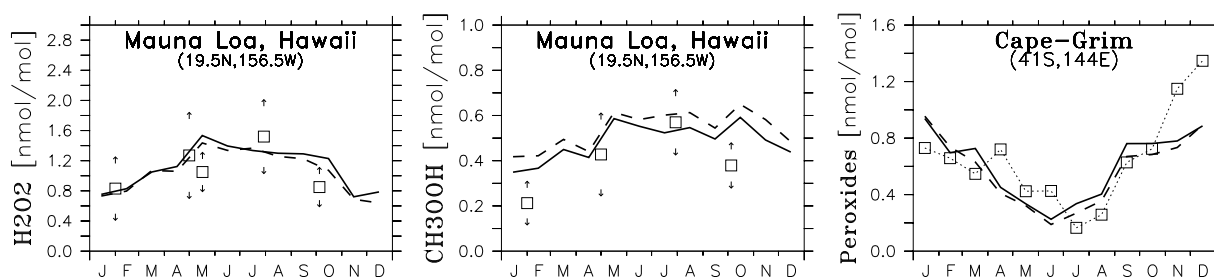

Figure 3.31: Surface measurements of peroxides (squares) compared to model result (T63: solid line; T21: dashed line). The data are from *Staffelbach et al.* (1996) (during MLOPEX 2) and *Ayers et al.* (1996). "Peroxides" at Cape Grim (Tasmania) is the sum of H_2O_2, CH_3OOH and higher peroxides.

The calculated budgets of MHP show that only a small fraction of the total amount formed photochemically in the troposphere (280 Tg-C/yr) is lost through dry (3%) and wet (1%) deposition, while the majority either reacts with OH (80%) or photolyzes (16%). Even in the upper troposphere ($\sigma < 0.341$) reaction with OH dominates over the photolysis reaction (63% and 37% of the total photochemical loss, respectively).

Comparison of observations with the model results are shown in Figures 3.31 and 3.32. Again, only a subset of the airborne observations is shown. The magnitudes and seasonal cycles of the surface observations of peroxides are reasonably well simulated by the model. The vertical profiles are well reproduced for H_2O_2, with no detectable general bias of the model. The unusually high values found over Brazil during the burning season are underestimated, a problem also found in other 3D-modeling studies (*Wang et al.* (1998c); *Hauglustaine et al.* (1998)), which even showed larger underestimations (2 nmol/mol H_2O_2 versus 3 nmol/mol in MATCH). The higher H_2O_2 mixing ratios in this study are likely due to the assumed emissions of other oxygenates (HCHO, CH_3CHO), neglected in the other studies, which can increase HO_x levels near the sources. It has been suggested (*Lee et al.* (1997)) that the high observed values indicate direct emissions from fires, which are not included in the models. Further investigations are needed to better understand this phenomenon.

---

[16]The sum of these compounds is denoted ISO_2H (=ISOOH) in the chemical mechanism in Appendix A.1.

The mixing ratios of MHP found during the MLOPEX campaigns are reasonably well reproduced, though an overestimate during winter and fall is apparent. This overestimate is especially surprising as NO_x levels in the model tend to be on the high side of the observations during these seasons (see Figure 3.22). The most notable differences in comparing observed vertical profiles with model results are found over Newfoundland (SONEX) and Tasmania (ACE-1). The maximum in the lower free troposphere is not seen in these measurements. For the SONEX campaign the model underestimates NO in that region, especially in the middle troposphere, which would be linked to the overestimate in MHP. During ACE-1, however, NO is in good agreement with the observations, and thus the different vertical profiles are not easily explained. Good agreement, on the other hand is found for the measurements influenced by biomass burning over "Brazil-E" and "Africa-S" during TRACE-A.

There are only few measurements of the hydroxy-hydroperoxides from isoprene (*Warneke et al.* (2001); *Sanhueza et al.* (2001)). It was found in Section 3.4.3 that comparison of isoprene mixing ratios with the model is difficult. Therefore, only the ratio ISOOH to isoprene is evaluated here. *Warneke et al.* (2001) report ratios between 0.28 and 0.46 during daytime over the rainforest in Surinam, with the higher values early in the morning. The 24h-average value from the model is about 0.15. The lower simulated value could be easily explained by rapid deposition of ISOOH during night, which is likely faster than the decrease of isoprene which is assumed to be due reaction with O_3 and NO_3 only. The surface measurements of *Sanhueza et al.* (2001) at a savanna site (Calabozo, Venezuela) resulted in approximate ISOOH/isoprene ratios of 0.1-0.2 (24h-means) which are also calculated by the model. However, it is noted that the agreement might be fortuitous, since the deposition of isoprene needed to explain the measurements is not included in the 3D simulation and calculated NO_x mixing ratios (0.97 nmol/mol) appear to be on the high side of the measurements at the site in the wet season by *de Serves et al.* (1996) (0.4-1 nmol/mol). These two errors tend to cancel each other out. Furthermore, the ratio is probably strongly affected by the deposition velocity of ISOOH, which is assumed to be fairly high (1.3 cm/s, only slightly slower than for HNO_3: 1.5 cm/s), but cannot be confirmed by observations.

3.6.2   Formaldehyde (HCHO)

Formaldehyde can photolyze and contribute to HO_x formation and is a precursor of CO. Its main source in the atmosphere is the oxidation of methane, but it is also produced from the oxidation of other VOCs. While a run only including methane chemistry results in a photochemical production of 340 Tg(C)/yr of HCHO, a run with the full chemistry scheme yields 500 Tg(C)/yr. The main loss pathways in the model are photolysis (64%) and reaction with OH (30%). Even though HCHO is quite soluble (about 10 times more than CH_3OOH, but 10 time less than H_2O_2[17]) only a small fraction of the total loss occurs via deposition (about 6%). This is because its annual mean tropospheric photochemical lifetime is calculated to be only about 5 hours, short enough that precipitation scavenging cannot make a significant contribution.

Surface and Airborne Measurements

Surface and airborne measurements of HCHO compared to model results are shown in Figures 3.33 (first two rows) and 3.32 (last two rows). The seasonal cycle in the northern mid-latitude

---

[17]This is in terms of effective uptake onto water as expressed by the effective Henry's Law constant which takes into account that HCHO hydrolyzes to $CH_2(OH)_2$ in the aqueous phase.
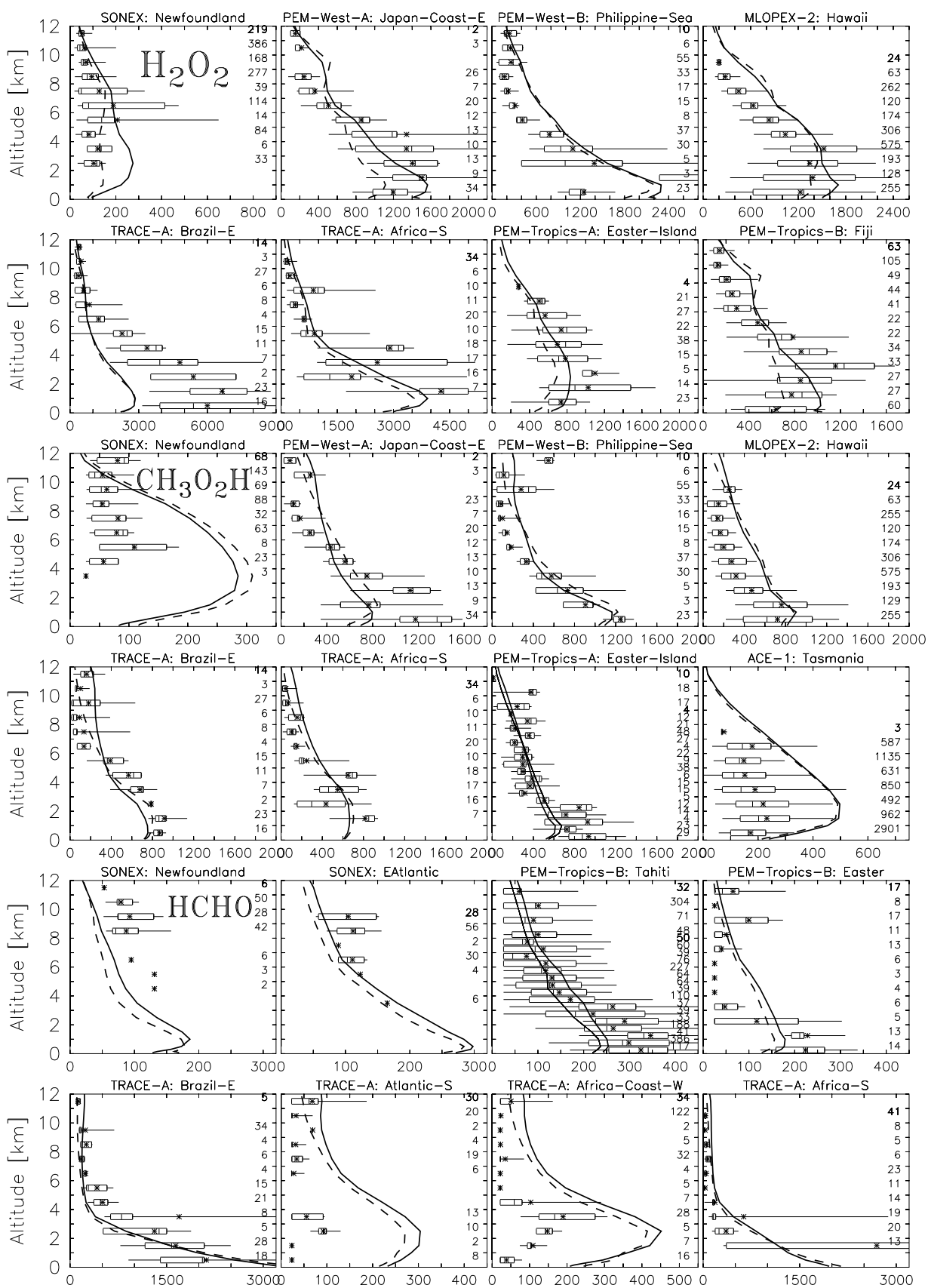
Figure 3.32: Comparison of airborne measurements of peroxides (H_2O_2 and CH_3OOH) and formaldehyde (HCHO) with model results (as in Figure 3.5).

has a maximum in summer, which is reproduced by the model. The model, however, tends to underestimate mixing ratios in winter, which could be explained by too low industrial emissions. Another 3D-global model, MOZART (*Brasseur et al.* (1998); *Hauglustaine et al.* (1998)), correctly predicts the winter mixing ratios using a two times higher industrial emission strength than used here, but MOZART overestimates the summer mixing ratios instead. The underestimate at Ispra is not easily explained, but the station also behaves differently for CH_3CHO and acetone, indicating that the site is not representative for a larger grid cell of a 3D-model. The overestimate of about 40% at Mauna Loa has also been found by an earlier version of MATCH (*Lawrence* (1996)) and could not be explained in that study. Since all other substances tested were either in good agreement (CO, NO_x, HNO_3, ONIT, H_2O_2, CH_3OOH; also O_3, see Section 3.7) or slightly too low (C_2H_6, C_3H_6) this discrepancy is not easily explained. The overestimate of PAN does not directly affect formaldehyde (only via NO_x, which is in agreement with observations).

Zhou et al. (1996) state that HCHO concentrations during downslope periods (for which the data used here is filtered) did not depend on air mass origin, suggesting that it does not have other significant precursors than methane at this site. This would mean that the phenomenon has to be explained by the chemistry of methane oxidation alone. It has been argued that oxidation of HCHO in the aqueous phase could reduce HCHO mixing ratios in the troposphere (*Lelieveld and Crutzen* (1991)), but *Dentener* (1993) only found about a 5-10% reduction in the zonal mean at the latitude of Mauna Loa. This should probably be regarded as an upper limit estimate, since the revised rate constant of the reaction of hydrated formaldehyde with OH is a factor of 2.6 slower than used by these authors (*Chin and Wine* (1994)). With only one compound significantly miss-calculated the problem is not likely caused by one model deficiency alone. A solution is probably more complex and remains yet unexplained.

Comparison with the airborne measurements also reveals some disagreement. While the SONEX observations are somewhat underestimated, values over the Atlantic Ocean during the burning season are overestimated significantly. Both findings confirm problems encountered in previous modeling studies. *Jaeglé et al.* (2000) concluded from box-model calculations constrained by the SONEX measurements that a source for HCHO is missing in the upper troposphere. They also found a correlation of high HCHO mixing ratios with methanol (CH_3OH) and cirrus clouds and hypothesize that heterogeneous reactions on ice crystals or aerosols converting methanol to formaldehyde could occur. The reaction probability needed to resolve the discrepancy was found to be $\gamma_{ice} \approx 0.01$.

The high concentrations over the biomass burning regions during the TRACE-A campaign are reasonably well reproduced (regions "Brazil-E" and "Africa-S"), but in the outflow regions over the Atlantic the model overestimates the measurements by more than a factor of 2. From these measurements (and also from other measurements in the marine boundary layer) *Jacob et al.* (1996) concluded that they point to a major gap in current understanding of HCHO chemistry in the MBL. However, HCHO measurements in the Pacific ocean made during PEM-Tropics-B are well reproduced (as exemplified in Figure 3.32 for 2 out of 6 regions), so that it can be argued that the problem does not always occur in the MBL and might be connected the biomass burning outflow conditions during TRACE-A.

Even underestimations are found for other MBL measurements: *Weller et al.* (2001) find mixing ratios in October/November over the Atlantic at the same latitudes as the TRACE-A airborne measurements as high as 600-1000 pmol/mol, whereas the model calculates only 200-400 pmol/mol. A similar underestimate of the model by a factor of 2 is also found for the clean
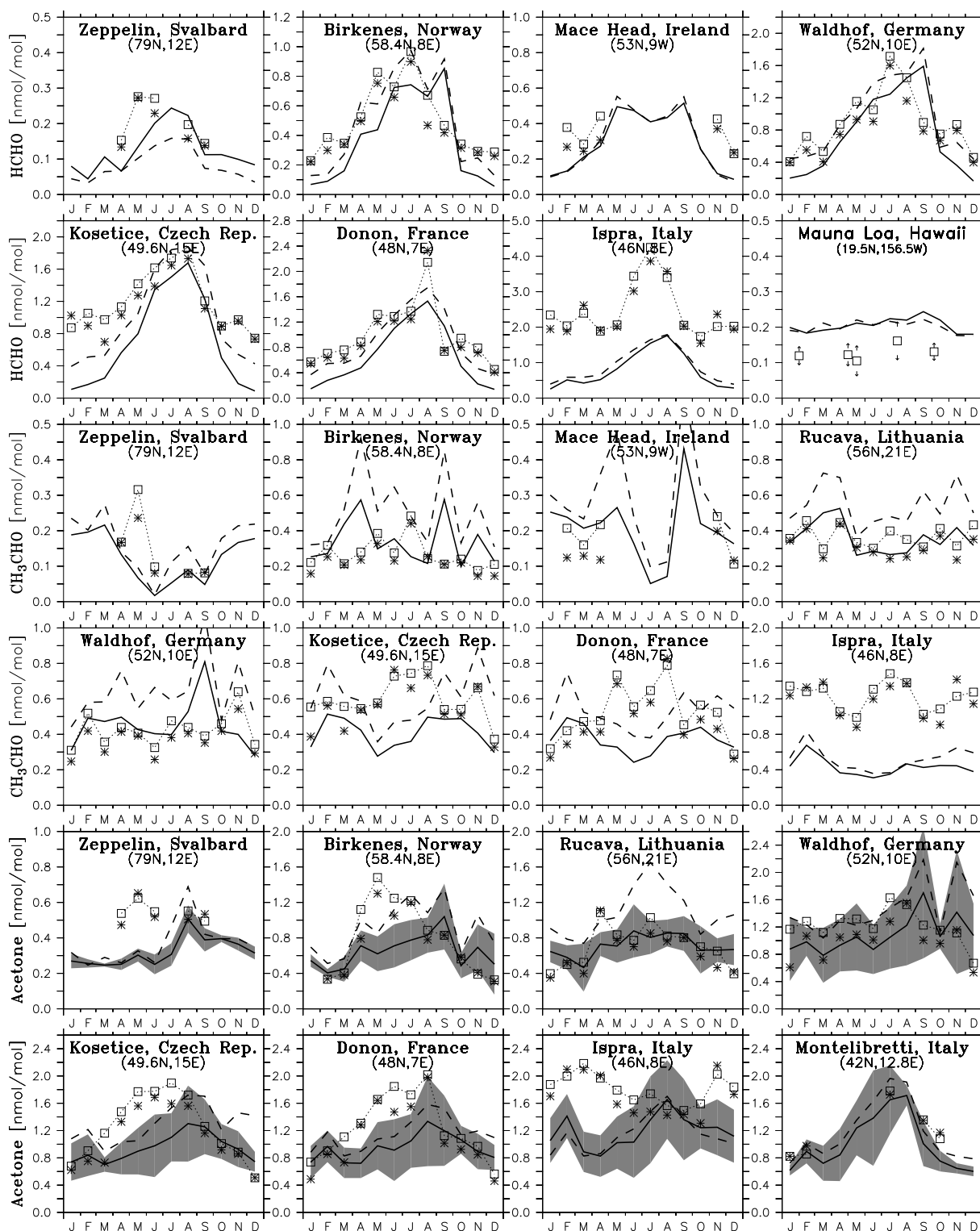
Figure 3.33: Comparison of model results with measurements of HCHO (first two rows), CH₃CHO (rows 3+4), and Acetone (bottom two rows) for different European stations (*Solberg et al.* (1996)) and for Mauna Loa (HCHO, *Zhou et al.* (1996)). Squares and stars are mean and median of observations (as Figure 3.11).

MBL data at Cape Grim of *Ayers et al.* (1997) and for measurements over the Pacific (*Arlander et al.* (1990)). The net flux of formaldehyde is very likely from air to sea, due its high solubility (including the hydrolysis) (*Zhou and Mopper* (1997)). Thus, other reasons than a direct emissions have to be found. *Ayers et al.* (1997) state that only 10 pmol/mol of isoprene could provide a substantial source of formaldehyde to MBL. In fact, isoprene mixing ratios of this magnitude were found sporadically over the southern oceans by *Yokouchi et al.* (1999).

Ayers et al. (1997) put forward another possibility to explain the underestimate of their model: There is a possibility for a minor channel of the $CH_3O_2 + HO_2$ reaction yielding formaldehyde instead of CH_3OOH. They could explain the observed mixing ratios of HCHO assuming a 40% yield for this channel. However, based on a literature review *Tyndall et al.* (2001) conclude that the channel is probably unimportant ($<10\%$) for temperatures higher than 295 K. No measurements are available at lower temperatures.

The over- and underestimations of the model occurring at different places or times strongly suggest that unknown factors are affecting formaldehyde concentrations in the marine boundary layer (provided the measurements are correct). More measurements are thus required to better understand the budget of formaldehyde in the MBL. Those studies should ideally include also measurements of a large suite of possible precursors of HCHO (NMHCs, oxygenates).
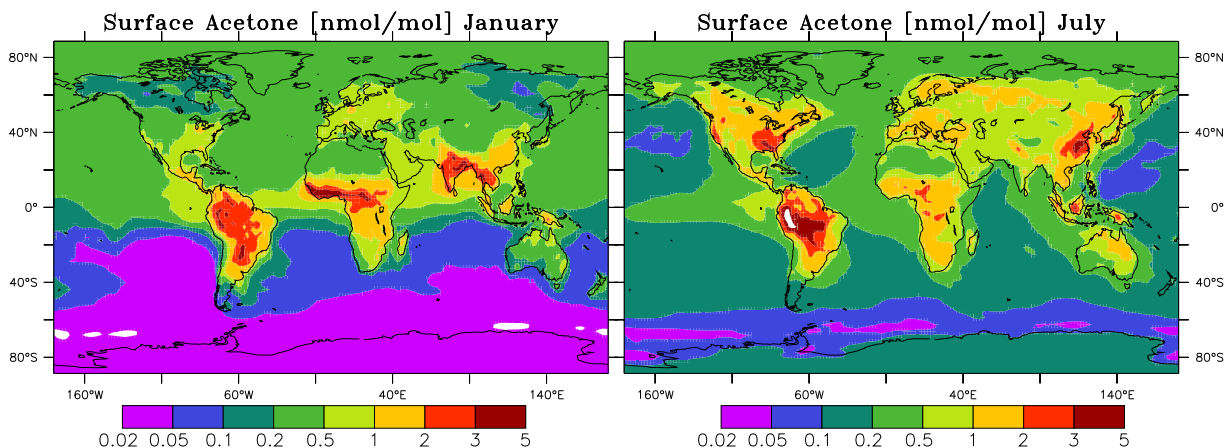
Figure 3.34: Surface distribution of acetone (CH_3COCH_3) for January and July from the high resolution simulation.

3.6.3 Acetone (CH_3COCH_3)

Acetone (CH_3COCH_3) is another oxygenated species that has gained strong interest over the last years as it has been measured in large amounts (up to several nmol/mol) at all altitudes (*Singh et al.* (1994, 1995, 2000, 2001); *Arnold et al.* (1997); *Wohlfrom et al.* (1999)) and is believed to contribute significantly to the upper tropospheric HO_x budget through photolysis (*Singh et al.* (1995); *McKeen et al.* (1997); *Collins et al.* (1999); *Müller and Brasseur* (1999); *Jaeglé et al.* (2001)).

The mean tropospheric lifetime of acetone is calculated to be 18 days, but can be as low as 5-10 days in the upper troposphere. Its direct sources to the atmosphere have been discussed in Section 2.3.6. The direct emissions used in MATCH sum up to a total of 46.2 Tg/yr, including 40 Tg/yr from three terrestrial biogenic sources (direct emissions, oxidation of terpenes, decaying

plant matter), which are not differentiated, 4.2 Tg/yr from biomass burning and 2 Tg/yr from industrial activities. It is noted that the biogenic emission strength is at the high side of the estimate of *Singh et al.* (2000) (21-43 Tg/yr) and higher than applied in other modeling studies (3.7 Tg/yr in *Roelofs and Lelieveld* (2000) to 24 Tg/yr in *Wang et al.* (1998c)). The photochemical source in the model is only from propane (9.3 Tg/yr); production from higher iso-alkanes and iso-alkenes has been neglected, but was estimated by *Singh et al.* (2000) to contribute only about 2 Tg/yr. The surface distribution of acetone calculated with these emissions is shown in Figure 3.34. Mixing ratios over land and in the northern hemisphere are higher. Maximal mixing ratios of a few nmol/mol are calculated over the biogenically active areas (Amazon, West Africa, parts of the Northern Hemisphere in summer).
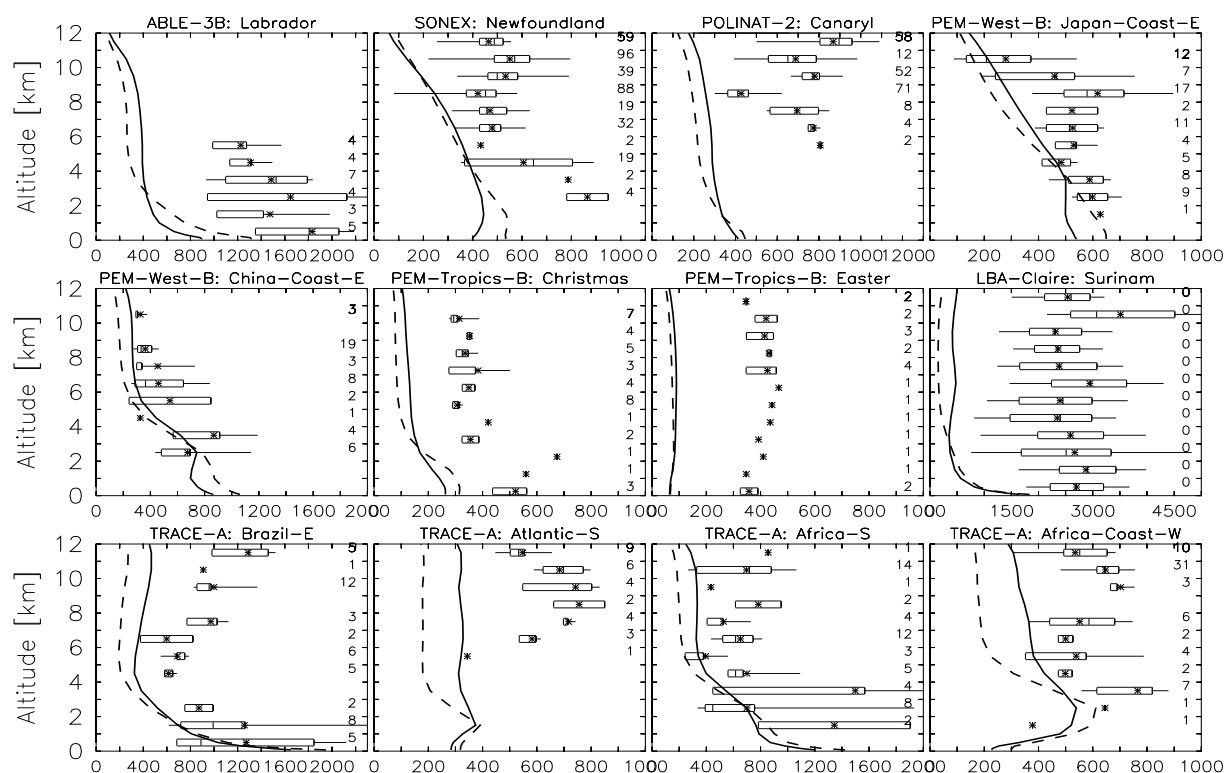
Figure 3.35: Comparison of model results with airborne measurements of acetone (CH_3COCH_3). Symbols and lines are as in Figure 3.5.

The photochemical loss pathways from the atmosphere are photolysis (54%) and reaction with OH (22%), the latter of which is usually more important in the lower troposphere. Dry deposition in MATCH is calculated based on the (fairly low) solubility and constitutes 23% of the total loss (18.8% over land, 4.5% over ocean). Loss to the stratosphere accounts for the remaining 1%.

A comparison of the model surface observations in Europe is depicted in Figure 3.33 (last two rows). The model tends to underestimate the measured concentrations especially in late spring. The seasonality with a summer maximum and a winter minimum is qualitatively reproduced, but discrepancies can be clearly seen in late spring at Zeppelin, Birkenes, Rucava, Kosetice, and Donon. The observed seasonal cycle at Ispra is actually reversed (for unknown reasons) and is not modeled correctly. As mentioned before, a local anomaly might be the cause. It appears

that an additional source having a seasonality peaking in early summer would be best suited to improve the agreement at most stations (not Ispra). Biogenic emissions are the most likely candidate, but the good agreement in fall actually suggests that the contribution to the biogenic source of acetone from decaying plant matter is not dominating. Direct emissions or oxidation of terpenes are therefore probably underestimated. Note that due to insufficient information all three biogenic source types where emitted with the same seasonality and horizontal distribution.

Comparing the model with airborne observations (Figure 3.35) one also finds indications of a larger than assumed source strength. The disagreement is especially marked during the PEM-Tropics-B campaign (March-April) over the Pacific ocean. The statement of *Singh et al.* (2001), that large widespread (most likely oceanic) sources must be present, is therefore supported by these results, even through here an almost two times larger terrestrial biogenic source of acetone is used. A large enrichment of acetone and also of other carbonyl compounds (e.g. acetaldehyde) have been measured by *Zhou and Mopper* (1997) in sea-water samples of the surface micro-layer of the ocean and a sea-air flux was suggested for the less soluble compounds (such as acetone and acetaldehyde).

The assumed terrestrial biogenic source of acetone appears to be too low as well, as suggested by the strong underestimation of the acetone measurements over the rain forest in Surinam during the LBA-Claire champaign (*Crutzen et al.* (2000); *Pöschl et al.* (2001)). Based on the correlation to acetonitrile, biomass burning was judged to be only a minor contribution to the observed acetone abundance. These measurements were also made with the aforementioned PTR-MS technique, and it should be kept in mind that propanal and glyoxal could also contribute to the same signal, but based on their shorter lifetimes than acetone it was argued that they are probably much less abundant (*Williams et al.* (2001)). A problem with this campaign might be that it took place very close to the coast (1-2 grid-cells inland at T63) and the influence of oceanic air could be overestimated in the model. However, even in the central Amazon region acetone model mixing ratios are lower than these observations. Mixing ratios in the model do not exceed 1.5 nmol/mol in the free troposphere and are about 3 nmol/mol near the surface. As mentioned by *Pöschl et al.* (2001), the lacking vertical gradient in the measurements can only be explained by either photochemical sources of acetone or advection of acetone-rich well-mixed air masses into the region. A correlation with the northerly wind component, but no dependence on the distance from the coast was also found, which also suggests that an oceanic source rather than additional terrestrial biogenic sources would result in better agreement of the model results with these observations.

The acetone mixing ratios over the biomass burning regions during TRACE-A are approximately correctly predicted in the lower troposphere, but appear to be too low in the upper troposphere (Brazil-E). However, as mentioned before, these measurement might not be representative since convective outflow was intentionally sampled and convection was unusually intense (*Pickering et al.* (1996)).

3.6.4   Acetaldehyde (CH₃CHO)

Acetaldehyde is produced in the oxidation of a variety of hydrocarbons. It can participate in HO_x production, but also produces PA-radicals and is thus an important precursor for PAN. In the mechanism employed in this thesis it is produced from ethane, n-butane (the surrogate for higher alkanes) and propene, totaling 100 Tg/yr. An additional 4.6 Tg/yr is emitted from biomass burning. Although this amount is low compared to the photochemical production, it

could be considerably more efficient in forming PAN, as is it emitted simultaneously with NO_x. Comparison with surface measurements over Europe (Figure 3.33) shows that the model usually agrees within a factor of 2 (except for the Ispra station, see above). No clear seasonal cycle is seen in the model, indicating that increased photochemical production and a shorter lifetime in summer are approximately in balance. In contrast, the observations show a summer maximum at some stations (Donon, Kosetice, Birkenes). This could point towards biogenic emissions peaking in summer (*Kesselmeier and Staudt* (1999)), but also additional photochemical sources are possible.

Airborne measurements have been recently reported from the LBA-Claire Campaign (*Crutzen et al.* (2000); *Williams et al.* (2001)) over the rain forest in Surinam. The mixing ratios of 1.7 nmol/mol in the boundary layer and 0.2-0.8 nmol/mol in the free troposphere are not reproduced by the model, which only computes 0.3 and 0.05 nmol/mol, respectively. Clearly, additional sources are needed to resolve the discrepancy. *Williams et al.* (2001) also report that the mixing ratios were actually higher over the ocean than over the forest. During the PEM-Tropics-B campaign (*Singh et al.* (2001)) acetaldehyde mixing ratios over the remote Pacific were measured to be about 60-100 pmol/mol, about 4-8 times higher than the MATCH results. As pointed out by *Singh et al.* (2001), wide-spread emissions are needed to reach such high values in the remote Pacific. As mentioned before *Zhou and Mopper* (1997) also found support for the hypothesis that acetaldehyde is formed in dissolved organic matter in the surface micro-layer of the oceans by photochemical processes which could result in a net flux from sea to air.

It is clear from this comparison that the budget of acetaldehyde is far from being understood (and correctly modeled). Due to its importance as a precursor for PAN and HO_x, further measurements of this compound should be given a high priority in future field campaigns.

3.6.5 Other Oxygenates (Methanol, Formic and Acetic Acid)

In this subsection three oxygenated species which are included in the photochemical mechanism and might be of importance to atmospheric chemistry are briefly discussed. The compounds methanol (CH_3OH), formic acid ($HCOOH$) and acetic acid (CH_3COOH) have in common that relatively few atmospheric measurements are available and knowledge about their sources and sinks is still quite uncertain. The photochemical lifetime with respect to gas phase oxidation of methanol, formic and acetic acid are 14, 20, and 11 days, respectively. Acetic and formic acids have lifetimes against deposition (both wet and dry) of about 7 days and only one day, respectively. This implies that most HCOOH is lost from the atmosphere by non-chemical processes, making it uninteresting for atmospheric chemistry, unless aqueous phase reactions are taken into account. It is noted that both carboxylic acids can contribute significant to acid deposition (*Chebbi and Carlier* (1996)). Formic acid is therefore only briefly discussed here. In fact, both acids have been found in the gas phase, as well as in aerosols and cloud droplets or rain water. For a review the reader is referred to *Khare et al.* (1999). Since the model only represents the gas phase chemistry of these acids, a good simulation of their distributions cannot be expected. Here, only the gas phase budgets are presented and a few general findings from a comparison with measurements can be made.

Methanol   Besides the total of 77 Tg/yr methanol from direct emissions, 28 Tg/yr are calculated to be produced from gas phase reactions of the methylhydroxy radical (CH_3O_2) with other alkyl-radicals, 90% of which stem from the self reaction of CH_3O_2. The loss in the model is

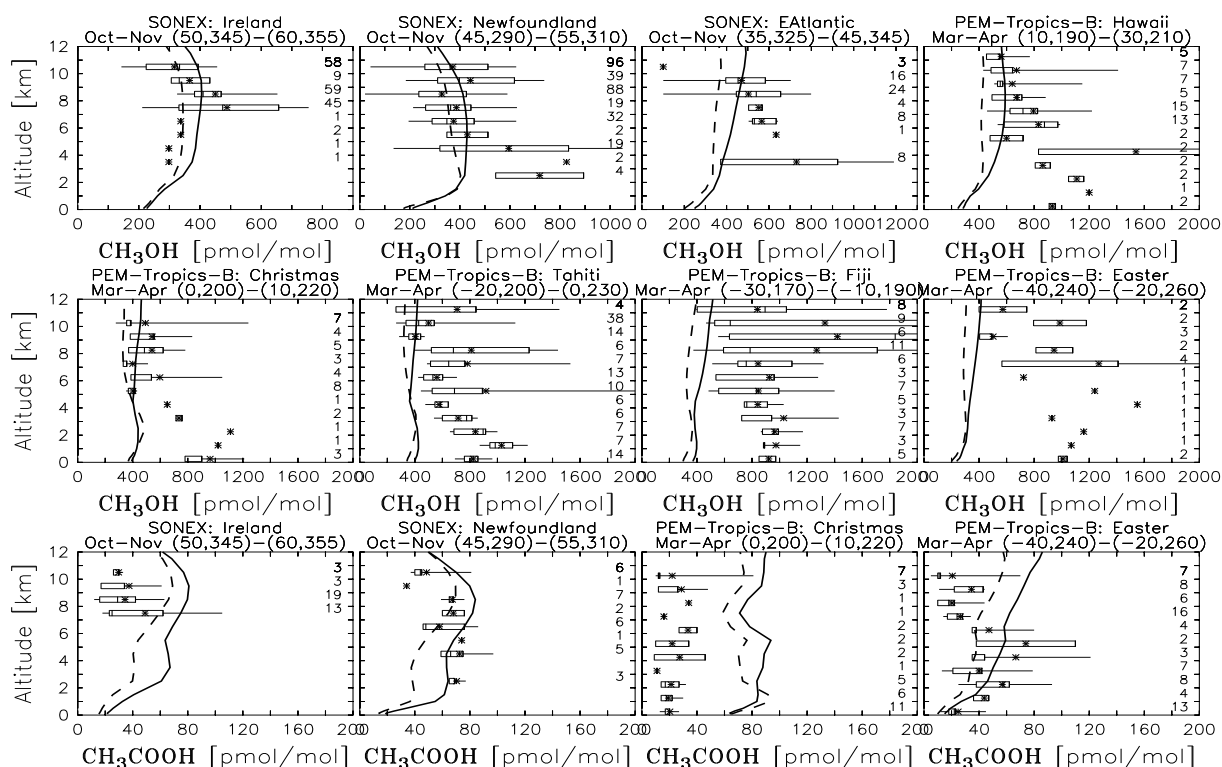Figure 3.36: Comparison of methanol (CH$_3$OH, first two rows) and acetic acid (CH$_3$COOH, last row) measurements with model results. Symbols and lines are as in Figure 3.5.

through reaction with OH (63%), through dry (30%) and wet deposition (7%). It is noted that dry deposition velocities of methanol have not been measured to date and this estimate is solely based on the Henry's Law constant using the relations of *Wesely* (1989).

During the LBA-Claire campaign boundary layer mixing ratios of 1.1 nmol/mol (< 3 km) and a mean free tropospheric value (> 3 km) of about 0.6 nmol/mol were found (*Crutzen et al.* (2000); *Williams et al.* (2001)). The model calculates up to 5 nmol/mol in the model surface layer (both resolutions) but decreases rapidly to 0.7 nmol/mol at about 800 hPa. In the free troposphere the values range between 0.7-1.6 in the high resolution run and only 0.4-0.8 in the T21 run due to weaker convection in that simulation. Thus, with the assumed biogenic emissions (60 Tg/yr = 22.5 Tg(C)/yr) free tropospheric concentrations can be reasonably reproduced. The boundary layer measurements are not sufficient to falsify the assumed 60 Tg/yr of direct biogenic emissions, taking into account the uncertainty in vertical mixing (see also the findings from the vertical profile of isoprene, Section 3.4.3). But it nevertheless appears that emissions in the that region are on the high side. Airborne measurements of methanol were also made during the SONEX and PEM-Tropics-B campaigns (*Singh et al.* (2000, 2001)). Figure 3.36 shows that the model is in reasonable agreement with the SONEX measurements, but mostly underestimates the mixing ratios observed over the Pacific, especially near the surface. The opposite vertical gradient (the model increases, whereas observations decrease with altitude) indicates that the ocean is more likely a net source than a sink in this region. Slow deposition to the ocean, accounting for about a third of the dry deposition loss, has been assumed in this study.

Finally, it is noted that mixing ratios of methanol, the most abundant of the three species

discussed in this subsection, could also be linked to the formaldehyde and formic acid budgets. *Monod et al.* (2000) found that both species can be produced in the aqueous phase oxidation of methanol (depending on pH-values) but the importance of these pathways to the atmospheric budget was not assessed.

Acetic and Formic Acid Acetic acid is photochemically produced mainly from reactions of the PA-radical (CH_3CO_3) with peroxy radicals (with HO_2: 63%, CH_3O_2: 28%) and from the reaction of OH with acetone (9%). It should be noted that only one channel of each of these reactions yields acetic acid. A total photochemical source strength of 75 (60) Tg/yr is calculated from the T63 (T21) simulation. These values are considerably smaller than that reported by *Baboukas et al.* (2000) (120 Tg/yr). This is probably due an erroneously interchanged branching ratio of the $CH_3CO_3+HO_2$ reaction used in that study (70% yield of acetic acid instead of 30%; see *Poisson et al.* (2000) for the chemical mechanism). Furthermore, more recent measurements by *Crawford et al.* (1999) found a CH_3COOH yield of only 12±4%. Following the recommendation of *Tyndall et al.* (2001), a branching of 0.2:0.8 at 298K was used here with a weak temperature dependence.

Comparing the MATCH simulation with the measurements of *Baboukas et al.* (2000) made over the Atlantic (25°W) indicates a strong underestimation of acetic acid in the model (by a factor of 3-9). The measurements are 200-500 pmol/mol, whereas in the model only 20-100 pmol/mol are calculated. On the other hand, comparison with aircraft measurements over the Atlantic and Pacific (Figure 3.36) shows that mixing ratios of acetic acid can be either over or underestimated by the model. However, the high calculated values in the remote Pacific might be due to the strong overestimate of PAN, which upon decomposition releases CH_3CO_3 that can efficiently form CH_3COOH in the NO_x-bereft environment. The agreement might therefore be fortuitous. The increase of mixing ratios with altitude in the model south of about 20°S (see also Figure 3.30, last panel) is not clearly seen in the measurements. Therefore, it appears that an additional source is needed over both the Atlantic and over the Pacific ocean. It is noted than increasing acetone to observed values would also cause somewhat increased production of acetic acid (Reaction R112, Table A.1).

Formic acid is only produced from the ozonolysis of alkenes (mainly isoprene) in the model totaling 17 Tg/yr (in basic agreement with *Baboukas et al.* (2000)). This and an additional 14 Tg/yr from biomass burning and the terrestrial biosphere only produce a few pmol/mol in oceanic regions, definitely too low compared to the observations of a few 100 pmol/mol (*Arlander et al.* (1990); *Baboukas et al.* (2000)). Also, most surface measurements compiled by *Poisson et al.* (2000) and also the measurements by *Quesada et al.* (2001) in Surinam are underestimated by a factor of 2 or more, except in the central Amazon, where model and observations consistently show about 500 pmol/mol. Several possible additional sources are discussed in the literature (see e.g. *Chebbi and Carlier* (1996); *Khare et al.* (1999); *Baboukas et al.* (2000)) including gas phase reactions and aqueous phase oxidation. Recent measurements, however, suggest that aqueous phase oxidation of HCHO is not an important source (see *Chebbi and Carlier* (1996); *Khare et al.* (1999) and references therein). Known gas phase production mechanisms for HCOOH are the alkene-ozone reactions (including isoprene+O_3), which are included in this study (except for higher alkene reactions) and the reaction of formaldehyde with HO_2, which has been judged to be unimportant (*Chebbi and Carlier* (1996); *Khare et al.* (1999)). The underestimate in alkene mixing ratios over oceans (see Section 3.4.2) could be another explanation, but even using much

higher emission rates of alkenes from oceans (see *Poisson et al.* (2000)), *Baboukas et al.* (2000) report 9 times too low mixing ratios of formic acid from gas-phase chemistry.

It is concluded that sources and sinks of methanol and the acetic and formic acids are not well understood. With the best guesses used in this study methanol and to a lesser extent acetic acid concentrations were calculated in reasonable agreement with observations. A widespread source of methanol in remote oceanic regions would improve the agreement with observations over the Pacific. Taking into account other model deficiencies, particularly the overestimation of PAN, an additional source of acetic acid is also probable. Likewise, for formic acid a large missing source, especially over the oceans, is clearly needed to match the observations.

3.7 Ozone (O_3)

In this section the global distribution of ozone is presented and compared to various types of observations. This comparison draws on the evaluations of other species done in the preceding sections. First, the distribution and budgets as calculated in MATCH are shown, followed by the evaluation with measurements. Also some results from a simulation using meteorological data from the NCAR Community Climate Model's (*Kiehl et al.* (1998)) middle atmosphere version (MACCM) are presented for comparison. The evaluation of ozone is mostly based on climatological multi-year data sets (ozone sondes and surface data), which should be favored over single-campaign data, but are not available for most other species.

In order to analyze further the origin of tropospheric ozone a "stratospheric ozone tracer" (O_{3S}) has also been included in the simulations, largely following the approach of *Follows and Austin* (1992) and *Roelofs and Lelieveld* (1997). O_{3S} is set equal to O_3 in the stratosphere after each time step and destroyed in the troposphere by photochemistry and deposition to the surface like ozone. The definition of the stratosphere in this procedure is based on the tropopause calculated online during the simulation. In order to eliminate fast null cycles within the O_x family, only a loss of odd oxygen ($O_x = O^1D + O_3 + NO_2 + 2\,NO_3 + 3\,N_2O_5 + HNO_3 + HNO_4 + PAN +$ other nitrates) is considered to be a loss of O_{3S}. It would thus be more precise to speak of "stratospheric odd oxygen", but since ozone is the dominating compound of O_x for tropospheric background conditions they are treated as equivalent hereafter. The odd oxygen family is also used to calculate 3D-fields of the gross production ($P(O_3)$) and gross loss ($L(O_3)$) of ozone, which is used to further analyze its budget. It is noted, however, that with this definition an equivalent of 148 Tg(O_3)/yr of odd oxygen is also lost from the atmosphere via wet and dry deposition of nitrogen species (=43 Tg(N)/yr). The stratospheric part of this loss is probably on the order of a few tens Tg(O_3)/yr, thus likely less than 10% of the stratospheric influx (see below). It is certainly small compared to the gross loss term and is neglected in this approach.

3.7.1 Tropospheric Distribution and Budgets

The annual zonal mean distribution of $P(O_3)$ and $L(O_3)$ and the net term are shown in Figure 3.37. The reactions mainly contributing to each total are listed in Table 3.8. Production of ozone is highest (5-9 nmol/mol/day) near the surface at northern mid-latitudes, where large NO emissions mainly from fossil fuel combustion occur. Locally, the production rate in the boundary layer can reach values up to about 25-35 nmol/mol/day over polluted regions, in agreement with the 3D results of *Hauglustaine et al.* (1998). In the uppermost tropical troposphere and the

stratosphere the effect of the photolysis of molecular oxygen can also be seen. While on the global average it contributes only 1% to the production of ozone, it can be a significant contribution to the ozone concentration above 200 hPa in the tropics. This was found in a sensitivity run neglecting this reaction, as done in the previous versions of MATCH and most other studies of tropospheric ozone. Up to about 35% less ozone was found (maximum percentage just below the tropopause), but the effect is only about 10% at 200 hPa and negligible below 300 hPa.

The source of ozone is mainly through reactions of NO with HO$_2$ and CH$_3$O$_2$ (followed by photolysis of NO$_2$), with only small contributions from other peroxy-radicals. It is noted that this does not mean that the influence of other VOCs than methane is negligible because they can increase the abundance of HO$_2$ and CH$_3$O$_2$ (see Chapter 4), as well as affect the NO concentrations.
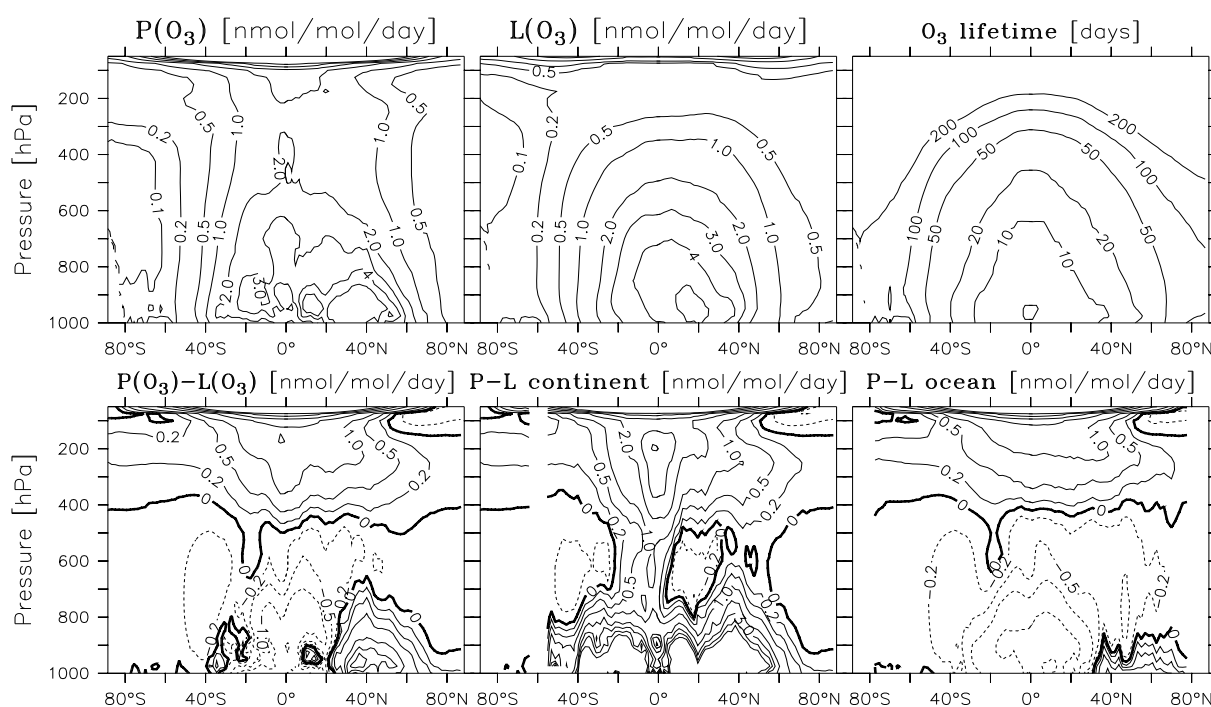
Figure 3.37: Calculated annual zonal mean gross production, loss and net production and lifetime of ozone (O$_x$, see text). The net production averaged only over continents and oceans is also shown.

The loss of ozone is strongest in the lower tropical troposphere, where the humidity and abundance of HO$_x$ are highest. These factors mainly determine the loss of ozone (Table 3.8). The associated photochemical lifetime of ozone is also plotted. A minimum annual zonal mean lifetime of about 5 days is calculated for the tropical boundary layer. The reaction of ozone with isoprene can cause the ozone lifetime to decrease to only 3-5 days in regions with substantial isoprene emissions. In the winter mid and high latitudes the lifetime exceeds 100 days.

The net tendency (P-L) of ozone calculated from these two terms results in net production above about 400 hPa and regions with net loss or production below (lower left panel in Figure 3.37). The net production restricted to regions over continents or oceans (as defined by the model's land/sea mask) are also shown. Except for small portions in the mid-troposphere net production of ozone occurs throughout the troposphere over the continents, whereas over oceans

Table 3.8: Annual mean production and loss terms of ozone in the troposphere in $\text{Tg}(O_3)/\text{yr}$ and percent of the total production and loss rate. Only terms contributing more than 0.5% are listed.

	Reaction	$\text{Tg}(O_3)/\text{yr}$	10^{10} molec/cm^2/s	Percent
Sources	$HO_2 + NO \rightarrow NO_2 + OH$	2819	22.0	61.8 %
	$CH_3O_2 + NO \rightarrow HCHO + HO_2 + NO_2$	1079	8.4	23.6 %
	$CH_3CO_3 + NO \rightarrow CH_3O_2 + NO_2 + CO_2$	237	1.8	5.2 %
	$MVKO_2 + NO \rightarrow NO_2 + .25\ CH_3CO_3\ldots$	124	1.0	2.7 %
	$ISO_2 + NO \rightarrow .956\ NO_2 + \ldots$	115	0.9	2.5 %
	$O_2 + h\nu \rightarrow 2\ O_3$	48	0.4	1.0 %
	$CH_3CO_3 + HO_2 \rightarrow CH_3COOH + O_3$	38	0.3	0.8 %
	$C_2H_5O_2 + NO \rightarrow CH_3CHO + \ldots$	33	0.3	0.7 %
	$C_3H_6O_2 + NO \rightarrow .98\ CH_3CHO \ldots$	32	0.3	0.7 %
	other reactions	47	0.4	1 %
Losses	$O^1D + H_2O \rightarrow 2\ OH$	−2436	19.0	56.8 %
	$O_3 + HO_2 \rightarrow OH + 2\ O_2$	−1211	9.4	28.3 %
	$O_3 + OH \rightarrow HO_2 + O_2$	−503	3.9	11.7 %
	$C_5H_8 + O_3 \rightarrow .58\ HCHO + .28\ HCOOH\ldots$	−33	0.3	0.8 %
	other reactions	−103	0.9	2.4 %

loss prevails below the 400 hPa level and production above. The net production seen north of about 40°N in the MBL is due to the relatively low loss rates combined with production near the coast downwind of the industrialized regions and also some production from ship NO_x emissions.

The annual mean budgets for several sub-domains of the troposphere calculated by the two model resolutions are summarized in Table 3.9. The range of values from other studies is also given, but it has to be kept in mind that different definitions of the troposphere were used, which makes a direct comparison difficult. For example, the calculated tropospheric burden of 294 $\text{Tg}(O_3)/\text{yr}$ is at the low end of the range from other studies, but integrating below $\sigma = 0.116$ yields 410 $\text{Tg}(O_3)/\text{yr}$, which may be compared to studies that use the region below 100 hPa. As already mentioned for the methane lifetimes the use of uniform definitions of the troposphere is recommended to increase the comparability of the different studies.

At first glance the tropospheric budget of O_3 appears to be a balance between losses through dry deposition and sources from the stratosphere and a smaller net photochemical production, but the net photochemical production (or net destruction as calculated by some studies) is actually the difference of two large terms (5-9 times larger any of the other terms) that are largely canceling out each other on the global average, but not regionally. In fact, using the monthly mean production and loss fields it can be calculated that in regions of the troposphere where production is larger than destruction about 1430 (1310) $\text{Tg}(O_3)/\text{yr}$ are produced in the high (low) resolution run, which are largely balanced by -1020 (-1110) $\text{Tg}(O_3)/\text{yr}$ in regions with net loss (mainly marine regions below 400 hPa, see below). Note that the difference in the net production compared to the numbers in Table 3.9 is due to the use of monthly mean fields and tropopause pressures as opposed to the online calculation used in Table 3.9. Thus, even if one argues that the two large global tropospheric production and loss terms are not independent

of each other, due to chemical coupling[18], this shows that only accounting for the net effect in regions of the troposphere yields more than two times higher values than the stratospheric influx.

Remember that the stratospheric input was artificially reduced to get better agreement with observations (next section) and other studies (*Murphy and Fahey* (1994); *Tie and Hess* (1997); *Gettelman et al.* (1997); *McLinden et al.* (2000)). The other values are in the range of previous studies, except for the gross production and loss terms, which are higher than previous estimates. Gross and net production of ozone (in molec/cm^2/s) is larger in the NH than in the SH and larger over continents than over the oceans. The tropics are also a photochemically very active region of the atmosphere (per area) but the net photochemical effect on ozone is low. This is the result of averaging over remote oceanic regions, where large destruction occurs, and regions with net production over the continents and in the free troposphere. The net transport over the continents is negative, despite some influx from the stratosphere. Assuming a stratospheric influx of about 220 Tg/yr[19] one can estimate that about 370 Tg(O$_3$)/yr are exported from the continental into the marine troposphere. This value is of the same order as the stratospheric input (about 320 Tg/yr) into that region, but it is much lower than the production term integrated over all net producing regions in the troposphere (1430 Tg/yr, see above).

The upper troposphere also exports ozone due to the large net production in that region (550 Tg/yr)[20]. This results in a total of 1090 Tg(O$_3$)/yr, about twice the stratospheric influx, transported into the lower troposphere ($\sigma > 0.341$), where it is balanced by dry deposition (820 Tg/yr) and net photochemical destruction (270 Tg/yr). This is an interesting point, because it demonstrates that photochemical production is as important as stratospheric influx even in the upper troposphere, where ozone is most efficient as a greenhouse gas (e.g. *Lacis et al.* (1990)).

The resulting distribution of O$_3$ as calculated with the high resolution run is shown in Figures 3.38 and 3.39. High surface mixing ratios (up to 80 nmol/mol) are calculated over the Mediterranean in summer (60-80 nmol/mol) and over the industrialized regions of the U.S (50-70 nmol/mol). It is interesting to note that the maximum values near the eastern U.S. are actually calculated off the coast. This is also seen off the coast of India in January, similar to observations by *Lal and Lawrence* (2001). The effect is probably due to the titration of ozone by freshly emitted NO (NO+O$_3$ $\rightarrow$ NO$_2$+O$_2$, as mentioned in Appendix B.2), which reduces ozone concentrations directly over the source region, but ozone production down wind of the sources and less deposition over the ocean probably also contribute to the effect. The titration effect can be more clearly seen in winter, when a distinct ozone minimum is calculated. The effect is equivalent to the low or zero ozone concentrations found in the center of large cities or streets, but is probably overestimated by the perfect mixing of the fresh NO emissions and O$_3$ (see also Appendix B.2). It is restricted mainly to the first few model layers. At 900 hPa mixing ratios of ozone over the source regions of NO$_x$ have recovered to about 30 nmol/mol already.

It is noted that mixing ratios over Amazonia are too high compared to measurements during the ABLE campaigns (6 and 12 nmol/mol at daytime during the wet and dry season respectively,

---

[18]Ozone production occurs mainly in regions with high NO$_x$, which also causes enhanced HO$_x$ concentration that increase the loss of ozone (see Table 3.8, loss reaction 2+3). Also, more ozone results in more OH which in turn causes enhanced ozone loss (see Table 3.8, loss reaction 1).

[19]This estimate is based on the fact that about 30% of the earth's surface is covered by land and considering that the stratosphere-troposphere flux (STF) is about 50% higher in the northern hemisphere (see also *Ebel et al.* (1996)) and mainly occurring north of about 30°, where land masses cover a larger fraction of the surface. Thus, roughly 40% of the STF is assumed to occur over the continents.

[20]The value for the T21 simulation calculation from the monthly mean fields (post-processed, since this region was not calculated online in that run) yields a lower value of 405 Tg(O$_3$)/yr.

Table 3.9: Budgets of O_3 in different regions of the troposphere from the standard simulations (in $Tg(O_3)$/yr and 10^{10}molec/cm^2/s in *italics*). Rates in Tg/yr are rounded to tens of Tg/yr.

Resolution Region[b]	Range[a] GT	T63 GT	T21 GT	T63 NH	T63 SH	T63 CT	T63 MT	T63 TT	T63 UT
Burden, Tg-O$_3$	294-401	294	306	171	123	92	202	108	102
(molec/cm^2)	—	*2.3*	*2.4*	*2.7*	*1.9*	*2.4*	*2.2*	*2.4*	*0.8*
Net transport[c]	390-1100	540	630	300	250	−150	690	270	−550
	—	*4.2*	*4.9*	*4.6*	*3.8*	*−3.9*	*7.6*	*6.0*	*−4.3*
Dry deposition	−534-1180	−820	−700	−550	−260	−570	−250	−290	—
	—	*−6.4*	*−5.5*	*−8.7*	*−4.0*	*−15*	*−2.8*	*−6.5*	—
P(O$_3$), chem. production	3020-4550	4560	4170	2820	1740	2210	2370	2390	760
	—	*35.6*	*32.5*	*43.6*	*26.2*	*58.9*	*25.8*	*53.2*	*5.9*
−L(O$_3$), chem. loss	2511-4000	−4290	−4090	−2560	−1730	−1500	−2740	−2370	−210
	—	*−33.4*	*−31.9*	*−39.4*	*−26.0*	*−39.8*	*−30.6*	*−52.7*	*−1.6*
P(O$_3$)–L(O$_3$)	−480-+550	+280	+80	+260	+16	+720	−440	+25	+550
	—	*+2.2*	*+0.6*	*+4.2*	*+0.27*	*+19*	*−4.9*	*+0.56*	*+4.3*
Lifetime	—	25 d	27 d	27 d	25 d	22 d	27 d	17 d	6 mo

[a]Ranges are based on previous 3D-modeling studies (*Hauglustaine et al.* (1998) and references therein, *Houweling et al.* (1998); *Müller and Brasseur* (1995); *Lawrence et al.* (1999b); *Roelofs and Lelieveld* (2000)). It is noted, however, that different definitions of the troposphere were used.

[b]Region definitions: GT: Global Troposphere (below WMO-tropopause, calculated online), SH: Southern Hemisphere, NH: Northern Hemisphere, CT: Continental Troposphere, MT: Marine Troposphere, TT: Tropical Troposphere (20°S-20°N), UT: Upper Troposphere ($\sigma < 0.341$).

[c]Net transport is the sum of individual terms: advection (443), convection (14), vertical mixing (4), and tropopause movements (82). Numbers in brackets are $Tg(O_3)$/yr for the T63-GT region. Net transport into the global troposphere is the net stratosphere-troposphere flux (STF).

Kirchhoff et al. (1990)). In part this is due to the too high calculated wet skin fraction in the T63 run. The T21 run using a corrected wet skin fraction is in better agreement, yielding about 10-15 nmol/mol but still on the high side of the measurements. This may be because even in the corrected version wet skin fractions can reach 50%, and by assuming that O_3 deposition is inefficient over wetted surfaces (*Ganzeveld and Lelieveld* (1995)) deposition of O_3 is still significantly hindered. As mentioned before (Section 2.3.4) the process is highly uncertain and more research is clearly needed to clarify the effect of wetted canopies on ozone deposition.

At 500 hPa in the NH winter a very smooth ozone distribution is calculated in agreement with observations (*Logan* (1999)) reflecting the long lifetime of ozone. Ozone minima are over the remote Pacific, where low NO_x mixing ratios and high humidities result in strong net destruction of ozone. Over the Middle East an O_3 maximum of about 80 nmol/mol is calculated, which is supported by measurements from the MOZAIC campaign and ozone soundings (*Li et al.* (2001)).

The distribution of ozone in the T21 run is very similar near the surface (except over the Amazon, see above), but O_3 mixing ratios are about 10 nmol/mol higher at 500 hPa in the winter hemisphere likely due to higher stratospheric influx in that run (Table 3.9).

The zonal mean mixing ratios, depicted in Figure 3.39 (contour lines), are lowest near the surface especially in the tropics and the southern latitudes and increase monotonically with height. This increase is the combined effect of stratospheric input, photochemical production in the upper troposphere, and deposition to the surface. In the tropics low surface ozone mixing ratios, which result from the net destruction in that region as shown above, are transported upward and maintain zonal mean mixing ratios of 30-40 nmol/mol up to about 200 hPa, and
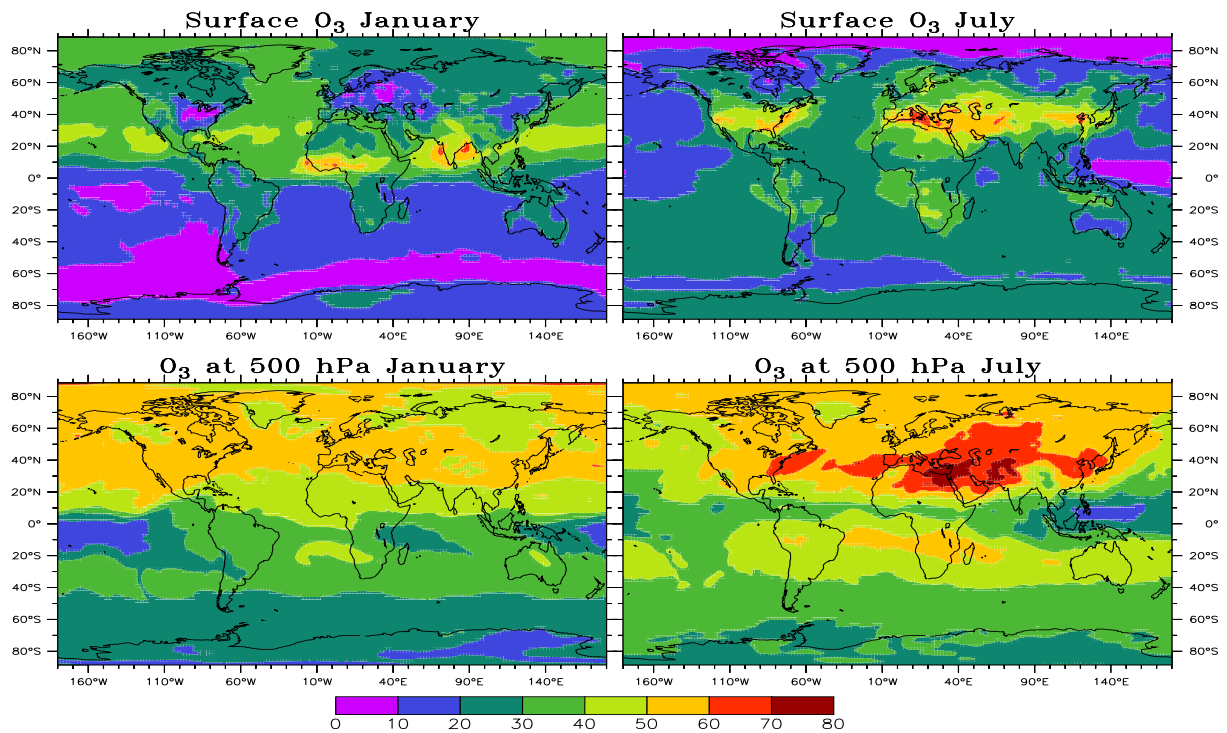
Figure 3.38: Modeled distribution of ozone in nmol/mol (T63) for January and July in the lowest model layer and at 500 hPa.
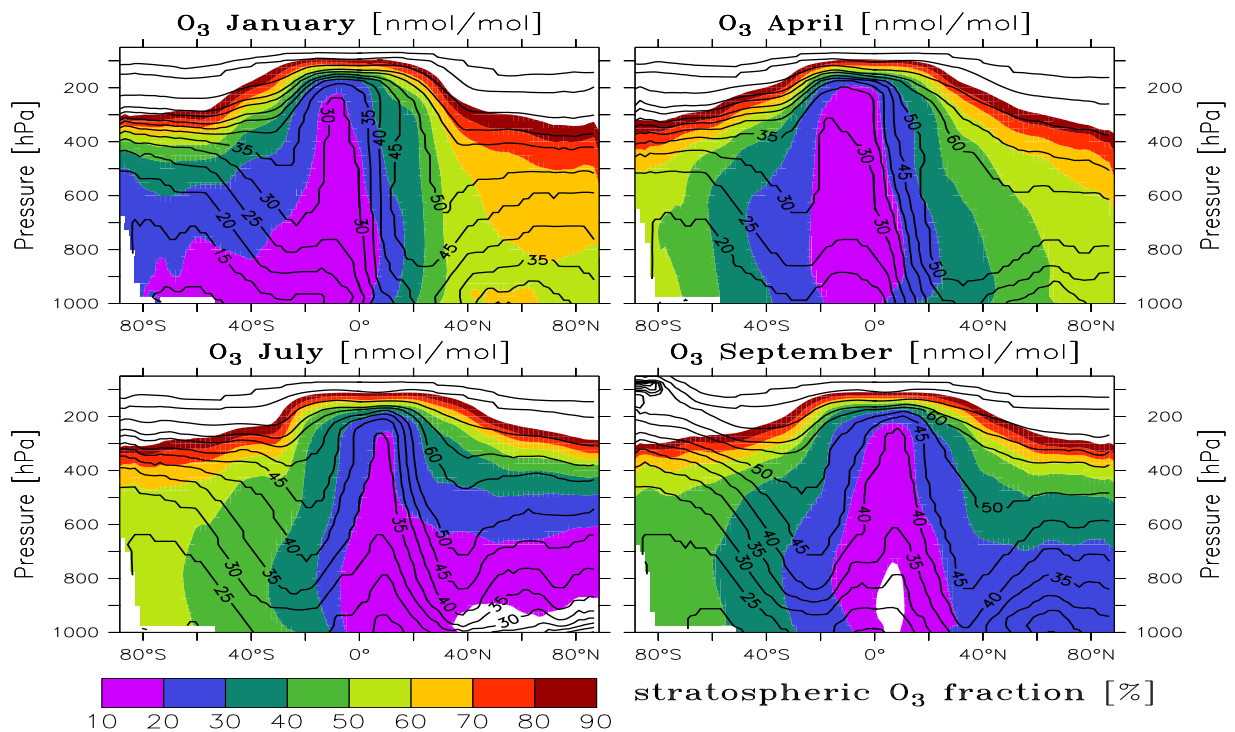

Figure 3.39: Zonal mean distribution of ozone from the T63 run for 4 months. Contour lines are O$_3$ mixing ratios in nmol/mol, color shading gives the contribution of the O$_{3S}$ tracer to the total ozone mixing ratio in percent.

much lower mixing ratios in specific regions such as the Pacific (*Kley et al.* (1996); *Lawrence et al.* (1999a)). The smallest monthly mean values are 12 nmol/mol in the upper troposphere in this region.

Additionally, the shading in Figure 3.39 gives the percent contribution of the O_{3S} tracer. A clear seasonality in the stratospheric influx of ozone, with the maximum in winter to spring in each hemisphere, can be seen. It is noted, however, that tropopause folding events, which are believed to cause a large part of the ozone flux into the troposphere, are not resolved even at T63 resolution. Therefore, as pointed out by *Lawrence et al.* (1999b) and *Crutzen et al.* (1999), it is well possible that the influx is not correctly distributed over the extratropical latitudes.

The stratospheric contribution to the total ozone concentration at the surface is calculated to be larger than 50% in winter and less than 10% in summer in the NH. Apart from a calculated higher stratosphere-troposphere flux (STF) in winter-spring, the high percentage is also due to the longer lifetime of O_3 in that season. During winter-spring in the extra-tropics, these calculations for stratospheric ozone are higher than the results of *Roelofs and Lelieveld* (1997) by about 5-10 nmol/mol. In the tropics there is agreement with that study, and in the southern hemisphere MATCH calculates about 5 nmol/mol less O_{3S}. These differences are in part due to the different advection schemes employed. *Roelofs and Lelieveld* (1997) use a Semi-Lagrangian transport algorithm, which was also use in MATCH 1.2 (*Lawrence* (1996)) and found to give a very different STF than the SPITFIRE scheme used here (*Lawrence et al.* (1999b); *Jöckel* (2000)). The annual mean tropospheric burden of O_{3S} is calculated to be 124 Tg, thus about 42% of the total ozone burden. The fraction appears to be very high in view of the global budgets presented above, but it can be explained by the fact that the stratospheric input is largest in winter (and spring) when the ozone-lifetime is very long. The value is only slightly higher than the one obtained by *Roelofs and Lelieveld* (1997) (40%) which may be due their lower STF of 459 $Tg(O_3)$/yr. This is also in line with the result for the sensitivity run using the MACCM meteorological input data (see Section 2.1), which yields a 35% stratospheric contribution with a STF of only 365 $Tg(O_3)$/yr. More results from this run are shown in ozone sonde comparison (Section 3.7.3).

3.7.2   Surface Measurements

A comparison of the seasonal cycle of modeled surface ozone mixing ratios with observations at 30 stations, compiled from the literature to represent background and polluted conditions in different parts of the world, is presented in Figure 3.40. At most stations the data set spans several years of observations. Like for CO, the model is sampled at a higher level for some mountain stations where the orography is not resolved by the model (Åreskutan, Hohenpeißenberg, Zugspitze, Niwot Ridge, Izaña, Mauna Loa).

The model generally reproduces the seasonal cycle at polluted and background station in both hemispheres and agrees in absolute abundance to within 10 nmol/mol in most cases. Some exceptions are discussed below. The O_{3S} tracer is also plotted to aid the discussion.

At the background northern high and mid latitude sites the springtime maximum (e.g. Reykjavik, Åreskutan, Mace Head) is well simulated. Since the maximum in ozone is later than that of the stratospheric ozone tracer, it appears to be caused by a combination of input from the stratosphere and photochemical production from precursors that have accumulated during winter (e.g. PAN; *Penkett and Brice* (1986); *Monks* (2000)). The seasonal cycle at Barrow is not correctly simulated. This is in line with results from other global models (*Wang et al.* (1998c);
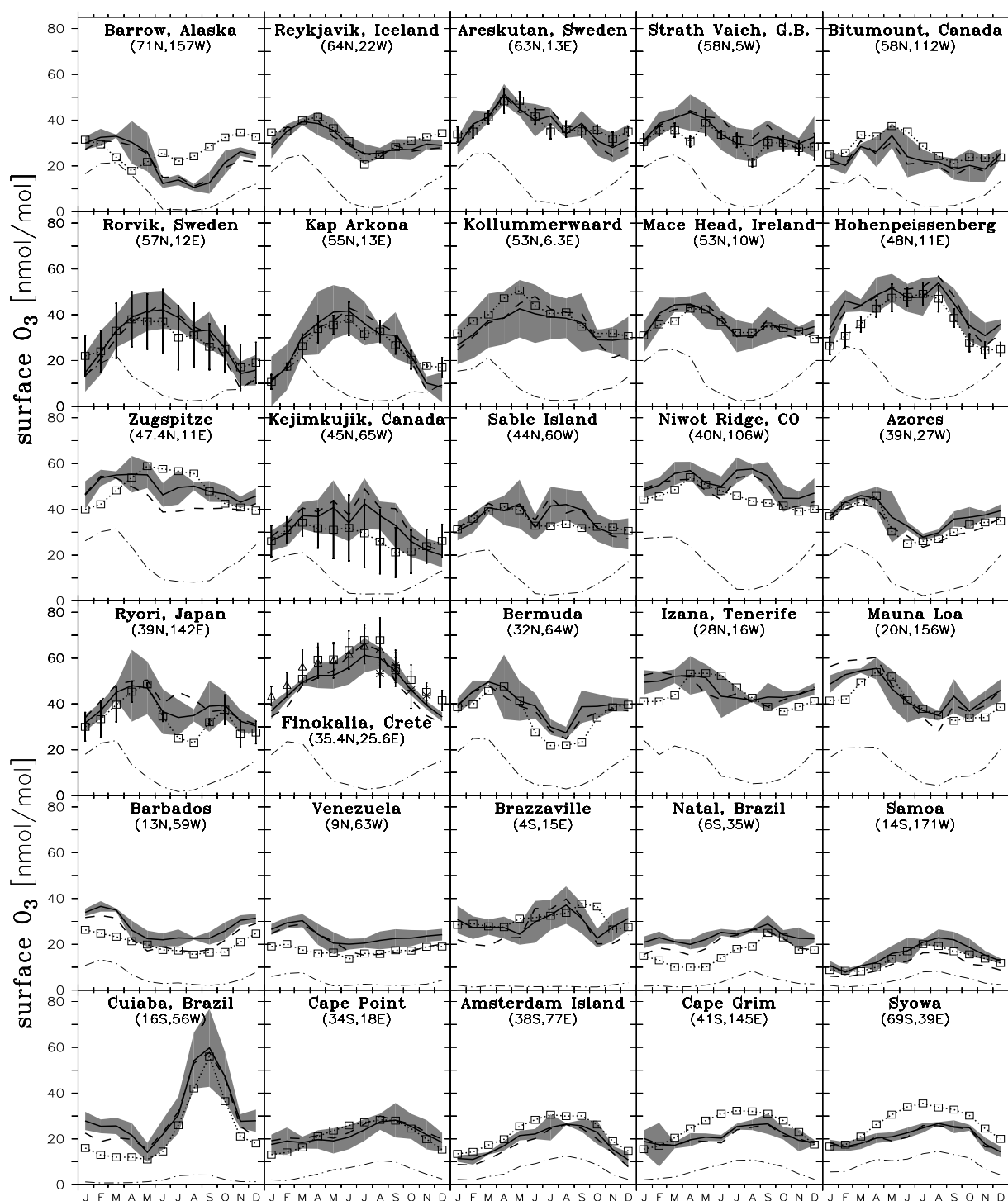
Figure 3.40: Comparison of surface ozone observations with model results (as Figure 3.3). The thin dash-dotted line is the stratospheric ozone tracer (O$_{3S}$) from the T63 run. Vertical bars are standard deviations of the monthly means, except for Rörvik, Kejimkujik and Finokalia, where they are from individual measurements. At Kollummerwaard observations and model are for O$_3$ + NO$_2$. The data are from *Oltmans and Levy* (1994); *Bazhanov and Rodhe* (1997); *Angle and Sandhu* (1986); *Lindskog and Moldanová* (1994); *Scheel et al.* (1997); *Bottenheim et al.* (1994); *Parrish et al.* (1998); *Kouvarakis et al.* (2000); *Sunwoo et al.* (1994); *Sanhueza et al.* (1985); *Cros et al.* (1988); *Kirchhoff et al.* (1989); *Gros et al.* (1998), and the WOUDC data archive (http://www.msc-smc.ec.gc.ca/woudc/).

Houweling et al. (1998); *Poisson et al.* (2000)). The spring time minimum at this site is believed to be caused by bromine-catalyzed ozone destruction (*Barrie et al.* (1988)), which is not included in the model. The underestimate during summer, fall and early winter is not clear. At Bitumount somewhat too low values are calculated. This site was also influenced by the high wet skin fraction, which led to higher ozone mixing ratios in the T63 run. Furthermore, the station is situated at the slope of a mountain ridge, and could thus be influenced by nighttime katabatic winds which could cause a low level mass divergence over the ridge and result in advecting upper tropospheric ozone-rich air to lower altitudes, as indicated by a nighttime maximum often observed at the site (*Angle and Sandhu* (1986)). The station might therefore not be representative for the larger area of the model grid cell.

The seasonal cycle at more polluted stations (e.g. Kap Arkona, Kollummerwaard) displays a summer maximum, which is well simulated. Note that at Hohenpeißenberg the titration effect discussed in the last section does not show up since the surface layer is not sampled, but rather the level at $\sigma = 0.942$ because the station is about 500 m higher that the resolved orography in the model. At high mountain sites (Zugspitze, Izaña, Mauna Loa, Niwot Ridge) the model tends to overestimate in winter which may be due to too excessive STF at this time. However, comparing with the results of MATCH-2.0 (*Lawrence et al.* (1999b)) it can be said that the 50% reduction in STF of ozone resulted in substantial improvement at these stations, which were overestimated by about 20 nmol/mol in MATCH-2.0 using only background chemistry. At the Zugspitze station the summer maximum is not modeled correctly (discussed later in the ozone sonde comparison). The bulge calculated by the model at Niwot Ridge during July to September is not seen in the observation. This phenomenom was also found in the MOZART model (*Hauglustaine et al.* (1998)). It is suspected that this is due to a local characteristic of the site, since at the nearby (< 1° to the east) ozone sounding station at Boulder close to the surface ($\approx$840 hPa) much higher ozone mixing ratios are observed (see below).

The extremely high background values measured on Crete (60-70 nmol/mol in summer) are reproduced by the model. A tendency to underestimate still remains, but is much less than in the MOGUNTIA model tested with these data by *Kouvarakis et al.* (2000).

The biomass burning at Cuiaba (Brazil) is correctly simulated in timing and magnitude, lending further credence to the *Galanter et al.* (2000) data set for this region. However, the dry season (January-May) mixing ratios are overestimated, especially for the high resolution simulation. This is in part due to the too large wet skin fraction in the T63 run (and the assumed hindrance of ozone uptake on wetted surfaces), but it appears that also in the T21 run ozone dry deposition may be underestimated. Dry deposition is also the likeliest reason for the overestimate at Natal (Brazil), considering that at 800 hPa (see below) the agreement is much better.

The seasonal cycles of southern hemispheric background stations peaking in July to September are well simulated in the model. However, at some stations, especially in Antarctica (Syowa but also South Pole, not shown) mixing ratios in austral winter-spring are underestimated. Since little photochemical production is expected during this time, it is probable that the stratospheric influence is underestimated. This bias could be easily introduced by the procedure to globally reduce the stratospheric influx by 50% (as described in Section 2.3.6). This would also fit with the idea that some of the stratosphere-troposphere exchange in the model is caused by fluctuations in the vertical velocity, which is calculated from the horizontal wind components. Thus, the internal consistency of the data set is an important factor. It has been observed for a comparison

over 10 days of data (*M. Lawrence*, personal communication, 2000) that the variation in the vertical velocity was smaller in the NCEP analysis than in the reanalysis used in this study. In the reanalysis the model is forced towards observations which might reduce the consistency of the horizontal wind fields and thus lead to stronger fluctuations in the vertical velocity. In the high southern latitudes observations to nudge the model are scarce, which could lead to a better consistency and subsequently to less fluctuations in the model. It is noted that these fluctuations are only a problem in the vicinity of large gradients, as is the case of ozone near the tropopause, in combination with too coarse a model discretization. Further evidence of problems near the tropopause are presented and discussed in the next section.

3.7.3 Ozone Sonde Data

Ozone sondes from the compilation of *Logan* (1999), which are mostly from the WOUDC archive, are used in this section to evaluate the modeled distribution of ozone in the free troposphere. It has been chosen to test the model at three pressure levels: 800, 500, and 300 hPa. Selected vertical profiles at some station are also presented.

The seasonal cycle at the three pressure levels is compared to the two model runs in Figures 3.41 and 3.42. The O$_{3S}$ tracer is also plotted for comparison. The comparison has been done for over 30 stations of the data set but only 15 stations, selected to represent the main regimes, are shown here.

Although many features of the observation are reproduced by the simulations, some differences are also apparent. The observations show a broad spring to summer maximum up to the tropopause in the northern mid and high latitudes, with the maximum appearing earlier for the high latitudes and later for more polluted sites (e.g. Hohenpeißenberg). In the lower troposphere this seasonal cycle is usually well reproduced, but in the middle and upper troposphere a tendency to overestimate in spring and underestimate in summer is seen.

The O$_{3S}$ mixing ratio at 300 hPa is sometimes higher than the ozone observations (e.g. Alert), showing that at the 300 hPa level, which is often in the stratosphere at high latitudes, the downward mixing of ozone is too efficient. As expected, in a run without the 50% reduction of STF applied in this study the results were in much larger contrast to these observations (not shown). The ozone summer maximum observed at some stations is underestimated at all levels (though not at the surface level, see e.g. Hohenpeißenberg), especially in the middle troposphere. An underestimation of photochemical production in the summer free troposphere must be considered the most probable explanation, but a miscalculated annual cycle in STF of ozone could also play a role. The findings of *Elbern et al.* (1998) that the frequency of tropopause folding events is significantly lower in summer than in other seasons, however, argues against the latter option. Reasons for underestimating of photochemical production could be the neglect of higher alkenes and aromatic compounds in the chemical scheme or too low abundance of NO$_x$ in the free troposphere. For the first option it questionable, though, whether this can enhance ozone in middle troposphere. Nevertheless, these results encourage testing of even more elaborate chemical schemes in MATCH, e.g. including aromatics and/or terpenes, in order to investigate whether the underestimate can be explained by neglected gas phase chemical processes. To little detrainment of precursors in the middle atmosphere could also contribute to the underestimate.

Comparison to the model results using the MACCM meteorological input data strongly suggests that the high winter-spring downward flux of ozone in northern mid and high latitudes is a phenomenom associated with the NCEP data. During this time period the results with the
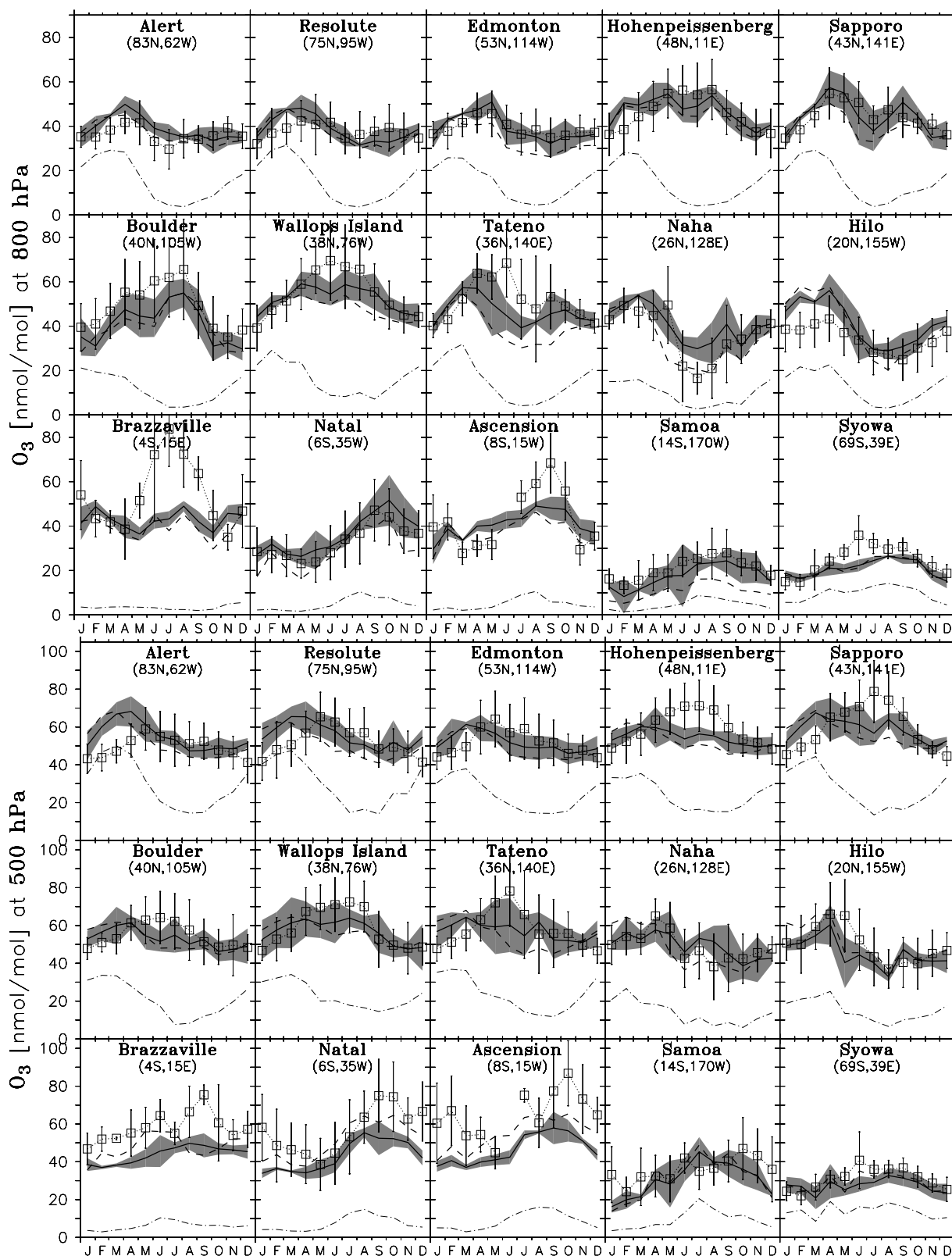
Figure 3.41: Comparison of model results (T63: solid line and shaded area, T21: dashed line) with monthly mean observations (squares) from ozone soundings (compiled by *Logan* (1999)) at 800 and 500 hPa. Vertical bars are standard deviations from the individual soundings. Dash-dotted line is the stratospheric ozone tracer (O_{3S}).
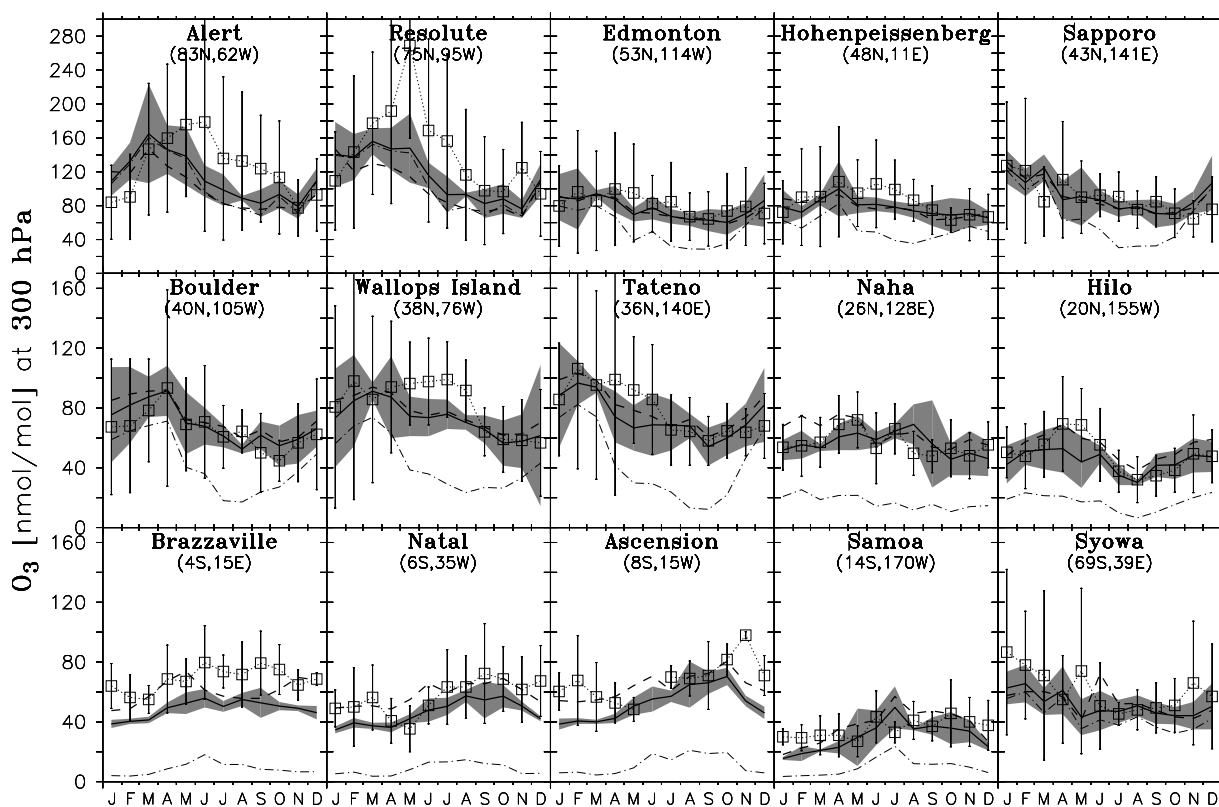
Figure 3.42: Same as Figure 3.41 but at 300 hPa.

MACCM data are in much better agreement to observations than the standard runs using NCEP data (Figure 3.43). The underestimate of ozone over polluted regions in summer (e.g. Hohen-peißenberg) is also seen in the MACCM-simulation, supporting the view that this is probably a photochemical rather than dynamical problem. Note that for the MACCM-simulation no artificial reduction of the STF of 50% was applied. The calculated STF of O_3 of only 365 $Tg(O_3)$/yr in this run is nevertheless lower than current estimates . This could be connected to other problems seen in this simulation, such as very weak convection especially in the tropics.
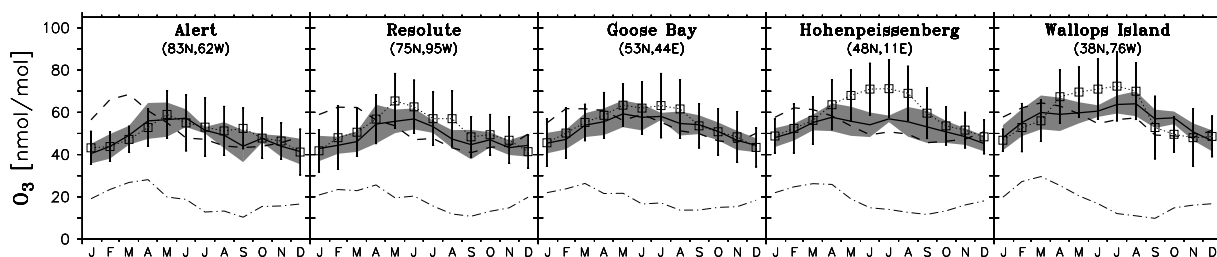
Figure 3.43: Comparison of ozone at 500 hPa. Sondes as in 3.41. Solid line and shaded area is from a MATCH simulation using the middle atmosphere version CCM meteorological data, dashed line is the standard T21 run.

At tropical stations influenced by biomass burning (Brazzaville, Ascension Island, Natal) the model tends to significantly underestimate ozone mixing ratios over large parts of the middle troposphere throughout the year, but especially during the burning season. An underestimate by

about 10-20 nmol/mol was also seen for the TRACE-A measurements (not shown). At Brazzaville the ozone maximum at 700-800 hPa in June-August is not reproduced (see the ozone sonde profile). Comparison of the GOME NO_2 column data over Brazzaville shows that seasonality is well reproduced, but the values are too low by about 30-50% (not shown). Thus, biomass burning at this site is probably underestimated, although it is noted that only 5 soundings from 2-3 years are included in some of the monthly means at this station, which according to *Logan* (1999) and *Lawrence* (2001) is not sufficient to reliably determine a representative ozone profile. The same also applies to Ascension Island, where even fewer soundings are included in the dataset per month. The model is in better agreement at the more remote tropical stations Samoa and Hilo (Hawaii). The seasonal cycles are well reproduced at these stations, but in the lower troposphere at Hilo too much ozone is predicted in winter and spring (as was already seen at Mauna Loa). During this time the station is mostly influenced by air from more northerly latitudes. Little ozone production would be expected for those airmasses and the seasonal cycle of the O_{3S} tracer suggests that too large a stratospheric contribution at those latitudes, which is subsequently advected to Hilo, is the reason for the discrepancy.

The vertical profile of ozone and particularly the location of the chemical tropopause[21] is best examined from plots of the profiles at individual stations. Results for five extratropical and five tropical stations are shown in Figures 3.44 and 3.45. The main features of the seasonally averaged profiles are well simulated at the extratropical sites. In the lowermost stratosphere (above about 250 hPa), however, too low ozone mixing ratios are calculated poleward of about 45° during some seasons in the model. This is a direct consequence of the procedure applied here to reduce the net influx of ozone from the stratosphere, and is another sign that dynamics near the tropopause and in the lowermost stratosphere are not well represented in the meteorological data set. The fact that this deficiency is seen at both resolutions shows that the problem is probably not caused by the procedure to produce this reduced resolution data set (which is simple linear averaging).

In the tropics a good simulation is found at some stations (Hilo, Samoa). Particularly the change in the gradient at about 800 hPa is correctly simulated. This indicates that turbulent mixing across the trade wind inversion is realistically modeled. However, the chemical tropopause is sometimes misplaced in the model by up to about 50 hPa. The reason why this occurs only at some stations in not clear, but it is suspected to be connected to the nudging of the NCEP model for the reanalysis, which would be more severe near the continents (Atlantic) that at the remote Pacific stations, because more observations are available there. It is important to mention, however, that this displacement of the tropopause only represents about 2 (at most 3) model layers. The MACCM run, which has a higher resolution near the tropopause region is in much better agreement at the three stations in the Atlantic region (Natal, Brazzaville, Ascension) (not shown), but the chemical tropopause is sometimes too low over the Pacific (Hilo, Samoa). The latter may be explained by too weak convection in combination with the important role of convection over the Pacific in maintaining low ozone mixing ratios in the uppermost troposphere (*Kley et al.* (1996); *Lawrence et al.* (1999a)). Missing processes such as in-cloud destruction of ozone and iodine chemistry were also suspected by *Kley et al.* (1996). Due to the problems with the MACCM-simulation in the tropics which also affected the simulation of other trace gases this model configuration is not considered in the following chapters.

Unfortunately, it cannot be easily judged whether the improvements in the MACCM-run are due the to higher vertical resolution near the tropopause or a better internal consistency of

---

[21]The region near the thermal tropopause, where large gradients of ozone (and also other tracers) occur.
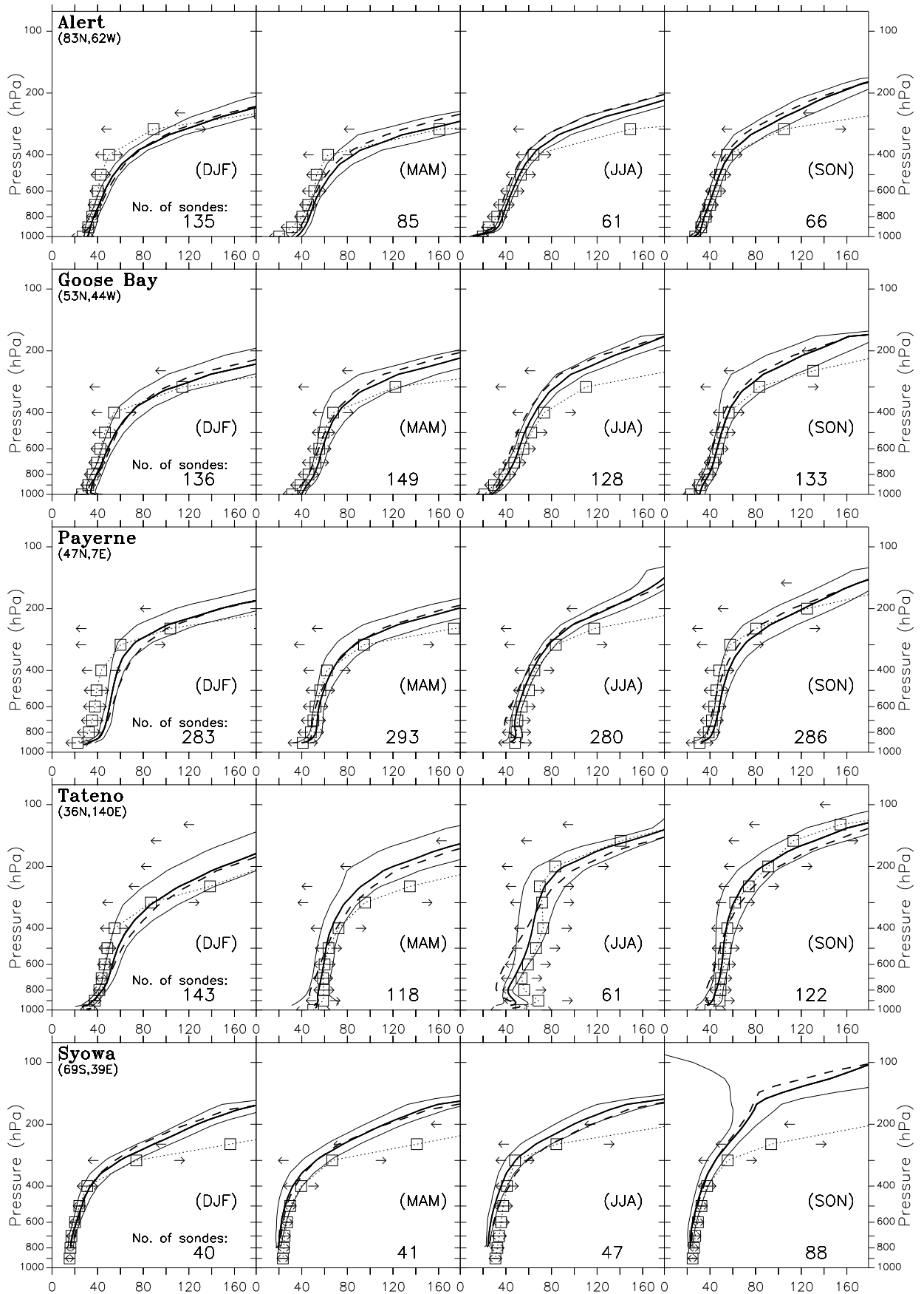
Figure 3.44: Observed (squares and dotted lines for means and arrows for $\pm\sigma$) and simulated (solid line: T63, thin solid lines $\pm\sigma$; T21: dashed line) vertical profiles of ozone during four seasons over extratropical locations. The number of soundings in the average is also given.
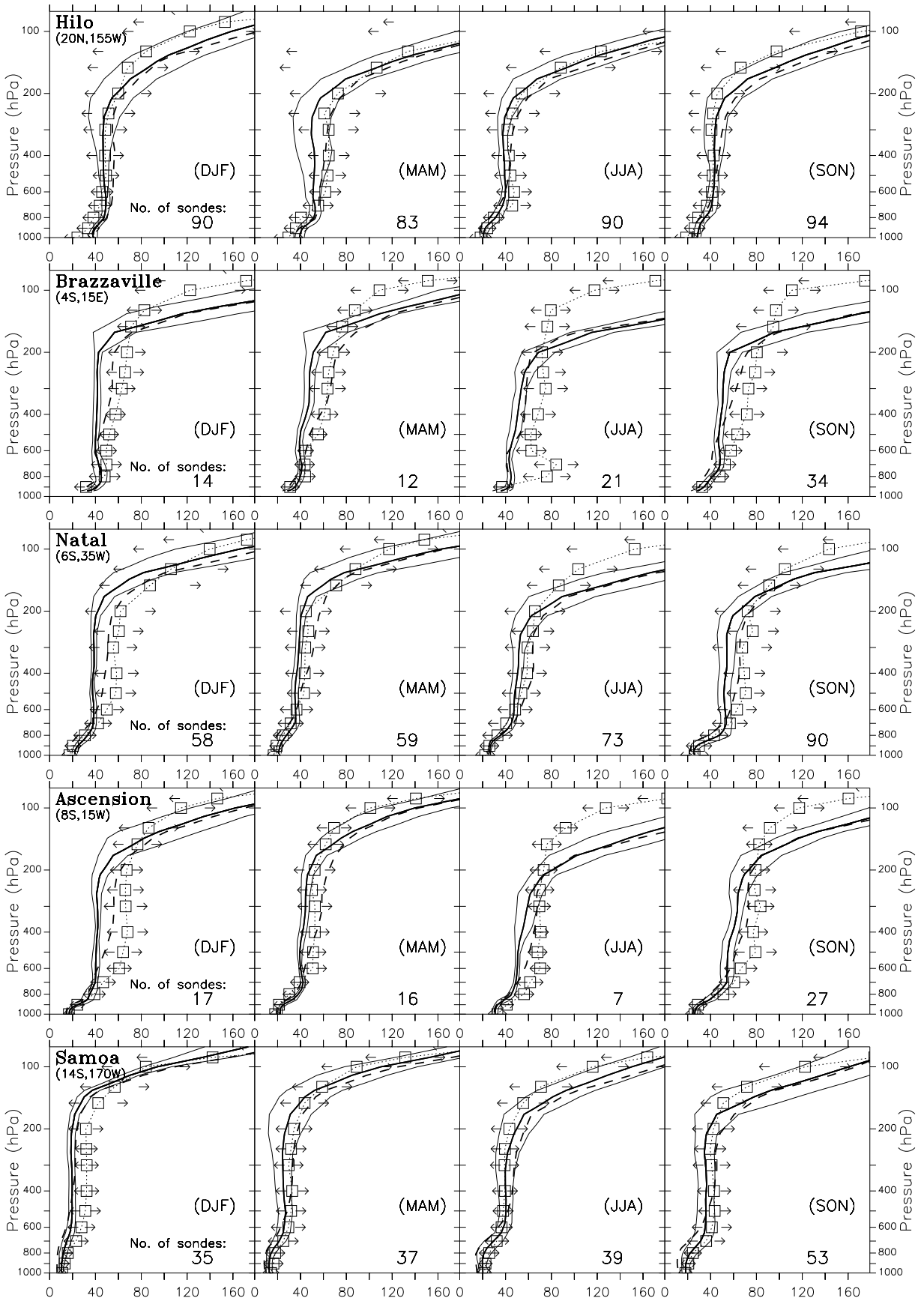
Figure 3.45: Same as Figure 3.44 but for five tropical stations.

the horizontal winds, but in view of the enormous gradient of ozone at the tropopause (with an increase from 100 to 1000 nmol/mol within 4-5 model layers in the NCEP data) a higher resolution such as in the CCM data set is clearly advantageous. Given the importance of the upper troposphere for photochemical production of ozone more research should be focused on this region of the atmosphere.

3.8 Synopsis of the Comparison to Observations

A short presentation of the calculated distributions and budgets of ozone and some of its precursors along with a thorough comparison to observations has been given in this Chapter. A large number of indications about the emissions inventories, chemistry and other aspects of the model has been gathered, and in particular some additional links between the findings for the different species are described below.

Many features of the observed distribution of ozone could be well simulated, but some discrepancies were also revealed. While surface observations are mostly reproduced to within ± 10 nmol/mol, the model tends to overestimate winter-springtime ozone in the middle and upper troposphere and underestimates ozone in summer over polluted regions. The former effect is probably related to model dynamics (STF), whereas the latter is probably mainly of photochemical origin. Ozone concentrations in the free troposphere over regions strongly influenced by biomass burning appeared to be underestimated by up to 20-30 nmol/mol, but this is based on only few soundings. The calculated photochemical production and destruction of ozone in the troposphere are 4560 Tg/yr and 4290 Tg/yr respectively (T63-run), which is higher than in previous studies. Other ozone budget terms (net photochemistry: +280, dry deposition: 820, stratospheric influx: 540 Tg/yr) are within the range of previous studies. The net production of ozone integrated over regions where production exceeds loss is calculated at about 1400 $Tg(O_3)$/yr stressing the role of photochemistry on the budget of ozone. The model budgets also imply that photochemical production is almost as important to the O_3 budget in the upper troposphere as stratosphere-troposphere exchange (about 400–600 Tg/yr each), providing support for further investigating the chemistry of the upper troposphere.

The comparison of model calculations with GOME NO_2 columns brought out a number of encouraging results, such as consistent seasonal cycle and magnitude of biomass burning emissions in most parts of Africa and South America, but also some interesting deviations. These include: too long lifetime or too large emissions of NO_x from aircraft and possibly from ships, too much lightning NO_x over the Amazon and Indonesia, too large industrial emissions over parts of eastern Europe and a significant underestimation of the biomass burning plume in the south-east Atlantic. The latter may also be connected to the underestimated ozone mixing ratios in the region. Some problems in the reliability of the observations and possible improvements in this comparison were also pointed out.

The predicted partitioning of nitrogen-species sometimes deviates from the observations. Too much PAN is often predicted in the remote free troposphere, as well as near the surface during the arctic winter (Zeppelin station). The simulated mixing ratios of PAN were, however, consistent with observations in freshly polluted airmasses (outflow from Asia, biomass burning over southern Africa and Brazil), which could imply too long a lifetime of PAN in the model. Calculated HNO_3 is mostly on the low side, especially for regions where aged airmasses are expected. NO levels are mostly reproduced in the lower troposphere, but in the upper troposphere too low values are

persistently calculated.

Interpretation of these results is difficult, but they help to identify key areas for future studies. Since the severalfold overestimation of HNO_3 common to other 3D-models was not found in MATCH and such extreme changes are not expected from the differences in the chemistry, it appears that the wet deposition parameterization for highly soluble substance is too efficient in MATCH. Possible reasons for this have already been discussed in Section 2.3.5. Further issues affecting HNO_3 are the uptake of HNO_3 on ice, the hypothesized additional conversion of HNO_3 to NO and also the overestimate of PAN. Too high PAN levels in tropical regions could be in part due to the overestimation of isoprene found in the Amazon region. Convection of isoprene and its oxidation products with subsequent reactions with the overestimated lightning-NO_x (inferred from GOME) could also contribute to the PAN overestimate. Further possibilities are misrepresentation and uncertainties of the chemistry of its precursors. The condensed isoprene mechanism (the MIM) was found by *Pöschl et al.* (2000b) to produce PAN concentrations in agreement with the Master Chemical Mechanism, but both mechanisms were mostly higher than the other tested mechanisms. Simplifications in other parts of the chemistry (propane, ethene) could also result in artificial PAN formation. A test run using a lower limit for the thermal stability of PAN gave better agreement in some instances, but could not fully explain the discrepancies.

A sensitivity study assuming no uptake of HNO_3 on ice, revealed that this process was effective in removing HNO_3 in most regions of the upper troposphere and leading to better agreement with observations. This results also implies that a mechanism for conversion of HNO_3 to NO_x, mediated by ice surfaces and UV-radiation, as proposed by *Honrath et al.* (2000a), could occur in the upper troposphere. Cases of underestimated NO mixing ratios in regions where HNO_3 is too high when uptake on ice is not allowed are often encountered in the MATCH simulations. This suggests that this conversion actually takes place in some regions of the upper troposphere troposphere, although more research is needed to better quantify the possible conversion rate and to assess other possible explanations.

The tropospheric photochemical methane lifetime, often used to indicate global mean OH levels, is 8.8 and 9.0 years in the high and low resolution run, which is within the range of previous studies. The methylchloroform test indicates that the mean methylchloroform-loss weighted OH levels are probably underestimated by about 10±20%. Comparison with the climatology of *Spivakovsky et al.* (2000) shows that lower values by up to a factor of two are calculated in the upper troposphere, especially in the southern hemisphere, and higher values are found in the lower troposphere (below about 800 hPa). The low OH concentrations in the UT are probably caused by the underestimated NO_x.

CO concentrations in northern hemispheric and tropical surface stations are generally quite well reproduced. This also holds for column CO observations. The agreement of the seasonal cycle at tropical stations gives credence to the biomass burning emissions. South of about 20°S, however, the model tends to overestimate the CO mixing ratio by about 30-40%. The low OH levels in the SH could be a reason for this discrepancy.

The concentrations of ethane and propane tend to be underestimated. This was especially seen for stations in North America and only in winter at the European stations. The NH column ethane data are in accordance with these findings. In the southern hemisphere simulated ethane is in reasonable agreement with observations, but propane is underestimated. Thus, too much PAN production from these alkanes is not the reason for the overestimated PAN levels. The comparison

with alkenes shows reasonable agreement at the European stations, but measurements over the oceans appear to be underestimated, even when canister measurements are discarded. Since the upper limit estimate of the study of *Plass-Dülmer et al.* (1995) who employed a relatively large dataset of sea water measurements to determine the oceanic alkene emissions was used in this study, systematic problems in their methodology are suspected.

The comparison of model results with oxygenated species gave mixed results. The simulation of peroxides (H_2O_2 and CH_3OOH) was mostly good. For formaldehyde the picture is more complicated: While mixing ratios at most European stations are reasonably reproduced, observations at Mauna Loa are overestimated. MBL measurements are over or underestimated indicating that unknown factors influence formaldehyde in this region. Acetone concentrations are often underestimated by the model. Significant additional sources are especially needed to explain observations over the remote South Pacific. Photochemical production of acetone in the surface micro-layer of the ocean (*Zhou and Mopper* (1997)), not included in this study, is the most likely cause for the discrepancies over remote ocean regions. The knowledge of sources and sinks of methanol, acetic and formic acid appears to be even more incomplete. While large missing sources of formic acid are evident from the MATCH simulation, this is not as clear for methanol and acetic acid. For acetic acid the observed mixing ratios are reasonably reproduced, but the overestimate of PAN, makes an interpretation difficult, because it implies too high a photochemical production of acetic acid from the reaction $CH_3CO_3 + HO_2$. It appears from the PEM-Tropics-B measurements over the Pacific that oceans are likely a source of methanol, but more evidence is needed to confirm this impression.

Improvements over the previous model version were achieved in several instances. Some improvements stem from the updated biomass burning data set (*Galanter et al.* (2000)), e.g. CO and O_3 at Cuiaba (Brazil), and better agreement with the seasonality and magnitude of the GOME NO_2 data, but the inclusion of non-methane hydrocarbon chemistry is also responsible for some improvements, as will be shown in the next chapter.

At the two resolutions mostly very similar results were obtained so that the low resolution run can be used for further sensitivity studies. Some of the differences seen at surface stations are probably due to nearby sources, which are better resolved in the T63 run. However, stronger convection was found in the T63 runs and influenced the distribution of several trace gases. The most notable differences were seen for PAN, which is lower and thus in better agreement with observations in the lower resolution run, indicating the importance of convection for this species.

Chapter 4

Effects of Higher Hydrocarbon Chemistry on the Distributions and Budgets of Trace Gases

In the last chapter simulations were considered which used the full chemical scheme, including both the typical background CO-CH_4-NO_x-HO_x chemistry plus the chemistry of non-methane volatile organic compounds (NMVOC). Here, the effects of the sum of these NMVOCs will be assessed by comparing the full chemistry run with one in which only the background chemistry is included, that is, only reactions R1–R45 in Table A.1 are considered, otherwise keeping the same setup as in the last chapter. This run will be referred to as the CH4-simulation. Due to the large emissions of isoprene, a third run, which only includes the reactions of the CH4-run and isoprene related reactions (reactions R46–R91), is also discussed. This run will be used to investigate the contribution of isoprene to the total effect of NMVOC. This latter run will be denoted by ISOP, and the simulation using the full chemistry scheme, including isoprene, will be referred to as the NMVOC-run.

The three runs are compared here to assess the influence of groups of compounds to the modeled distributions of trace gases. This approach can only give an approximation of the actual effect of each group of compounds in the full chemistry simulation. However, it is not straightforward, if possible at all, to separate the contribution of a species within a single simulation. For the case of the contribution of methane oxidation to the formation of ozone this difficulty has been pointed out by *Pöschl et al.* (2000a) in response to a method proposed by *Johnston and Kinnison* (1998).

Although these runs are mainly intended to illuminate the role of hydrocarbon chemistry on the distributions and budgets of these species, they may also help explain why agreement or disagreement was found in the last chapter, and whether or not changes in the gas phase chemistry alone are likely to explain some of the discrepancies found, or if other model errors are also involved.

The stepwise increase in complexity of the chemistry scheme can (together with some additional assumptions) also be used to estimate the yield of CO from methane, isoprene and the other NMVOCs considered. Furthermore, a detailed analysis of the pathways for the loss of carbon during the oxidation sequence, calculated in the model budget routines, will be given. All simulations are performed at T21 ($5.6° \times 5.6°$) resolution. The discussion here is focused

on the main species O_3, CO, OH, NO_x and PAN. Global budget details, some of which are also summarized in Table 4.3 on page 147, are discussed in each section and compared to other studies.

4.1   Effects on CO

Carbon monoxide is a common product from the oxidation of VOCs. Compared to a simulation without NMVOC-chemistry, therefore, an increase in CO is expected. It is noted that no additional emissions to compensate for the CO production from the omitted hydrocarbons are assumed in the CH4-run, as done by *Roelofs and Lelieveld* (2000). The 100 Tg(CO)/yr from vegetation, however, which were in part meant to include some CO from biogenic compounds not treated in the chemistry scheme (e.g. terpenes) were also included in the CH4-run.

The annual zonal mean relative increase is shown in Figure 4.1 for the NMVOC and the ISOP run. Except in the high northern latitudes the largest part of the increase is due to isoprene alone. Due to the inclusion of isoprene chemistry alone zonal mean CO is enhanced by more than 20% in the tropics, with a maximum effect of about 26% in the upper troposphere. Inclusion of other NMVOC increases the effect to about 28% near the surface and 36% in the upper troposphere. This corresponds to about 24 nmol/mol higher CO mixing ratios near the surface and 20 nmol/mol in the UT in the NMVOC run compared to the CH4 run. The large relative increase in the upper troposphere indicates that a substantial fraction of the additional hydrocarbons is oxidized to CO at higher altitudes, since conversion to CO in the PBL would be similar to an additional surface CO source, which should result in a more uniform relative increase.
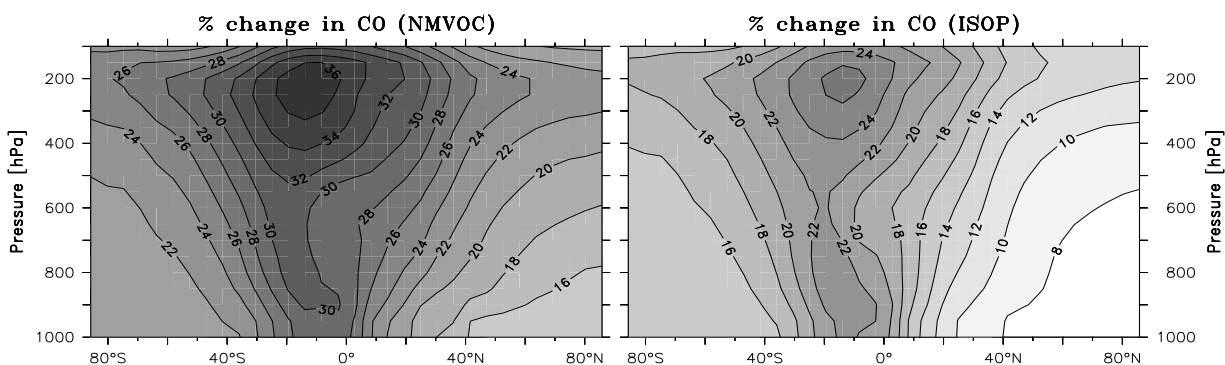
Figure 4.1: Percent change in the annual zonal mean mixing ratios of CO due to the consideration of all NMVOC (including isoprene) or isoprene only (computed as $(CO_{NMVOC/ISOP}-CO_{CH4})/CO_{CH4} \cdot 100\%$, where the subscript refers to the acronym of the run).

A comparison of the modeled CO mixing ratios with measurements at selected NOAA/CMDL stations (*Novelli et al.* (1998); see Section 3.1) is shown in Figure 4.2. It can be seen that the increase only yields small improvements in the NH, while the overestimate in the SH is worsened by the inclusion of NMVOCs. The same effect can also be achieved with additional CO or HCHO emissions in the CH4 run, replacing the CO from the oxidation of higher hydrocarbons. This method has been successfully applied by *Roelofs and Lelieveld* (1995) and *Lawrence et al.* (1999b).

Figure 4.2: Comparison of model simulations of CO to CMDL/NOAA measurements (symbols and error bars, arrows indicate extreme monthly values). Solid line is simulation with full-chemistry (NMVOC), dashed line is background chemistry plus isoprene (ISOP), and dash-dotted line is methane-CO background chemistry.

Since the modeled CO mixing ratios at remote southern latitude stations are too high even in the CH4 run, other factors besides too high biogenic emissions or too high a yield of CO from the NMVOC must contribute to the overestimate. Possible explanations whi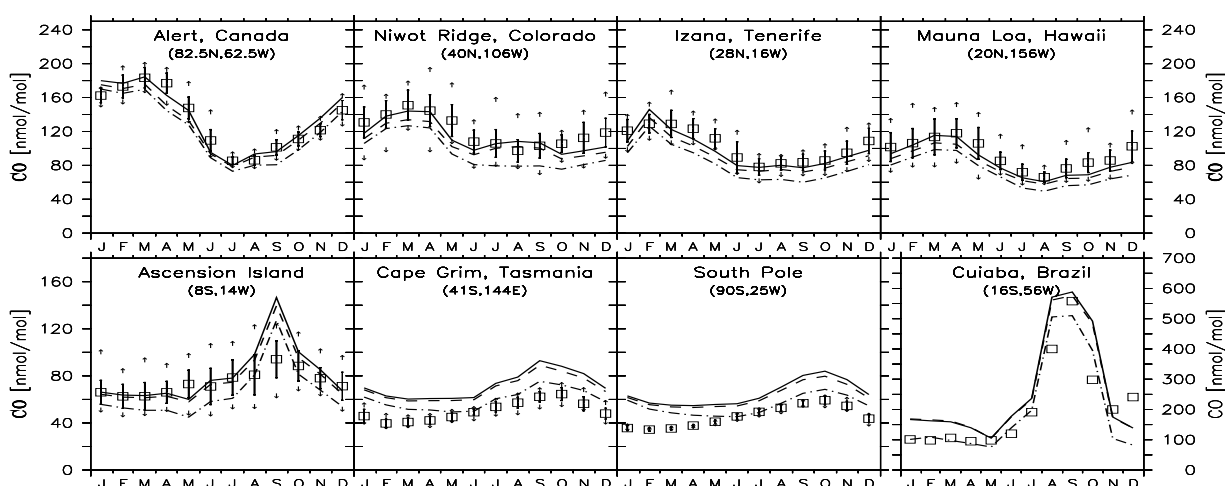ch would also apply to the CH4-run are too high biomass burning emissions, too little OH at these latitudes or too high a yield of CO from methane. In the next section this yield is determined to be 0.92 CO molecules per CH_4 molecule oxidized, which is somewhat higher than estimated by *Bergamaschi et al.* (2000a) based on an inversion study of CO and its isotopes. A value of about 0.86 (0.80–0.88) was found in that study, but it was also stated that values as low as 0.69 may be possible. Assuming that about 20-25 nmol/mol CO are from methane oxidation (*Holloway et al.* (2000)), a reduction of this yield in MATCH by as much as 0.2 would only result in about 5 nmol/mol smaller CO mixing ratios explaining only part of the ≈20 nmol/mol overestimate. These findings and the fact that *Holloway et al.* (2000) obtained good agreement employing the same biomass burning emissions as used in this study suggest that OH levels in the SH in MATCH are probably a major factor for the overestimate of CO. This would fit with studies indicating more OH in the SH than in the NH (*Brenninkmeijer et al.* (1992); *Spivakovsky et al.* (2000); *Montzka et al.* (2000); *Prinn et al.* (2001))[1] as opposed to MATCH (and most other 3D global chemical transport models), which calculates a higher mean OH abundance in the NH. In addition, the CO-yield from NMVOC (primarily biogenic) could also contribute significantly (see Section 4.2).

The global production and burden have increased in the NMVOC run by 52% and 30%, or 406 Tg(CO)/yr and 78 Tg-CO, respectively, compared to the CH4 simulation. Note that the loss rate has also increased in the NMVOC simulation, thus reducing the effect on the global burden. More than half of this increase is already caused by the oxidation of isoprene. Interestingly, by comparing these results to the values given by *Poisson et al.* (2000), it can be found that the relative and absolute increase in global photochemical production is larger but the increase in burden is lower than found by *Poisson et al.* (2000). This can only be explained by a different

---

[1]It is noted, however, that these estimates are highly uncertain (see *Jöckel* (2000) and Section 3.3.2).

response of the global mean OH concentrations to the inclusion of NMVOCs . In fact, global mean (mass weighted) OH has decreased much less in this study compared to *Poisson et al.* (2000) (see Section 4.4).

4.2   The Yield of CO — A Detailed Analysis of Loss Pathways of Carbon

As was seen in the last section, NMVOCs are a large source of CO in the troposphere. Due to deposition processes and direct production of CO_2, some fraction of the carbon in the oxidized hydrocarbon does not result in CO. Utilizing the budget computations in MATCH and some assumptions, these yields and the loss pathways are derived from the model output. Another method would be to label carbon atoms from different hydrocarbons (e.g. *Granier et al.* (2000)) and follow how much of each results in CO, but with this method all intermediates that can be produced from several hydrocarbons (e.g. HCHO, CH_3OOH) have to be treated separately for each "parent" hydrocarbon in the transport and in the chemical schemes, which significantly enhances the computational burden.

4.2.1   The CO-yield from Methane

First, the CH4-run is considered and used to determine the CO yield from CH_4. All subsequent numbers here are in Tg(C)/yr. Out of the 346 units of methane oxidized, 27.9 (15.8 via HCHO, 8.1 via CH_3OOH, 4.0 via CH_3OH) are lost through dry or wet deposition. In this calculation, the deposition of some directly emitted CH_3OH and HCHO (total emission strengths are 28.7 and 3.6, see Section 2.3.6) is already subtracted assuming that the loss fraction of emitted molecules is not significantly different from the loss fraction of molecules produced by CH_4. Thus, a CO yield from methane of γ_{CH_4}=0.92 is found, as noted above.

   This value is significantly higher than several other estimates. *Logan et al.* (1981) estimated a value of 0.8; *Tie et al.* (1992) showed small seasonal and latitudinal variations with a global average of about 0.82. Both studies, however, used a very simple parameterization of heterogeneous losses (rainout and assumed loss on aerosols), employing a constant rate only depending on height and did not account for the formation of methanol. Outdated kinetic data could also be a problem in the former study. Using measurements of ^{13}C and ^{12}C isotopes in the southern hemisphere fitted with a 2D-zonally averaged model, *Manning et al.* (1997) conclude that their data are difficult to reconcile with a yield of 0.8 or more and suggest a value of 0.7 for the SH. However, significant uncertainties in the ^{13}C enrichment from some CO sources are also stated. *Bergamaschi et al.* (2000a,b) use CO measurement and the isotopic ratios $^{13}C/^{12}C$ and $^{18}O/^{16}O$ in CO as constraints in an inversion study with a 3D global transport model. The CO yield from methane was treated as a tunable parameter and a value of 0.86 (0.8-0.88) was derived. It was also stated that with certain further assumptions the value could be as low as 0.69. On the other hand, in another 3D modeling study by *Kanakidou and Crutzen* (1999) a similar value to that found here is stated (γ_{CH_4} =0.9).

   It was argued before (Section 2.3.5) that the wet deposition scheme is probably too efficient in MATCH, as it assumes instantaneous equilibrium with the gas phase and efficient mixing of cloudy with cloud-free air within a grid cell. Furthermore, the inclusion of a fraction of methanol (3%) formed in the oxidation of methane would also tend to result in a slightly higher loss

rate, since methanol is very unreactive and a higher fraction than for HCHO and CH_3OOH is deposited. Therefore it seems difficult to reach values as low as 0.7 or 0.8 only with dry deposition and wet scavenging. Heterogeneous processes occurring in cloud droplets or on aerosols offer a potential explanation but too little information is available to quantify their impact. Aqueous phase production of formic acid would be a process that could lead to a larger loss of carbon, but it has been concluded to be probably of minor importance (*Chebbi and Carlier* (1996); *Khare et al.* (1999)). Minor gas-phase reaction pathways which could potentially form highly soluble hydroxyhydroperoxide (HMHP, $HOCH_2OOH$) and/or formic acid were also discussed:

$$HCHO + HO_2 \quad \leftrightarrow \quad HOCH_2O_2 \tag{4.1}$$

$$HOCH_2O_2 + HO_2 \quad \rightarrow \quad HOCH_2OOH + O_2 \tag{4.2}$$
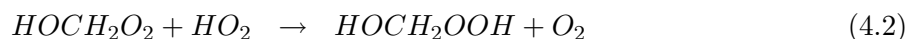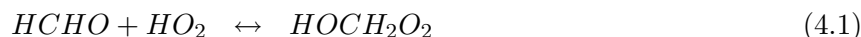
These pathways were also judged by the aforementioned two reviews to be unimportant as sources of formic acid, which can be formed upon further reactions of HMHP. In a short test simulation these additional reactions have been added to the methane oxidation sequence using the recommended rate constants from *Atkinson* (1997) (see *Chebbi and Carlier* (1996)) and indeed resulted in less than 1 Tg-C/yr of formic acid (which is later shown to deposit by 97%). However, it is noted that some of the involved kinetic parameters are very uncertain and have only been measured for temperatures higher than 275 K (e.g. equilibrium reactions 4.1).

Nevertheless, the strong underestimation of formic acid in MATCH compared to observations (in agreement with *Baboukas et al.* (2000)) indicate that understanding the production pathways of this compound could also help to bring the CO yield from methane in better agreement with the CO isotope inversion studies (*Manning et al.* (1997); *Bergamaschi et al.* (2000a,b)).

4.2.2   The CO-yield from Isoprene

Next, we assume that the CO yield from methane does not change significantly when adding more chemistry to the model. Also, the above mentioned assumption, that directly emitted molecules have the same chance to deposit than photochemically produced ones, has to be made for more substances. From the total photochemical production of CO (464 Tg-C/yr) and the methane oxidation (338 Tg-C/yr) in that run one can estimate that about 39% of the carbon in isoprene get oxidized to CO, thus constituting a source of 321 Tg(CO)/yr.

Previous estimates of the CO yield from isoprene obtained a large range of values. Early estimates of this yield by *Zimmerman et al.* (1978) were 0.6–0.8 CO per carbon in isoprene oxidized. Employing a one-dimensional model and using the parameters for heterogeneous loss from *Logan et al.* (1981) (assuming same properties of ROOH and CH_3OOH) *Brewer et al.* (1984) obtained a yield of 0.22 – 0.27 CO per C in isoprene oxidized. Estimates of this yield under high NO_x conditions is probably more reliable because deposition processes are less important. Furthermore, the reaction mechanism of isoprene is better know under these conditions since smog chamber studies upon which the mechanism development heavily relies are usually conducted with very high NO_x concentrations. Value obtained from these conditions are 0.68 and 0.6 per carbon (*Paulson and Seinfeld* (1992); *Miyoshi et al.* (1994)), but cannot be extrapolated to a global value. Additional analysis of the most probable reaction pathways under low NO_x conditions, along with the simple assumptions of *Logan et al.* (1981) for the heterogeneous loss of hydroperoxides, were combined by *Miyoshi et al.* (1994) to arrive at an estimated global mean CO yield of $\gamma_{C_5H_8} = 0.30^{+0.09}_{-0.08}$ (on a per carbon basis).

It is asserted here that these estimates cannot be readily compared to the results from a 3D-global model, which transports and treats wet and dry deposition of many intermediate species based on a physical parameterization of these processes. In the case of the deposition processes these are based on Henry's Law constants. In the previous studies another major difficulty lies in judging the contributions from the high and low NO_x regimes.

A more comparable study by *Granier et al.* (2000) yielded a value of $\gamma_{C_5H_8} = 0.23$ per carbon based on a 3D simulation of tagged carbon. In the chemical mechanism employed (which was based on *Müller and Brasseur* (1995) and *Paulson and Seinfeld* (1992)) the hydroperoxides from isoprene (denoted ISO_2H and $MACRO_2H$ in this study) are not explicitly treated. It was assumed that 70% of these substances gets lost from the atmosphere by non-chemical processes. This assumption was based on a modeling study of the PBL in the wet season in the Amazon basin by *Jacob and Wofsy* (1990). *Granier et al.* (2000) also state that this high loss fraction extrapolated to the global troposphere could result in an underestimate of the CO yield. Also, in the mechanism of *Müller and Brasseur* (1995) some other substances (e.g. formic and acetic acid, methylglyoxal, alcohols, organic nitrates from isoprene) are assumed to be removed from the atmosphere through deposition or reactions on aerosols. *Granier et al.* (2000) state that some changes have been made to the mechanism, but it is unclear whether these assumptions were also affected. In the MATCH simulation, which explicitly considers transport and dry and wet deposition rates for most of these compounds, however, a significant gas-phase oxidation is calculated (see next section), which might explain the smaller yield of CO from isoprene in the study of *Granier et al.* (2000).

4.2.3   The yield of CO from other NMVOCs and Analysis of Loss Pathways

Finally, the full NMVOC chemistry simulation is analyzed in more detail to assess the most important pathways of carbon loss in the model. From the calculated total CO production of 511.4 Tg-C/yr and the total input of carbon of 857.8 Tg-C/yr in that run (methane oxidation: 332.8, isoprene emissions: 350, other NMVOC emissions: 175 Tg-C/yr) an overall yield of CO from hydrocarbons of about 60% can be calculated. Assuming again that the above calculated yields (92% from methane, 39% from isoprene on a per carbon basis) are not significantly different in the NMVOC simulation an average yield of $\gamma_{NMVOC} = 0.39$ is calculated. Apparently this number contains the largest uncertainties from the calculation method as is relies on the most assumptions. Varying γ_{CH_4} and $\gamma_{C_5H_8}$ by 0.02 and 0.05, respectively, in order to mimic possible changes of these numbers due to the changes in the chemistry, results in changes in γ_{NMVOC} of ± 0.1. The value obtained here is in agreement with the value of 0.39 obtained by *Kanakidou et al.* (1991) for ethane and propane oxidation in a 2D-model and by *Poisson et al.* (2000) (γ_{NMVOC} $= 0.4$)[2] for other NMVOCs than isoprene in a 3D modeling study.

An analysis of the loss pathways as calculated in MATCH for the full chemistry simulation is given in Table 4.1. The loss of carbon is occurring through 3 main and 2 minor processes: dry and wet deposition account for about 68% (dry: 37%, wet: 31%) and direct CO_2 production, bypassing CO production, accounts for 28% of the total loss in the conversion of NMVOC to CO. The two minor pathways (not listed in Table 4.1) are loss by assumptions within the chemical mechanism (3.9%) and transport into the stratosphere (0.2%). Note that by using the methane

---

[2]In the paper the overall yield from hydrocarbons and the yield from isoprene alone are given as 0.4, thus it was inferred here, that the value from all hydrocarbons but isoprene must also be 0.4. A method how the effect of the different hydrocarbons was separated was not given.

Table 4.1: Loss pathways of carbon from the oxidation of hydrocarbons before yielding CO (in Tg-C/yr).

Species[a] in [Tg-C/yr]	Total Deposition	Dry Deposition	Wet Deposition	Total Production	% Loss by Depos.
$ISO_2H+MACRO_2H$	81.5	19.6	61.9	244.2	33.4 %
HCHO	33.8	20.4	13.4	500.3	6.8 %
CH_3COOH	21.1	11.4	9.7	24.9	66.0 %
CH_3OH	16.8	14.6	2.2	38.9	43.2 %
MACR	13.8	13.8	—	215.0	6.4 %
CH_3COCH_3	11.0	11.0	—	34.3	32.1 %
ISON	9.8	3.4	6.4	20.6	47.6 %
CH_3OOH	9.6	8.4	1.2	279.5	3.4 %
CH_3COCHO	8.4	4.1	4.3	90.0	9.3 %
CH_3CO_3H	6.9	4.9	2.0	51.9	13.3 %
HCOOH	8.2	3.9	4.3	8.4	97.6 %
other deposition	14.2	13.1	1.1		
Sum deposition	235.1	128.6	106.5		

production of CO_2	Tg(C)/yr	% of total
$CH_3CO_3 + NO$	53.8	55.4 %
$ISO_2H + OH$	14.6	15.0 %
$CH_3CO_3 + CH_3O_2$	9.4	9.6 %
CH3COOH + OH	5.5	5.6 %
MVKO2 + NO	3.7	3.8 %
other reactions	10.1	10.6 %
total CO_2 production	97.1	100.0 %

[a]For some abbreviations see species list in Table 2.1.

oxidation instead of methane emissions as input to the carbon budget, methane oxidation in the stratosphere has not been counted as input into the system. The loss of carbon by assumptions in the chemical mechanism is mostly from the oxidation of isoprene. It stems from the formation of either unknown products or products which are expected to be very soluble and lost from the atmosphere by deposition (e.g. multi-functional alcohols). Compared to other chemical mechanisms, however, (e.g. *Houweling et al.* (1998); *Müller and Brasseur* (1995); *Brasseur et al.* (1998)) the chemical scheme employed in this study is fairly strict in conserving carbon (see also *Pöschl et al.* (2000b)).

The single largest loss of carbon (81.5 Tg-C/yr) is through the deposition of hydroxy-hydroperoxides from the oxidation of isoprene. Note that the C_4 (MACRO$_2$H) and the C_5-hydroperoxides (ISO$_2$H) are transported together in this study and their deposition properties (parameterized by the Henry's Law constant) are assumed to be the same. Only the combined effect is therefore shown in Table 4.1. Since no laboratory data are available for these compounds, the solubility of the simplest hydroxy-hydroperoxide, hydroxy-methylhydroperoxide (HMHP, HOCH$_2$O$_2$H), has been used instead. Information on the solubility of other similar substances could not be found in the literature. As shown in Section 2.3.4 (Table 2.4) this assumption leads to dry deposition velocities almost as large as those of the highly soluble HNO$_3$. The assumed Henry's Law coefficient of $1.7 \cdot 10^6$ mol/l/atm at 298 K should result in almost 100%

wet scavenging efficiency (*Crutzen and Lawrence* (2000)). In the annual global mean this results in about one third of these substances being lost by deposition processes, thus much lower than the assumed 70% in *Müller and Brasseur* (1995) and *Granier et al.* (2000). Computing this fraction for the continental PBL in the Amazon Basin (10°S-0°N, 70W-30W, below 800 hPa) one finds that about 58% of the hydroperoxides photochemically formed from the oxidation of isoprene are lost by wet or dry deposition on the annual mean. During the wet season this value is about 70% in agreement with the study of *Jacob and Wofsy* (1990). It should be mentioned that only uptake by water droplets is taken into account in the current version. If significant amounts can reach higher altitudes and would also be taken up by ice crystals, the loss of carbon via these compounds could increase further.

Other large deposition loss terms in Table 4.1 include acetic acid (CH_3COOH) which is very soluble and a common product in the oxidation of isoprene, alkenes and acetone. The large loss fraction of methanol (CH_3OH) and acetone (CH_3COCH_3), despite their fairly low solubility and thus low dry deposition velocities (0.16 and 0.28 cm/s over land and ocean for methanol, less than 0.1 cm/s for acetone for both surfaces), is due to the relatively long lifetimes of these compounds against chemical processes (methanol: 13 days, acetone: 18 days, annual tropospheric mean values). In the case of MACR, which is a surrogate species of two main oxidation products of isoprene, methyl-vinyl-ketone (MVK) and methacrolein, a significant amount of carbon is lost due to the large total production of this compound group. Indications that dry deposition of these two compounds is actually occurring was first reported by *Sanhueza et al.* (2001), based on measurements of the diurnal cycle and box modeling. It was concluded that the decrease observed during the night cannot be explained by chemical reactions alone. A quantitative estimation of the deposition velocity, however, was hindered by lacking information on the height of the nocturnal boundary layer. Wet deposition has not been taken into account for this surrogate species due to the low Henry's Law constants ($4.1 \cdot 10^1$ for MVK, 6.5 mol/l/atm for methacrolein at 298 K). However, *Helmig et al.* (1998b) found evidence of wet scavenging of both of these compounds, with the loss being more efficient for MVK in agreement with its higher Henry's Law constant. It is further interesting to note that roughly half of the organic C_5 nitrates from isoprene (denoted as ISON) are also lost through deposition processes. For this compound group, also a high value for the Henry's Law constant was used in this study based on measurements of other hydroxy-nitrates (*Treves et al.* (2000)).

Out of the 28% lost by direct production of CO_2 most is lost via the reaction of the peroxyacyl radical with NO. Thus, the yield of CO_2 is expected to be dependent on NO_x concentration. Since the other NMVOC than isoprene are mostly emitted in regions with high NO_x concentrations this might partially explain why the yield of CO from other hydrocarbons was not significantly higher that from isoprene, although a large loss in the isoprene oxidation sequence occurs through deposition of the hydroxy-hydroperoxides.

In this study heterogeneous processes on aerosols and in cloud droplets are not considered. No information of sticking coefficients and possible reaction products of oxygenated organic compounds have been found in the literature. The possible effect on the carbon budget would also depend on the the vapor pressure of the reaction products in the aerosol media, which would influence whether or not revolatilization occurs.

Based on these model results and the literature cited above (see also references in *Kanakidou and Crutzen* (1999)) uncertainty ranges of the conversion factors are estimated as follows: γ_{CH_4}= 0.7-0.92, $\gamma_{C_5H_8}$= 0.2-0.4, γ_{NMVOC}=0.3-0.6 (all numbers on a per carbon basis). Note that the

result from this study are often at the high end of this estimated range. With theses yields and using the emissions and methane oxidation rate from the NMVOC run a range in the resulting secondary CO production from all hydrocarbons of about 1060±230 Tg(CO)/yr can be derived. This uncertainty estimate does not include uncertainties from the emission strengths of these hydrocarbons. Terpene oxidation, and other potential compounds are also not considered in the model at present (see e.g. *Kesselmeier and Staudt* (1999) for a review on compounds that may be emitted by vegetation). These compounds are taken into account by 100 Tg(CO)/yr of additional biogenic emissions, which include also some direct emissions from the biosphere. This may be compared to the range of uncertainty in the primary emissions from fossil fuel combustion and biomass burning, which can be approximately summarized as 1150±450 Tg(CO)/yr (*IPCC* (1996)).

The uncertainties due to deposition processes and chemistry (CO$_2$ yield) thus add significantly to the overall uncertainty in the source of CO in the atmosphere. More information on various related parameters, like deposition velocities, sticking coefficients, Henry's Law constants of some oxygenated compounds, especially the hydroperoxides from isoprene are clearly desirable.

4.3 Effects on the distribution of NO$_x$ and PAN

The distribution of NO$_x$ is strongly influenced by the inclusion of hydrocarbon chemistry. The changes of the zonal annual means depicted in Figure 4.3shows that isoprene chemistry is responsible for a large part of the effect. Up to about 80% increase in the zonal mean is found in the ISOP run, and 120% in the NMVOC simulation. The maximum relative effect is found between about 600 and 800 hPa, corresponding to the altitude where most of the PAN transported down from the upper troposphere in remote regions decomposes and releases NO$_x$ (see PAN profiles in Figures 3.26 and 3.25). The absolute zonal mean values for NO$_x$ at this altitude are a few tens of pmol/mol. In the northern mid-latitudes a net reduction in the seasonal zonal mean is seen, reflecting the formation of organic nitrates (mainly PAN and ONIT in MATCH) over the polluted regions. At the high northern latitudes in the lower troposphere in turn an increase of NO$_x$ is predicted which is likely the combined effect of PAN decomposition and the oxidation of the organic nitrate pool ONIT. ONIT is mainly formed from the oxidation of C$_4$H$_{10}$, which represents all higher alkanes and is the NMVOC species with the largest industrial emissions. The chemistry of n-butane and a constant nitrate yield from the peroxyradical-NO reaction of 16% was used. The lumping of different nitrate yields and the neglect of some known temperature dependence of this yield make this estimate rather uncertain.

At 700 hPa where the maximum relative zonal mean effect is found and near the surface the patterns look very similar to Figure 4.4, but the depletion/enhancement is even more severe with up to 5 times higher NO$_x$ levels in the NMVOC run. However, at these locations NO$_x$ mixing ratios are extremely low (less than 5 pmol/mol) even in the NMVOC simulation.

In the upper troposphere (above 500 hPa) the total effect of taking into account NMVOCs is rather small, generally less than 20% in the zonal mean. Locally, however, enhancements in remote oceanic regions and reductions over the continents of about 30-50% are also predicted. The results for the zonal means are in contrast to the study of *Wang et al.* (1998b), who found 50-100% more NO$_x$ over the northern high latitudes and 20-50% more over the tropics in the upper troposphere in a run omitting NMVOCs chemistry[3]. Below 500 hPa in the *Wang et al.*

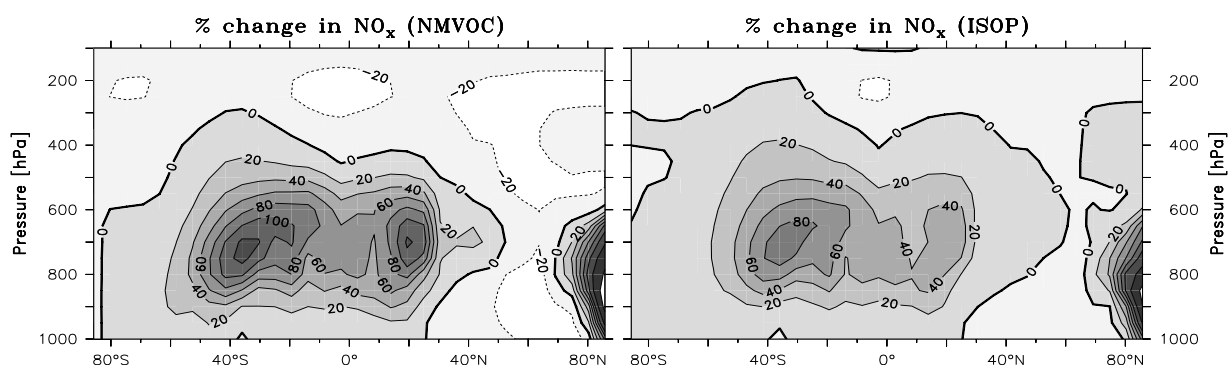[3]Note that in the study of *Wang et al.* (1998b) sensitivities are expressed relative to the simulation with full

Figure 4.3: Percent change in the annual zonal mean mixing ratios of NO_x due to the consideration of all NMVOC or isoprene only (same as Figure 4.1, but for NO_x).

(1998b) study the effect appears to be smaller, which could be due to the relatively high PAN concentrations in MATCH compared to observations. *Moxim et al.* (1996), on the other hand, found only a 10%-effect of PAN-chemistry on upper tropospheric NO_x. However, due to many strong simplifications in the latter study (parameterized zonal mean offline chemical conversions of the NO_x-PAN-HNO_3 system; no diurnal cycle; isoprene chemistry is not included in the parameterization, but instead enhanced boundary layer concentrations of ethane and propane are assumed) the results are difficult to interpret and are not further discussed.

The budget of NO_x in the upper troposphere ($\sigma < 0.535$) was analyzed to find the reason for the relatively weak net effect in MATCH. Note that for both simulations NO_x in the upper troposphere is calculated to be in chemical steady state (i.e. total loss $\approx$ total production) and thus it cannot be judged from these budgets whether the average NO_x concentrations have increased or decreased, but only the shift in the source and loss processes is shown. It was found that a net decrease from the inclusion of PAN chemistry (-0.7 Tg-N/yr) and slightly less transport into the region (mainly by convection from the lower troposphere; -0.07 Tg-N/yr) are compensated by increased formation of HNO_3, with a net effect of HNO_3 chemistry of $+0.39$ Tg-N/yr (0.46 Tg-N/yr lower sink and 0.07 less production in the NMVOC run), and by decomposition of other nitrates (0.38 Tg-N/yr). The net positive effect of HNO_3-NO_x interactions is mainly from a decrease in the formation reaction $OH + NO_2$ (+M) $\rightarrow$ HNO_3 (+M), which is due to the decease in OH in the upper troposphere (see Figure 4.6 and the next section). Since PAN chemistry caused the largest increasing loss term in the upper troposphere, its formation must be seen as the reason for the slight decrease of NO_x in that region.

Inspection of the horizontal distribution of other nitrates considered in the chemistry (MPAN, ISON, NACA, and ONIT) reveals that PAN is also the dominant reason for the long-range transport of reactive nitrogen. This follows from the fact that no significant amounts of other nitrates are found in the remote regions. An exception to this are up to about 100 pmol/mol of ONIT in the northern high latitudes (not shown). Evidence for the dominant role of PAN in the additional long range transport of reactive nitrogen can also be found in the model budgets. It is calculated that 42% of the total export of NO_y out of the global continental troposphere[4] is in the form of PAN, while NO_x and HNO_3 contribute 28% and 16%, respectively. The isoprene nitrates (ISON, MPAN, NACA) together contribute about 11% and the organic nitrate pool

---

chemistry, as opposed to relative to the CH4 simulation as done in this study.
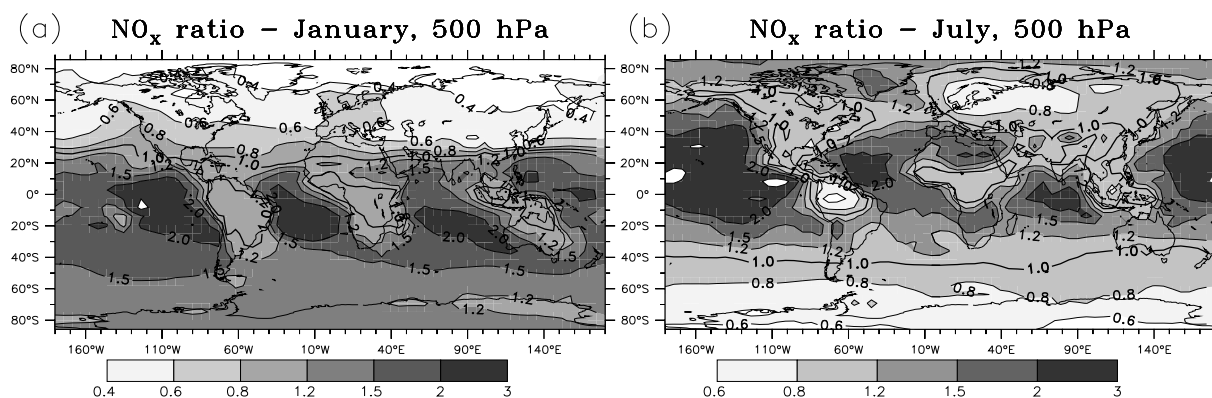
[4]As defined by the models land-sea mask.

Figure 4.4: Ratio of NO$_x$ mixing ratios from the NMVOC and CH4 simulation (NO$_{x, NMVOC}$/NO$_{x, CH4}$) at 500 hPa for January (a) and July (b). White within dark are values higher than 3.

from alkanes only 3%. It must be noted that only for PAN a significant fraction could also be reentering the budget region (e.g. by being advected from over the the U.S. to Europe), while for the other species usually the lifetime is too short. Calculating the same fraction for the global continental boundary layer, one gets a higher fraction of NO$_y$ escaping as NO$_x$ (36%) and a smaller term for PAN (25%), which indicates that significant amounts of PAN are formed in the free troposphere e.g., from lightning NO$_x$ and precursors convected from the boundary layer.

The horizontal distribution of the changes in NO$_x$ at 500 hPa is depicted in Figure 4.4. It can be seen that in the remote tropical mid troposphere NO$_x$ is significantly enhanced in the NMVOC simulation (up to a factor of 3) mainly due to the decomposition of PAN, whereas over the NO source regions it is depleted, due to the formation of PAN or nitrates from isoprene. In the northern latitudes in winter a strong reduction is seen in the upper troposphere, but below about 600 hPa an enhancement is found in all seasons (see annual zonal mean in Figure 4.3). In the winter upper troposphere loss through nitrogen capture in PAN appears to dominate over the additional source through ONIT in the region. The net positive effect below 600 hPa is probably also mainly caused by PAN. This can be seen from the change in the ISOP run, where organic nitrates from alkanes (ONIT) are not included, but almost the same increase is seen below 600 hPa.

Finally, the contribution of isoprene to the total PAN abundance is shown in Figure 4.5 for July. It can be seen that isoprene accounts for more than half of the production of PAN in the tropics, but its contribution in the northern extra-tropics is lower. This is even more pronounced during the NH winter, when the contribution in the tropics is about the same but the contribution at northern mid and high latitudes is only 10% or less (not shown). The resulting annual mean contribution from isoprene chemistry at 40°N is about 20%. The low fraction of isoprene related PAN near the Arabian Peninsula is due to large emissions of alkanes and NO$_x$, presumably from oil and gas production in the region.

The global tropospheric mass of PAN in the ISOP run is 79 Gg-N, which is 39% of the value in the NMVOC run. Whereas the fraction of isoprene related PAN to that calculated in the NMVOC simulation is only 16% (by mass) in the NH extra-tropics (north of 30°N), it is 65% south of 30°N.
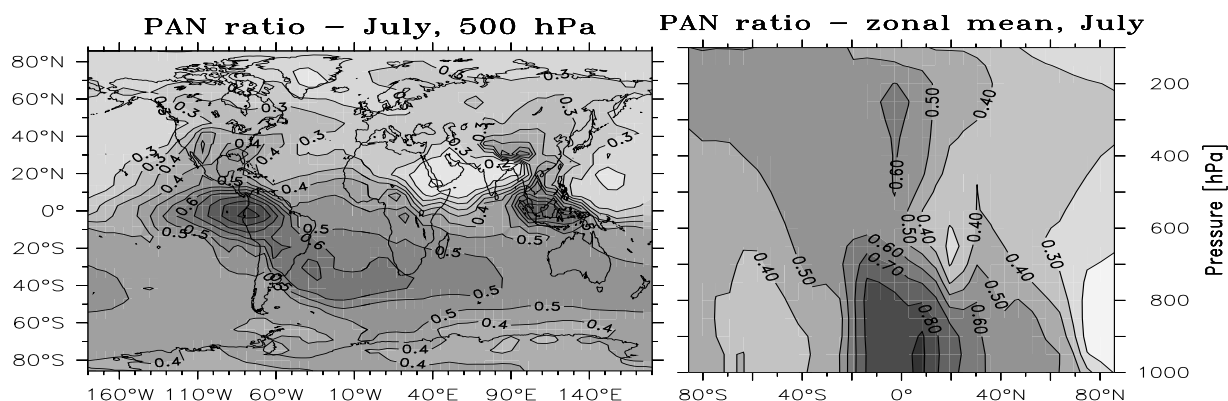
Figure 4.5:   Ratio of PAN mixing ratios from the ISOP and NMVOC simulation (PAN_{ISOP}/PAN_{NMVOC}) in July. Ratio from the two runs at 500 hPa (left) and of the zonal means (right) are plotted.

4.4   Effects on the distribution of OH and HO_x

The zonal mean effect of NMVOCs on the distribution of OH shows four regimes (Figure 4.7). The structure of the relative effect is similar in the ISOP and the NMVOC run and it can be seen that isoprene alone accounts for more than half the total effect.

In the PBL a net reduction of OH is seen which is due to the reaction of OH with the more reactive hydrocarbons (isoprene, alkenes) and their oxidation products (including CO). In the region between about 600 and 800 hPa enhanced zonal mean OH levels are found which are most likely caused be the higher NO_x concentrations in that region. Moving higher up another region with less OH in the NMVOC and ISOP run is found (about 200 – 500/600 hPa). Here, NO_x has only slightly increased or decreased. In combination with larger mixing ratios of CO and other sinks for OH this results in a net reduction of this compound.
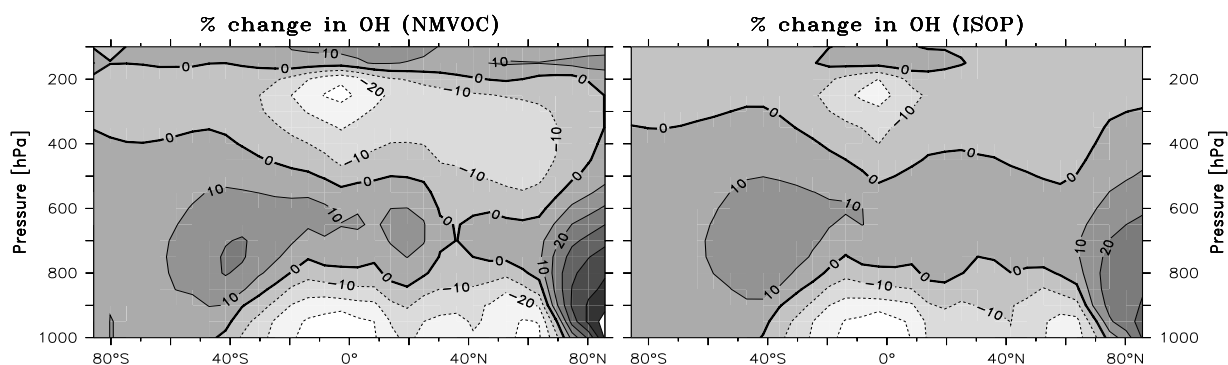
Figure 4.6: Percent change in the annual zonal mean mixing ratios of OH due to the consideration of all NMVOC or isoprene only (same as Figure 4.1, but for OH).

In this explanation one aspect is still missing: Many hydrocarbons (aldehydes, ketones, and hydroperoxides) can produce OH and HO_2 upon photolysis. This is especially important for OH levels in the upper troposphere were photolysis reactions are fastest and other sources of OH are small. Thus, the increase of OH in the fourth regime in Figure 4.6 (above 200 hPa) is attributed to the effect of these hydrocarbons which are pumped up into these altitudes by deep

convection in the rising branch of the Hadley cell. The overall enhancement of HO$_x$ in the ISOP and NMVOC run can be seen in Figure 4.7. The largest absolute zonal mean increase is found at about 700 hPa (not shown), where also a large relative effect is seen, probably linked to the increase in NO$_x$. The largest relative increase, however, of about 30% and 50% for the ISOP and NMVOC, respectively, is seen in the region of the uppermost troposphere (and lowermost stratosphere in the extra-tropics, but the absolute increase is very small), corresponding to the region of convective outflow. The fact that a significant impact (more than half the effect in the tropical uppermost troposphere) is seen already in the ISOP simulation shows that acetone, which is not included in that run, is not the dominant source of HO$_x$ from NMVOCs in the upper troposphere, but rather a contributor among other carbonyl compounds.

Figure 4.7: Relative increase of HO$_x$ concentrations when including isoprene chemistry and all NMVOC compared to the CH4-simulation (computed as (HO$_{x,ISOP/NMVOC}$ − HO$_{x,CH4}$)/HO$_{x,CH4}$·100%).
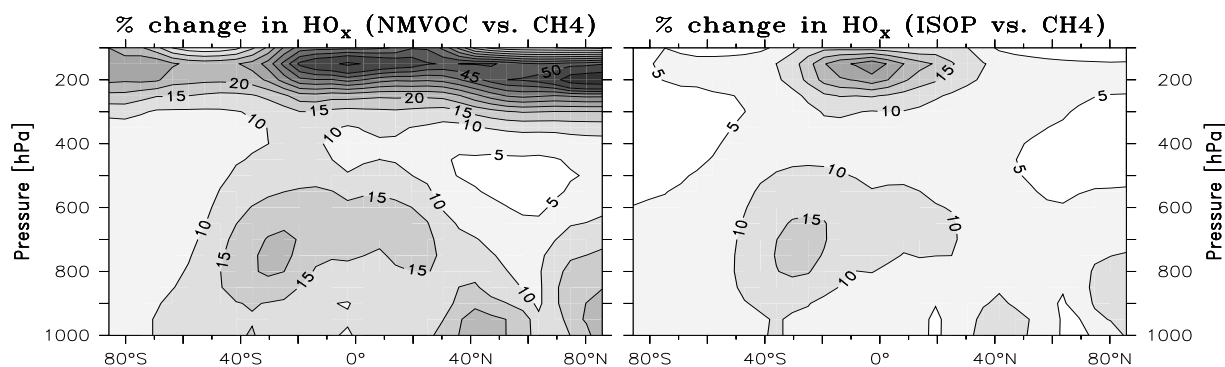
These results can be compared to those of *Wang et al.* (1998b). The region of higher OH in the full-chemistry simulation at 600-800 hPa is not seen in that study but a decrease of 20% or more was found over most parts of the troposphere. This difference may be explained by the different effects found for NO$_x$, which appear to be larger in MATCH, consistent with the higher PAN mixing ratios as compared to the model of *Wang et al.* (1998a,c). The increase in the uppermost troposphere was also observed by *Wang et al.* (1998b).

The changes of OH in the PBL are plotted in Figure 4.8. OH mixing ratios are strongly depleted in the continental boundary layer (by up to a factor of 10), mainly due to the reaction with isoprene. In the remote oceanic regions on the other hand an increase of about 20% or more is seen. This is caused by the increased NO$_x$ levels, which seem to have a larger effect than the increased loss of OH through reaction with CO. An increase is also seen for some clean continental regions, with no isoprene emissions, like the Sahara desert or Siberia in winter.

The resulting tropospheric annual mean average OH, weighted by air density has changed only little (Table 4.3 in Section 4.6). In the NMVOC run it is about 4% lower than in the simulation without NMVOCs. The methane lifetime as another measure of global mean OH has increased by 4% in the NMVOC run. Large effects, however are found for the global turnover rate of OH as can be seen in Table 4.2. In the NMVOC run source and loss terms are about 24% larger than in the CH4 simulation. The so-called primary production of OH through O^{1}D + H$_2$O → 2 OH also increases by about the same percentage due to the increase in ozone (which can form O^{1}D upon photolysis). In fact, it can be seen that the percentage contribution of several reactions only varies slightly on the global mean.
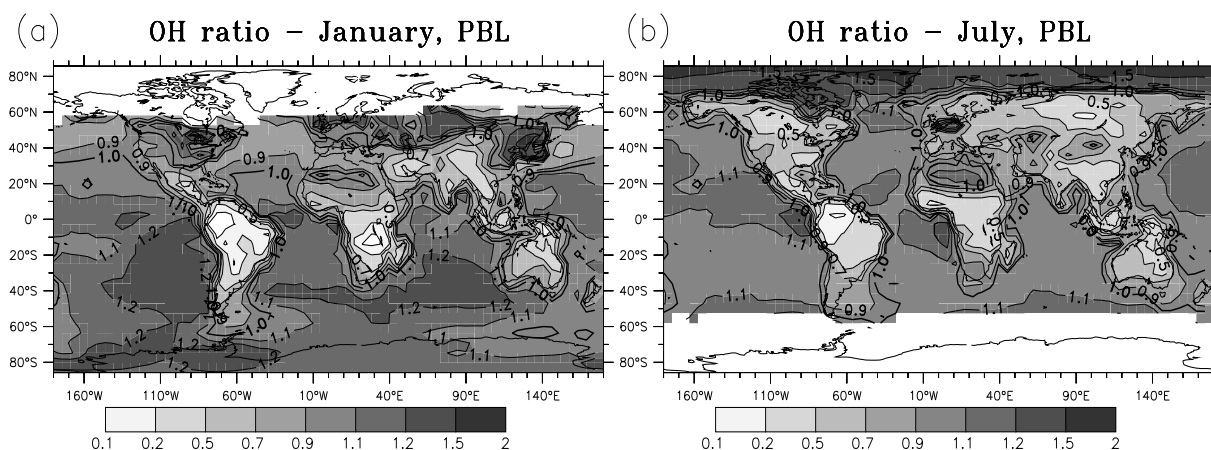
Figure 4.8: Ratio of OH concentration in the PBL (below σ=0.9) from the NMVOC and the CH4 run (OH_{NMVOC}/OH_{CH4}). Only regions with monthly mean OH concentrations more than 10^4 molec/cm^3 are plotted.

The low global mean effect on OH is in agreement with *Houweling et al.* (1998), who also observed little difference in their methylchloroform test, but lower than found by *Poisson et al.* (2000) and *Wang et al.* (1998b) (–14% and –20%, respectively). The difference is not easy to explain, as different aspects like the yield of CO in the chemical scheme, the nitrogen-chemistry (PAN) and the vertical mixing are involved. It is clear, however, that the overestimation of PAN in MATCH often found compared to observations (Section 3.5) will tend predict too large an increase of the OH concentrations in remote regions, which in this study appear to almost compensate for the increased loss of OH due to additional CO. A rather too large effect from PAN transport is also consistent with larger effect found for zonal mean NO_x at about 500-700 hPa than in *Wang et al.* (1998b).

4.5   Effects on the distribution of O_3

The zonal mean effects on the concentrations of ozone are also depicted in Figure 4.9. A maximum increase of about 25% and 35% is calculated for the ISOP and NMVOC simulation, respectively, compared to the CH4 run, with the largest effects in the southern tropics. The annual zonal mean absolute increase in the NMVOC run is about 4-9 nmol/mol in the lower and mid-troposphere and up to 12 nmol/mol in the uppermost troposphere.

In Figure 4.10 the change in the annual zonal mean production and loss rate of O_3, based on the O_x concept (Section 3.7) are shown. Both rates have increased over most parts of the atmosphere, which demonstrates the buffering of the chemistry of ozone. The production has increased especially in the uppermost troposphere and in the mid-troposphere (600-800 hPa). The latter region corresponds well with the region of the largest increase of NO_x (Figure 4.3), whereas in the former region NO_x has changed little compared to the CH4 run and the increase in ozone production can be mainly attributed to the increase in HO_x (Figure 4.7). E.g. the reaction HO_2+NO followed by photolysis of NO_2 results in production of ozone. Production of ozone has also increased by up to 80% over the northern mid-latitudes despite the decrease in NO_x in these regions. This is because chemistry in the strongly polluted regions is VOC and/or HO_x limited rather than NO_x limited (e.g. *Jacob et al.* (1995)), and thus the decease of NO_x due

Table 4.2: Turnover rates of OH in the simulations with and without NMVOCs. Turnover is in 10^8 molec/cm^3/s. Percent contribution to total turnover is also given.

Reaction	Turnover	Percent	Turnover	Percent
Source reactions	CH4	CH4	NMVOC	NMVOC
$O^1D + H_2O$ (2×)	2834	48.9%	3511	48.8%
$NO + HO_2$	1705	29.4%	2016	28.0%
$O_3 + HO_2$	598	10.3%	852	11.8%
$H_2O_2 + \nu$ (2×)	506	8.7%	638	8.9%
$CH_3OOH + \nu$	145	2.5%	150	2.1%
Loss reactions	CH4	CH4	NMVOC	NMVOC
$OH + CO = HO_2$	−2551	44.1%	−2980	41.4%
$CH_4 + OH$	−1078	18.6%	−1051	14.6%
$CH_3OOH + OH$	−440	7.6%	−485	6.7%
$HCHO + OH$	−363	6.3%	−464	6.4%
$O_3 + OH = HO_2$	−316	5.5%	−373	5.2%
$HO_2 + OH = H_2O$	−341	5.9%	−366	5.1%
$H_2 + OH = HO_2$	−331	5.7%	−323	4.5%
$OH + H_2O_2 = HO_2$	−227	3.9%	−279	3.9%
Total (loss ≈ source)	−5790	100%	−7200	100%
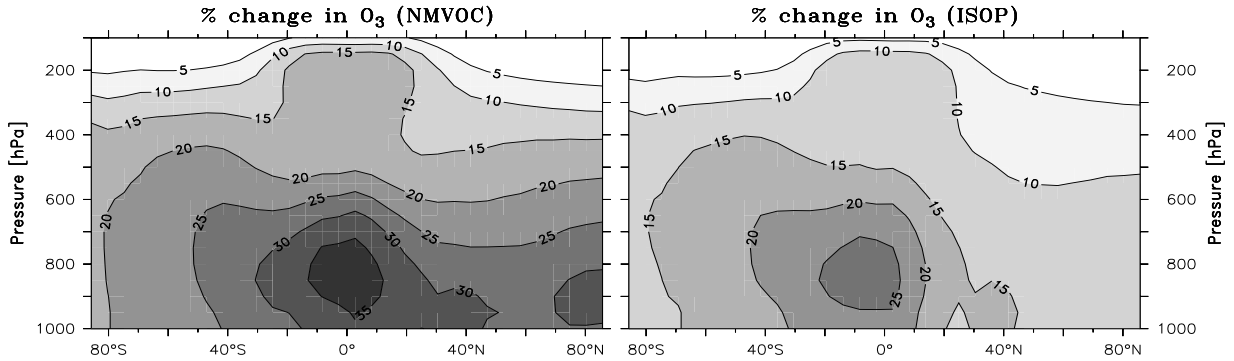
Figure 4.9: Percent change in the annual zonal mean mixing ratios of O_3 due to the consideration of all NMVOC or isoprene only (same as Figure 4.1, but for O_3).

to the formation of nitrates does not significantly hamper ozone production.

The only other study that investigated the effect of hydrocarbon chemistry on the production rate of ozone is the study of *Wang et al.* (1998b). These authors also found an intermittent region in the atmosphere between 300 and 500 hPa where ozone production is lower when higher hydrocarbon chemistry is included. However, the effect is more pronounced in the model of *Wang et al.* (1998b) which computed over 20% less production of ozone when including NMVOCs. On the other hand, the increase in the lower free troposphere (600-800 hPa) is larger in MATCH. The two maxima at 40°S and 20°N are associated with NO_x biomass burning and emissions from East Asia, respectively. In these regions relatively high NO_x mixing ratios are present and the additional hydrocarbons are especially effective in enhancing ozone production.

The increase of the loss reactions in the free troposphere correspond mainly to the increase in HO_x (loss reactions 2+3 in Table 3.8), but in the PBL near the equator also the influence of the
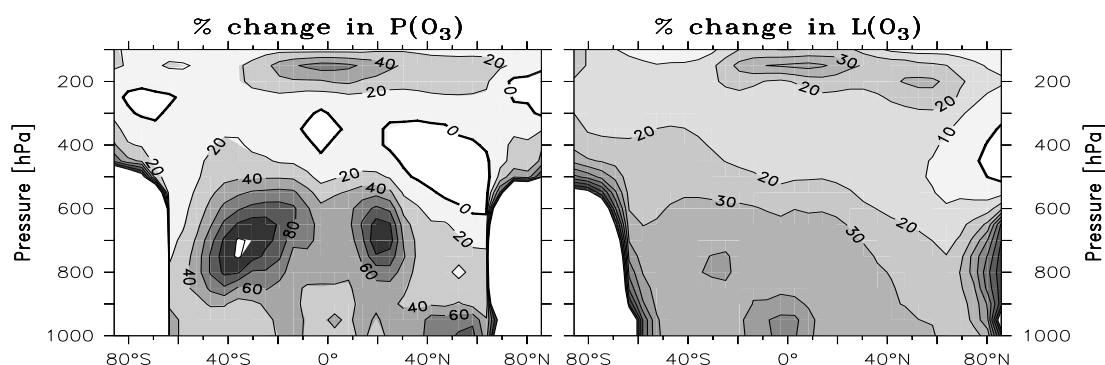
Figure 4.10: Percent change in the annual zonal mean gross production and loss rate of ozone (defined by the O_x-family in Section 3.7.

ozonolysis reaction of isoprene ($C_5H_8 + O_3 \rightarrow$ products) can be seen. In the polar regions the changes are only large in a relative sense, because very little NO_x is calculated in the methane-only run in these regions, due to the lack of a long-lived reservoir species other than HNO_3, which is efficiently removed by precipitation during transport into these regions.
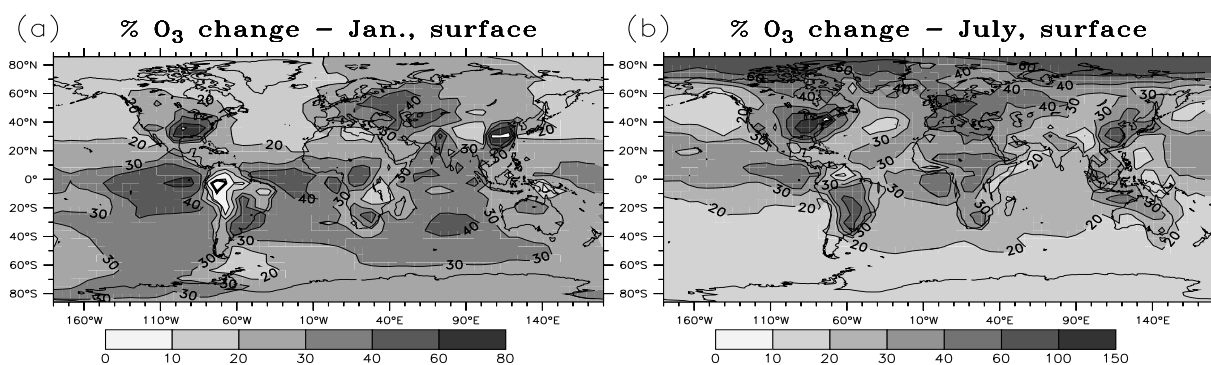
Figure 4.11: Percent change in the surface mixing ratio of ozone when including NMVOCs ($O_{3,NMVOC}$ - $O_{3,CH4}$)/$O_{3,CH4}\cdot100\%$).

The horizontal distribution of the relative change in ozone is depicted in Figure 4.11. Like in the study of *Houweling et al.* (1998) the largest effect is found in regions with high NO_x concentrations (South-East USA, Europe, East China, India, South Brazil). The enhancement of ozone in remote oceanic regions also reaches 30-40%, but the absolute increase is only about 1-3 nmol/mol. A slight decrease can be seen over the Amazon region in January due to the ozonolysis of isoprene, but not in July as in *Houweling et al.* (1998).

The inclusion of NMVOC-chemistry significantly improves the agreement at many surface measurement stations as demonstrated in Figure 4.12. The absolute increase is largest in the NO_x-rich regions, i.e. industrialized regions of the northern hemisphere (e.g. Kap Arkona, Hohenpeißenberg, Crete) and biomass burning regions (Cuiaba). While at these stations the increase due to isoprene and other NMVOCs is largest in summer (or the burning season, respectively) it is rather constant over the year at all remote stations. Thus, for those stations the seasonal cycle is not improved. At all other southern hemispheric stations almost the full effect is caused by isoprene chemistry alone, reflecting its large emissions in that region, compared to other NMVOC emissions which are assumed to be very low. The large widespread (most likely oceanic) emis-

sions of acetone and acetaldehyde suggested by *Singh et al.* (2000) and by the comparison in the last chapter could change this picture somewhat.

Although the agreement could be improved by the inclusion of NMVOCs at the southern low latitudes (south of 30°S), the mixing ratios are still too low (Amsterdam Island, Cape Grim). Since PAN is usually overestimated and thus also NO$_x$ concentrations are probably rather too high than too low in these regions, the reason is probably not photochemical. Note however, that other sources of NO$_x$ into the region (e.g. oceanic methyl nitrate, *Jones et al.* (1999)) cannot be ruled out. It is suspected that the global reduction of the stratospheric influx of ozone (Section 2.3.6) might not be necessary for the southern hemisphere, possibly because the internal consistency of the meteorological data is better (less "disturbed") in that region as discussed in Section 3.7.2.
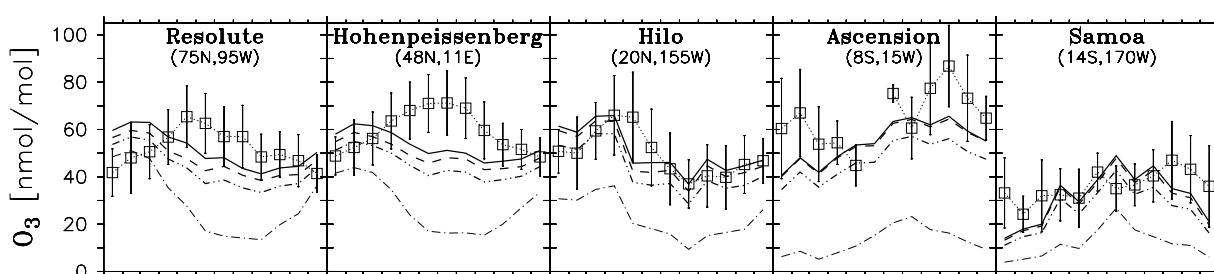
(a) At 500 hPa.
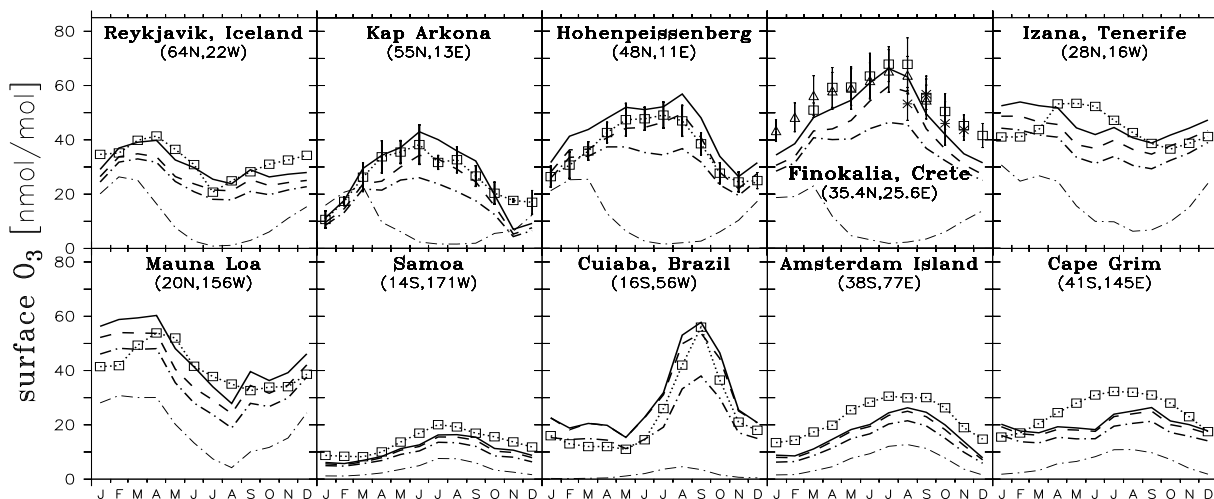
(b) At the surface.

Figure 4.12: Comparison of calculated ozone with selected surface observations (b) and at 500 hPa (a). Lines are as in Figure 4.2.

The changes in the middle and upper troposphere are also independent of the season (Figure 4.12a), thus are not predominantly the result of locally increased ozone production but rather of enhanced background concentrations due to enhanced production in other or more widespread regions. Consequently the seasonal cycle does not change or improve. This is especially interest-

ing for the polluted northern mid latitude stations (e.g. Hohenpeißenberg), where the summer maximum is still markedly underestimated by the model. Since a seasonal increase is found near the surface, a possible issue here is vertical mixing of precursors, which could be too slow in the model. Also an increased detrainment rate could help increase the production of ozone in the middle atmosphere. Inclusion of additional chemistry alone, e.g. aromatics or terpenes, would not suffice to solve the problem, because they should have similar effects than isoprene or the other hydrocarbons, which could not significantly change the seasonal cycle. As was seen in Section 3.7.3 the use of a different dataset had a much larger effect on the seasonal cycle, improving the agreement in the winter/spring season but also some in summer (see Hohenpeißenberg in Figure 3.43). This also suggests that meteorological instead of chemical parameters are important for a solution of this problem.

As summarized in Table 4.3 the increase of ozone when including NMVOC chemistry is the result of an increasing production rate (increased globally averaged by 1253 $Tg(O_3)$/yr) and an only partially compensating increase in the loss rate (+1055 $Tg(O_3)$/yr). It is interesting to analyze how much these respective increases are actually connected, thus whether this large compensation occurs in the same regions or if additional regional imbalances are caused. For this purpose the net tendencies in regions with net production and net loss (as in Section 3.7.1) are separately integrated for each run. The results show that in the regions where net production is found in the CH4 run, the net production increases only by 199 $Tg(O_3)$/yr, while for the "loss region" a slight decrease in net loss of 6 Tg/yr is found. It is noted that by defining the loss and production region based on the CH4 run for the integration of both net terms, small regions that actually switch signs are ignored. In these "switching regions" a net loss of –30 Tg/yr changes to a positive tendency of +26 Tg/yr. These numbers may be added to those given above, but do not change the interpretation significantly.

The total change in photochemical tendencies averaged separately over the two different chemical regimes thus results in terms which are only about 20% of the change in global loss or production and about 80% of the increase is buffered away within the respective region. Although it is recognized that at smaller spatial scales larger imbalances could be caused by the inclusion of NMVOC chemistry, this nevertheless illustrates the strong buffering effect in ozone chemistry. This underlines that an analysis of ozone chemistry should focus rather on the net photochemistry term than on the gross production and loss term, since these seem to be strongly coupled.

The resulting increase in burden is calculated to be 18% (12% from isoprene chemistry), which is in good agreement with *Houweling et al.* (1998) and *Poisson et al.* (2000), but larger than found by *Wang et al.* (1998b) (Table 4.3). Note, however, that these studies used different region definitions (< 150 hPa in *Wang et al.* (1998b), and < 100 hPa in the other two studies). The absolute increase of 46 $Tg(O_3)$ is well within the range of the other three studies (+56, +45 and +25 $Tg(O_3)$).

4.6   Summary and Conclusions

In this chapter the effects of non-methane volatile organic compounds (NMVOC) on atmospheric chemistry were investigated by comparing model simulations with and without this group of compounds. A third run was used to find the contributions of isoprene alone to these effects. The distribution of key atmospheric constituents O_3, CO, NO_x and HO_x were found to be strongly affected by NMVOCs chemistry. Isoprene chemistry alone is responsible for about half of the

Table 4.3: Effect of isoprene and NMVOC chemistry on global tropospheric budgets.

	CH4	ISOP	change[a]	NMVOC	change[a]	other studies[b]
global O_3 burden [Tg]	260	291	+12%	306	+18%	+16%[P],17%[H],9%[W]
strat. influx [Tg/yr]	650	634	–2%	627	–3%	+4%[H]
dry deposition [Tg/yr]	529	644	+22%	704	+33%	+31%[P],+28%[H]
$P(O_3)$ [Tg/yr]	2916	3809	+31%	4169	+43%	+31%[P],+38%[H]
$L(O_3)$ [Tg/yr]	3036	3799	+25%	4091	+35%	+17%[P],+29%[H]
$P(O_3)$–$L(O_3)$ [Tg/yr]	–120	+10	(+130)	+78	(+198)	+255[P],+169[H]
$\tau(CH_4)_{OH}$ [yr]	8.78	8.98	+2.3%	9.13	+4.0%	+15%[P]
$[\overline{OH}]_M$ [10^5molec/cm^3]	9.99	9.85	–1.4%	9.60	–3.9%	–14%[P],–20%[W],small[H]
CO prod. [Tg/yr]	787	1082	+37%	1193	+52%(+406)	+41%(+377)[P]
CO burden [Tg]	264	314	+19%	342	+30%(+78)	+38% (+86)[P]

[a]Relative to the CH4 simulation in percent or in the respective absolute units.

[b]Superscripts P, H, W denote the studies of *Poisson et al.* (2000); *Houweling et al.* (1998) and *Wang et al.* (1998b), respectively.

observed effects, with even larger contributions in the tropics and the Southern Hemisphere and lower effects in the northern hemispheric extra-tropics.

While the annual mean tropospheric burden of ozone increased by 18%, zonal mean concentrations in the tropics have increased by 20-35% in the lower troposphere (Table 4.3). Local increases in industrial and biomass burning regions can be as large as 50% or more. The global production and loss rates of ozone have both increased by about 30%, with a somewhat larger increase in the production term. In regions of net ozone production, about 80% of the increased production is compensated or buffered by an increase in loss rate.

The oxidation of non-methane hydrocarbons considered in the chemical scheme produce about 480 Tg(CO)/yr[5], of which about 320 Tg(CO)/yr are from isoprene. For comparison, methane oxidation produces another 714 Tg(CO)/yr. The tropospheric burden of CO is increased by 30% when all NMVOC are included. A detailed analysis of the loss pathways of carbon during the oxidation of hydrocarbons to CO reveals that roughly one third is lost through dry and wet deposition and direct production of CO_2 each. The total fraction lost through the deposition pathways is 72%[6]. Loss of peroxides formed in the oxidation of isoprene via deposition (mainly wet) is the largest single loss pathway and probably at the same time also the most uncertain. In these calculations loss via these compounds accounts for about 40% of the carbon loss in the oxidation of isoprene (or 82 Tg-C/yr) corresponding to a third of these compounds lost by dry deposition. In these estimate loss on aerosols is not considered. The CO-yields from methane, isoprene and other hydrocarbons is estimated to be 0.92, 0.39, and 0.39 respectively. The range of uncertainty obtained by reviewing the literature corresponds to an uncertainty in the CO production of up to about ±200 Tg(CO)/yr. More information on the deposition pathways of oxygenated compounds in the atmosphere is thus judged to be important in order to better quantify the production of CO from biogenic and anthropogenic hydrocarbons.

The distributions of NO_x and HO_x are also changed significantly by the inclusion of hydrocarbon-

---

[5]Note that methane oxidation has decreased in the simulation including NMVOC. Also, directly emitted methanol and formaldehyde is included in this estimate of additional CO production, but is also included in the CO production of the CH4 run (787 Tg/yr in Table 4.3). This explains the difference to the net increase of CO production of 406 Tg/yr given in Table 4.3.

[6]Here, the small loss due to violation of strict carbon conservation in the chemical scheme is counted as deposition.

chemistry. Formation of PAN in the boundary layer or free troposphere, above the continents, and subsequent long-range transport has been demonstrated to be the dominant mechanism for the redistribution of NO_x. PAN constitutes the largest reactive nitrogen reservoir exported from the continental troposphere, where most NO_x emissions occur. As a consequence NO_x concentrations are reduced by about 20-60% over the source areas when NMVOCs are considered and enhanced over the remote regions, especially around 700 hPa where most PAN decomposes. Above about 300 hPa the zonal mean net effect is a slight reduction in NO_x mainly due to its capture in PAN.

OH concentrations are largely depleted over forested regions (up to a factor of 10) due to the oxidation of isoprene. In remote regions the change in OH is strongly coupled to the change in NO_x, plus some additional loss due to the enhanced CO concentrations. In the uppermost troposphere an increase in OH but especially in HO_x is predicted, consistent with convective transport and photolysis of aldehydes, ketones, and peroxides into the region. The overall effect on global OH levels, as measured by the methane lifetime ($\tau(CH_4)_{OH}$) and the mass weighted mean OH concentration $[\overline{OH}]_M$, is calculated to be rather small ($\approx 4\%$ increase in methane lifetime), suggesting that the decrease due to enhanced CO levels is almost compensated by a net positive effect from the redistribution of NO_x.

Most results obtained with MATCH are in reasonable agreement with other studies. Some global budget numbers are also listed in Table 4.3 for comparison. However, some differences to other studies and disagreements between these studies were also found. For the increase in global burden of ozone three studies including this one consistently compute an increase of about 17%, whereas *Wang et al.* (1998b) get only 9%. Differences were also found in the effects on the distributions of NO_x and on the global mean OH concentration. Larger increase of NO_x in the remote mid-troposphere and less decrease in the upper troposphere when including NMVOCs were found in this study compared to *Wang et al.* (1998b). The difference is probably mainly caused by PAN chemistry and convection. It has already been found in the previous chapter that the intensity of convection can significantly influence the PAN abundance in the upper troposphere. The different redistribution of NO_x, is also linked to prediction of OH and HO_x enhancement in remote regions, which is probably larger in this study, leading to the low net effect in the global mean OH, consistent with *Houweling et al.* (1998), but different from *Poisson et al.* (2000) and *Wang et al.* (1998b).

These results and the comparison to other studies indicate that in assessing the effect of NMVOC chemistry the estimate for ozone is probably the most robust, which might be due the buffering effect seen in the photchemical tendencies. This statement, however, does not include other uncertainties which affect the net production of ozone in the troposphere (stratosphere, dry deposition). The accuracy in calculating the effect on CO is limited mainly by the uncertain deposition of intermediates and the change in OH. The effects on OH (HO_x) and especially NO_x are probably most uncertain and appear to be strongly dependent on PAN chemistry and probably convection. A realistic simulation of PAN is therefore also an important factor for correctly predicting the response of the atmosphere to changes in emissions. Unfortunately, agreement between model results and observations of this compound are often only achieved within a factor of 2 (*Roelofs and Lelieveld* (2000); *Poisson et al.* (2000), this study - Section 3.5.4).

Chapter 5

Sensitivities in Modeling Isoprene in a Global Model

An important function of atmospheric models is that they allow an assessment of the impact on the calculated results. This can give indications of where additional experimental research would be valuable and also helps provide an estimate of the uncertainty in predictions of future changes with the model (see e.g. *IPCC* (2001)). It is clear, however, that due to the enormous complexity of global chemistry-meteorology models, only the influence of a small fraction of the assumptions and parameters can be examined in a single study.

In the last chapter large changes in the distributions and even global abundances of several key trace gases in the atmosphere have been demonstrated to occur when the chemistry of hydrocarbons other than methane are considered in the simulation. Isoprene has been found to be a very large contributor to the calculated effects. This chapter thus focuses on possible influences of its chemistry and related parameters on the model results.

In Chapter 3 several deviations from observations were found, some of which could possibly be related to the treatment of isoprene chemistry or to interactions of isoprene chemistry and other model assumptions. Examples of discrepancies would the overestimate of isoprene in the Amazon region, the overestimate of CO in the Southern Hemisphere or the overestimate of PAN in the remote tropical free troposphere. Sensitivity runs could help to support or exclude potential reasons for these deviations.

In a box model study *Pöschl et al.* (2000b) compared one detailed and five condensed isoprene oxidation mechanisms with each other under various scenarios relevant to the atmosphere. While the Mainz Isoprene Mechanism (MIM), which was developed in that study and is also used here, was in relatively close agreement to the detailed mechanisms (the Master Chemical Mechanisms – MCM, *Jenkin et al.* (1997); *Saunders et al.* (1997a,b)), large deviations were found between the other mechanisms, both relative to each other and to the MCM.

The study in this chapter expands upon this work in two ways. Firstly, selected condensed isoprene mechanisms have been implemented into MATCH in order to investigate whether the effects found in the box model study are also relevant in the 3D context. Secondly, the global 3D model also allows the influence of non-chemical assumptions on the calculated results to be examined.

All simulations include only "background" CH_4-CO-NO_x-HO_x chemistry (Reactions R1-R45 in Table A.1 on page 171) and isoprene chemistry. Other non-methane hydrocarbons have not

been included in these tests in order to simplify the test conditions. Since in the last chapter isoprene has been shown to cause more than half of the effects of all NMVOCs and the sensitivities examined in this chapter are mainly in the tropics, where the contribution of isoprene was especially large, it can be assumed that the results obtained here would not change qualitatively, if the full NMVOC scheme was used instead. It is judged, however, that the effects obtained here will tend to be larger than one would get by varying isoprene sensitivities within the full chemistry scheme, because the influence of factors common to all test simulations would be higher in that case.

All simulations start with the meteorology of the 2nd of March 1998. The chemical initialisation for that day (at 0:00 o'clock) is calculated from a spin-up run which started on January 1st (1998) with the monthly mean tracer fields of January from the T21 base run (considering all NMVOCs) of Chapter 3. This lower resolution (T21) is used for all simulations in this Chapter. Only the monthly mean results for May are analysed here, which means that a spin-up period of 2 months is allowed for each simulation. This period has been chosen because it is characterised by frequent rainfall over large parts of the tropical continents south of the ITCZ[1] (wet season). During this season very little burning activity is occurring and thus the NO_x concentrations are relatively low (*Jacob and Wofsy* (1990)). Under these conditions isoprene chemistry is expected to be most uncertain, since the mechanisms are only tested with smog chamber data with NO_x concentrations in the hundred nmol/mol to mmol/mol range. Formation of the hydroxy-hydroperoxides should thus maximise during this season. On the other hand, during the dry season when biomass burning enhances the NO_x concentration in large parts of the southern tropics the influence of the treatment of organic nitrates would probably be larger than in May. Thus, no reliable extrapolations of the results from May to other seasons is strictly possible.

The discussion will focus on the effects in the tropics and especially over the Amazon rain forest, although global budget information is also collected and presented from each run to show the global mean effect. The effects of isoprene and its uncertainties in the extra-tropics are not very large in May and probably maximise later (July-August), when the isoprene emissions are strongest.

Each discussion of a group of sensitivity studies is based on the same two tables (Table 5.2 and 5.3) which comprise the main results from all sensitivity runs. Additionally, some plots of the 2-dimensional distributions of the changes are shown and discussed in the respective subsections.

5.1   Description of the Sensitivity Runs

A total of 13 sensitivity simulations have been performed, including a BASE simulation and a simulation only including the background chemistry (denoted CH4). An acronym for each run and a short description is given in Table 5.1. Most of the modified assumption in these runs can be considered to be within the range of uncertainties of our current knowledge or have been used in the recent literature. Not all tests are equally relevant and some simulations are therefore only discussed briefly. The sensitivity simulations in Table 5.1 can be subdivided into four groups, which are discussed separately in the following four sections.

The first group consists of three simulations (including the base run) with different condensed isoprene mechanisms. The Mainz Isoprene Mechanism (MIM, *Pöschl et al.* (2000b)) is compared to two other mechanisms used in recent global modelling studies. These two mechanisms have

---

[1]Intertropical Convergence Zone

Table 5.1: Short descriptions and acronyms of the sensitivity simulations discussed in this chapter.

Name	Description
CH4	Only backgound CH_4-CO-NO_x-HO_x chemistry.
BASE	Base run with background and isoprene chemistry (no other NMVOCs).
MOZART	Isoprene chemistry from the MOZART model (*Brasseur et al.* (1998)).
CBM	Isoprene chemistry of the modified CBM-IV mechanism by *Houweling et al.* (1998).
LOWISOP	Isoprene emissions reduced by 50% in the tropics (20°S-20°N).
LOWSOIL	Soil-NO_x emissions reduced by 50% over forested areas in the tropics (20°S-20°N).
LOWLTNG	Production of NO from lightning reduced by 60% over the continental tropical South America.
HIGHISON	Doubled yield of isoprene nitrates from the ISO_2+NO reaction.
INHNO3	Production of isoprene nitrates is channeled into HNO_3.
NONACA	Reaction products of the oxidation of the isoprene nitrates with OH are assumed to be lost from the atmosphere (thus product NACA is omitted).
LOWDEP	Deposition properties (dry+wet) of hydroxy-hydroperoxides from isoprene assumed to be the same as for CH_3OOH.
VLOWDEP	Deposition of intermediates of isoprene oxidation switched off.
HIGHDEP	Assumed loss of 70% of hydroxy-hydroperoxides from isoprene (as in *Brasseur et al.* (1998)).

been implemented in MATCH for this purpose using the flexible integration technique as presented in Section 2.3.3. In order to focus on mechanistic differences in the isoprene oxidation scheme, the rate parameters for the initial reactions of isoprene with OH, O_3 and NO_3, and also the PAN chemistry have been unified for all three mechanisms. An exception to this is the treatment of peroxy-acetic acid ($CH_3C(O)O_2H$), which is not included in the CBM scheme. The same photolysis rates are also used for reactions common to the three mechanisms.

The isoprene chemistry of the MIM has already been introduced in Section 1.2 (see Figure 1.3 on page 14). It contains about 45 isoprene related reactions and 16 species additional to the background methane chemistry. Each stage of the degradation is represented by a few species so that the reaction pathways prevailing under low and high NO_x conditions can be adequately represented by the surrogate species. Hydroxy-hydroperoxides from isoprene, which are assumed to form in NO_x-bereft environments and have likely been identified in two isoprene emitting ecosystems in South America (rainforest in Surinam: *Crutzen et al.* (2000); *Warneke et al.* (2001) and savanna in Venezuela: *Sanhueza et al.* (2001)), are explicitly treated in the chemistry and transport part of the model.

The mechanism used in another 3D chemistry-transport model named MOZART (*Brasseur et al.* (1998)), which is mainly based on *Müller and Brasseur* (1995), is similar in complexity to the MIM (about 19 species and 50 reactions). The main differences are the neglected treatment of hydroxy-hydroperoxides. Instead, 70% of these compounds are assumed to be lost through heterogeneous processes and the remainder is immediately oxidised to smaller products. The main C_4-products of the oxidation of isoprene, methylvinylketone (MVK) and methacrolein (MACR) are treated separately, as opposed to the method of lumping them into a single compound (also denoted MACR) in the MIM. The hypothetical reactions of MVK and MACR (as

well as methylglyoxal) with sulfate aerosols assumed in *Brasseur et al.* (1996) are not included in the implementation in MATCH.

Another difference is the relatively low reactivity assumed for the isoprene nitrates in the MOZART scheme, which may be used because isoprene nitrates are lumped together with other less reactive alkyl nitrates. The reaction rate with OH is $6.8 \cdot 10^{-13}$ molec/cm^3/s compared to $1.3 \cdot 10^{-11}$ used in the MIM. The latter value has been estimated using the structure-reactivity relationship (SAR) method of *Kwok and Atkinson* (1995). However, it is noted that this method not very reliable for organic nitrates (*Neeb* (2000)) and the reactivity of these nitrates must be seen as another uncertainty in the oxidation of isoprene.

A very simple oxidation scheme of isoprene has been constructed by *Houweling et al.* (1998), based on the CBM-IV mechanism of *Gery et al.* (1989). The lumping approach used in the CBM-IV to reduce the complexity of the degradation schemes of higher hydrocarbons is different than used in the MIM or the MOZART scheme. A structural lumping, which groups species according to their bond type (e.g. single or paraffinic bonds, double or olefinic bonds) is used, as opposed to molecular lumping in MIM and MOZART, where groups of reactions of entire molecules are combined. The initial reaction of isoprene with OH, for example, reads in the CBM mechanism of *Houweling et al.* (1998):

$$C_5H_8 + OH \quad \rightarrow \quad 0.85\,XO2 + 0.61\,HCHO + 0.85\,HO_2 + 0.03\,MGLY$$
$$+0.58\,OLE + 0.15\,XO2N + 0.63\,PAR$$
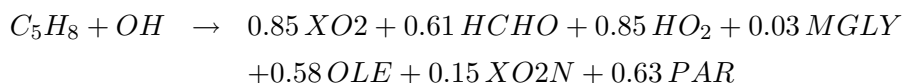
Here, XO2 and XO2N are peroxy-radical operators and OLE and PAR denote olefinic and paraffinic carbon bonds. The XO2(N) operators react like HO_2 but carry no carbon load, with the difference that the XO2N (NO-to-nitrate) operator converts NO to organic nitrates whereas XO2 converts it to NO_2. It is noted that upon this first reaction already 50% of the carbon is lost and replaced by carbon-free operators[2]. It was not stated by *Houweling et al.* (1998) whether this is due to chemical assumptions (CO_2 production), omission of products, or if it reflects the implicit assumption of loss of intermediates by deposition or heterogeneous processes.

In the next group of simulations some relevant emission strengths are varied. The direction of the changes (increase or decrease of the emissions strengths) is chosen so as to give better agreement with observations as presented in Chapter 3. Despite the caution with which comparison of a global model with point measurements has to be seen, it has been found in Section 3.4.3 that isoprene concentrations in the tropical rainforest are probably overestimated. It is unclear whether this is due to overestimated emissions or neglect of unknown deposition processes, but the difference is not relevant for modelling purposes, unless it significantly changes the diurnal cycle in the net flux of isoprene to the atmosphere. Therefore, a test simulation with isoprene emissions reduced by 50% in the tropics was made, resulting in an emission strength of about 215 Tg(C)/yr instead of 350 Tg/yr in the standard run, which is about equal to the value of 220 Tg(C)/yr used by *Brasseur et al.* (1998). The isoprene mixing ratios calculated with this emission strength are still on the high side of measurements at the tropical rainforest sites (e.g. *Rasmussen and Khalil* (1988); *Greenberg and Zimmerman* (1984); *Helmig et al.* (1998a)).

Soil emissions and lightning are the most important emissions in tropical ecosystems in the wet season when biomass burning activity is low. A critical issue in determining the actual flux

---

[2]Note that in the original CBM-IV by *Gery et al.* (1989) the carbon load in this reaction was conserved by 100%.

of nitrogen into the atmosphere is canopy recapture. A large part of the NO emitted by the forest soil is believed to be converted to NO_2 or organic nitrates and deposited to the canopy before being actually released to the atmosphere. In the soil emission data set used in this study (*Yienger and Levy* (1995)) this is taken into account by simple mechanistic assumptions. For tropical rain forest the canopy reduction factor, which expresses the fraction of nitrogen that is actually exported from the canopy, is given in *Yienger and Levy* (1995) as 0.25. In the LOWSOIL test simulation it was assumed that the soil emission over forested regions of the tropics is 50% smaller. This would correspond to a canopy reduction factor of about 0.13, or a 50% reduced primary soil emission strength with an unchanged reduction factor. The change in the global source strength, however, was found to be only about 5% (or 0.3 Tg(N)/yr), probably because tropical forest soils during the wet season are not very productive and most soil NO is released to the atmosphere over less forested regions (e.g. savanna). Therefore, this test probably does not span the full range of uncertainty of NO emissions from soils.

The production by lightning is calculated to be an even larger source of NO to the Amazon region in MATCH (vertically integrated). In the comparison to the GOME column NO_2 data it was found that this source is apparently overestimated in MATCH over this region during the wet season (Section 3.5.2). In another sensitivity run (LOWLTNG) therefore the NO production from lightning has been reduced by 60% over this region (continental South America, north of about 15°S). This reduction applied globally would result in a total source strength of 2 Tg(N)/yr in MATCH, which is near the low end of current estimates (e.g. *Lawrence et al.* (1995)). Due to the regional restriction of the reduction the global source strength is only reduced by 0.6 Tg(N)/yr or 13% (from 4.8 to 4.2 Tg/yr).

Since *Pöschl et al.* (2000b) pointed out that the different treatment of organic nitrates formed in the course of isoprene oxidation were responsible for a large part of the differences seen in box model simulations with various isoprene oxidation schemes, some tests were also performed to explore their role in the 3D model (3rd group of test runs). In the HIGHISON simulation a doubled yield of isoprene nitrates (denoted ISON in the MIM) is used. The value of 8.8% corresponds to the best estimate of *Carter and Atkinson* (1996), which is, however, in disagreement with the value of 4.4% obtained by *Chen et al.* (1998) and used in all other runs here.

Uncertainty also exists in the fate of these nitrates. In most reduced mechanisms, including the three tested here, two different groups of nitrates are represented by a single compound: The products of the reaction of isoprene with NO_3 and the group of β-hydroxy-nitrates from the peroxy radicals which are formed from the C_5H_8+OH reaction (see Figure 1.3 on page 14). The former will be mainly formed at night, because NO_3 concentrations are very low during the day. Since both groups still include a double bond they can react readily with OH, but the products and properties of the reaction products are not well known (see e.g. *Chen et al.* (1998)). *Chen et al.* (1998) argued that permanent removal of NO_x will generally occur. In the MIM an intermediate product, denoted NACA (for nitrooxy-acetaldehyde) is formed which can also deposit. In the sensitivity run NONACA it was assumed that all products of the ISON+OH reaction are assumed to deposit. Another assumption (*Roelofs and Lelieveld* (2000)) is that ISON is quickly reacts to HNO_3, which is tested in the "INHNO3" run. It is noted, however, that experimental evidence of this assumption is lacking.

A last group of sensitivity runs is performed to assess the role of deposition processes of soluble intermediates in the oxidation of isoprene. As discussed in the last chapter hydroxy-hydroperoxides produced by the reaction of hydroxy-peroxyradicals with HO_2 are probably very

soluble and can be efficiently taken up by cloud droplets and possibly to other surfaces. The special role and properties of these hydroxy-hydroperoxides compared to other peroxyradicals (ROOH) is often neglected (e.g. *Berntsen and Isaksen* (1997); *Collins et al.* (1999); *Zaveri and Peters* (1999)). This is imitated in the LOWDEP run, where the solubility of CH_3OOH is assumed to also be valid for these compounds, with effect of a lower wet and dry deposition efficiency.

An even more extreme case is tested in VLOWDEP, where deposition (dry and wet) of several intermediates (ISOOH, MACROOH, HACET, MPAN, MACR, ISON[3]) in the MIM are neglected completely. On the other extreme, in the "HIGHDEP" simulation a 70% loss of ISOOH and MACROOH[4] is assumed as in *Müller and Brasseur* (1995); *Brasseur et al.* (1998) and *Granier et al.* (2000).

5.2 Sensitivity to the Chemical Scheme

The horizontal distribution of ozone and PAN along with the changes resulting from the different isoprene oxidation mechanisms is shown in Figure 5.1. As expected, the changes are largest over the tropical rainforest regions, where isoprene emissions are highest. The effect in the extra-tropics is not fully developed in early summer. However, in the south-eastern U.S. there is a region where ozone production from industrial NO_x and isoprene has already increased ozone mixing ratios significantly above the background values. The three mechanisms agree to within a few percent in their prediction in this region.

In the tropical continental regions, where NO_x concentration are lower, however, differences of up to 50% are seen. The MOZART scheme results in about 15-30% lower ozone concentrations in the source region, whereas the CBM mechanisms yields even lower values, especially in the clean Amazon basin. The exact reason for such a behaviour is very difficult to track down to specific reactions, especially in a 3D model. More test simulations with changed assumptions in the two mechanisms would be necessary to find the most critical aspects in the scheme.

In case of the CBM scheme, in the Amazon region a decrease in surface mixing ratios of NO_x (10-20%), PAN (20-50%) and OH (25-45%), but an increase in HO_2 is found compared to the BASE run. For the MOZART scheme, on the other hand, NO_x, HO_2 and OH have only changed slightly (<5%, not shown), but PAN is also decreased over the Amazon region by 20-40%. A likely cause for the lower PAN levels are the implicit assumptions of large losses of intermediates in both schemes. In the CBM mechanism this is expressed in the 50% loss of carbon upon the initial reaction with OH; in MOZART 70% of the hydroxy-hydroperoxides are assumed to be lost. In the BASE run a global loss fraction of 35% is calculated. The corresponding value for the Amazon boundary layer is 68%. The fraction is found to depend strongly on the OH concentrations since they limit the lifetimes of these compounds. Consequently in the free troposphere (above 800 hPa) the fraction of hydroxy-hydroperoxides lost via deposition is only about 10% in the model, because the photochemical loss via reaction with OH is faster (24h-average lifetime is about 12 hours for those conditions). This also means that the loss of carbon via this pathway will actually depend on the assumed emission strength of isoprene, because this largely controls the abundance of OH in the boundary layer where most of the loss occurs. The reactivity of the group of intermediates will also be importance, adding to the overall uncertainty.

---

[3]For an explanation of these species see Table 2.1 on page 23.

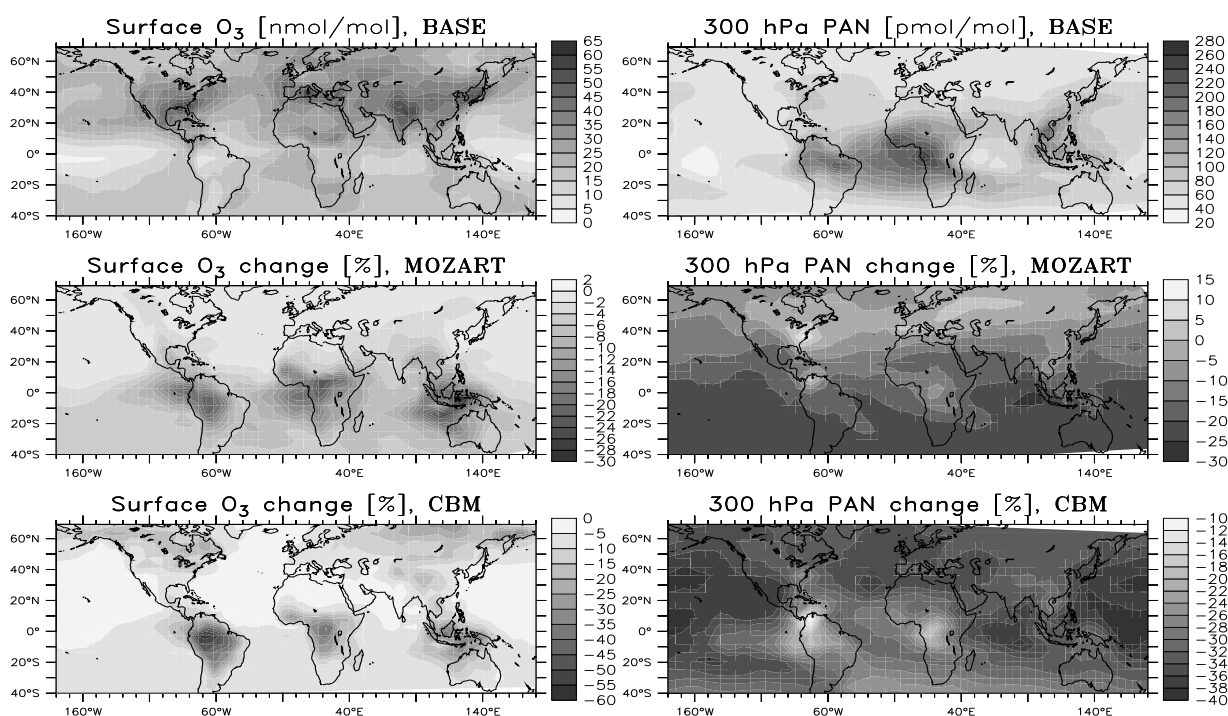[4]The two lumped hydroxy-hydroperoxide species in the MIM.

Figure 5.1: Distribution of surface ozone and PAN at 300 hPa in the BASE run (upper two panels) and relative difference (in %) of the results from the MOZART (middle panels) and CBM (lower panels) from the BASE run (e.g. $(X_{MOZART}-X_{BASE})/X_{BASE} \cdot 100\%$).

While the MIM cannot be claimed to perform "better" in these issues, it is argued here that it is nevertheless advantageous to be able to treat these aspects in the model when more data become available. All these aspects cannot be taken into account in the two other tested mechanisms, since these compounds are not explicitly treated.

The deviations in the PAN concentration in the upper troposphere are also plotted in Figure 5.1. The upper tropospheric values are plotted here because they determine the large scale transport of NO_x and give a better indication of the impact of the chemical scheme on the background level of this compound. Interestingly, for MOZART higher PAN concentrations are calculated near the surface in the northern hemispheric extra-tropics (+40-60%), but the change in the upper troposphere is much smaller ($\pm 5\%$). In these regions the treatment of the hydroxy-hydroperoxides is probably not important due to higher NO_x and OH concentrations. Therefore the differences found must be due to other differences in the chemical schemes.

In CBM the calculated concentration of upper tropospheric PAN is lower by about 20-40% compared to the MIM-chemistry (BASE run) over large regions including the NH-extra-tropics. Near the surface the CBM scheme tends to calculate lower mixing ratios over the continents and most parts of the ocean (not shown).

These results are consistent with the findings in the box model simulations (*Pöschl et al.* (2000b)), where PAN from the MIM was bracketed by the two schemes in the high NO_x scenarios, with MOZART being higher and CBM being lower, and was higher than the two other schemes in the low NO_x scenarios.

Some budget numbers from all simulations are collected in Table 5.2. Not all will be discussed here, but are listed for documentation and completeness. It can be seen that the global burden

Table 5.2: Selected budgets numbers from the sensitivity simulations for May. Units are Tg/yr unless stated differently.

Test case[a]	CH4	BASE	MOZ-ART	CBM	LOW-ISOP	LOW-SOIL	LOW-LTNG	HIGH-ISON	IN-HNO3	NO-NACA	VLOW-DEP	LOW-DEP	HIGH-DEP
O_3 Troposphere													
Burden [Tg]	273	304	290	291	296	304	298	303	297	298	322	308	300
Dry deposition	-604	-724	-684	-707	-713	-719	-718	-705	-702	-705	-765	-730	-715
$P(O_3)$–$L(O_3)$[b]	-80	90	37	54	56	85	86	71	58	63	190	115	66
$P(O_3)$	3087	3956	3645	3669	3758	3938	3881	3908	3785	3808	4345	4041	3860
–$L(O_3)$	-3167	-3865	-3609	-3615	-3702	-3853	-3795	-3837	-3727	-3745	-4155	-3927	-3793
O_3 Cont. PBL[c]													
Transport[d]	4	-50	-6	13	-52	-45	-52	-32	-29	-31	-58	-41	-53
$P(O_3)$–$L(O_3)$	410	564	487	495	559	554	561	527	525	530	603	559	561
CH_4–Lifetime [yr]	8.70	8.91	9.25	9.23	8.75	8.94	9.08	8.98	9.21	9.20	8.75	9.07	8.82
CO Troposphere													
Burden [Tg]	271	302	298	300	288	302	305	302	304	305	315	313	294
Chem. Prod.	787	1081	958	1023	989	1078	1066	1071	1037	1045	1234	1138	1031
Chem. Loss.	-2068	-2244	-2136	-2159	-2184	-2240	-2223	-2232	-2194	-2201	-2360	-2270	-2212
NO_y													
Troposph. Burden [Gg-N]	198	314	310	278	273	313	305	317	294	299	419	349	285
Transp. Cont. PBL	-2.86	-4.42	-4.13	-3.98	-4.04	-4.36	-4.39	-4.42	-3.85	-3.97	-5.93	-4.64	-4.26
Transp. UT Tropics[e]	0.270	0.111	-0.094	0.075	0.24	0.098	0.143	0.094	0.07	0.103	0.136	0.045	0.202
PAN													
Troposph. Burden [Gg-N]	—	84	72	57	53	84	81	85	78	82	147	111	60
Transport, Cont. PBL	—	-0.766	-0.832	-0.595	-0.639	-0.756	-0.754	-0.705	-0.701	-0.72	-1.174	-0.887	-0.689
Transport, UT Tropics	—	-0.227	-0.173	-0.14	-0.08	-0.23	-0.206	-0.243	-0.218	-0.227	-0.386	-0.298	-0.135

[a]For a list of acronyms of the runs see Table 5.1.
[b]Net photochemical production, based on O_x family (Section 3.7). $P(O_3)$ is gross chemical production and $L(O_3)$ chemical loss of ozone.
[c]Continental boundary layer (below about 800 hPa, $\sigma > 0.778$). Continents are defined by the model's land–sea mask.
[d]Sum of advection, convection and vertical diffusion tendencies. Negative numbers indicate net export from the continental boundary layer.
[e]Tropical (20°S–20°N) upper troposphere ($\sigma < 0.34$).

of PAN is lower in MOZART (-14%) and in the CBM run (-32%) compared the BASE run. The export from the continental troposphere is largest in MOZART and significantly smaller in CBM. The net export of PAN from the tropical upper troposphere shows that in this region chemistry is a source of PAN. Significant deviations are also found for total reactive nitrogen (NO_y), with the lowest values in each category for the CBM simulation.

The global tropospheric burden of ozone is lower by about 5% in the two other chemistry schemes. The results from a "methane-only" (CH_4-CO-NO_x-HO_x) simulation are also listed in order to assess the error in the overall effect of isoprene. While in the BASE run an increase of 31 $Tg(O_3)$ is calculated, it is only 17 or 18 Tg in the other two runs. The gross production of ozone ($P(O_3)$) varies by as much as 300 $Tg(O_3)$/yr in the different isoprene runs, compared to an increase from the "CH4" simulation of about 700-800 Tg/yr. However, the change (decrease or increase) in the loss rate is always acting against the production, so that the change in net production is not as large. This shows again that the two terms are not independent of each other.

For the export (or import) of ozone from the continental boundary layer even different signs are predicted. The BASE run has the highest photochemical production of ozone and despite a compensating higher dry deposition rate calculates the largest export of ozone from this region.

The CO burden is only marginally different in the runs, but it could be that the spin-up time of 2 months is not sufficient to fully develop the effect for this longer lived species. The production rate is significantly lower in MOZART (–123 $Tg(CO)$/yr or 11%) and CBM (–58 Tg/yr, 5%). Despite the lower production rates and burdens of CO in these two runs, the oxidation efficiency of the atmosphere with respect to methane is somewhat lower (corresponding to a 0.3 yr longer methane lifetime). This is probably caused by the lower PAN amounts and thus less long-range transport of NO_x in these runs.

Locally, the effects on CO mixing ratios can also be significant. A summary of the relative and absolute deviations of all simulations compared to the BASE run are presented in Table 5.3 for the key species O_3, CO, NO_x, PAN, OH and HO_2. Again, not all numbers will be discussed here, but they illustrate the magnitude of the perturbation by each of the sensitivity simulations. It can be seen that the MOZART and CBM simulation can be as much as 11 and 22 nmol/mol lower in CO. For the CBM scheme regions with higher CO mixing ratios (up to 12 nmol/mol) are also found, which is probably due the faster oxidation of isoprene to CO resulting from the omission of several intermediate stages in the mechanism. The maximum perturbation in O_3 is as large as about 10 nmol/mol for the two runs. Local deviations are also found for the two HO_x species (OH and HO_2), especially for the CBM simulation.

5.3 Sensitivity to the Emissions Strengths

As discussed above the three tests to investigate the effect of changing the emissions strengths are probably all within the range of uncertainty. In the test of the soil emissions only the sensitivity to the canopy reduction factor and not the overall uncertainty in the source strength is considered.

The effects on surface ozone and and PAN at 300 hPa are shown in Figure 5.2. The perturbation of upper tropospheric PAN in the LOWSOIL simulation was small ($\pm2\%$) so that only the change in surface NO_x concentrations is shown instead.

The reduction of the isoprene emissions in the tropics (LOWISOP) results in an increase of O_3 in the source regions, which is due to the reduced ozonolysis reaction of isoprene with

Table 5.3: Maximal relative and absolute deviations of the test runs from the BASE run. The relative deviations have been restricted to regions where the mixing ratios are more than 5% of the corresponding lower tropospheric (<500 hPa) average.

Test run[a]	CH4	MOZ-ART	CBM	LOW-ISOP	LOW-SOIL	LOW-LTNG	HIGH-ISON	IN-HNO3	NO-NACA	VLOW-DEP	LOW-DEP	HIGH-DEP
O_3												
max. relative change [%][b]	4.7	0.5	0.4	15.8	0.2	0.3	3.6	0.2	0.2	41.8	16.0	2.0
min. relative change [%][c]	-48.2	-34.5	-63.4	-14.6	-15.7	-25.1	-28.4	-19.1	-17.1	-0.5	-11.6	-3.8
max. absolute change [nmol/mol][d]	11.0	6.6	4.6	4.2	0.15	4.1	0.7	1.8	1.5	8.1	2.1	1.0
min. absolute change [nmol/mol]	-23.9	-11.2	-12.5	-5.7	-2.5	-8.6	-5.1	-6.5	-5.8	-6.2	-3.2	-1.1
CO												
max. relative change [%]	1.4	1.4	12.8	0.1	0.6	5.2	1.1	2.0	2.3	25.0	15.7	0.0
min. relative change [%]	-42.9	-10.2	-10.3	-18.9	-1.4	-0.5	-3.6	-2.0	-1.4	0.0	0.0	-5.1
max. absolute change [nmol/mol]	1.8	1.9	16.0	0.01	0.6	3.5	1.3	1.4	1.9	35.8	20.6	0
min. absolute change [nmol/mol]	-77.9	-11.7	-22.4	-33.7	-1.6	-0.6	-4.0	-2.3	-1.7	-0	-0	-5.9
NO_x												
max. relative change [%]	83.2	14.3	24.7	52.2	8.3	11.9	20.4	5.8	5.5	179.7	105.8	20.7
min. relative change [%]	-79.2	-70.0	-73.4	-49.6	-38.1	-54.8	-32.3	-41.4	-38.0	-23.1	-48.1	-17.1
max. absolute change [pmol/mol]	2486	31.8	1537	89.6	3.5	15.6	98.7	25.4	25.5	89.5	23.9	42.2
min. absolute change [pmol/mol]	-260	-127	-173	-46.7	-223	-79.1	-74.0	-64.1	-57.3	-267	-39.1	-13.6
PAN												
max. relative change [%]	—	79.5	114.0	13.8	19.9	31.6	69.4	44.0	51.0	1924	1072	0.8
min. relative change [%]	—	-81.1	-85.6	-88.8	-24.2	-33.4	-38.0	-45.1	-39.6	-14.0	-19.5	-48.3
max. absolute change [pmol/mol]	—	497	37	2.2	4.0	2.1	13.5	0.6	1.2	617	195	1.0
min. absolute change [pmol/mol]	—	-118	-189	-352	-29.0	-54.8	-80.1	-64.9	-52.6	-1.2	-1.6	-78.4
OH												
max. relative change [%]	6854	11.6	51.0	229	1.2	7.2	3.4	3.2	1.7	35.5	11.9	25.8
min. relative change [%]	-49.8	-59.8	-67.9	-14.7	-25.4	-59.1	-45.7	-27.4	-26.0	-60.3	-60.4	-7.2
HO_2												
max. relative change [%]	45.7	21.9	142	23.7	3.0	36.4	6.9	7.8	8.7	38.5	22.4	6.1
min. relative change [%]	-93.7	-20.1	-39.2	-39.7	-8.1	-13.4	-12.5	-12.6	-10.9	-12.3	-19.1	-14.2

[a] For a list of acronyms of the runs see Table 5.1.
[b] Percentage by which the mixing ratio in the test run is maximally higher than the BASE run.
[c] Percentage by which the mixing ratio in the test run is maximally lower than the BASE run.
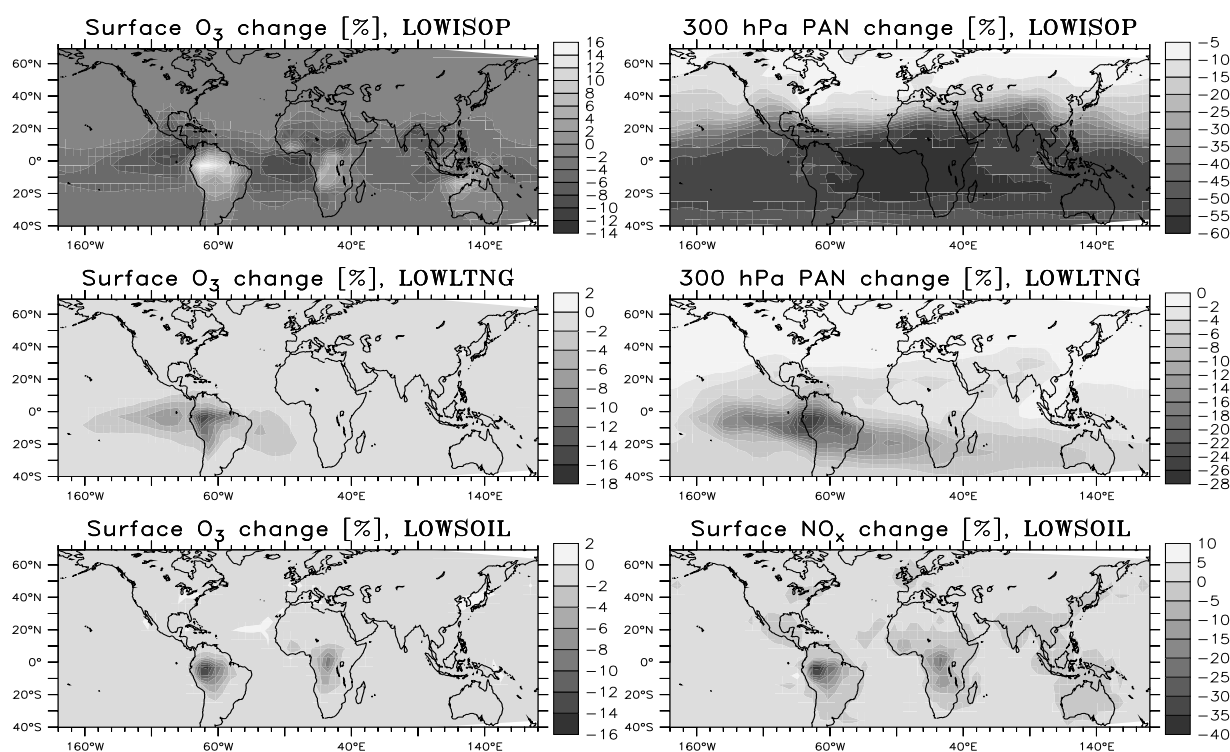[d] Like relative changes, but for maximum difference in mixing ratios.

Figure 5.2: Relative change (in %) in surface ozone and PAN at 300 hPa in the sensitivity runs with changed emissions. For the LOWSOIL simulation the change in surface NO_x is plotted.

O_3. On the other hand, a decrease in remote regions and also in the free troposphere above the source regions is calculated (not shown), which is likely connected to less PAN formation and thus less NO_x in remote regions. The absolute difference (Table 5.3) of about ± 5 nmol/mol is not as large as in the last group of tests. The predicted increase in the total ozone column in the BASE run compared to a "methane-only" simulation (CH4) of 31 Tg(O_3) is reduced by 8 Tg (26% of the effect). Interestingly, the global burden and the net production term of O_3 in the LOWISOP simulation are still higher that for the MOZART and the CBM runs, whereas other budget numbers like the global CO burden and chemical production and the global PAN burden are significantly lower in the LOWISOP run. This shows that the impact of the isoprene oxidation scheme on O_3 is as large as the 50% reduction in isoprene source strength, whereas most other species are slightly less affected.

A larger impact is predicted for PAN, which is reduced by about 40-60% at 300 hPa in the LOWISOP run, which corresponds well to the 50% reduction in tropical isoprene emissions. Clearly, the overestimation of isoprene in MATCH over tropical locations together with the fact that a large (>50%) fraction of PAN in the tropics is from isoprene can explain a large part of the overestimate in PAN found in Section 3.5.4.

The reduction of the soil emissions (or the canopy reduction factor) results in maximum reduction of NO_x of 38% (Table 5.3 and Figure 5.2) over the central Amazon and a reduction in O_3 of about 15%, only 2.5 nmol/mol. In the free troposphere the effect on ozone and as mentioned above also on PAN is negligible (O_3: $< \pm 1\%$). Recall, however, that the absolute change in the emission strength was only small in this test run.

A much larger effect is found when reducing lightning over a major isoprene source region

(South America). The 60% reduction in the lightning NO source reduces PAN concentrations by up to 30% in that region in the LOWLTNG run, which means that about half of the PAN formed from isoprene in that region is from the interaction of isoprene oxidation products and lightning NO_x. The remainder is from biomass burning (in Venezuela), some surrounding industrial emissions (e.g. from cities at the west coast of South America) and from NO_x emissions from soils. Recall that the overestimate of the NO_2-column over the central Amazon in May was as large as a factor of 10. Thus, even when considering the uncertainties in that comparison, it is likely that the 60% reduction was too mild and the effects could be much larger with an "optimal" lightning source in the region. A better quantification of the source strength of lightning in this region, especially in the wet season, when other NO_x sources are weak (and deposition loss is strongest), in connection with a realistic representation of vertical transport (PBL turbulence, convection) appears to be a key to a better simulation of the chemistry over the Amazon, and significantly influences the export of PAN from that region.

5.4 Sensitivity to the Fate of Isoprene-Nitrates

The nitrates formed in the oxidation of isoprene are usually represented by only a few surrogate species in the condensed mechanisms, due to a lack of more detailed knowledge of their individual chemistry and computational restrictions. Apart from the uncertainty in their formation rate, it is also largely unknown what products are formed upon their reaction with OH or photolysis.

The changes of surface ozone in the HIGHISON and NONACA simulations are shown in Figure 5.3 and further results are listed in Tables 5.2 and 5.3. Ozone concentrations decrease by about 20% in the central Amazon region, which is comparable to the changes found in the last section. In the simulation where all products of the reaction of isoprene nitrates with OH (ISON+OH) are assumed to deposit (NONACA), the changes are somewhat more widespread due to the lifetime of ISON of about one day in the MIM. The results from the third run in which all ISON is quickly converted to HNO_3 (INHNO3) is not shown, since it actually yielded very similar results than the NONACA simulation. This is understandable, because forming HNO_3 from ISON will also result in a high likelihood of permanent nitrogen removal from the atmosphere, this time via deposition of nitric acid, instead of an explicit assumption in the scheme.
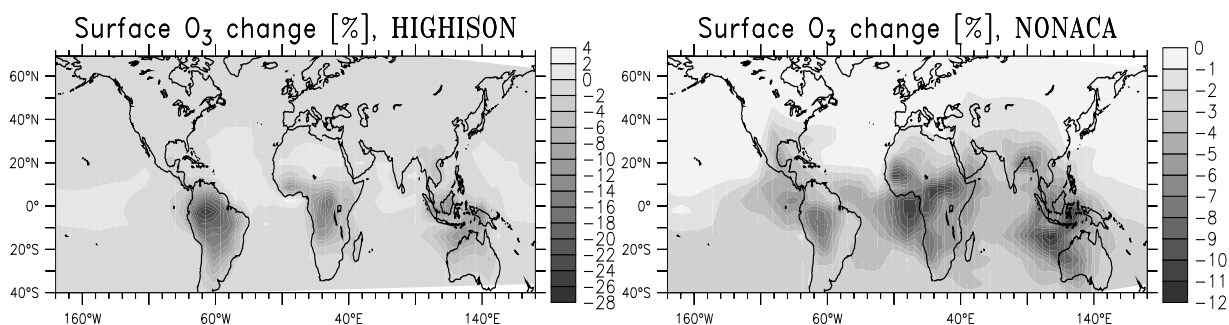

Figure 5.3: Relative change (in %) in surface ozone in the HIGHISON and NONACA sensitivity runs compared to the BASE run.

At this point it might be interesting to analyse the global average sources and sinks of these nitrates in the MIM. It can be seen in Table 5.4 that actually more than 60% of the ISON surrogate in MIM is formed from the nighttime reaction of isoprene with NO_3. 'The isoprene-NO_3-adduct could in principle react with NO, NO_3, HO_2, OH or decompose (*Jenkin et al.* (1997)), but no mechanistic information is available at present and as mentioned before the SAR estimation method for nitrates is not very reliable. This has to be kept in mind, when more elaborate formulations of their chemistry are attempted. The basic question to answer will be how much of the nitrogen is eventually lost from the atmosphere without releasing NO_2. In the BASE implementation about 53% is lost via dry and wet deposition in May on the global average, which is somewhat higher than the annual average of 48% calculated in Section 4.2.3. This high fraction is the result of a relatively high Henry's Law constant assumed for this species (see Table 2.4 on page 32).

Table 5.4: Tropospheric budgets of C_5-isoprene nitrates in the BASE simulation (MIM chemistry) in May. Numbers are in Tg(N)/yr.

Sources	$C_5H_8+NO_3$	+2.9
	ISO_2+NO	+1.8
Sinks	$ISON+OH$	–2.2
	$ISON+h\nu$	–0.1
	dry deposition	–1.0
	wet deposition	–1.5

More extreme assumption have been made by *Müller and Brasseur* (1995), who assume 100% loss, and by *Houweling et al.* (1998), who neglect their deposition loss completely. The first assumption should be similar to the NONACA case tested here, since only a small fraction of ISON photolyses to give back NO_2 (Table 5.4). The latter assumption is unrealistic and probably a compromise needed because the nitrates from isoprene are not differentiated from the alkyl nitrate pool in this CBM version[5]. The tests performed here should thus give a good indication of the actual range of uncertainty from the treatment of isoprene nitrates.

Although the global effects on ozone and PAN are smaller than seen in the test with different chemistry schemes, the local differences in O_3 are not negligible (up to 5 nmol/mol). The net production in the INHNO3 simulation (58 Tg/yr compared to 90 in the BASE run) is almost as low as in the CBM simulation (54 Tg/yr).

5.5 Sensitivity to Deposition of Intermediates

In the last chapter it has been calculated that on the global annual average 33% of the hydroxy-hydroperoxides are lost in the standard MATCH simulation using a relatively high Henry's Law coefficients. Two other assumptions which have been used in other studies were tested here. The VLOWDEP case, were no deposition of intermediate species from the oxidation of isoprene is allowed, is probably unrealistic and is only used to assess the maximal effect of the deposition of intermediates. In view of the 33% mentioned above, the high loss rate in the HIGHDEP

---

[5]See *Zaveri and Peters* (1999) for an alternative formulation of isoprene chemistry in another modification of the CBM-IV scheme.

simulation on the other hand appears to be only possible when heterogeneous loss on aerosols occurs, which is well possible but speculative at present.

The effect of these assumptions on ozone is quite small (< 3 nmol/mol) for the two more realistic cases (LOWDEP and HIGHDEP), but are predicted to be in the range $\pm 6 - 8$ nmol/mol for the VLOWDEP case (Table 5.2 on page 156). For that case also the highest global burden of O_3 of all test simulations is calculated, which corresponds to an increase of 49 Tg(O_3) compared to the CH4 run (31 Tg in the BASE run). The global CO burdens have changed by only little as in all the other test runs: -4% in LOWDEP and +2% in HIGHDEP. But local differences can be especially large in the LOWDEP run (+15% or 20 nmol/mol), though the resulting decrease in CO in the remote SH at the surface is also small ($\approx 5\%$, not shown). This is about the magnitude that was found by reducing the source strength of isoprene. The photochemical source of CO is changed by ± 50 Tg(CO)/yr ($< 5\%$) in the two more realistic scenarios and +150 Tg/yr in the VLOWDEP case. Note that the magnitude of these effects are also coupled to the total source strength which was reduced by 30% from the original data set (*Guenther et al.* (1995), 500 Tg(C)/yr).

An interesting point can be seen in the change in the methane lifetime. While in the two more realistic simulations the methane lifetime changes consistently with the increase or decrease of CO production, in the VLOWDEP the methane lifetime is shorter than in the BASE simulation despite the higher production of CO. This behaviour is probably the result of also neglecting the deposition of two nitrates from isoprene oxidation (ISON and MPAN) and the strongly increased PAN abundance (Table 5.2 on page 156 and 5.3 on page 158), which lead to enhancement of global OH via more transport of NO_x into remote regions.

Since the assumptions added to the BASE run for the HIGHDEP simulation are basically adopted from the MOZART mechanism, one can examine the impact of these assumptions on the total difference between MOZART and the BASE run. The results of the MOZART and HIGHDEP runs are much closer to each other than MOZART and BASE, which means that the assumption of 70% loss of hydroxy-hydroperoxides from isoprene probably also has a significant impact on the results of the MOZART run. Some discrepancies, however, remain and must be due to other factors in the chemical schemes. For example the global PAN and NO_y burden are even smaller in the HIGHDEP than in the MOZART run which confirms the tendency of the MOZART scheme to predict high PAN levels. Since PAN-related rate parameters were unified in this study, this means that differences in the reaction rates were not the reason for the higher PAN yield in the MOZART mechanism, which was also found in the box model study of *Pöschl et al.* (2000b).

The largest effects in this group of test cases is in fact found for PAN, which is depicted in Figure 5.4. Especially in the LOWDEP case the deviations are large: A 30-45% increase in PAN levels can be seen in the upper troposphere of the SH and the northern tropics when the deposition properties of CH_3OOH are used for all peroxides (LOWDEP run). The decrease in PAN due to even higher deposition rate is not as large: about 15-20% over large parts of the SH. The changes in the lower atmosphere are even higher with peak changes of a factor of 10 (see Table 5.3 on page 158), but these occur in regions with less than 1 pmol/mol of PAN (e.g. in the south east Pacific).

Since photolysis of peroxides is believed to contribute to upper tropospheric HO_x production it is instructive to see the effect of the different treatment of hydroxy-hydroperoxides on the HO_x mixing ratios in the upper troposphere. In the LOWDEP simulation a 10% higher zonal mean
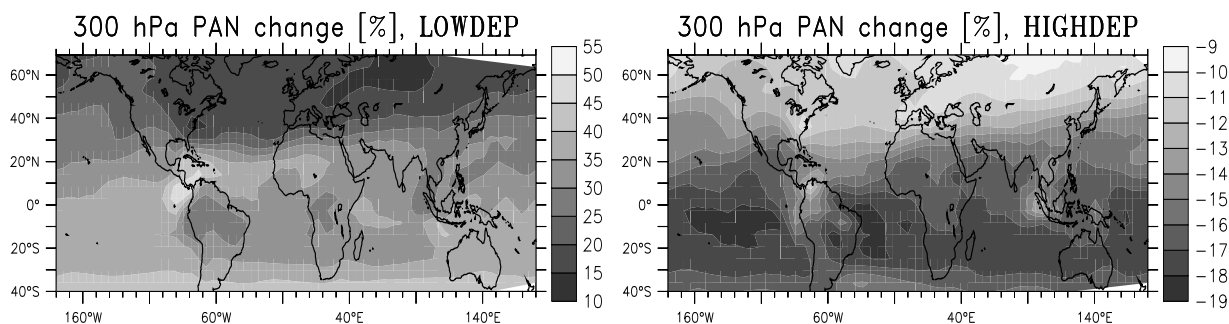
Figure 5.4: Change in the PAN mixing ratios (in %) at 300 hPa for the LOWDEP and HIGHDEP simulations.

HO_x abundance in the uppermost tropical troposphere (100-200 hPa) is found. The HIGHDEP runs results in about 5% lower values than in the BASE case.

In the study of *Collins et al.* (1999) the effect of convection of different compounds on upper tropospheric HO_x levels was studied. In that study the same assumptions as in the LOWDEP run were made. The largest effect was found for isoprene and its largest oxidation products. It is difficult to judge quantitatively the effect of the results from this study within the framework of their test setup, where only one substance was allowed to be convected per test run. However, from the above results it can be said that the effects found by *Collins et al.* (1999) when switching on the convection of isoprene and its oxidation products were probably overestimated, due to too little wet scavenging of the hydroxy-hydroperoxides.

5.6   Summary and Conclusions

A number of different sensitivities in the treatment of isoprene in a global model have been examined. Different chemical schemes, changed emission rates, and different assumptions about the fate of isoprene nitrates and about the deposition efficiency of certain intermediates have been tested and analysed for one month of the year (May).

The overall picture obtained in these tests is that global average budget numbers of O_3 and CO vary in the different sensitivity runs by about 5% or less, whereas the changes in total NO_y burden and PAN burden are larger (10% and 30-40%, respectively). Local deviations of the key species can be substantial. In judging this, however, one has to keep in mind that the total effect of isoprene chemistry on global tropospheric ozone is probably of the order of 20% or less (see Chapter 4), because a large part of the tropospheric chemistry is driven by methane and CO. Thus, a 50% uncertainty in isoprene-related factors would only result in a global mean effect of about 10%.

The deviations induced when exchanging the chemical scheme were found to be largest among all test simulations (except for the VLOWDEP run, which is discarded here as unrealistic). The simulation with the highly condensed CBM-scheme by *Houweling et al.* (1998) produces the largest local deviations in O_3 from the base simulation (up to 60% and 12 nmol/mol). The global burden of O_3 calculated for the three runs with different chemistry is increased compared to the background methane chemistry by 24±7 Tg(O_3) (or ±30%). This range of uncertainty and the much larger local deviations found in the test runs show that the treatment of isoprene chemistry in global models can only be seen as a first order estimate at present.

The reason for the deviations of the results from different isoprene oxidation mechanisms cannot easily be identified, but in the case of the CBM scheme (*Houweling et al.* (1998)) it is suspected that the large loss of carbon and thus also of some functional groups and the direct channelling into smaller products produces the different behaviour in that scheme. The MOZART mechanism tends to produce more PAN than the MIM-scheme used in the reference run, but this is in part prevented by the implicit assumption of a high (and constant) loss rate of soluble intermediate species (the hydroxy-hydroperoxides from isoprene). It could be shown that the actual fraction of these compounds which is deposited in a certain environment will also depend on the abundance of OH. Although no mechanism can be judged superior over the other schemes, it appears advantageous that these compounds are explicitly included in the MIM. As new data on their reactivities and deposition properties become available, they can be readily implemented in the scheme or the surrounding model.

While deposition of soluble intermediates appeared to have a relatively small impact on ozone, it was found to be much more important for the formation of PAN and thus the resulting total burden of NO_y. The effect of an increased deposition rate (HIGHDEP run) resulted in a reduction in global PAN burden (–24 Gg-N, or –29%) which was comparable to the run with a 50% reduction in the isoprene source strength (–31 Gg-N, –37%). Overall, it appears that the overestimation of modeled PAN compared to observations in the tropics found in Section 3.5.4 can be largely explained by a combination of the three factors found in this chapter to have the largest impact on PAN: total source strength of isoprene (or alternatively an additional deposition process), source strength of NO from lightning and loss of intermediates through deposition or heterogeneous processes. All of these parameters need to be quantified better in order to improve the simulation of the long-range transport of NO_x in the tropics.

The effects of exchanging the chemical scheme are of the same magnitude as a reduction of tropical isoprene emissions by 50%. While the variation of NO emissions from forest soils had only minor effects, changing the source strength of lightning over the Amazon region resulted in larger deviations (up to 20% in O_3) and the true lightning source strength could still be outside the tested range. The interaction of lightning NO and biogenic hydrocarbons, including those other than isoprene, should therefore be studied further.

The effect of the fate of nitrates from the oxidation of isoprene was rather small, but this could be in part due to the chosen season in this study. Larger effects would e.g. be expected during the biomass burning season in the southern tropics and sub-tropics. This season and the peak summer months in the NH (July-August) would be interesting to investigate. During the latter time period a significant underestimate of ozone in the middle troposphere over polluted regions was seen in Section 3.7.3 and during the biomass burning season ozone was also underestimated by up to 20 nmol/mol in the middle troposphere. From the results obtained here, it is not expected that either of these problems can be solved by changes in the implementation of isoprene in the model.

Overall it can be said that isoprene chemistry is still a relatively uncertain point in current chemistry models. Additional to the uncertainties in the the gas-phase mechanisms, deposition and potential heterogeneous processes on aerosols, are also problems in 3D-models, which require further research. However, the importance of these uncertainties is limited by the total effect of isoprene on global tropospheric chemistry, which was discussed in Chapter 4.

Chapter 6

Conclusions and Outlook

6.1 Conclusions

The 3-dimensional chemistry-meteorology model MATCH-MPIC has been used to study the chemistry of tropospheric ozone, the hydroxyl radical (OH) and other related species, such as reactive nitrogen compounds, hydrocarbons and oxygenated species.

For this purpose the treatment of non-methane volatile organic compounds (NMVOCs) has been added to the model. This included the development of a simplified representation of their photochemistry and the implementation of deposition processes and emissions. Also, a reevaluation and some updates on emission datasets and the implementation of a more detailed dry deposition scheme has been performed. The chemical scheme applied in this studies includes background CH_4-CO-NO_x-HO_x chemistry, ethane and propane (and acetone), isoprene, and simple representations for ethene and propene chemistry. The chemistry of n-butane is used to represent higher alkanes. For newly included photolysis rates a simple parameterisation was developed, which couples the new reaction rates to other rates previously used in the model.

For the solution of the coupled system of stiff ordinary differential equations of the chemistry a fast Rosenbrock method has been adopted and implemented using a preprocessor environment, which allows for easily changing the set of chemical reactions in future studies with the model. Sufficient speed and accuracy of the solution could be achieved by the use of asymmetric subdivisions of the dynamic time step within the chemistry integration. A first[1] assessment of the accuracy of the chemical integration method in the 3D context (but excluding splitting errors) has also been presented.

A extensive comparison of the model results with observations in various regions was carried out. The model was able to reproduce large parts of the observations, but some discrepancies could also be identified. Both, agreement and disagreement, can help promote our understanding of the life cycles of the key species and quantify the anthropogenic and biogenic contributions to the species budgets.

For carbon monoxide (CO) the agreement was generally good in terms of seasonal cycle and magnitude, with the exception of a significant overestimate in the Southern Hemisphere (SH) extra-tropics. No single reason for the too high CO concentrations in the SH could be identified and it is judged that a combination of several factors is probably responsible.

The evaluation of calculated global OH with methyl-chloroform (MCF) and by comparison

---

[1]To the best of the authors knowledge.

to other studies could not detect an unequivocal over- or underestimate, although the MCF-test suggests a slight underestimate of the correspondingly weighted global mean OH. It was also found that the capabilities of the methyl-chloroform test to derive this quantity were probably seen too optimistic by previous studies. This statement may, however, not apply to the information included in the rapid decrease of MCF after 1992.

The abundance and seasonal cycle of the two alkanes, ethane and propane, is somewhat underestimated in the Northern Hemisphere (NH), especially over the North America, which must be connected to the heavy weighting of the emission data set (*Olivier et al.* (1996)) towards the Eurasian continent. In the SH only propane appears to be underestimated, while ethane is in agreement with surface and column observations. The abundance of the alkenes show reasonable agreement, but measurements over oceans (even when discarding canister sample measurements) were mostly higher than the model. Since we have used an upper limit estimate of the emission strength (from *Plass-Dülmer et al.* (1995)) this points towards a lack of understanding of the processes governing the sea-to-air flux of these substances from the ocean. This can also be said about the role of oceans for several oxygenated species (see below).

The comparison of point measurements of short lived species such as isoprene (2-methyl-1,3-butadiene) with results have to be seen with caution. Nevertheless, it is argued that the several-fold overestimation of the model over the Amazon rainforest points either towards a major overestimate of the emission strength from this ecosystem or unknown deposition processes are present.

The comparison of the model with NO_2 columns retrieved from the GOME satellite instrument proofed to be particularly fruitful, despite the large uncertainties associated with the comparison. Due to the global coverage of this data set a large number of indications, in fact too numerous to be listed here, of erroneous or consistent emission data could be pointed out. Among the encouraging results are consistent seasonal cycles and magnitudes of biomass burning in Africa and South America (though with some local exceptions) and in western Europe. Deviations include too large industrial emissions in parts of eastern Europe, too high lightning NO_x production over the Amazon during the wet season and over Indonesia, and an underestimation of the biomass burning plume in the south-east Atlantic. The latter could be another indication of a missing process that converts HNO_3 to NO_x and could be connected to the underestimate of O_3 during the burning season in that region.

Another interesting point found in the comparison is that aircraft emissions and possibly ship emissions over the North Atlantic in winter appear to be too long lived or too large in the model. Too long a lifetime of NO_x would be consistent with studies of plume-processing in aircraft plumes (*Meijer et al.* (1997)) and would mean that the influence of aircraft NO_x emissions (and potentially also ship-NO_x emissions) would be overestimated in large scale models. The GOME data in conjunction with 3D model results provide the first large scale observational support for this hypothesis.

The comparison to air-borne and surface measurements of nitrogen species revealed a general tendency of the model to overestimate PAN (peroxy-acetyl nitrate) and underestimate HNO_3 in remote regions. Near the pollution sources, however, the model results were mostly consistent with the observations. It is argued that HNO_3 can be easily brought in agreement with observation, by modifying the wet scavenging parameterisation, which is likely too efficient. A heterogeneous conversion, as hypothesised by some authors does not seem necessary for a good simulation of this compound, however, it could help explain problems with too low upper tropo-

spheric NO levels in the model.

A test simulation was performed to assess the effects of HNO_3 uptake on ice particles. It could be shown that allowing for efficient uptake significantly improves the agreement with observations in the upper troposphere. Together with a proposed conversion of HNO_3 to NO_x, via photolysis of the nitrate ion (NO_3^-) on ice surfaces (*Honrath et al.* (2000a)), this would consistently improve the simulation of both compounds (NO and HNO_3). The fact that the overestimate of HNO_3 in the run without uptake on ice and the underestimate of NO often coincide, lends support for this conversion process. However, more quantitative model and laboratory studies are needed to arrive at firmer conclusions.

Several factors that can affect the formation of PAN have been identified in this work. These include, the isoprene emission strength, convection, loss of intermediates in the oxidation of isoprene, the thermal equilibrium rate constants and the availability of NO_x in and above the production regions of the PAN precursor radical (CH_3CO_3). For the latter factor the interaction of isoprene oxidation products and lightning NO_x were especially found to be effective in producing PAN. Furthermore, sub-grid chemistry near the NO_x source could have an effect on the partitioning of nitrogen species.

The knowledge on sources and sinks for some oxygenated species appears to be incomplete. While for the peroxides H_2O_2 and CH_3OOH the agreement was mostly good, the simulation of formaldehyde gave mixed results. Acetone is mostly underestimated despite the relatively high terrestrial biogenic emissions (40 Tg/yr) applied in this work. The existence of widespread, likely oceanic, sources of acetone proposed by *Singh et al.* (2001) are therefore supported by these results. Similar results were found for acetaldehyde, which is underestimated over the rainforest in Surinam and over the remote Pacific. Additional sources are clearly needed for this compound.

The simulation of methanol and acetic acid yielded reasonable agreement with observations, though an additional oceanic source would improve the results. For acetic acid the interpretation is unclear, because this compound may also be affected by the overestimate in PAN. In the case of formic acid a clear need for additional sources was found.

The budget and distribution of tropospheric ozone was examined in detail. The upper troposphere (above about 400 hPa) and the continental boundary layer have been identified as the main regions of photochemical production of ozone, whereas net loss occurs mainly in the marine lower troposphere (below 400 hPa). The magnitude of the corresponding net terms in the production and loss regions (about +1400 Tg(O_3)/yr and –1100 Tg(O_3)/yr) compared to the net stratospheric influx (about +600 Tg/yr) and deposition to the ground (–700-800 Tg/yr) demonstrate the importance of photochemistry for the abundance and distribution of ozone in the troposphere. The production in the upper troposphere was actually of the same magnitude as the stratospheric influx, thus doubling the net import of ozone into the lower troposphere.

The gross production and loss terms (each calculated to be about 4200 Tg/yr) have been found to be less meaningful since they are largely coupled to each other. Focus in future studies should therefore be on the results for the net tendencies. Considering that identical emissions and chemistry were used, the difference between results from the high ($1.9° \times 1.9°$) and low resolution ($5.6° \times 5.6°$) simulation for the net photochemical production of ozone in the troposphere (+280 Tg/yr and +80 Tg/yr, respectively) indicate that this number is still quite uncertain.

The agreement between surface observations and the model was relatively good agreement, mostly within ±10 nmol/mol or better. In the northern extra-tropical upper troposphere too high ozone values are calculated in winter/spring. With the aid of a stratospheric ozone tracer and

the use of an alternative meteorological data set it was shown that this problem can be largely attributed to the stratosphere-troposphere exchange implied by the standard meteorological data employed (NCEP, *Kalnay et al.* (1996)). In summer over polluted regions (mid troposphere), on the other hand, the model is too low in ozone by 10-20 nmol/mol. The results from the sensitivity runs with different chemical mechanisms have shown, that this is not easily explained by missing or erroneous chemistry, and thus dynamical factors (e.g. detrainment rates) are probably also involved.

The few observations from tropical ozone sounding stations indicate that the model is underestimating ozone in the tropical mid troposphere, especially during the burning season. These results, however, need reconfirmation with a statistically more valid data set. Comparison with vertical ozone profiles revealed that the location of the chemical tropopause is sometimes not correctly simulated, which is probably due to the meteorological input data or their treatment in the model. The determination of vertical velocities in chemical tracer models is suspected to be a crucial issue for a good simulation of tracers with large gradients in the tropopause region.

The influence of non-methane volatile organic compounds (NMVOC) on global tropospheric chemistry and specifically the influence of isoprene was further studied with the model. It could be shown that the inclusion of NMVOC in the model significantly changes the distributions of several key species. Ozone levels are enhanced by 20-35% on the zonal mean and even more at specific locations, such as in the polluted boundary layer. The result including NMVOC are in much better agreement with observations than the model version without their consideration. CO levels are also higher in the NMVOC simulation by about 15-30%, but this only improves the agreement in the NH. In the SH extra-tropics it increases the overestimate, which shows that other factors than the source of CO from NMVOC (mainly isoprene) must play a role.

The distribution of NO_x is changed significantly when NMVOC are taken into account, mainly due to the formation and long-range transport of PAN. The result is less NO_x over polluted regions and an enhancement in the mid and lower troposphere of remote regions, where PAN decomposes. The comparison with observation does not significantly improvement, which shows that other e.g. physical/meteorological factors, such as wet scavenging rates and potential heterogeneous processes also play a role. While OH is strongly depleted in source regions of isoprene, it is enhanced due to the increased NO_x levels in remote regions. Higher CO concentrations also tends to result in lower OH, but the overall global average effect is found to be small. Isoprene alone caused about half of the effects of all hydrocarbons considered, and was therefore examined further.

A sensitivity study of the treatment of isoprene and related parameters was conducted with the model. The sensitivity to different chemical oxidation schemes, changes in emissions strengths, the treatment of nitrates from isoprene and deposition of intermediates was studied. It was shown that the differences from exchanging the isoprene oxidation scheme were largest among the tested scenarios with respect to ozone. The largest differences in the formation of PAN were found when the isoprene emission strength was reduced by 50% or in tests with increased or decreased efficiency of the deposition of intermediates. Overall, the uncertainty in predicting the effect of uncertainties associated with isoprene on the global ozone burden was on the order of 30%, or 5% of the total burden. Considering also the large local deviations found it is judged that this can only be seen as a first order estimate at present.

6.2 Outlook

From the experiences collected based on the interplay of observations and model calculations a number of interesting studies can be proposed that may help to reduce the discrepancies or uncertainties found in this study.

Two main regions of the atmosphere deserve special focus in future research: the upper troposphere and the polluted boundary layer. In the upper troposphere the understanding of dynamical processes appears to be incomplete and their treatment in large scale Eulerian model oversimplified. It was shown that in this region also a large amounts of ozone are produced, which are radiatively most effective at these altitudes. The polluted boundary layer is also important, because many processes are initiated near the sources, e.g. partitioning of NO_y species or production of ozone. When anthropogenic emissions of ozone precursors increase, this will be the region where the largest effects are probably found and where human health and plants can be affected. In these two regions also the largest increase in ozone was predicted by several models, including MATCH (*IPCC* (2001)), for the end of the century. As mentioned above, it is suspected that in those regions also the largest absolute uncertainties are associated with the prediction.

Several key aspects in modeling atmospheric chemistry are also closely linked to the two regions. Convection as a link between the regions and as a sub-grid process should be further studied. Closely linked to convective activity are the processes of wet scavenging, which was found to be a key player in determining the lifetime of NO_y in the atmosphere, and lightning. The distribution and magnitude of lightning NO emissions is probably the most uncertain term among the emissions of NO_x to the atmosphere, and since only about 20% of the surface emissions of NO_x leave the boundary layer (as NO_y) this free tropospheric source can be even more important. The use of satellite data (OTD, LIS, GOME) in connection with case studies with a global or a regional model should help to improve our understanding of these processes. The interaction of lightning NO with non-methane hydrocarbons will also be an interesting field for further studies.

In the case of isoprene, several key areas of uncertainties have been pointed out. A major problem is still the disagreement between emission estimates and modeled concentrations on the one hand, and observations in the tropics on the other hand. Some indications on deposition processes have been observed, but the information is insufficient to explain or even quantify the importance in the tropical rainforests. Thus, it is concluded that the overestimate of isoprene in tropical ecosystems remains an unsolved problem, which requires further research. Better kinetic data on the oxidation products are needed to reduce uncertainties associated with the soluble intermediates and nitrates formed. Controlled laboratory experiments with atmospherically relevant NO_x concentrations would be clearly valuable. Deposition properties and information on processes potentially occurring on aerosol surfaces would also be helpful, but are certainly difficult to obtain.

Testing more complex chemistry schemes including interesting groups of compounds such as terpenes, aromatics or halogens appears to be feasible in terms of computer requirements (at least for low resolution simulations) and can provide additional informations on a number of current research questions. Employing the flexible integration technique used in this study should facilitate these tasks enormously.

An advantage of an offline model such as MATCH has actually not been exploited in this study: Using the meteorology of the actual time of the measurement can significantly reduce the

uncertainties, which are associated with the approach to use an arbitrary year for the evaluation of measurement campaigns which have taken place during the last 10 years or so. A long-term integration of the last decade, which writes out the necessary information for each campaign that falls within the time span, would provide a wealth of information of high quality to be analysed.

In several instances the neglect of sub-grid chemical processes was suspected to have a significant influence on the modeled results. There should be continuing efforts to find efficient ways to include these into large-scale models. In doing so attention should not only be given to ozone production, but also to the lifetime and partitioning of nitrogen species.

The model MATCH can be used in several ways to clarify some open question which were encountered during this study. The use of different meteorological input data sets is recommended, since it can help to differentiate between primarily chemical and dynamical errors in the model. After the encouraging results from the comparison to GOME NO_2 data, the use of satellite data should be expanded. More detailled regional studies, improvements in the methodology of the comparison and the evaluation of data for other substances (HCHO, O_3, CO), which are either already available or will be in the near future, are clearly promising projects. The tropical tropospheric ozone (TTO) product from the TOMS instrument is another interesting data set, which could help to analyse and improve the model performance in the tropics. In order to confirm the tendency of MATCH in the tropics to underestimate ozone, comparison with ozone soundings from the recent SHADOZ[2] program should be performed.

Overall, it can be said that the multitude of data available or soon available hold promise to give many new insights into the chemical and dynamical processes of the atmosphere that surrounds us and will help to continually improve atmospheric models and their ability to predict future developments.

---

[2]Southern Hemisphere ADditional OZonesondes

Appendix A

Details on the Chemical Module

A.1 Reactions included in the Chemical Scheme

The following table lists all gas phase reactions considered in the standard simulation with MATCH. For some complex reaction rate expressions only references to the cited literature are given for brevity here. M denotes air molecules. For a list of all transported species see Table 2.1 in Chapter 2.3.1.

Table A.1: Chemical Reactions considered in the standard simulation.

No.	Reaction	Rate	Ref.,Notes
R1	$O_3 + h\nu \longrightarrow O(^1D) + O_2$	J_1	L+C98, 1
R2	$O(^1D) + O_2 (\longrightarrow O(^3P) + O_2^*) \xrightarrow{O_2} O_3 (+O_2^*)$	$k_2 = 3.2 \cdot 10^{-11}\exp(70/T)$	JPL97
R3	$O(^1D) + N_2 (\longrightarrow O(^3P) + N_2^*) \xrightarrow{O_2} O_3 (+N_2^*)$	$k_3 = 1.8 \cdot 10^{-11}\exp(110/T)$	JPL97
R4	$O(^1D) + H_2O \longrightarrow 2\ OH$	$k_4 = 2.2 \cdot 10^{-10}$	JPL97
R5	$O_2 + h\nu (\longrightarrow 2\ O(^3P)) \xrightarrow{2O_2} 2\ O_3$	J_2	L+C98
R6	$O_3 + OH \longrightarrow HO_2 + O_2$	$k_6 = 1.5 \cdot 10^{-12}\exp(-880/T)$	JPL00
R7	$O_3 + HO_2 \longrightarrow OH + 2\ O_2$	$k_7 = 2.0 \cdot 10^{-14}\exp(-680/T)$	JPL00
R8	$HO_2 + OH \longrightarrow H_2O + O_2$	$k_8 = 4.8 \cdot 10^{-11}\exp(250/T)$	JPL00
R9	$HO_2 + HO_2 \longrightarrow H_2O_2 + O_2$	$k_9=$complex$,f(T,[M],[H_2O])$	JPL97
R10	$H_2O_2 + h\nu \longrightarrow 2\ OH$	J_3	L+C98
R11	$OH + H_2O_2 \longrightarrow HO_2 + H_2O$	$k_{11} = 2.9 \cdot 10^{-12}\exp(-160/T)$	JPL97, 1
R12	$OH + CO \longrightarrow HO_2 + CO_2$	$k_{12} = 1.5 \cdot 10^{-13}(1 + 0.6 \cdot P_{atm})$	JPL97, 1
R13	$CH_4 + OH \longrightarrow CH_3O_2 + H_2O$	$k_{13} = 2.8 \cdot 10^{-14}T^{0.667}\exp(-1575/T)$	JPL97
R14	$CH_3O_2 + HO_2 \longrightarrow CH_3O_2H + O_2$	$k_{14} = 4.15 \cdot 10^{-13}\exp(750/T)$	Tyn00
R15	$CH_3O_2 + NO \longrightarrow HCHO + HO_2 + NO_2$	$k_{15} = 2.8 \cdot 10^{-12}\exp(300/T)$	Tyn00
R16	$CH_3O_2 + CH_3O_2 \longrightarrow 2\ HCHO + 2\ HO_2$	$k_{16}=9.5 \cdot 10^{-14}\exp(390/T) /(1+1/(26.2\cdot\exp(-1130/T)))$	Tyn00
R17	$CH_3O_2 + CH_3O_2 \longrightarrow HCHO + CH_3OH$	$k_{17}=9.5 \cdot 10^{-14}\exp(390/T) /(1+26.2\cdot\exp(-1130/T))$	Tyn00
R18	$CH_3O_2 + NO_3 \longrightarrow HCHO + HO_2 + NO_2$	$k_{18} = 1.3 \cdot 10^{-12}$	Atk99
R19	$CH_3O_2H + h\nu \longrightarrow HCHO + HO_2 + OH$	J_4	L+C98
R20	$CH_3O_2H + OH \longrightarrow 0.7\ CH_3O_2 + 0.3\ HCHO + 0.3\ OH + H_2O$	$k_{20} = 3.8 \cdot 10^{-12}\exp(200/T)$	JPL97

Table A.1 continued

No.	Reaction	Rate	Ref.,Notes
R21	HCHO + $h\nu$ $\xrightarrow{2O_2}$ CO + 2 HO$_2$	J_5	L+C98
R22	HCHO + $h\nu$ $\longrightarrow$ CO + H$_2$	J_6	L+C98, 1
R23	HCHO + OH $\longrightarrow$ CO + HO$_2$ + H$_2$O	$k_{23} = 1.0 \cdot 10^{-11}$	JPL97
R24	HCHO + NO$_3$ $\longrightarrow$ HNO$_3$ + CO + HO$_2$	$k_{24} = 3.4 \cdot 10^{-13}$exp(-1900/T)	JPL97
R25	NO + O$_3$ $\longrightarrow$ NO$_2$ +O$_2$	$k_{25} = 3.0 \cdot 10^{-12}$exp(-1500/T)	JPL00
R26	NO + HO$_2$ $\longrightarrow$ NO$_2$ + OH	$k_{26} = 3.5 \cdot 10^{-12}$exp(250/T)	JPL97
R27	NO$_2$ + $h\nu$ $\xrightarrow{O_2}$ NO + O$_3$	J_7	L+C98
R28	NO$_2$ + O$_3$ $\longrightarrow$ NO$_3$	$k_{28} = 1.2 \cdot 10^{-13}$exp(-2450/T)	JPL97
R29	NO$_2$ + OH + M $\longrightarrow$ HNO$_3$ + M	k_{29} = complex	Dra99
R30	NO$_2$ + HO$_2$ + M $\longrightarrow$ HNO$_4$ + M	k_{30} = complex	JPL97
R31	HNO$_3$ + $h\nu$ $\longrightarrow$ OH + NO$_2$	J_8	L+C98
R32	OH + HNO$_3$ + M $\longrightarrow$ NO$_3$ + H$_2$O + M	k_{32} = complex	JPL00
R33	NO$_3$ + $h\nu$ +O$_2$ $\longrightarrow$ NO$_2$ + O$_3$	J_9	L+C98
R34	NO$_3$ + $h\nu$ $\longrightarrow$ NO	J_{10}	L+C98
R35	NO$_3$ + NO $\longrightarrow$ 2 NO$_2$	$k_{35} = 1.5 \cdot 10^{-11}$exp(170/T)	JPL97
R36	NO$_3$ + NO$_2$ + M $\longrightarrow$ N$_2$O$_5$ + M	k_{36} = complex	JPL00
R37	N$_2$O$_5$ + $h\nu$ $\longrightarrow$ NO$_3$ + NO$_2$	J_{11}	L+C98
R38	NO$_3$ + HO$_2$ $\longrightarrow$ 0.8 NO$_2$ + 0.8 OH + 0.2 HNO$_3$	$k_{38} = 3.5 \cdot 10^{-12}$	JPL97
R39	N$_2$O$_5$ + M $\longrightarrow$ NO$_3$ + NO$_2$ + M	$k_{39} = k_{36}/(3.0 \cdot 10^{-27}$ exp(10991/T))	JPL00
R40	N$_2$O$_5$ + H$_2$O $\longrightarrow$ 2 HNO$_3$	k_{40}=2.5·10^{-22}+[H$_2$O]1.8·10^{-39}	Wah98
R41	HNO$_4$ + $h\nu$ $\longrightarrow$ 0.39 NO$_3$ + 0.39 OH + 0.61 NO$_2$ + 0.61 HO$_2$	J_{12}	L+C98,Atk97
R42	HNO$_4$ + M $\longrightarrow$ HO$_2$ + NO$_2$ + M	k_{42}=k_{30}/(2.1·10^{-27}exp(10900/T))	JPL97
R43	HNO$_4$ + OH $\longrightarrow$ NO$_2$ + H$_2$O + O$_2$	$k_{43} = 1.3 \cdot 10^{-12}$exp(380/T)	JPL97
R44	H$_2$ + OH $\longrightarrow$ HO$_2$ + H$_2$O	$k_{44} = 5.5 \cdot 10^{-12}$exp(-2000/T)	JPL97
R45	CH$_3$OH + OH $\longrightarrow$ HCHO + HO$_2$	$k_{45} = 6.7 \cdot 10^{-12}$exp(-600/T)	JPL97
R46	C$_5$H$_8$ + OH $\longrightarrow$ ISO$_2$	$k_{46} = 2.54 \cdot 10^{-11}$exp(410/T)	Poe00
R47	C$_5$H$_8$ + NO$_3$ $\longrightarrow$ ISON	$k_{47} = 3.03 \cdot 10^{-12}$exp(-446/T)	Poe00
R48	C$_5$H$_8$ + O$_3$ $\longrightarrow$ 0.28 HCOOH + 0.65 MACR + 0.1 MACRO$_2$ + 0.1 CH$_3$CO$_3$ + 0.14 CO + 0.58 HCHO + 0.09 H$_2$O$_2$ + 0.08 CH$_3$O$_2$ + 0.25 OH + 0.25 HO$_2$ + 0.22 CO$_2$	$k_{48} = 7.86 \cdot 10^{-15}$exp(-1913/T)	Poe00
R49	ISO$_2$ + HO$_2$ $\longrightarrow$ ISO$_2$H	$k_{49} = 2.05 \cdot 10^{-13}$exp(1300/T)	Poe00
R50	ISO$_2$ + NO $\longrightarrow$ 0.956 NO$_2$ + 0.956 MACR + 0.956 HCHO + 0.956 HO$_2$ + 0.044 ISON	$k_{50} = 2.54 \cdot 10^{-12}$exp(360/T)	Poe00
R51	ISO$_2$ + ISO$_2$ $\longrightarrow$ 2 MACR + HCHO + HO$_2$ + CO$_2$	$k_{51} = 2.0 \cdot 10^{-12}$	Poe00
R52	ISO$_2$ + CH$_3$O$_2$ $\longrightarrow$ 0.5 MACR + 1.25 HCHO + HO$_2$ + 0.25 MGLY + 0.25 HACET + 0.25 CH$_3$OH	$k_{52} = 2.0 \cdot 10^{-12}$	RvK01
R53	ISO$_2$H + $h\nu$ $\longrightarrow$ MACR + HCHO + HO$_2$ + OH	$J_{13} = J_4$	as CH$_3$O$_2$H
R54	ISO$_2$H + OH $\longrightarrow$ MACR + OH + CO$_2$	$k_{54} = 1.0 \cdot 10^{-10}$	Poe00
R55	MACR + OH $\longrightarrow$ MACRO$_2$	k_{55}=0.5(4.1 $\cdot$ 10^{-12}exp(452/T) +1.9·10^{-11}exp(175/T))	Poe00

Table A.1 continued

No.	Reaction	Rate	Ref.,Notes
R56	$MACR + h\nu \longrightarrow CH_3CO_3 + HCHO + CO + HO_2 + 0.125\ CO_2$	$J_{14} = 0.5(0.037 \cdot J_6 + 0.031 \cdot J_{19})$	RvK01
R57	$MACR + O_3 \longrightarrow 0.45\ HCOOH + 0.9\ MGLY + 0.1\ CH_3CO_3 + 0.19\ OH + 0.22\ CO + 0.32\ HO_2 + 0.15\ CO_2$	$k_{57}=0.5(1.4 \cdot 10^{-15}\exp(-2112/T)+7.5 \cdot 10^{-16}\exp(-1521/T))$	Poe00
R58	$MACRO_2 + NO \longrightarrow NO_2 + 0.25\ CH_3CO_3 + 0.25\ HACET + 0.75\ HCHO + 0.25\ CO + 0.75\ HO_2 + 0.5\ MGLY + 0.125\ CO_2$	$k_{58} = 2.54 \cdot 10^{-12}\exp(360/T)$	Poe00
R59	$MACRO_2 + HO_2 \longrightarrow MACRO_2H$	$k_{59} = 1.82 \cdot 10^{-13}\exp(1300/T)$	Poe00
R60	$MACRO_2H + h\nu \longrightarrow OH + 0.5\ CH_3COCHO + 0.25\ CH_3COCH_2OH + 0.75\ HCHO + 0.75\ HO_2 + 0.25\ CH_3CO_3 + 0.25\ CO + 0.22\ CO_2$	$J_{15} = J_4$	as CH_3O_2H
R61	$MACRO_2H + OH \longrightarrow MACRO_2$	$k_{61} = 3 \cdot 10^{-11}$	Poe00
R62	$MACRO_2 + NO_2 + M \longrightarrow MPAN + M$	$k_{62} = $ complex	Poe00
R63	$MACRO_2 + MACRO_2 \longrightarrow HACET + MGLY + 0.5\ CO + 0.5\ HCHO + HO_2 + CO_2$	$k_{63} = 2.0 \cdot 10^{-12}$	Poe00
R64	$MACRO_2 + CH_3O_2 \longrightarrow 0.5\ MGLY + 0.375\ HACET + 0.125\ CH_3CO_3 + 1.125\ HCHO + 0.875\ HO_2 + 0.125\ CO + 0.25\ CH_3OH$	$k_{64} = 2.0 \cdot 10^{-12}$	RvK01
R65	$ISON + OH \longrightarrow HACET + NALD$	$k_{65} = 1.3 \cdot 10^{-11}$	Poe00
R66	$ISON + h\nu \longrightarrow MACR + HCHO + NO_2 + HO_2$	$J_{16} = J_{26}$	RvK01
R67	$MPAN + OH \longrightarrow HACET + NO_2 + CO_2$	$k_{67} = 3.6 \cdot 10^{-12}$	Poe00
R68	$MPAN + M \longrightarrow MACRO_2 + NO_2 + M$	$k_{68} = k_{86}$	Poe00
R69	$MPAN + h\nu \longrightarrow CH_3COCH_2OH + NO_2 + CO_2$	$J_{16} = J_{22}$	Poe00
R70	$NALD + OH \longrightarrow NO_2 + HCHO + CO$	$k_{70} = 5.6 \cdot 10^{-12}\exp(270/T)$	Poe00
R71	$NALD + h\nu \longrightarrow NO_2 + HCHO + CO$	$J_{17} = J_{23}$	Poe00
R72	$HACET + OH \longrightarrow MGLY + HO_2$	$k_{72} = 3.0 \cdot 10^{-12}$	Atk99
R73	$HACET + OH \longrightarrow MGLY + HO_2$	$J_{18} = 0.11 \cdot J_5$	RvK01
R74	$MGLY + OH \longrightarrow CH_3CO_3 + CO$	$k_{74} = 8.4 \cdot 10^{-13}\exp(830/T)$	Tyn95
R75	$MGLY + h\nu \longrightarrow CH_3CO_3 + CO + HO_2$	J_{19}	RvK01,L+C98
R76	$CH_3CO_3 + HO_2 \longrightarrow CH_3CO_3H$	$k_{76} = 4.3 \cdot 10^{-13}\exp(1040/T)/(1+1/(37 \cdot \exp(-660/T)))$	Tyn00
R77	$CH_3CO_3 + HO_2 \longrightarrow CH_3COOH + O_3$	$k_{77} = 4.3 \cdot 10^{-13}\exp(1040/T)/(1+37 \cdot \exp(-660/T))$	Tyn00
R78	$CH_3CO_3 + NO \longrightarrow CH_3O_2 + NO_2 + CO_2$	$k_{78} = 8.1 \cdot 10^{-12}\exp(270/T)$	Tyn00
R79	$CH_3CO_3 + NO_2 \longrightarrow PAN$	$k_{78} = $ complex	Tyn00
R80	$CH_3CO_3 + CH_3O_2 \longrightarrow HCHO + HO_2 + CH_3O_2 + CO_2$	$k_{80} = 2.0 \cdot 10^{-12}\exp(500/T)/(1+1/(2.2 \cdot 10^6\ \exp(3820/T)))$	Tyn00,JPL97
R81	$CH_3CO_3 + CH_3O_2 \longrightarrow CH_3COOH + HCHO + CO_2$	$k_{80} = 2.0 \cdot 10^{-12}\exp(500/T)/(1+2.2 \cdot 10^6\ \exp(-3820/T))$	Tyn00,JPL97
R82	$CH_3CO_3 + CH_3CO_3 \longrightarrow 2\ CH_3O_2 + 2\ CO_2 + O_2$	$k_{82} = 2.5 \cdot 10^{-12}\exp(500/T)$	Tyn00
R83	$CH_3CO_3 + NO_3 \longrightarrow CH_3O_2 + NO_2 + CO_2$	$k_{83} = 4 \cdot 10^{-12}$	Can96
R84	$CH_3CO_3H + h\nu \longrightarrow CH_3O_2 + OH$	$J_{20} = 0.025 \cdot J_5$	RvK01
R85	$CH_3CO_3H + OH \longrightarrow CH_3CO_3$	$k_{85} = k_{20}$	as CH_3O_2H
R86	$CH_3COCH_2OH + h\nu \longrightarrow CH_3CO_3 + HCHO + HO_2$	$J_{21} = 0.11 \cdot J_5$	RvK01

Table A.1 continued

No.	Reaction	Rate	Ref.,Notes
R87	PAN + M $\longrightarrow$ CH$_3$CO$_3$ + NO$_2$	$k_{87} = k_{79}/(9\cdot10^{-29}\exp(-14000/T)$	JPL97
R88	PAN + $h\nu$ $\longrightarrow$ CH$_3$CO$_3$ + NO$_2$	J_{22}	RvK01,L+C98
R89	PAN + OH $\longrightarrow$ HCHO + NO$_2$ + CO$_2$	$k_{89} = 2\cdot10^{-14}$	JPL97, 2
R90	CH$_3$COOH + OH $\longrightarrow$ CH$_3$O$_2$ + CO$_2$	$k_{90} = 4\cdot10^{-13}\exp(200/T)$	JPL97
R91	HCOOH + OH $\longrightarrow$ HO$_2$ + CO$_2$	$k_{91} = 4\cdot10^{-13}$	JPL97
R92	C$_2$H$_6$ + OH $\longrightarrow$ C$_2$H$_5$O$_2$ + H$_2$O	$k_{92} = 8.7\cdot10^{-12}\exp(-1070/T)$	JPL97
R93	C$_2$H$_5$O$_2$ + HO$_2$ $\longrightarrow$ C$_2$H$_5$O$_2$H	$k_{93} = 7.4\cdot10^{-13}\exp(700/T)$	Tyn00
R94	C$_2$H$_5$O$_2$ + CH$_3$O$_2$ $\longrightarrow$ 0.76 HCHO + 1.04 HO$_2$ + 0.76 CH$_3$CHO + 0.24 CH$_3$OH	$k_{94} = 1.18\cdot10^{-13}\exp(158/T)$	V+L96,K+S96
R95	C$_2$H$_5$O$_2$ + CH$_3$CO$_3$ $\longrightarrow$ 0.82 CH$_3$O$_2$ + CH$_3$CHO + 0.82 HO$_2$ + 0.18 CH$_3$COOH	$k_{95} = 4.9\cdot10^{-12}\exp(211/T)$	Atk99,K+S96
R96	C$_2$H$_5$O$_2$ + NO $\longrightarrow$ CH$_3$CHO + HO$_2$ + NO$_2$	$k_{96} = 2.7\cdot10^{-12}\exp(350/T)$	Tyn00
R97	C$_2$H$_5$O$_2$ + NO$_3$ $\longrightarrow$ CH$_3$CHO + HO$_2$ + NO$_2$	$k_{97} = 2.3\cdot10^{-12}$	Atk99
R98	CH$_3$CHO + OH $\longrightarrow$ CH$_3$CO$_3$ + H$_2$O	$k_{98} = 5.6\cdot10^{-12}\exp(270/T)$	JPL97
R99	CH$_3$CHO + $h\nu$ $\longrightarrow$ CH$_3$O$_2$ + HO$_2$ + CO	$J_{23} = 0.19\cdot J_5$	RvK01
R100	CH$_3$CHO + NO$_3$ $\longrightarrow$ CH$_3$CO$_3$ + HNO$_3$	$k_{100} = 1.4\cdot10^{-12}\exp(-1900/T)$	JPL97
R101	C$_2$H$_5$O$_2$H + OH $\longrightarrow$ 0.3 C$_2$H$_5$O$_2$ + 0.7 CH$_3$CHO + 0.7 OH	$k_{101} = k_{20}$	as CH$_3$O$_2$H
R102	C$_2$H$_5$O$_2$H + $h\nu$ $\longrightarrow$ CH$_3$CHO + HO$_2$ + OH	$J_{24} = J_4$	as CH$_3$O$_2$H
R103	C$_3$H$_8$ + OH $\longrightarrow$ 0.82 C$_3$H$_7$O$_2$ + 0.18 C$_2$H$_5$O$_2$ + H$_2$O	$k_{103} = 1\cdot10^{-11}\exp(-660/T)$	JPL97, 3
R104	C$_3$H$_7$O$_2$ + NO $\longrightarrow$ 0.96 CH$_3$COCH$_3$ + 0.96 HO$_2$ + 0.96 NO$_2$ + 0.04 C$_3$H$_7$ONO$_2$	$k_{104} = 2.7\cdot10^{-12}\exp(360/T)$	Atk99,MCM
R105	C$_3$H$_7$O$_2$ + HO$_2$ $\longrightarrow$ C$_3$H$_7$O$_2$H	$k_{105} = 1.9\cdot10^{-13}\exp(1300/T)$	Atk97
R106	C$_3$H$_7$O$_2$ + CH$_3$O$_2$ $\longrightarrow$ CH$_3$COCH$_3$ + 0.8 HCHO + 0.8 HO$_2$ + 0.2 CH$_3$OH	$k_{106} = 9.46\cdot10^{-14}\exp(431/T)$	K+S96
R107	C$_3$H$_7$O$_2$H + $h\nu$ $\longrightarrow$ CH$_3$COCH$_3$ + HO$_2$ + OH	$J_{25} = J_4$	as CH$_3$O$_2$
R108	C$_3$H$_7$O$_2$H + OH $\longrightarrow$ 0.3 C$_3$H$_7$O$_2$ + 0.7 CH$_3$COCH$_3$ + 0.7 OH	$k_{108} = k_{20}$	as CH$_3$O$_2$H
R109	C$_3$H$_7$ONO$_2$ + OH $\longrightarrow$ CH$_3$COCH$_3$ + NO$_2$	$k_{109} = 6.2\cdot10^{-13}\exp(-230/T)$	Atk99
R110	C$_3$H$_7$ONO$_2$ + $h\nu$ $\longrightarrow$ CH$_3$COCH$_3$ + NO$_2$ + HO$_2$	$J_{26} = 3.7\cdot J_{22}$	RvK01
R111	CH$_3$COCH$_3$ + OH $\longrightarrow$ CH$_3$COCH$_2$O$_2$ + H$_2$O	$k_{111} = 8.8\cdot10^{-12}\exp(-1320/T)$	Wol00
R112	CH$_3$COCH$_3$ + OH $\longrightarrow$ CH$_3$COOH + CH$_3$O$_2$	$k_{112} = 1.7\cdot10^{-14}\exp(423/T)$	Wol00
R113	CH$_3$COCH$_3$ + $h\nu$ $\longrightarrow$ CH$_3$CO$_3$ + CH$_3$O$_2$	J_{27}	RvK01,L+C98
R114	CH$_3$COCH$_2$O$_2$ + NO $\longrightarrow$ NO$_2$ + CH$_3$CO$_3$ + HCHO	$k_{114} = 2.8\cdot10^{-12}\exp(300/T)$	Tyn00
R115	CH$_3$COCH$_2$O$_2$ + HO$_2$ $\longrightarrow$ CH$_3$COCH$_2$O$_2$H	$k_{115} = 8.6\cdot10^{-13}\exp(700/T)$	Tyn00
R116	CH$_3$COCH$_2$O$_2$ + CH$_3$O$_2$ $\longrightarrow$ 0.5 MGLY + 0.5 CH$_3$OH + 0.3 CH$_3$CO$_3$ + 0.8 HCHO + 0.3 HO$_2$ + 0.2 HACET	$k_{116} = 7.5\cdot10^{-13}\exp(500/T)$	Tyn00
R117	CH$_3$COCH$_2$O$_2$H + OH $\longrightarrow$ 0.3 CH$_3$COCH$_2$O$_2$ + 0.7 MGLY + 0.7 OH	$k_{117} = k_{20}$	as CH$_3$O$_2$H
R118	CH$_3$COCH$_2$O$_2$H + $h\nu$ $\longrightarrow$ CH$_3$CO$_3$ + HO$_2$ + OH	J_{28}	as CH$_3$O$_2$H
R119	C$_3$H$_6$ + OH + M $\longrightarrow$ C$_3$H$_6$OHO$_2$ + M	$k_{119} = $ complex	Atk99

Table A.1 continued

No.	Reaction	Rate	Ref.,Notes
R120	$C_3H_6 + O_3 \longrightarrow 0.57\ HCHO + 0.47\ CH_3CHO + 0.33\ OH + 0.26\ HO_2 + 0.07\ CH_3O_2 + 0.06\ C_2H_5O_2 + 0.23\ CH_3CO_3 + 0.04\ MGLY + 0.06\ CH_4 + 0.31\ CO + 0.22\ HCOOH + 0.03\ CH_3OH + 0.13\ CO_2$	$k_{120} = 6.5 \cdot 10^{-15}\exp(-1900/T)$	Z+P99,JPL97
R121	$C_3H_6 + NO_3 \longrightarrow ONIT$	$k_{121} = 4.6 \cdot 10^{-13}\exp(-1155/T)$	RvK01,Atk99
R122	$C_3H_6OHO_2 + NO \longrightarrow 0.98\ CH_3CHO + 0.98\ HCHO + 0.98\ HO_2 + 0.98\ NO_2 + 0.02\ ONIT$	$k_{122} = 4.2 \cdot 10^{-12}\exp(180/T)$	M+B95,MCM
R123	$C_3H_6OHO_2 + HO_2 \longrightarrow C_3H_6OHO_2H$	$k_{123} = 6.5 \cdot 10^{-13}\exp(650/T)$	M+B95
R124	$C_3H_6OHO_2H + OH \longrightarrow 0.5\ C_3H_6O_2 + 0.5\ HACET + 0.5\ OH + H_2O$	$k_{124} = 3.8 \cdot 10^{-12}\exp(200/T)$	M+B95
R125	$C_2H_4 + OH + M \longrightarrow 0.667\ C_3H_6O_2 + M$	$k_{125} = $ complex	M+B95,JPL97
R126	$C_2H_4 + O_3 \longrightarrow HCHO + 0.22\ HO_2 + 0.12\ OH + 0.23\ CO + 0.54\ HCOOH + 0.1\ H_2 + 0.23\ CO_2$	$k_{126} = 1.2 \cdot 10^{-14}\exp(-2630/T)$	Nee98,JPL97
R127	$C_4H_{10} + OH \longrightarrow C_4H_9O_2 + H_2O$	$k_{127} = 9 \cdot 10^{-12}\exp(-395/T)$	Atk99
R128	$C_4H_9O_2 + NO \longrightarrow 0.84\ NO_2 + 0.56\ MEK + 0.56\ HO_2 + 0.28\ C_2H_5O_2 + 0.84\ CH_3CHO + 0.16\ ONIT$	$k_{12} = k_{104}$	Poi00,Z+P99
R129	$C_4H_9O_2 + HO_2 \longrightarrow C_4H_9O_2H$	$k_{129} = k_{105}$	Poi00
R130	$C_4H_9O_2 + CH_3O_2 \longrightarrow 0.88\ MEK + 0.68\ HCHO + 1.23\ HO_2 + 0.12\ CH_3CHO + 0.12\ C_2H_5O_2 + 0.18\ CH_3OH$	$k_{130} = k_{106}$	Poi00
R131	$C_4H_9O_2H + OH \longrightarrow 0.15\ C_4H_9O_2 + 0.85\ MEK + 0.85\ OH + 0.85\ H_2O$	$k_{131} = k_{20}$	Poi00
R132	$C_4H_9O_2H + h\nu \longrightarrow OH + 0.67\ MEK + 0.67\ HO_2 + 0.33\ C_2H_5O_2 + 0.33\ CH_3CHO$	$J_{29} = J_4$	as CH_3O_2H
R133	$MEK + OH \longrightarrow MEKO_2$	$k_{133} = 1.3 \cdot 10^{-12}\exp(-25/T)$	Atk99
R134	$MEK + h\nu \longrightarrow CH_3CO_3 + C_2H_5O_2$	$J_{30} = 0.42 \cdot J_5$	RvK01
R135	$MEKO_2 + NO \longrightarrow 0.985\ CH_3CHO + 0.985\ CH_3CO_3 + 0.985\ NO_2 + 0.015\ ONIT$	$k_{136} = k_{104}$	Poi00,MCM
R136	$MEKO_2 + HO_2 \longrightarrow MEKO_2H$	$k_{137} = k_{105}$	Atk97
R137	$MEKO_2H + OH \longrightarrow 0.8\ CH_3COCOCH_3 + 0.8\ OH + 0.2\ MEKO_2$	$k_{138} = k_{20}$	Poi00
R138	$CH_3COCOCH_3 + h\nu \longrightarrow 2\ CH_3CO_3$	$J_{31} = 2.2 \cdot J_{19}$	RvK01,MCM
R139	$MEKO_2H + h\nu \longrightarrow CH_3CO_3 + CH_3CHO + OH$	$J_{32} = J_4$	as CH_3O_2H
R140	$ONIT + OH \longrightarrow MEK + NO_2 + H_2O$	$k_{140} = 1.7 \cdot 10^{-12}$	Atk99
R141	$ONIT + h\nu \longrightarrow NO_2 + 0.67\ MEK + 0.67\ HO_2 + 0.33\ C_2H_5O_2 + 0.33\ CH_3CHO$	$J_{33} = J_{26}$	RvK01

References: JPL00 is *Sander et al.* (2000), JPL97 is *DeMore et al.* (1997), Tyn00 is *Tyndall et al.* (2001), Poe00 is *Pöschl et al.* (2000b), L+C98 is *Landgraf and Crutzen* (1998), Atk99 is *Atkinson et al.* (1999), Atk97 is *Atkinson et al.* (1997), Dra99 is *Dransfield et al.* (1999), Wah98 is *Wahner et al.* (1998), RvK01: this work (see e.g. Chapter 2.3.2), Tyn95 is *Tyndall et al.* (1995), V+L96 is *Villenave and Lesclaux* (1996), Can96 is *Canosa-Mas et al.* (1996), MCM is *Jenkin et al.* (1997) and *Saunders et al.* (1997a,b), Wol00 is *Wollenhaupt et al.* (2000) and *Wollenhaupt and Crowley* (2000), Z+P99 is *Zaveri and Peters* (1999), M+B95 is *Müller and Brasseur* (1995), Nee98 is *Neeb et al.* (1998), Poi00 is *Poisson et al.* (2000).

Notes:

1: O_2, H_2O, CO_2 and H_2 are not calculated in the chemistry code, but are only listed here for completeness.

2: One half of the maximum rate constant given in *DeMore et al.* (1997) is used.

3: Only formation of secondary peroxyradicals is taken into account. Instead of the primary peroxyradicals ethylperoxyradicals are formed, which effectively parameterizes formation of PPN (peroxypropionyl nitrate) as PAN formation.

A.2   Implementation of the dry deposition scheme

Some additional details on the dry deposition scheme and its implementation in MATCH are given here. Mainly aspects not given in *Ganzeveld and Lelieveld* (1995) and *Ganzeveld et al.* (1998) or those needed to explain differences in the implementation are described here. As mentioned the dry deposition velocity of the gas indexed i is calculated from three main resistances:

$$V_d^i = (R_a + R_b^i + R_c^i)^{-1} \,, \tag{A.1}$$

where R_a is the aerodynamic resistance, R_b^i is the quasi-laminar sublayer resistance, and R_c^i is the total surface resistance of the gas.

The calculation of the aerodynamic resistance is coupled to the boundary layer parameterization in MATCH. As pointed out by *Ganzeveld et al.* (1998), the use of macroscale parameters from the dynamical part of the model can lead to unrealistically high values of the deposition of very soluble substances in mountainous areas. This is the result of a very large surface roughness for momentum (with z_0 being as large as 20m) used in the model to represent the sub-grid scale orographic roughness. This leads to a very low aerodynamic resistance, which is the controlling resistance for highly soluble gases. Therefore over land a local roughness length is used for the calculation of surface albedo instead, based on a preexisting field used for the albedo calculations in MATCH. The friction velocity u_* and the stability parameter (Obukhov-Length) have been corrected to represent this local parameter. Over the oceans, the roughness length and the friction velocity are iteratively calculated from the Charnock relation (*Charnock* (1955)) and assuming neutral conditions, to approximate the wind speed dependence of z_0 and u_*:

$$z_0 = 0.032 \cdot \frac{u_*^2}{g} \quad and \quad u_* = \frac{0.4 \cdot u_h}{\ln(z_r/z_0)} \,,$$

where u_h is the horizontal wind speed at the reference height z_r, for which the heigh of the first model layer's mid point is used.

The quasi-laminar resistance R_b^i only depends on the molecular diffusivity of the trace gas in air (see *Ganzeveld and Lelieveld* (1995) for more details).

For the calculation of the total surface resistance each grid cell is subdivided into fractions corresponding to snow cover, sea ice, ocean, vegetation, wetted surface and bare soil. The total surface resistance for non-vegetated areas is simply the corresponding ground resistance, while for vegetated areas three uptake pathways exist: 1) uptake by the plant stomata, represented by a serial stomatal and mesophyllic resistance, 2) uptake by the waxy surface of the plants (the cuticle) and 3) uptake by the soil, including also an aerodynamic canopy resistance, which represents the turbulent transport of the trace gas through the canopy to the soil.

Thus for vegetated areas:

$$R_c^i = \frac{1}{LAI/r_{leaf} + 1/(r_{can} + r_{soil})}$$

where LAI is the single-side total leaf area index (in m^2 leaf surface per m^2 area surface), r_{can} is the in-canopy resistance according to *Erisman et al.* (1994), and r_{soil} is the soil resistance and r_{leaf} is calculated as

$$r_{leaf} = \frac{1}{1/(r_{stom} + r_{mes}) + 1/r_{cut}}$$

with the stomatal, mesophyllic and cuticular resistance involved. The stomatal resistance depends again on the photosynthetic active radiation (PAR), the LAI, which is used to take into account the extinction of PAR by the canopy, and a water stress factor. The latter is based on the procedure in the global climate model ECHAM (*DKRZ* (1993)) and on monthly mean ECHAM output fields of the soil wetness and the field capacity *(L. Ganzeveld*, pers. comm., 1999). The water stress factor is only in effect in very arid regions and in the dry season of semi-arid regions. The wet skin fraction is also calculated with the procedure as in ECHAM using monthly mean fields of the skin reservoir content, i.e. the amount of water held by the vegetation or soil.

PAR is defined as the total radiation (diffuse and direct) in the wavelength interval 0.4–0.72 μm. It is calculated online in MATCH from the 8th fixed wavelength (580 nm) of the photolysis scheme in the same way as photolysis rates are parameterized by *Landgraf and Crutzen* (1998), except that h/λ (with Planck's constant h and the wavelength λ) is used instead of the cross section of a species, and a polynomial fit is calculated to relate the photon flux at the central wavelength to the integral over the interval, which then gives the PAR in W/m^2. This method ensures a better consistency with the actual meteorology (cloudiness) than using time averaged radiance data. The LAI is derived from the AVHRR (Advanced Very High Resolution Data Radiometer) satellite instrument (*Brown et al.* (1985)) using the algorithm of *Guenther et al.* (1995). The data were additionally limited to values less than 8 in order to be in better agreement with measurements in tropical forests (e.g. *Fan et al.* (1990)). The distribution of the LAI, as kindly provided by *L. Ganzefeld* (pers. comm., 1999), is shown in Figure A.1 for the months January and July.

The resistances for O_3, HNO_3, NO_2 and NO are taken from *Ganzeveld and Lelieveld* (1995). Parameters for SO_2, which is used as a reference for other soluble substances, are from *Ganzeveld et al.* (1998). *Ganzeveld and Lelieveld* (1995) apply a constant soil resistance of 400 s/m for all types of soil throughout the year, which might overestimate O_3 deposition in winter mid-latitudes and underestimate it in summer. For CO, a soil resistance of 2000 s/m and a high mesophyllic resistance is used, which resulted in an annual average deposition rate of 150 Tg(CO)/yr. This is in basic agreement but on the low end of the estimate given in *Moxley and Cape* (1997) (540± 430 Tg/yr) and in good agreement with the study of *Sanhueza et al.* (1998) (115–230 Tg(CO)/yr). Like in *Lawrence et al.* (1999b) uptake of CO, which is mediated by soil bacteria, has been limited to regions where the temperature is above 5°C and the relative humidity is higher than 40% in order to exclude cold tundra and desert soils.

The resistances of other species are calculated from the formulas given by *Wesely* (1989) and *Walmsley and Wesely* (1996), which are based on the effective Henry's law constants and a reactivity factor f_0. The relations are not repeated here, but the reactivity factors used are listed in Table A.2. The same temperature dependent Henry's law constants as in the wet deposition

LAI (Jan.)

LAI (July)
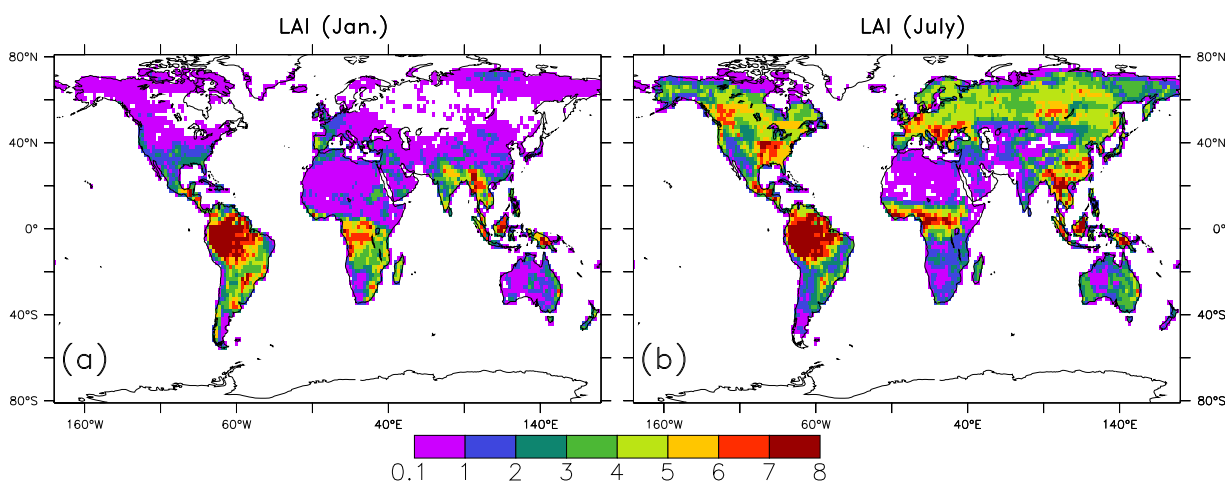
Figure A.1: Leaf area index (LAI) for January and July as used in MATCH calculation of the dry deposition velocities.

Table A.2: Reactivity factors (if larger than zero) used in the relations by *Wesely* (1989) as applied in MATCH. Values after the semicolon are added species compared to *Wesely* (1989).

Reactivity factor f_0	Species
highly reactive, $f_0 = 1$	O_3, H_2O_2; NO_3
slightly reactive, $f_0 = 0.1$	NO_2, CH_3O_2H, CH_3CO_3H, PAN;
	$MPAN$, ISO_2H, $MACRO_2H$, ISON, NALD

scheme are used for consistency (Table 2.4 in Chapter 2.3.4). For ocean surfaces a pH value of 8.1 is assumed in calculating the effective Henry's law constants. The deposition of the NOX-family is calculated separately for each species, instead of applying an averaged deposition velocity. N_2O_5 deposition is assumed to be as effective as that of HNO_3. The Henry's Law constant and the acidity parameter K_A for HNO_4 are taken from *Regimbal and Mozurkewich* (1997). However, due to the fast interaction in this family (especially of NO and NO_2) this is an uncertain point in modeling dry deposition and future studies are needed to arrive at a more accurate representation of NO_x deposition. A minimum value for the surface and aerodynamic resistance of 10 s/m and 5 s/m respectively is applied, which avoids unrealistically high peaks in the deposition of HNO_3 or organic acids under unstable conditions in the planetary boundary layer.

Appendix B

Tests of the Numerics

In this appendix some of the numerical tests are presented which have been performed during this thesis. These tests have been placed in an appendix because the focus of a reasonably developed model should be on the scientific interpretation of the model results. However, it needs to be ensured that basic numerical assumptions or procedures do not interfere with the interpretation. Obviously, in a strict sense such interferences always occur and thus have to be included in the discussion if they appear to be important enough. Here, consequences of some numerical assumptions are investigated, focusing on tests of the chemical integration method (sections B.1 and B.2), which is fairly new to 3D atmospheric modeling and thus needs more thorough evaluation, than other assumptions that have been used by many researcher during the last two or three decades. By testing the method of how the emissions are handled numerically, the issue of operator splitting is also touched upon.

B.1 Box Model Tests of the Chemical Integration Method

In order to test the accuracy of the Rosenbrock solver, which was chosen for this study due to its high performance, numerous box model tests covering different scenarios where conducted. One type of test was between the results of a standard implementation of ROS2 with long time steps and the ROS2 results obtained with a much smaller time step. Note that the update frequency of photolysis rates or emitted species was maintained independend of the time step, because otherwise different results are to be expected. An outer time step (Δt) of 30 minutes and the same reactions as in MATCH (listed in Table A.1) were used for these box model simulations. This procedure assumes that ROS2 converges to the true solution when the time step is decreased to very small values. This is to be expected since ROS2 is a 2nd-order consistent method, which means that the result is an approximation to the true solution to the order $O(\Delta t^2)$. Nevertheless in order to check the correctness of the implementation and coding (also of the kinetic preprocessor KPP), ROS2 with a small step size of around 1 second was compared to results obtained with the commercial program FACSIMILE (*Malleson et al.* (1990)), which is based on the ordinary differential equation solver of *Gear* (1971). The agreement was excellent.

It was found that in general under low and medium NO_x conditions (< 500 nmol/mol), with and without specified sources of NO, the solution using a single (un-split) time step of 30 minutes was sufficient to achieve good agreement with the solution obtained using very small time steps (which will hereafter be called the *exact solution*). This result was also independent

of the amount of NMVOC (e.g. isoprene) used, which do not seem to represent a significant difficulty to the solver. However, when NO_x levels where high and/or a strong NO source was included, the solution with a time step of 30 minutes was inaccurate.

An example is shown in Figure B.1. It can be seen that the ROS2 solution with the sources added externally every 30 minutes (1st order operator splitting, see Section 2.3.3; dash-dotted line), which is also the frequency at which the photolysis rate coefficients are updated, strongly deviates from the "exact" solution (dotted line) in which, the source is added using the same method. The same scenario was also computed specifying the NO source like a first order reaction rate within the solver. This is often referred to as "1st-order source splitting" (e.g. *Verwer et al.* (1998)), which is a splitting method that can also be used for the advective tendencies in the 3D context. Thus, actually two "exact" solutions exist and the difference between the two is the splitting error associated with splitting the source terms from the chemistry integration. When 1st order source splitting is used, the ROS2 solution using a large time step of 30 minutes agrees much better with the corresponding exact solution. The largest errors for this solution occur for the species N_2O_5, NO_3 and HNO_3 which are always underestimated by the operator split single step solution. This might be connected to the fact that ROS2 is a 2-stage solver, i.e. only one intermediate solution is calculated, which probably makes it difficult for the solver to convert the emitted NO all the way through the chain $NO \rightarrow NO_2 \rightarrow NO_3 \rightarrow N_2O_5 \rightarrow HNO_3$ in one time step. A much better agreement is found when the 30-minute time step is split into 2 sub-steps. This method was introduced in Section 2.3.3.

It is noted that the heterogeneous conversion of N_2O_5 to HNO_3 is included in these runs as a pseudo-first order reaction with a rate constant of $9 \cdot 10^{-5}\,s^{-1}$, which is about twice the maximum zonal mean value (northern hemisphere near the surface) given in *Dentener and Crutzen* (1993). When setting this reaction rate to zero the deviations are much smaller (except for NO_3 and N_2O_5 at night), because in that case nearly all NO_3 and N_2O_5 is converted back to NO_x in the morning instead of forming the longer lived HNO_3, and thus the underestimated N_2O_5 during night has less impact on the daytime NO_x concentration. This explanation is also supported by the fact that the overestimation of NO_x in the operator split solution (dash dotted line in Figure B.1) is indeed compensated by an underestimation of HNO_3 (not shown). When no heterogeneous conversion of N_2O_5 is assumed, then one step using source splitting or 2 sub-steps with operator splitting, respectively, are accurate enough for the high NO_x scenario.

The sub-stepping technique greatly improves the results, especially in connection with the source splitting method (Figure B.2). It can be seen that using 2 and 3 sub-steps largely diminishes the deviation from the exact solution. Note also the changed scales for O_3 and NO_x compared to Figure B.1. The solution using 4 sub-steps is indistinguishable from the reference solution.

The actual intervals in the asymmetric sub-stepping can actually be optimized to some degree using a high NO_x scenario where differences are actually visible. This has been done using even higher NO_x conditions and also using perturbation tests, where the NO and NO_2 are multiplied by ten every 2 hours and divided by ten after another 2 hours. The results, which did not follow a strict optimization procedure, are listed in Table 2.3 in Chapter 2.3.3. These extreme and probably unrealistic tests attempt to mimic the situation of a grid box embedded in the 3D global model in the context of operator splitting, when NO_x levels can suddenly change in a grid box because e.g. fresh NO_x plumes are advected into the grid box. These simulations also indicated that 2 sub-steps already gave a very good approximation to the exact solution.
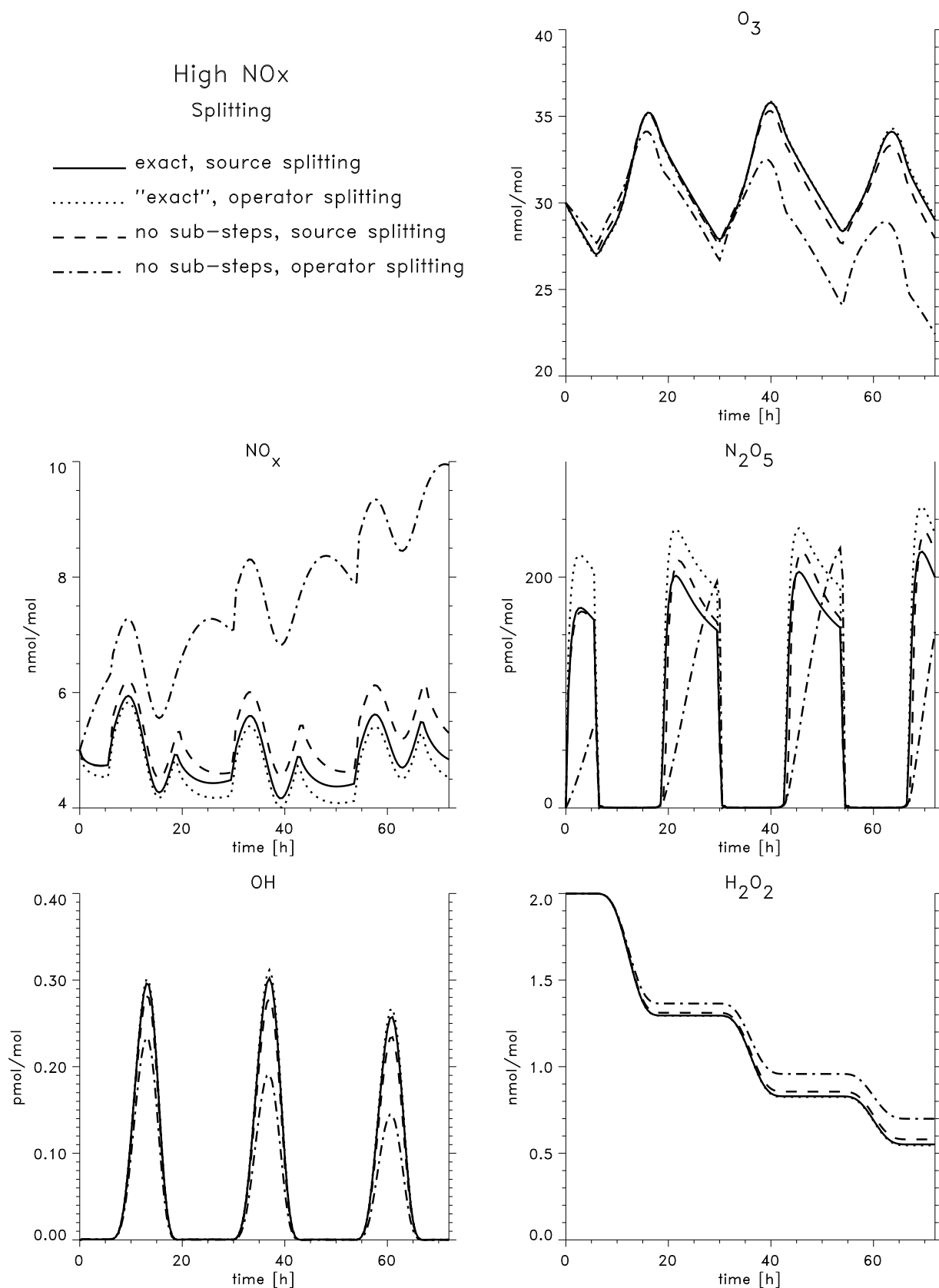
Figure B.1: Boxmodel results for a high NO$_x$ scenario with a strong NO source. Exact solutions here were obtained using a timestep of about a second. See text for explanation of the different splitting techniques.
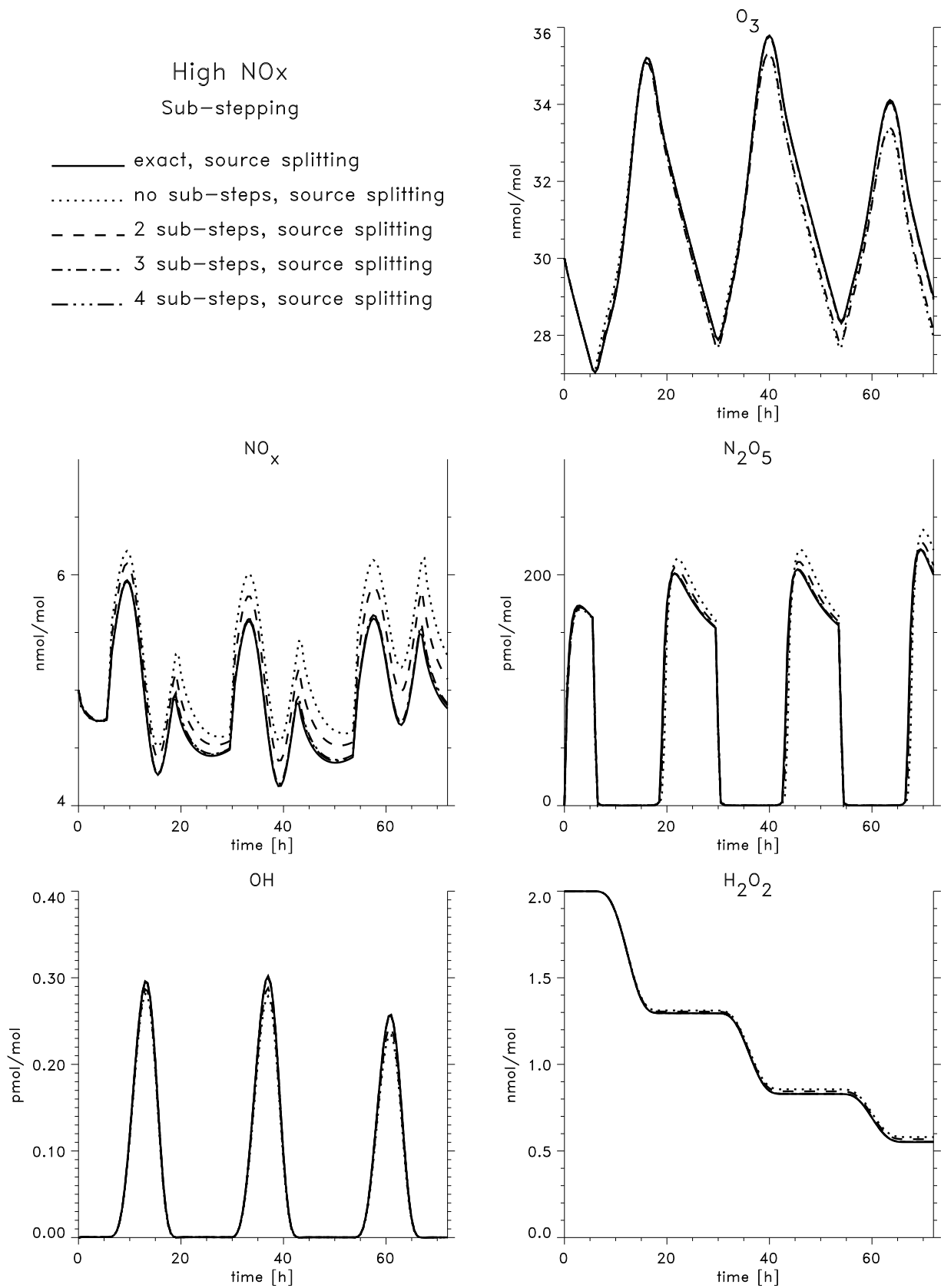
Figure B.2: Solutions using asymmetric sub-stepping calculated for the same scenario as in Figure B.1. All calculation in this plot use the source splitting technique (see text).

From these box model simulation is it concluded that source splitting appears to be advantageous and that additionally using 2 sub-steps (optimally with a ratio of the two sub-steps of about 20/80) appears to be sufficient, given the fact that most tests are probably more vigorous than the actual situation in the 3D model and also considering that such difficult situations may only occur occasionally and at a few locations. However, a profound judgment about whether the accuracy is also sufficient in the 3D application cannot be made on the basis of box model tests, but only in the context of simulations with the 3D implementation of the solver.

B.2   3D Tests of the Chemical Integration Method

As in the boxmodel runs, a solution using ROS2, but with many more sub-steps is used as a reference solution. Four times five sub-steps were used for this purpose. With a general model timestep of 30 minutes this means that for the chemistry the following sequence of 20 time steps is used: 4×9 sec, 4×54 sec, 4×99 sec, 4×135 sec, 4×153 sec. Using 30 subdivisions of the 30 minute time step does not change the concentration of any species by more than 0.01%. This number and most subsequent relative numbers are restricted to regions where appreciable amounts (more than 0.1% of the global maximum) of the species are present. Thus, the 20-step solution can be confidently used as a reference solution.

A comparison run starting in September is performed with the minimum requirement inferred from the box model tests, which is 2 sub-steps in connection with source splitting, i.e. treating the source terms directly within the chemical integration. In these runs only background CH_4-CO-NO_x-HO_x chemistry and isoprene chemistry are included. The relative difference of the 5-day averages compared to the reference solution after a two months simulation is shown in Figure B.3. The figure shows the key species O_3 and NOX (=NO+NO_2+NO_3+2 N_2O_5+HNO_4), along with PAN at 500 hPa, which is important for the long range transport of reactive nitrogen and H_2O_2 because its production depends quadratically on the HO_2 abundance and is thus a good indicator for HO_x. The relative differences are generally quite low, below 1 or 2%. Somewhat higher relative differences for H_2O_2 of up to 4% usually occur in single grid cells and at high latitudes where the absolute concentration are very low (below the 0.1% criterion mentioned above). Comparison with HNO_3 indicates that in these grid cells strong rain events have largely depleted the concentrations of highly soluble gases. Apart from these grid points the difference is mostly lower that 0.1%.

One can judge from this test that already two sub-steps yield sufficient accuracy for the chemistry scheme applied. It has, however, been observed that for a different chemical mechanism the stability properties can vary somewhat. This behavior is already noticeable in boxmodel simulations. It is therefore recommendable to test each mechanism separately. For this thesis a more conservative number of sub-steps have (historically) been used (see Section 2.3.3). It has been found that better results are obtained even if only the source regions of NO_x, which are mainly surface sources, are calculated with more sub-steps. When using 3 sub-steps in the lowest 7 model layers and 5 in the first model layer, which also includes the emissions, for example the error in O_3 shown in Figure B.3 is reduced to less that 0.25% compared to 0.7% using 2 sub-steps uniformly in the whole model domain. A similar error is found when the pair of simulations are repeated using operator splitting for the NO emissions (not shown), which is somewhat surprising in view of the box model tests in the last chapter, where the source split simulations were found to agree more closely with their respective reference simulations. This indicates that the box
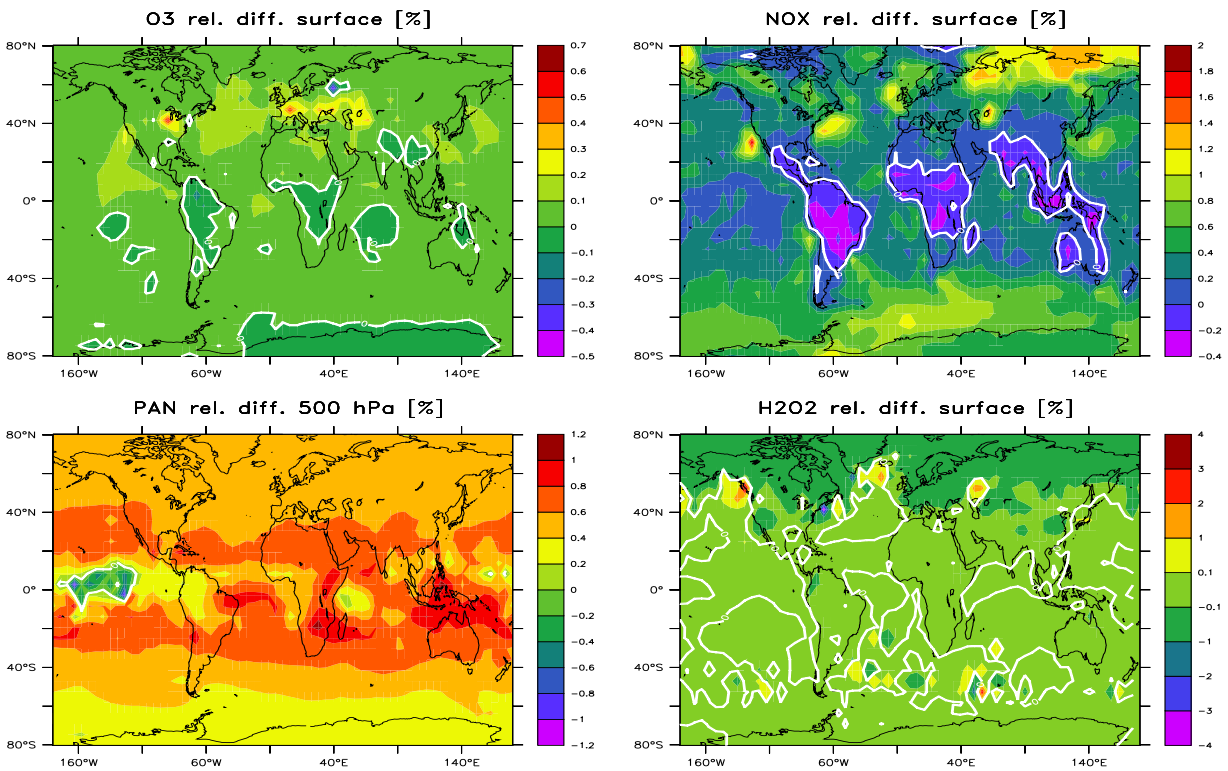
Figure B.3: Relative difference between the reference solution (see text) and a simulation with only 2 sub-steps globally. All values are thus (2-step - reference)/reference×100%. White contour lines mark 0%. Note that values for PAN are at 500hPa and first model layer values are given for the other species.
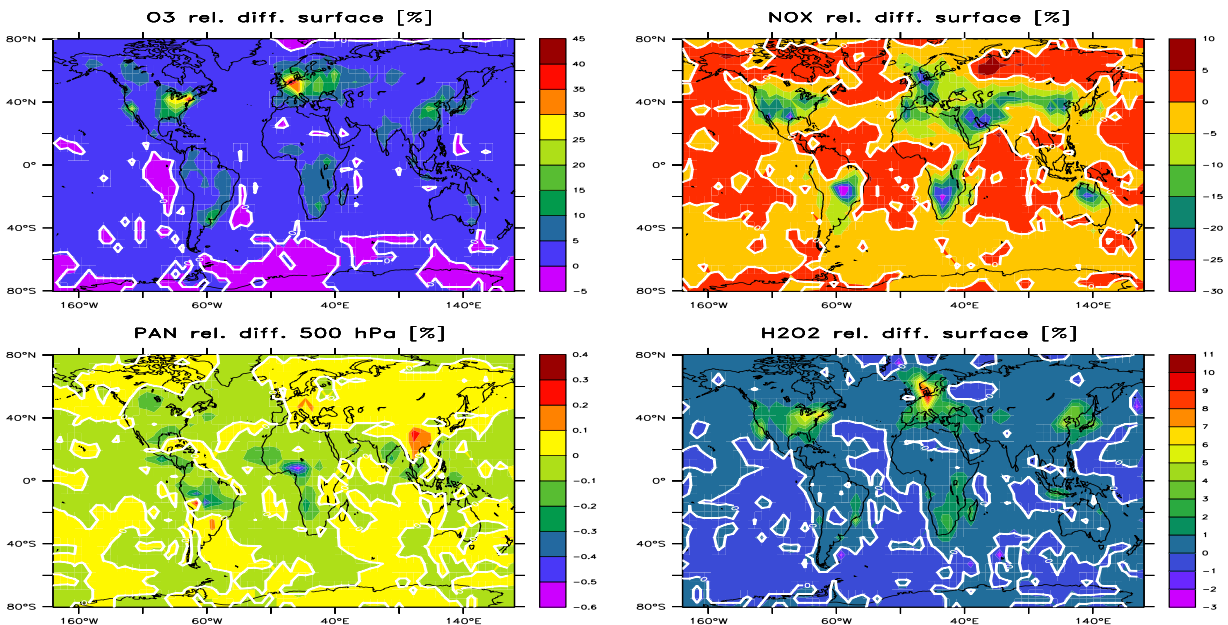
Figure B.4: Same as Figure B.3, but for the different source splitting solutions for the NO/NOX emissions. Thus, a simulation with a direct NO source within the chemistry (reference) and an external NOX source are compared. The average over the first 5 days in November is shown.

model perturbation tests were probably more difficult for the solver than the average situation in the 3D-model or that errors are canceling or smearing out in the 3D simulation.

It is, however, interesting to compare the two reference solutions and look at the associated "splitting error", which in this case also overlaps with the effect of the implicit assumption that the NOX-family is then usually emitted instead of NO. When the emitted NO is added outside the chemistry it is necessary to emit it as the family NOX, since this is the quantity which is transported and known to all the other processes except for the chemistry. The concentration of each family member is then calculated by scaling each member with a constant factor to be consistent with the updated (advected) total concentration of the family. Thus, effectively all family members are emitted instead of just NO. This detail appears to be a frequently-made assumption (e.g. *G.-J. Roelofs* and *M. Lawrence*, pers. comm., 1998-2000) although information from the literature is rarely available (only *Wang et al.* (1998a) state that they constantly emit 90% NO and 10% NO_2).

The effect, however, is significant as can be seen in Figure B.4. Over the most polluted regions in the winter hemisphere local deviations in O_3 of up to about 40% occur, with the source split solution being lower (it has been used as the reference in Figure B.4). Also NOX significantly differs. It should be noted that the region of the largest relative effect is also a region were an "ozone hole" appears in the model in winter (see Section 3.7), with O_3 values even below 5 nmol/mol, which are not supported by measurements. It appears that these deviations do not strongly propagate in the model, which can be seen by the relatively small relative change in PAN at 500 hPa. The difference in O_3 is also smaller than 1% at this pressure level. The most likely solution for the low ozone values near the surface is efficient titration by the freshly emitted NO:

$$NO + O_3 \rightarrow NO_2 + O_2 \tag{B.1}$$

The titration is actually very likely too efficient in the model, because both NO and O_3 are averaged in the large grid boxes (as well as the emissions). For a further discussion of sub-grid scale effects, see Section 1.3. The reason why the operator split solution yields more ozone over the heavily polluted regions is then easy to understand. Since now a portion is emitted e.g. as NO_2 one molecule of O_3 is artificially "saved" from destruction via Reaction B.1 per emitted NOX molecule other than NO compared to the case where only NO is emitted. Actually for emission of NO_3 or N_2O_5 accounts for two or three saved O_3 molecules respectively. Especially during night, when the competing reaction to B.1,

$$NO + HO_2 \rightarrow NO_2 + OH \,, \tag{B.2}$$

ceases because HO_2 is hardly available, this will be effective and basically one (or more) molecule O_3 is artificially saved per emitted NOX. This also explains why the effect is lower over the biomass burning regions of South Africa and Brazil, which have similar NOX concentrations. The difference is that here much more HO_2 is available due to enhanced solar insulation and probably due to the oxidation of NMHCs. This leads to increased reaction of NO via Reaction B.2 and smaller NO/NO_2 ratio and thus to less ozone titration.

The NOX concentration in the operator split solution is probably lower, because more NO_2 is available (it is directly emitted in part) so that the conversion to HNO_3 via reaction with OH is therefore enhanced and dry deposition of HNO_3 then represents a stronger sink for NOX. A similar argumentation also holds for N_2O_5, which is assumed to deposit as efficiently as HNO_3.

It is thus concluded from these tests that the exact method of how nitrogen oxides (as NOX or NO or NO_2) are emitted is of importance for the concentrations of O_3, NO_x and also HO_x near strong sources at least at medium to high latitude winter situations. For other situations (e.g. in the tropics) the effect is not as large. Since a direct emission of NO (and potentially a small fraction of NO_2) is physically more correct, this is a typical example of where resolving one "error" uncovers another (the sub-grid error).

Appendix C

List of Acronyms

For a list of species see Table 2.1 on page 23.

AMF	Air Mass Factor
AVHRR	Advanced Very High Resolution Radiometer
CAPE	Convective Available Potential Energy
CCM	Community Climate Model
DOAS	Differential Optical Absorption Spectroscopy
EBI	Euler Backward Iterative
ECHAM	European Community - HAMburg model
GEIA	Global Emissions Inventory Activity
GOME	Global Ozone Monitoring Experiment
HALOE	HALogen Occultation Experiment
IPCC	Intergovernmental Panel on Climate Change
IUPAC	International Union of Pure and Applied Chemistry
KPP	Kinetic PreProcessor
LAI	Leaf Area Index
LBA	Large-scale Biosphere-Atmosphere experiment
LBA-CLAIRE	Cooperative LBA Airborne Regional Experiment
MATCH	Model of Atmospheric Transport and CHemistry
MBL	Marine boundary layer
MCF	Methyl-chloroform
MCM	Master Chemical Mechanism
MIM	Mainz Isoprene Mechanism
MLOPEX	Mauna Loa Observatory Photochemistry Experiment
MOZAIC	Measurement of OZone and wAter vapour by Airbus In-Service airCraft
MOZART	Model of OZone And Related Tracers
NCAR	National Center of Atmospheric Research
NCEP	National Centers for Environmental Prediction
NH	Northern Hemisphere
NMHC	Non-methane Hydrocarbons
NMVOC	Non-methane Volatile Organic Compounds

NOAA/CMDL	National Oceanic and Atmospheric Administration / Climate Monitoring and Diagnostics Laboratory
OPE	Ozone production efficiency
PAR	Photosynthetic Active Radiation
PBL	Planetary Boundary Layer
PEM-Tropics	Pacific Exploratory Mission in the tropical Pacific
PEM-West	Pacific Exploratory Mission — West
PTR-MS	Proton-Transfer-Reaction Mass Spectrometer
QSSA	Quasi steady-state assumption
SAR	Structure Reactivity Relationship
SCF	Sampling Correction Factor
SH	Southern Hemisphere
SOA	Secondary Organic Aerosol
SONEX	SASS (Subsonic Assessment) Ozone and NO_x Experiment
SPITFIRE	Split Implementation of Transport Using Flux Integral Representation
STE	Stratosphere-Troposphere Exchange
STF	Stratosphere-Troposphere Flux
TRACE-A	Transport and Atmospheric Chemistry in the Atlantic
UT	Upper Troposphere
UV	Ultra-violett
VOC	Volatic organic compounds
WMO	World Meteorological Organisation
WOUDC	World Ozone and Ultraviolet Radiation Data Centre

Bibliography

Abbatt, J. P. D. Interaction of HNO_3 with water-ice surfaces at temperatures of the free tropo-sphere. *Geophys. Res. Lett.*, *24*, 1479–1482, 1997.

Allen, J., W. X. Balcavage, B. Ramachandran, and A. L. Shrout. Determination of Henry's law constants by equilibrium partitioning in a closed system using a new in situ optical absorbance method. *Environ. Toxicol. Chem.*, *17*, 1216–1221, 1998.

Andreae, M. O. *Biomass burning: Its history, use, and distribution and its impact on environ-mental quality and global climate*, pages 3–21. MIT Press, Cambridge, Mass., 1991.

Andreae, M. O. and P. Merlet. Emission of trace gases and aerosols from biomass burning. *submitted to Global Biogeochem. Cycles*, 2000.

Andronache, C., W. L. Chameides, M. O. Rodgers, J. Martinez, P. Zimmerman, and J. Green-berg. Vertical distribution of isoprene in the lower boundary layer of the rural and urban southern United States. *J. Geophys. Res.*, *99*, 16 989–16 999, 1994.

Angle, R. P. and H. S. Sandhu. Urban and rural ozone concentrations in Alberta, Canada. *Atmos. Environ.*, *20*, 1221–1228, 1986.

Ariya, P., R. Sander, and P. J. Crutzen. Significance of HO_x and peroxides production due to alkene ozonolysis during fall and winter: A modeling study. *J. Geophys. Res.*, *105*, 17 721–17 738, 2000.

Arlander, D. W., D. R. Cronn, J. C. Farmer, F. A. Menzia, and H. H. Westberg. Gaseous oxygenated hydrocarbons in the remote marine troposphere. *J. Geophys. Res.*, *95*, 16 391–16 403, 1990.

Arnold, F., V. Bürger, B. Droste-Fanke, F. Grimm, A. Krieger, J. Schneider, and T. Stilp. Acetone in the upper troposphere and lower stratosphere: Impact on trace gases and aerosols. *Geophys. Res. Lett.*, *24*, 3017–3021, 1997.

Arora, O., D. Cziczo, A. Morgan, J. Abbatt, and R. Niedziela. Uptake of nitric acid by sub-micron-sized ice particles. *Geophys. Res. Lett.*, *26*, 3621–3624, 1999.

Atkinson, R. Gas-Phase Tropospheric Chemistry of Volatile Organic Compounds: 1. Alkanes and Alkenes. *J. Phys. Chem. Ref. Data*, *26*, 215–290, 1997.

Atkinson, R. Atmospheric chemistry of VOCs and NO_x. *Atmos. Environ.*, *34*, 2063–2101, 2000.

Atkinson, R., D. L. Baulch, R. A. Cox, R. F. Hampson, Jr, J. A. Kerr, M. J. Rossi, and J. Troe. Evaluated Kinetic and Heterogeneous Data for Atmospheric Chemistry: Supplement V. *J. Phys. Chem. Ref. Data*, *26*, 521–1011, 1997.

Atkinson, R., D. L. Baulch, R. A. Cox, R. F. Hampson, Jr, J. A. Kerr, M. J. Rossi, and J. Troe. Evaluated kinetic and photochemical data for atmospheric chemistry, Organic species: Supplement VII. *J. Phys. Chem. Ref. Data*, *28*, 191–393, `http://www.iupac-kinetic.ch.cm.ac.uk/`, August 1999.

Atlas, E. and B. A. Ridley. The Mauna Loa Observatory Photochemistry Experiment: An introduction. *J. Geophys. Res.*, *101*, 14 531–14 541, 1996.

Ayers, G. P., R. W. Gillett, H. Granek, C. de Serves, and R. A. Cox. Formaldehyde production in clean marine air. *Geophys. Res. Lett.*, *24*, 401–404, 1997.

Ayers, G. P., S. A. Penkett, R. W. Gillett, B. Bandy, I. E. Galbally, C. P. Meyer, C. M. Elsworth, S. T. Bentley, and B. W. Forgan. The annual cycle of peroxides and ozone in marine air at Cape Grim, Tasmania. *J. Atmos. Chem.*, *23*, 221–252, 1996.

Baboukas, E. D., M. Kanakidou, and N. Mihalopoulos. Carboxylic acids in gas and particulate phase above the Atlantic Ocean. *J. Geophys. Res.*, *105*, 14 459–14 471, 2000.

Bakwin, P. S., S. C. Wofsy, and S.-M. Fan. Measurements of reactive nitrogen oxides (NO_y) within and above a topical forest canopy in the wet season. *J. Geophys. Res.*, *95*, 16 765–16 772, 1990a.

Bakwin, P. S., S. C. Wofsy, S.-M. Fan, M. Keller, S. E. Trumbore, and J. M. da Costa. Emission of Nitric Oxide (NO) from tropical forest soils and exchange of NO between the forest canopy and atmospherc boundary layers. *J. Geophys. Res.*, *95*, 16 755–16 764, 1990b.

Barrie, L. A., J. W. Bottenheim, P. J. Crutzen, and R. A. Rasmussen. Ozone destruction at polar sunrise in the lower Arctic atmosphere. *Nature*, *334*, 138–141, 1988.

Bates, T. S., K. C. Kelly, J. E. Johnson, and R. H. Gammon. Regional and seasonal variations in the flux of oceanic carbon monoxide to the atmosphere. *J. Geophys. Res.*, *100*, 23 093–23 101, 1995.

Baughcum, S. L., S. C. Henderson, P. S. Hertel, D. R. Maggiora, and C. A. Oncina. Stratospheric emissions effects database developement. Contr. Rep. CR-4592, NASA, 1994.

Bazhanov, V. and H. Rodhe. Tropospheric Ozone at the Swedish Mountain Site Åreskutan: Budget and Trends. *J. Atmos. Chem.*, *28*, 61–76, 1997.

Beine, H. J. and T. Krognes. The seasonal cycle of peroxyacetyl nitrate (PAN) in the European Arctic. *Atmos. Environ.*, *34*, 933–940, 2000.

Beker, K. H., J. Bechara, and K. J. Brockmann. Studies on the formation of H_2O_2 in the ozonolysis of alkenes. *Atmos. Environ.*, *27A*, 57–61, 1993.

Beker, K. H., K. J. Brockmann, and J. Bechara. Production of hydrogen peroxide in forest air by reaction of ozone with terpenes. *Nature*, *436*, 256–258, 1990.

Bergamaschi, P., R. Hein, C. A. M. Brenninkmeijer, and P. J. Crutzen. Inverse modeling of the global CO cycle, 2. Inversion of $^{13}C/^{12}C$ and $^{18}O/^{16}O$ isotope ratios. *J. Geophys. Res.*, *105*, 1929–1945, 2000a.

Bergamaschi, P., R. Hein, M. Heimann, and P. J. Crutzen. Inverse modeling of the global CO cycle, 1. Inversion of CO mixing ratios. *J. Geophys. Res.*, *105*, 1909–1927, 2000b.

Berkvens, P. J. F., M. A. Botchev, J. G. Verwer, M. C. Krol, and W. Peters. Solving vertical transport and chemistry in air pollution models. MAS-R0023, Centrum voor Wiskunde en Informatica, Amsterdam, 2000.

Berntsen, T. K. and I. S. A. Isaksen. A global three-dimensional chemical transport model for the troposphere, 1. Model description and CO and ozone results. *J. Geophys. Res.*, *102*, 21 239–21 280, 1997.

Betterton, E. A. and M. R. Hoffmann. Henry's law constants of some environmentally important aldehydes. *Env. Sci. Tech.*, *22*, 1415–1418, 1988.

Bode, K., G. Helas, and J. Kesselmeier. *Biogenic contribution to atmospheric organic acids*, pages 157–170. SPB Academic Publishing bv, 1997.

Bonsang, B. . and C. Boissard. *Global distribution of reactive hydrocarbons in the atmosphere*, pages 209–265. Acadamic Press, 1999.

Bonsang, B., M. Kanakidou, G. Lambert, and P. Monfray. The Marine Source of C_2–C_6 Aliphatic Hydrocarbons. *J. Atmos. Chem.*, *6*, 3–20, 1988.

Bottenheim, J. W. and B. F. Shepherd. C_2–C_6 hydrocarbon measurements at four rural locations across Canada. *J. Geophys. Res.*, *29*, 647–664, 1995.

Bottenheim, J. W., A. Sirois, K. A. Brice, and A. J. Gallant. Five years of continuous observations of PAN and ozone at a rural location in eastern Canada. *J. Geophys. Res.*, *99*, 5333–5352, 1994.

Bradshaw, J., D. Davis, G. Grodzinsky, S. Smyth, R. Newell, S. Sandholm, and S. Liu. Observed distribution of nitrogen oxides in the remote free troposphere from the NASA global tropospheric experiment programs. *Rev. Geoph.*, *38*, 611–116, 2000.

Brasseur, G. P., D. A. Hauglustaine, and S. Walters. Chemical compounds in the rempote Pacific troposphere: Comparison between MLOPEX measurements and chemical transport model calculations. *J. Geophys. Res.*, *101*, 14 795–14 813, 1996.

Brasseur, G. P., D. A. Hauglustaine, S. Walters, P. J. Rasch, and J.-F. Müller. MOZART, a global chemical transport model for ozone and related chemical tracers, 1, Model description. *J. Geophys. Res.*, *103*, 28 265–28 269, 1998.

Brenninkmeijer, C. A. M., M. R. Manning, D. C. Lowe, G. Wallace, R. J. Sparks, and A. Volz-Thomas. Interhemispheric asymmetry in OH abundance inferred from measurements of atmospheric ^{14}CO. *Nature*, *356*, 50–52, 1992.

Brewer, D. A., M. A. Ogliaruso, T. R. Augustsson, and T. R. Levine. The oxidation of isoprene in the troposphere: mechanism and model calculations. *Atmos. Environ.*, *18*, 2723–2744, 1984.

Brown, O. W., J. W. Brown, and R. H. Evans. Calculation of advanced Very High Resolution Radiometer observations. *J. Geophys. Res.*, *90*, 11 667–11 677, 1985.

Brühl, C. and P. J. Crutzen. On the disproportional role of tropospheric ozone as a filter against solar UV-B radiation. *Geophys. Res. Lett.*, *16*, 703–706, 1989.

Brühl, C., S. R. Drayson, J. M. Russel III, P. J. Crutzen, J. M. McInerney, P. N. Purcell, H. Claude, H. Gernandt, T. J. McGee, I. S. McDermid, and M. R. Gunson. Halogen Occultation Experiment ozone channel validation. *J. Geophys. Res.*, *101*, 10 217–10 240, 1996.

Canosa-Mas, C. E., M. D. King, R. Lopez, C. J. Percival, R. P. Wayne, D. E. Shallcross, J. A. Pyle, and V. Daell. Is the reaction between $CH_3(O)O_2$ and NO_3 important in the nigh-time troposphere? *J. Chem. Soc., Faraday Trans.*, *92*, 2211–2222, 1996.

Carter, W. P. L. and R. Atkinson. Alkyl nitrate formation from the atmospheric photooxidation of alkanes: A revised estimation method. *J. Atmos. Chem.*, *8*, 165–173, 1989.

Carter, W. P. L. and R. Atkinson. Development and Evaluation of a Detailed Mechanism for the Atmospheric Reactions of Isoprene and NO_x. *Int. J. Chem. Kinet.*, *28*, 497–530, 1996.

Chameides, W. L. and J. C. G. Walker. A photochemical theory of tropospheric ozone. *J. Geophys. Res.*, *78*, 8751–8760, 1973.

Charnock, M. Wind stress on a water surface. *Q. J. R. Meteorol. Soc.*, *81*, 639–640, 1955.

Chatfield, R. B. Anomalous HNO_3/NO_x ratio of the remote tropospheric air: Conversion of nitric acid to formic acid and NO_x? *Geophys. Res. Lett.*, *21*, 2705–2708, 1994.

Chatfield, R. B. and P. J. Crutzen. Are there interactions of iodine and sulfur species in the marine air photochemistry? *J. Geophys. Res.*, *95*, 22 319–22 341, 1990.

Chatfield, R. B. and A. C. Delany. Convection links biomass burning to increased tropical ozone: however, models will tend to overpredict O_3. *J. Geophys. Res.*, *95*, 18 473–18 488, 1990.

Chebbi, A. and P. Carlier. Carboxylic acids in the troposphere, occurrence, sources, and sinks: A review. *Atmos. Environ.*, *30*, 4233–4249, 1996.

Chen, X., D. Hulbert, and P. B. Shepson. Measurement of the organic nitrate yield from OH reaction with isoprene. *J. Geophys. Res.*, *103*, 25 563–25 568, 1998.

Chin, M. and P. H. Wine. *Biogenic contribution to atmospheric organic acids*, pages 85–98. Lewis, Boca Raton, Florida, 1994.

Christian, H. J., R. J. Blakeslee, and S. J. Goodman. The detection of Lightning from Geostationary Orbit. *J. Geophys. Res.*, *94*, 13 329–13 337, 1989.

Christian, H. J., R. J. Blakeslee, S. J. Goodman, D. A. Mach, M. F. Stewart, D. E. Buechler, W. J. Koshak, J. M. Hall, W. L. Boeck, K. T. Driscoll, , and D. J. Bocippio. The Lightning Imaging Sensor. In *Proceedings of the 11th International Conference on Atmospheric Electricity*, pages 746–749, `http://thunder.msfc.nasa.gov/lis`. Guntersville, Alabama, June 7-11, 1999.

Clarkson, T. S., R. J. Martin, and J. Rudolph. Ethane and propane in the southern marine troposphere. *Atmos. Environ.*, *31*, 3763–3771, 1997.

Cleveland, C. C. and J. B. Yavitt. Consumption of atmospheric isoprene in soil. *Geophys. Res. Lett.*, *24*, 2379–2382, 1997.

Collins, W. J., D. S. Stevenson, C. E. Johnson, and R. G. Derwent. Tropospheric Ozone in a Global-Scale Three-Dimensional Lagrangian Model and Its Response to NO_x Emission Controls. *J. Atmos. Chem.*, *26*, 223–274, 1997.

Collins, W. J., D. S. Stevenson, C. E. Johnson, and R. G. Derwent. Role of convection in determining the budget of odd hydrogen in the upper troposphere. *J. Geophys. Res.*, *104*, 26 927–26 941, 1999.

Conklin, M. A. H., A. Sig, A. Neftel, and R. Bales. Atmosphere-snow transfer function for H_2O_2: Microphysical considerations. *J. Geophys. Res.*, *98*, 18 367–18 376, 1993.

Corbett, J. J. and P. S. Fischbeck. Emissions from ships. *Science*, *278*, 823–824, 1997.

Corbett, J. J., P. S. Fischbeck, and S. N. Pandis. Global nitrogen and sulfur inventories for oceangoing ships. *J. Geophys. Res.*, *104*, 3457–3470, 1999.

Crawford, J. et al. Photostationary state analysis of the NO_2-NO system based on airborne observations from the western and cetnral North Pacific. *J. Geophys. Res.*, *101*, 2053–2072, 1996.

Crawford, M. A., T. J. Wallington, J. J. Szente, M. M. Maricq, and J. S. Francisco. Kinetics and mechanism of the acetylperoxy + HO_2 reaction. *J. Phys. Chem. A*, *103*, 365–378, 1999.

Cros, B., R. Delmas, D. Nganga, B. Claira, and J. Fontan. Seasonal trends of ozone in equatorial Africa: experimental evidence of photochemical formation. *J. Geophys. Res.*, *93*, 8355–8366, 1988.

Crutzen, P. and M. O. Andreae. Biomass burning in the tropics: Impact on atmospheric chemistry and biogeochemical cycles. *Science*, *250*, 1669–1678, 1990.

Crutzen, P. and P. H. Zimmermann. The changing photochemistry of the troposphere. *Tellus*, *43 AB*, 136–151, 1991.

Crutzen, P. J. Gas-phase nitrogen and methane chemistry in the atmosphere. Report AP-10, University of Stockholm, 1972.

Crutzen, P. J. A discussion of the chemistry of some minor constituents in the stratosphere and troposphere. *Pure and Applied Geophysics*, *106–108*, 1385–1399, 1973.

Crutzen, P. J. Photochemical reactions initiated by and influencing ozone in unpolluted tropospheric air. *Tellus*, *16*, 47–56, 1974.

Crutzen, P. J. The role of NO and NO_2 in the chemistry of the stratosphere and troposphere. *Ann. Rev. Earth Planet Sci.*, *7*, 443–472, 1979.

Crutzen, P. J. *Ozone in the troposphere*, chapter 10, pages 349–393. Von Nostrand Reinold Publ., New York, 1995.

Crutzen, P. J. and M. G. Lawrence. The impact of precipitation scavenging on the transport of trace gases: A 3-dimensional model sensitivity study. *J. Atmos. Chem.*, *37*, 81–112, 2000.

Crutzen, P. J., M. G. Lawrence, and U. Pöschl. On the background photochemistry of tropospheric ozone. *Tellus*, *51*, 123–146, 1999.

Crutzen, P. J., J. Williams, U. Pöschl, P. Hoor, H. Fischer, C. Warneke, R. Holzinger, A. Hansel, W. Lindinger, B. Scheeren, and J. Lelieveld. High spatial and temporal resolution measurements of primary organics and their oxidation products over the tropical forests of Surinam. *Atmos. Environ.*, *34*, 1161–1165, 2000.

Damian-Iordache, V. *KPP — Chemistry Simulation Developement Environment*. Master's thesis, University of Iowa, Iowa City, Iowa, 1996.

Davidson, E. A. and W. Kingerlee. A global inventory of nitric oxide emissions from soils. *Nutrient Cycling in Agroecosystems*, *48*, 37–50, 1997.

de Serves, C., A. Rondón, and P. Oyola. Photochemical Studies in the Savannah Boundary Layer During the wet Season. *Atmos. Environ.*, *30*, 1419–1427, 1996.

Delmas, R., D. Serça, and C. Jambert. Global inventory of NO_x sources. *Nutrient Cycling in Agroecosystems*, *48*, 51–60, 1997.

DeMore, W. B., S. P. Sander, C. J. Howard, A. R. Ravishankara, D. M. Golden, C. E. Kolb, R. F. Hampson, M. J. Kurylo, and M. J. Molina. Chemical Kinetics and Photochemical Data for Use in Stratospheric Modeling. Evaluation 12, 97-4, Jet Propulsion Laboratory, Pasadena, California, 1997.

Denning, A. S., M. Holzer, K. R. Gurney, M. Heimann, R. M. Law, P. J. Rayner, I. Y. Fung, S.-M. Fan, S. Taguchi, P. Friedlingstein, Y. Balkanski, J. Taylor, M. Maiss, and I. Levin. Three-dimensional transport and concentration of SF_6 — A model intercomparison study (TransCom 2). *Tellus*, *51 B*, 266–297, 1999.

Dentener, F. J. *Heterogeneous chemistry in the troposphere*. Ph.D. thesis, Universiteit Utrecht, Utrecht, Netherlands, 1993.

Dentener, F. J. and P. J. Crutzen. Reaction of N_2O_5 on Tropospheric Aerosols: Impact on the Global Distributions of NO_x, O_3, and OH. *J. Geophys. Res.*, *98*, 7149–7163, 1993.

Dickerson, R. R., K. P. Rhoads, T. P. Carsey, S. J. Oltmans, J. P. Burrows, and P. J. Crutzen. Ozone in the remote marine boundary layer: A possible role for halogens. *J. Geophys. Res.*, *104*, 21 385–21 395, 1999.

DKRZ. The ECHAM 3 Atmospheric General Circulation Model. No. 6 (Revision 2), Deutsches Klima Rechenzentrum, Hamburg, 1993.

Donahue, N. M. and R. G. Prinn. Non-methane Hydrocarbon Chemistry in the Remote Marine Boundary Layer. *J. Geophys. Res.*, *95*, 18 387–18 411, 1990.

Donahue, N. M. and R. G. Prinn. In Situ Nonmethane Hydrocarbon Measurements on SAGA 3. *J. Geophys. Res.*, *98*, 16 915–16 932, 1993.

Donoso, L., R. Romero, A. Rondon, E. Fernandez, P. Oyola, and E. Sanhueza. Natural and anthropogenic C_2 to C_6 Hydrocarbons in the Central-Eastern Venezuelan Atmosphere during the rainy season. *J. Atmos. Chem.*, *25*, 201–214, 1996.

Dransfield, T. J., K. K. Perkins, N. M. Donahue, J. G. Anderson, M. M. Sprengnether, and K. L. Demerjian. Temperature and Pressure Dependent Kinetics of the Gas-Phase Reaction of the Hydroxy Radicals with Nitrogen Dioxide. *Geophys. Res. Lett.*, *26*, 687– 690, 1999.

Ebel, A., H. Elbern, J. Hendricks, and R. Meyer. Stratosphere-troposphere exchange and its impact on the structure of the lower stratosphere. *J. Geomagn. Geoelectr.*, *48*, 135–144, 1996.

Elbern, H., J. Hendricks, and A. Ebel. A climatology of tropopause folds by global analyses. *Theor. Appl. Climatol.*, *59*, 81–200, 1998.

Emmons, L. K., M. A. Carroll, D. A. Hauglustaine, G. P. Brasseur, C. Atherton, J. Penner, S. Sillman, H. Levy II, F. Rohrer, W. M. F. Wauben, P. F. J. V. Velthoven, Y. Wang, D. Jacob, P. Bakwin, R. Dickerson, B. Doddridge, C. Gerbig, R. Honrath, G. Hübler, D. Jaffe, Y. Kondo, J. W. Munger, A. Torres, and A. Volz-Thomas. Climatologies of NOx and NOy: a comparison of data and models. *Atmos. Environ.*, *31*, 1851–1904, 1997.

Emmons, L. K., D. A. Hauglustaine, J.-F. Müller, M. A. Carroll, G. P. Brasseur, D. Brunner, J. Staehelin, V. Thouret, and A. Marenco. Data composites of airborne observations of tropospheric ozone and its precursors. *J. Geophys. Res.*, *105*, 20 497–20 538, 2000.

Erickson, D. Ocean to atmosphere carbon monoxide flux: global inventory and climate implications. *Global Biogecles*, *3*, 305–314, 1989.

Erisman, J. W., A. van Pul, and P. Wyers. Parametrization of surface-resistance for the quantification of atmospheric deposition of acidifying pollutants and ozone. *Atmos. Environ.*, *28*, 2595–2607, 1994.

Fall, R. *Biogenic Emissions of Volatile Organic Compounds from Higher Plants*, pages 41–96. Acadamic Press, 1999.

Fan, S.-M., D. J. Jacob, D. L. M. an dJ. D. Bradshaw, S. T. Sandholm, D. R. Blake, H. B. Singh, R. W. Talbot, G. L. Gregory, and G. W. Sachse. Photochemistry of reactive nitrogen in the sub-Arctic troposphere in summer 1990: Observations and modeling. *J. Geophys. Res.*, *99*, 16 867–16 878, 1994.

Fan, S.-M., S. C. Wofsy, P. S. Bakwin, D. J. Jacob, and D. R. Fitzjarrald. Atmosphere-biosphere exchange of CO_2 and O_3 in the Central Amazon forest. *J. Geophys. Res.*, *95*, 16 851–16 864, 1990.

Fischer, H., C. A. M. Brenninmeijer, R. von Kuhlmann, M. Lawrence, J. Mühle, U. Parchatka, C. Schiller, V. Wagner, A. Zahn, and P. J. Crutzen. Indian Ocean Experiment (INDOEX) — In-situ Messungen anthropogener und natürlicher Spurengase zum Studium der chemischen ABbbaumechanismen und Transformationen in der maritimen Grenzschicht des Indischen Ozeans. BMBF Abschlußbericht 01 LA 9831/2, MPI für Chemie, Mainz, 2001.

Fishman, J., V. Brackett, E. Browell, and W. Grant. Tropospheric ozone derived from TOMS/SBUV measurements during TRACE-A. *J. Geophys. Res.*, *101*, 24 069–24 082, 1996.

Fishman, J., F. Fakhruzzaman, B. Cros, and D. Nganga. Identification of widespread pollution in the southern hemisphere from satellite analysis. *Science*, *252*, 1693–1696, 1991.

Fishman, J., C. E. Watson, J. C. Larsena, and J. A. Logan. Distribution of tropospheric ozone determined from satellite data. *J. Geophys. Res.*, *95*, 3599–3618, 1990.

Fitzjarrald, D. R., B. L. Stormwind, G. Fisch, and O. M. R. Cabral. Turbulent transport observed just above the Amazon forest. *J. Geophys. Res.*, *93*, 1551–1563, 1988.

Follows, M. J. and J. F. Austin. A zonal average model of the stratospheric contributions to the tropospheric ozone budget. *J. Geophys. Res.*, *97*, 18 047–18 060, 1992.

Fuentes, J. D., B. P. Hayden, M. Garstang, M. Lerdau, D. Fitzjarrald, D. D. Baldochi, R. Monson, B. Lamb, and C. Geron. New Directions: VOCs and biosphere-atmosphere feedbacks. *Atmos. Environ.*, *35*, 189–191, 2001.

Fuentes, J. D., M. Lerdau, R. Atkinson, D. Baldocchi, J. W. Bottenheim, P. Ciccioli, B. Lamb, C. Geron, L. Gu, A. Guenther, T. D. Sharkey, and W. Stockwell. Biogenic Hydrocarbons in the Atmospheric Boundary Layer: A Review. *Bull. Am. Met. Soc.*, *81*, 1537–1575, 2000.

Fung, I., J. John, J. Lerner, E. Matthews, M. Prather, L. P. Steele, and P. J. Fraser. 3-dimensional synthesis of the global methane cycle. *J. Geophys. Res.*, *96*, 13 033–13 065, 1991.

Galanter, M., H. Levy, and G. R. Carmichael. Impacts of biomass burning on tropospheric CO, NO_x, and O_3. *J. Geophys. Res.*, *105*, 6633–6653, 2000.

Ganzeveld, L. and J. Lelieveld. Dry Deposition parameterization in a chemical general circulation model and its influence on the distribution of reactive trace gases. *J. Geophys. Res.*, *100*, 20 999–21 012, 1995.

Ganzeveld, L., J. Lelieveld, and G.-J. Roelofs. A dry deposition parameterization for sulfur oxides in a chemistry and general circulation model. *J. Geophys. Res.*, *103*, 5679–5694, 1998.

Ganzeveld, L. N. *Surface-Atmosphere Trace Gas and Aerosol Exchanges on the Global Scale*. Ph.D. thesis, Universiteit Utrecht, Utrecht, Netherlands, 2001.

Gear, C. W. *Numerical initial value problems in ordinary differential equations*. Englewood Cliffs, N.J. Prentice-Hall, 1971.

Geron, C., R. Rasmussen, R. A. Arnts, and A. Guenther. A review and synthesis of monoterpene speciation from forests in the United States. *Atmos. Environ.*, *34*, 1761–1781, 2000.

Gery, M. W., G. Z. Whitten, J. P. Killus, and M. C. Dodge. A photochemical kinetics mechanism for urban and regional scale computer modeling. *J. Geophys. Res.*, *94*, 12 925–12 956, 1989.

Gettelman, A., J. R. Holton, and K. H. Rosenlof. Mass fluxes of O_3, CH_4, N_2O and CF_2Cl in the lower stratosphere calculated from observational data. *J. Geophys. Res.*, *102*, 19 149–19 159, 1997.

Gierczak, T., J. B. Burkholder, S. Bauerle, and A. R. Ravishankara. Photochemistry of acetone under tropospheric conditions. *Chem. Phys.*, *231*, 229–244, 1998.

Gierczak, T., J. B. Burkholder, R. K. Talukdar, A. Mellouki, S. B. Barone, and A. R. Ravishankara. Atmospheric fate of methyl vinyl ketone and methacrolein. *J. Photochem. Photobiol.*, *110*, 1–10, 1997.

Giguère, P. A. and A. W. Olmos. Sur le spectre ultraviolet de l'acide peracétique et l'hydrolyse des peracétates. *Can. J. Chem.*, *34*, 689–691, 1956.

Glasius, M., S. Wessel, C. S. Christensen, J. K. .Jacobsen, H. E. Jørgensen, K. C. Klitgaard, L. Petersen, J. K. Rasmussen, T. Stroyer Hansen, C. Lohse, E. Boaretto, and J. Heinemeier. Sources to formic acid studied by carbon isotopic analysis and air mass characterization. *Atmos. Environ.*, *34*, 2471–2479, 2000.

Goldstein, A. H., S. M. Fan, M. L. Goulden, J. W. Mungern, and S. C. Wofsy. Emissions of ethene, propene, and I-butene by a midlatitude forest. *J. Geophys. Res.*, *101*, 9149–9157, 1996.

Goldstein, A. H., S. C. Wofsy, and C. M. Spivakovsky. Seasonal variation of nonmethane hydrocarbons in rural New England: Constraints on OH concentrations in northern midlatitudes. *J. Geophys. Res.*, *100*, 21 023–21 033, 1995.

Granier, C., G. Pétron, J.-F. Müller, and G. Brasseur. The impact of natural and anthropogenic hydrocarbons on the tropospheric budget of carbon monoxide. *Atmos. Environ.*, *34*, 5255–5270, 2000.

Greenberg, J. P., D. Helmig, and P. R. Zimmerman. Seasonal measurements of nonmethane hydrocarbons and carbon monoxide at the Mauna Loa Observatory during the Mauna Loa Observatory Photochemitry Experiment 2. *J. Geophys. Res.*, *101*, 14 581–14 598, 1996.

Greenberg, J. P. and P. R. Zimmerman. Nonmethane hydrocarbons in remote tropical, continental, and marine atmospheres. *J. Geophys. Res.*, *89*, 4767–4778, 1984.

Gros, V., B. Bonsang, D. Martin, P. C. Novelli, and V. Kazan. Carbon monoxide short term measurements at Amsterdam Island: estimation of biomass burning emission rates. *Chemosphere: Global Change Science*, *1*, 163–172, 1999.

Gros, V., D. Martin, N. Poisson, M. Kanakidou, B. Bonsang, and F. Le Guern. Ozone and C_2–C_5 hydrocarbons in the marine boundary layer between 45^oS and 77^oS. *Tellus*, *50B*, 430–448, 1998.

Guenther, A., C. Geron, T. Pierce, B. Lamb, P. Harley, and R. Fall. Natural emissions of nonmethane volatile organic compounds, carbon monoxide, and oxides of nitrogen from North America. *Atmos. Environ.*, *34*, 2205–2230, 2000.

Guenther, A., C. N. Hewitt, D. Erickson, R. Fall, C. Geron, T. Graedel, P. Harley, L. Klinger, M. Lerdau, W. A. McKay, T. Pierce, B. Scholes, R. Steinbrecher, R. Tallamraju, J. Taylor, and P. Zimmerman. A global model of natural volatile organic compound emissions. *J. Geophys. Res.*, *100*, 8873–8892, 1995.

Guenther, A., P. R. Zimmerman, P. C. Harley, R. K. Monson, and R. Fall. Isoprene and Monoterpene Emission Rate Variability: Model Evaluations and Sensitivity Analysis. *J. Geophys. Res.*, *98*, 12 609–12 617, 1993.

Haagen-Smit, A. J. Chemistry and physiology of Los Angeles smog. *Ind. Eng. Chem.*, *44*, 1342–1346, 1952.

Hack, J. J. Parameterization of moist convection in the National Center for Atmospheric Research community climate model (CCM2). *J. Geophys. Res.*, *99*, 5551–5568, 1994.

Hack, J. J., B. A. Boville, B. P. Briegleb, J. T. Kiehl, P. J. Rasch, and D. L. Williamson. Describtion of the NCAR Community Climate Model (CCM2). NCAR Tech. Note NCAR/TN-382+STR, National Center for Atmospheric Research, Boulder, CO, 1993.

Hanson, P. J. and S. E. Lindenberg. Dry deposition of reactive nitrogen compounds: A review off leaf, canopy and non-foliar measurements. *Atmos. Environ.*, *25 A*, 1615–1634, 1991.

Hao, W. M. and M.-H. Liu. Spatial and temporal distribution of tropical biomass burning. *Global Biogecles*, *8*, 495–503, 1994.

Hao, W. M., M.-H. Liu, and P. J. Crutzen. *Estimates of annual and regional releases of CO_2 and other trace gases to the atmosphere from fires in the tropics, based on FAO statistics for the period 1975-1980*, pages 440–462. Springer Verlag, New York, 1990.

Harries, J. E., H. E. Brindley, P. J. Sagoo, and B. R. J. Increases in greenhouse forcing inferred from the outgoing longwave radiation spectra of the Earth in 1970 and 1997. *Nature*, *410*, 355–357, 2001.

Harries, J. E., J. M. Russel III, A. F. Tuck, L. L. Gordley, P. Purcell, K. Stone, R. M. Bevilacqua, M. Gunson, G. Nedoluha, and W. A. Traub. Validation of measurements of water vapor from the Halogen Occultation Experiment (HALOE). *J. Geophys. Res.*, *101*, 10 205–10 216, 1996.

Hauglustaine, D. A., G. P. Brasseur, S. Walters, P. J. Rasch, J.-F. Müller, L. K. Emmons, and M. A. Carroll. MOZART, a global chemical transport model for ozone and related chemical tracers, 2: model results and evaluation. *J. Geophys. Res.*, *103*, 28 291–28 335, 1998.

Hauglustaine, D. A., B. A. Ridley, S. Solomon, P. G. Hess, and S. Madronich. HNO_3/NO_x ratio in the remote troposphere during MLOPEX 2: Evidence for nitric acid reduction on carbonaceous aerosols? *Geophys. Res. Lett.*, *23*, 2609–2612, 1996.

Helas, G. and J. Kesselmeier. Estimates on sinks and sources of formic and acetic acid. In J. Slanina, G. Angeletti, and S. Beilke, editors, *General Assessment of Biogenic Emissions and Deposition of Nitrogen Compounds, Sulphur Compounds and Oxidants in Europe*, number CEC Air Polution Research Report 47, ISBN 2-87263-095-3, pages 299–304. E. Guyot SA, Brussels, 1993.

Helmig, D., B. Balsley, K. Davis, L. R. Kuck, M. Jensen, J. Bognar, T. S. Jr., R. V. Arrieta, R. Rodriguez, and J. W. Birks. Vertical profiling and determination of landscape fluxes of biogenic nonmethane hydrocarbons within the planetary boundary layer in the Peruvian Amazon. *J. Geophys. Res.*, *103*, 25 519–25 532, 1998a.

Helmig, D., J. Greenberg, and A. Guen. Volatile organic compounds and isoprene oxidation products at a temperate deciduous forest site. *J. Geophys. Res.*, *103*, 22 397–22 414, 1998b.

Hertel, O., R. Berkowicz, and J. Christensen. Test of two numerical schemes for use in atmopsheric transport-chemistry models. *Atmos. Environ.*, *27A*, 2591–2611, 1993.

Hesstvedt, E., Ø. Hov, and I. Isaksen. Quasi-steady-state-approximation in air pollution modelling: Comparison of two numerical schemes for oxidant predictions. *Int. J. Chem. Kinet.*, *10*, 971–994, 1978.

Hilst, G. R. Segregation and chemical reaction rates in air quality models. *Atmos. Environ.*, *32*, 3891–3895, 1998.

Hoekstra, E. J., J. H. Duyzer, E. W. B. de Leer, and U. A. T. Brinkmann. Chloroform — concentration gradient in soil air and atmospheric air, and emissions from soil. *Atmos. Environ.*, *35*, 61–70, 2001.

Hoell, J. M., D. D. Davis, S. C. Liu, R. Newell, H. Akimoto, R. J. McNeal, and R. J. Bendura. Pacific Exploratory Mission – West Phase B: February – March 1994. *J. Geophys. Res.*, *102*, 28 223–28 239, 1997.

Hoell, J. M., D. D. Davis, S. C. Liu, R. Newell, M. Shipham, H. Akimoto, R. J. McNeal, R. J. Bendura, and J. W. Drewry. Pacific Exploratory Mission – West A (PEM–West A): September – October 1991. *J. Geophys. Res.*, *101*, 1641–1653, 1996.

Hoffmann, T., J. R. Odum, F. Bowman, D. Collins, D. Klockow, R. C. Flagan, and J. H. Seinfeld. Formation of Organic Aerosols from the Oxidation of Biogenic Hydrocarbons. *1997*, *26*, 189–222, 1997.

Holloway, T., H. Levy II, and P. Kasibhatla. Global distribution of carbon monoxide. *J. Geophys. Res.*, *105*, 12 123–12 147, 2000.

Holtslag, A. A. M. and B. A. Boville. Local Versus Nonlocal Boundary-Layer Diffusion in a Global Climate Model. *J. Climate*, *6*, 1825–1841, 1993.

Honrath, R. E., S. Guo, M. C. Peterson, M. P. Dziobak, J. E. Dibb, and M. A. Arsenault. Photochemical production of gas phase NO_x from ice crystal NO_3^-. *J. Geophys. Res.*, *105*, 24 183–24 190, 2000a.

Honrath, R. E., M. C. Peterson, M. P. Dziobak, J. E. Dibb, and M. A. Arsenault. Release of NO_x from Sunlight-irrigated midlatitude snow. *Geophys. Res. Lett.*, *27*, 2237–2240, 2000b.

Honrath, R. E., M. C. Peterson, S. Guo, J. E. Dibb, P. B. Shepson, and B. Campbell. Evidence of NO_x production with or upon ice particles in the Greenland Snowpack. *Geophys. Res. Lett.*, *26*, 695–698, 1999.

Horowitz, L. W., J. Liang, G. M. Gardener, and D. J. Jacob. Export of reactive nitrogen form North America during summertime: Sensitivity to hydrocarbon chemistry. *J. Geophys. Res.*, *103*, 13 451–13 476, 1998.

Houweling, S., F. Dentener, and J. Lelieveld. The impact of non-methane hydrocarbon compounds on tropospheric photochemistry. *J. Geophys. Res.*, *103*, 10 673–10 696, 1998.

Houweling, S., T. Kaminski, F. Dentener, J. Lelieveld, and M. Heimann. Inverse modeling of methane sources and sinks using the adjoint of a global transport model. *J. Geophys. Res.*, pages 26 137–26 160, 1999.

IPCC. *(Intergovernmental Panel on Climate Change), Climate Change 1995: The Science of Climate Change*. Cambridge University Press, Cambridge, UK, 1996.

IPCC. *Climate Change 2001: The Scientific Basis — Contribution of Working Group I to the Third Assessment Report of the Intergovernmental Panel on Climate Change (IPCC)*. Cambridge University Press, Cambridge, UK, 2001.

Iraci, L. T., B. M. Baker, G. S. Tyndall, and J. J. Orlando. Measurements of the Henry's law coefficients of 2-methyl-3-buten-2-ol, methacrolein, and methylvinyl ketone. *J. Atmos. Chem.*, *33*, 321–330, 1999.

Iraci, L. T. and M. Tolbert. Heterogeneous interaction of formaldehyde with cold sulfuric acid: Implication for the upper troposphere and lower stratosphere. *J. Geophys. Res.*, *102*, 16 099–16 107, 1997.

Iribarne, J. V. and T. Pyshnov. The effect of freezing on the composition of supercooled droplets — I. Retention of HCl, HNO_3, NH_3, and H_2O_2. *Atmos. Environ.*, *24A*, 383–387, 1990.

Jacob, D. J. Heterogeneous Chemistry and Tropospheric Ozone. *Atmos. Environ.*, *34*, 2131–2159, 2000.

Jacob, D. J., B. G. Heikes, S.-M. Fan, J. A. Logan, D. L. Mauzerall, J. D. Bradshaw, H. B. Singh, G. L. Gregory, R. W. Talbot, D. R. Blake, and G. W. Sachse. Origin of ozone and NO_x in the tropical troposphere: A photochemical analysis of aircraft observations over the South Atlantic basin. *J. Geophys. Res.*, *101*, 24 235–24 250, 1996.

Jacob, D. J., L. W. Horowitz, J. W. Munger, B. G. Heikes, R. R. Dickerson, R. S. Artz, and W. C. Keene. Seasonal transition from NO_x- to hydrocarbon limited conditions for ozone production over the eastern United States in September. *J. Geophys. Res.*, *100*, 9315–9324, 1995.

Jacob, D. J. and S. Wofsy. Budgets of Reactive Nitrogen, Hydrocarbons, and Ozone Over the Amazone Forest during the Wet Season. *J. Geophys. Res.*, *95*, 16 737–16 754, 1990.

Jaeglé, L., D. J. Jacob, W. H. Brune, I. Faloona, D. Tan, B. G. Heikes, Y. Kondo, G. W. Sachse, B. Anderson, G. L. Gregory, H. B. Singh, R. Pueschel, G. Ferry, D. R. Blake, and R. Shetter. Photochemistry of HO_x in the upper troposphere at northern mid-latitudes. *J. Geophys. Res.*, *105*, 3877–3892, 2000.

Jaeglé, L., D. J. Jacob, W. H. Brune, and P. O. Wennberg. Chemistry of HO_x radicals in the upper troposphere. *Atmos. Environ.*, *35*, 469–489, 2001.

Jaeglé, L., D. J. Jacob, P. O. Wennberg, C. M. Spivakovsky, T. F. Hanisco, E. J. Lanzendorf, E. J. Hintsa, D. W. Fahey, E. R. Keim, M. H. Proffitt, E. L. Atlas, F. Flocke, S. Schauffler, C. T. McElroy, C. Midwinter, L. Pfister, and J. C. Wilson. Observed OH and HO_2 in the upper troposphere suggest a major source from convective injection of peroxides. *Geophys. Res. Lett.*, *24*, 3181–3184, 1997.

Jenkin, M., S. M. Saunders, and M. J. Pilling. The Tropospheric Degradation of volatile organic compounds: A protocol for mechanism development. *Atmos. Environ.*, *31*, 81–104, 1997.

Jenkin, M. E. and K. C. Clemitshaw. Ozone and other secondary photochemical pollutants: chemical processes governing their formation in the planetary boundary layer. *Atmos. Environ.*, *34*, 2499–2527, 2000.

Jobson, B. T., Z. Wu, H. Niki, and L. A. Barrie. Seasonal trends of isoprene, alkanes, and acetylene at a remote boreal site in Canada. *J. Geophys. Res.*, *99*, 1589–1599, 1994.

Jöckel, P. *Cosmogenic ^{14}CO as a tracer for atmospheric chemistry and transport*. Ph.D. thesis, Universität Heidelberg, 2000.

Jöckel, P., R. von Kuhlmann, M. G. Lawrence, B. Steil, C. A. M. Brenninkmeijer, P. J. Crutzen, P. J. Rasch, and B. Eaton. On a fundamental problem in implementing flux-form advection schemes for tracer transport in 3-dimensional general circulation and chemistry transport models. *Q. J. R. Meteorol. Soc.*, *127*, 1035–1052, 2001.

Johnson, B. J., E. A. Betterton, and D. Craig. Henry's law coefficients of formic and acetic acids. *J. Atmos. Chem.*, *24*, 113–119, 1996.

Johnston, H. and D. Kinnison. Methane photooxidation in the atmosphere: Contrast between two methods of analysis. *J. Geophys. Res.*, *103*, 21 967–21 984, 1998.

Jones, A. E., R. Weller, A. Minikin, E. W. Wolff, W. T. Sturges, H. P. McIntyre, S. R. Leonard, O. Schrems, and S. Bauguitte. Oxidized nitrogen chemistry and speciation in the Antarctic troposphere. *J. Geophys. Res.*, *104*, 21 355–21 366, 1999.

Jones, A. E., R. Weller, E. W. Wolff, and H.-W. Jacobi. Speciation and rate of photochemical NO and NO_2 production in Antarctic snow. *Geophys. Res. Lett.*, *27*, 345–348, 2000.

Jonson, J. E. and I. S. A. Isaksen. Tropospheric Ozone Chemistry. The Impact of Cloud Chemistry. *J. Atmos. Chem.*, *16*, 99–122, 1993.

Junge, C. E. Global ozone budget and exchange between stratosphere and troposphere. *Tellus*, *14*, 363–377, 1962.

Kalnay, E., M. Kanamitsu, R. Kistler, W. Collins, D. Deaven, L. Gandin, M. Iredell, S. Saha, G. White, J. Woollen, Y. Zhu, M. Chelliah, W. Ebisuzaki, W. Higgins, J. Janowiak, K. Mo, C. Ropelewski, J. Wang, A. Leetmaa, R. Reynolds, R. Jenne, and D. Joseph. The NCEP/NCAR 40-year reanalysis project. *Bull. Am. Meteorol. Soc.*, *77*, 437–471, 1996.

Kames, J. and U. Schurath. Alkyl nitrates and bifunctional nitrates of atmospheric interest: Henry's law constants and their temperature dependencies. *J. Atmos. Chem.*, *15*, 79–95, 1992.

Kames, J., S. Schweighoeffer, and U. Schurath. Henry's Law Constant and Hydrolysis of Peroxyacetyl Nitrate. *J. Atmos. Chem.*, *12*, 169–180, 1991.

Kanakidou, M. and P. J. Crutzen. Scale problems in global tropospheric chemistry modeling: comparison of results obtained witha three-dimensional model, adopting longitudinal uniform and varying emissions of NO_x and NMHC. *Chemosphere*, *26*, 787–801, 1993.

Kanakidou, M. and P. J. Crutzen. The photochemical source of carbon monoxide: Importance, uncertainties and feedbacks. *Chemosphere: Global Change Science*, *1*, 91–109, 1999.

Kanakidou, M., F. J. Dentener, G. P. Brasseur, T. K. Berntsen, W. J. Collins, D. A. Hauglustaine, S. Houweling, I. S. A. Isaksen, M. Krol, M. G. Lawrence, J.-F. Müller, N. Poisson, G.-J. Roelofs, Y. Wang, and W. M. F. Wauben. 3-D global simulations of tropospheric CO distributions — results of the GIM/IGAC intercomparison 1997 exercise. *Chemosphere: Global Change Science*, *1*, 263–282, 1999.

Kanakidou, M., F. J. Dentener, G. P. Brasseur, W. J. Collins, T. K. Berntsen, D. A. Hauglustaine, S. Houweling, I. S. A. Isaksen, M. Krol, K. S. Law, M. G. Lawrence, J.-F. Müller, P. H. Platevin, N. Poisson, G.-J. Roelofs, Y. Wang, and W. M. F. Wauben. 3-D global simulations of tropospheric chemistry with focus on ozone distributions — Results of the GIM/IGAC 1997 intercomparison. EUR 18842, Eur. Comm., 1998.

Kanakidou, M., H. B. Singh, K. M. Valentin, and P. J. Crutzen. A two-dimensional study of ethane and propane oxidation in the troposphere. *J. Geophys. Res.*, *96*, 15 395–15 413, 1991.

Kanakidou, M., K. Tsigaridis, F. J. Dentener, and P. J. Crutzen. Human-activity-enhanced formation of organic aerosols by biogenic hydrocarbon oxidation. *J. Geophys. Res.*, *105*, 9243–9254, 2000.

Kasibhatla, P., H. Levy II, W. J. Moxim, S. N. Pandis, J. J. Corbett, M. C. Peterson, R. E. Honrath, G. J. Frost, K. Knapp, D. D. Parrish, and T. B. Ryerson. Do emissions from ships have a significant impact on concentrations on nitrogen oxides in the marine boundary layer? *Geophys. Res. Lett.*, *27*, 2229–2232, 2000.

Kasibhatla, P. S., H. Levy, and W. J. Moxim. Global NO_x, HNO_3, PAN, and NO_y Distributions From Fossil Fuel Combustion Emissions: A Model Study. *J. Geophys. Res.*, *98*, 7165–7180, 1993.

Kesselmeier, J. and M. Staudt. Biogenic Volatile Organic Compounds (VOC): An Overview on Emission, Physiology and Ecology. *J. Atmos. Chem.*, *33*, 23–88, 1999.

Khare, P., N. Kumar, K. M. Kumari, and S. S. Srivastava. Atmospheric formic and acetic acids: an overview. *Rev. Geoph.*, *37*, 227–248, 1999.

Kiehl, J. T., J. J. Hack, G. B. Bonan, B. A. Boville, D. L. Williamson, and P. J. Rasch. The National Center for Atmospheric Research Community Climate Model: CCM3. *J. Climate*, *11*, 1131–1178, 1998.

Kirchhoff, V. W. J. H., I. M. O. da Silva, and E. V. Browell. Ozone Measurement in Amazonia: Dry Season Versus Wet Season. *J. Geophys. Res.*, *95*, 16 913–16 926, 1990.

Kirchhoff, V. W. J. H. and E. V. A. Marinho. Surface carbon monoxide measurements in Amazonia. *J. Geophys. Res.*, *95*, 16 933–16 943, 1990.

Kirchhoff, V. W. J. H., A. W. Setzer, and M. C. Pereira. Biomass burning in Amazonia: Seasonal effects on atmospheric O_3 and CO. *Geophys. Res. Lett.*, *16*, 469–472, 1989.

Kley, D., P. J. Crutzen, H. G. J. Smit, H. Vömel, S. J. Oltmans, H. Grassl, and V. Ramanathan. Observations of near-zero ozone concentrations over the convective Pacific: Effects on Air Chemistry. *Science*, *274*, 230–233, 1996.

Koch, S. and G. K. Moortgat. Photochemistry of Methylglyoxal in the Vapor Phase. *J. Phys. Chem.*, *102*, 9142–9153, 1998.

Kouvarakis, G., K. Tsigaridis, M. Kanakidou, and N. Mihalopoulos. Temporal variations of surface regional background ozone over Crete Island in the southeast Mediterranean. *J. Geophys. Res.*, *105*, 4399–4407, 2000.

Kraus, A. B., F. Rohrer, E. S. Grobler, and D. H. Ehhalt. The global tropospheric distribution of NO_x estimated by a three-dimensional chemical tracer model. *J. Geophys. Res.*, *101*, 18 587–18 604, 1996.

Krol, M., P. J. van Leeuwen, and J. Lelieveld. Global OH trend inferred from methyl-chloroform measurements. *J. Geophys. Res.*, *103*, 10 697–10 711, 1998.

Kwok, E. S. C. and R. Atkinson. Estimation of hydroxyl radical reaction rate constants for gas-phase organic compounds using a structure-reactivity relationship: an update. *Atmos. Environ.*, *29*, 1685–1695, 1995.

Labrador, L., M. G. Lawrence, and R. von Kuhlmann. Evaluation of lightning parameterisations in a global chemistry-transport model. *Geophys. Res. Abstr.*, *3*, 5793, 2001.

Lacis, A. A., D. J. Wuebbles, and J. A. Logan. Radiative forcing of climate by changes in the vertical distribution of ozone. *J. Geophys. Res.*, *95*, 9971–9981, 1990.

Lal, S. and M. G. Lawrence. Elevated mixing ratios of surface ozone over the Arabian Sea. *Geophys. Res. Lett.*, *28*, 1487–1490, 2001.

Lamb, B., E. Allwine, S. Dilts, H. Westberg, T. Pierce, C. Geron, D. Baldocchi, A. Guenther, L. Klinger, P. HArley, and P. Zimmerman. Evaluation of forest canopy models for estimating isoprene emissions. *J. Geophys. Res.*, *101*, 22 787–22 798, 1996.

Landgraf, J. *Modellierung photochemisch relevanter Strahlungsvorgänge in der Atmopshäre unter Berücksichtigung des Einflusses von Wolken*. Ph.D. thesis, Johannes Gutenberg-Universität Mainz, Mainz, Germany, 1998.

Landgraf, J. and P. J. Crutzen. An Efficient Method for Online Calculations of Photolysis and Heating Rates. *Bull. Am. Met. Soc.*, *25*, 863–878, 1998.

Lawrence, M. G. *Photochemistry in the Tropical Pacific Troposphere: Studies with a Global 3D Chemistry-Meteorology Model*. Ph.D. thesis, Georgia Institute of Technology, 1996.

Lawrence, M. G. Evaluating trace gas sampling strategies with assistance from a global 3D photochemical model: case studies for CEPEX and NARE O_3 Profiles. *Tellus*, *53B*, 22–39, 2001.

Lawrence, M. G., W. L. Chameides, P. S. Kasibhatla, H. Levy II, and W. Moxim. *Lightning and atmospheric chemistry: The rate of atmospheric NO production*, volume I, pages 189–202. CRC Press, Inc., 1995.

Lawrence, M. G. and P. J. Crutzen. The impact of cloud particle gravitational settling on soluble trace gas distributions. *Tellus*, *50B*, 263–289, 1998.

Lawrence, M. G. and P. J. Crutzen. Influence of NO_x emissions from ships on tropospheric photochemistry and climate. *Nature*, *402*, 167–170, 1999.

Lawrence, M. G., P. J. Crutzen, and P. J. Rasch. Analysis of the CEPEX ozone data using a 3D chemistry-meteorology model. *Q. J. R. Meteorol. Soc.*, *125*, 2987–3009, 1999a.

Lawrence, M. G., P. J. Crutzen, P. J. Rasch, B. E. Eaton, and N. M. Mahowald. A model for studies of tropospheric photochemistry: Description, global distributions, and evaluation. *J. Geophys. Res.*, *104*, 26 245–26 277, 1999b.

Lawrence, M. G., P. Jöckel, and R. von Kuhlmann. What does the global mean OH concentration tell us? *Atmos. Chem. Phys. Discuss. (in press)*, 2001.

Lee, M., B. G. Heikes, D. J. Jacob, G. Sachse, and b. Anderson. Hydrogen peroxide, organic hydroperoxide, and formaldehyde as primary pollutants from biomass burning. *J. Geophys. Res.*, *102*, 1301–1309, 1997.

Leighton, P. A. *Photochemistry of air pollution*. Academic Press, 1961.

Lelieveld, J. and P. J. Crutzen. Influences of cloud photochemical processes on tropospheric ozone. *Nature*, *343*, 227–233, 1990.

Lelieveld, J. and P. J. Crutzen. The Role of Clouds in Tropospheric Photochemistry. *J. Atmos. Chem.*, *12*, 229–267, 1991.

Lelieveld, J. and F. J. Dentener. What controls tropospheric ozone? *J. Geophys. Res.*, *105*, 3531–3551, 2000.

Levy, H. Normal Atmosphere: Large radical and formaldehyde concentrations predicted. *Science*, *173*, 141–143, 1971.

Levy, H. Photochemistry of the lower tropopshere. *Planet. Space. Sci.*, *20*, 919–935, 1972.

Levy, H. Photochemistry of minor constituents in the troposphere. *Planet. Space. Sci.*, *20*, 919–935, 1973.

Levy, H., W. J. Moxim, A. A. Klonecki, and P. S. Kasibhatla. Simulated Tropospheric NO_x: Its evaluation, global distribution and individual source contributions. *J. Geophys. Res.*, *104*, 26 279–26 306, 1999.

Li, Q., D. J. Jacob, J. A. Logan, I. Bey, R. M. Yantosca, H. Liu, R. V. Martin, A. M. Fiore, and B. N. Duncan. A Tropospheric Ozone Maximum over the Middle East. *submitted to Geophys. Res. Lett.*, 2001.

Liang, J., L. W. Horowitz, D. J. Jacob, Y. Wang, A. M. Fiore, J. A. Logan, G. M. Gardner, and J. W. Munger. Seasonal budgets of reactive nitrogen species and ozone over the United States, and export fluxes to the global atmosphere. *J. Geophys. Res.*, *103*, 13 435–13 450, 1998.

Liang, J. and D. J. Jacob. Effect of aqueous phase cloud chemistry on tropospheric ozone. *J. Geophys. Res.*, *102*, 5993–6001, 1997.

Liang, J. and M. Z. Jacobson. Effects of subgrid segregation on ozone production efficiency in a chemical model. *Atmos. Environ.*, *34*, 2975–2982, 2000.

Lide, D. R., editor. *CRC Handbook of Chemistry and Physics*. CRC Press Inc., 80th edition, 1999.

Lin, S.-J. and R. B. Rood. Multidimensional Flux-Form Semi-Lagrangian Transport Schemes. *Mon. Weather Rev.*, *124*, 2026–2070, 1996.

Lin, X., M. Trainer, and S. C. Liu. On the Nonlinearity of the tropospheric ozone production. *J. Geophys. Res.*, *93*, 15 879–15 888, 1988.

Lind, J. A. and G. L. Kok. Henry's law determinations for aqueous solutions of hydrogen peroxide, methylhydroperoxide, and peroxyacetic acid. *J. Geophys. Res.*, *91D*, 7889–7895, 1986.

Lindskog, A. and J. Moldanová. The Influence of the Origin, Season and Time of the day on the Distribution of Individual NMHC Measured at Rörvik, Sweden. *Atmos. Environ.*, *28*, 2383–2398, 1994.

Liu, S. C., M. Trainer, F. C. Fehsenfeld, D. D. Parrish, E. J. Williams, D. W. Fahey, G. Hübler, and P. C. Murphy. Ozone Production in the Rural Troposphere and the Implications for Regional and Global Ozone Distributions. *J. Geophys. Res.*, *92*, 4191–4207, 1987.

Lobert, J. M., W. C. Keene, J. A. Logan, and R. Yevich. Global chlorine emissions from biomass burning: Reactive chlorine emissions inventory. *J. Geophys. Res.*, *104*, 8373–8389, 1999.

Logan, J. A. An analysis of ozone-sonde data for the troposphere: Recommendations for testing 3-D models and development of a gridded climatology for tropospheric ozone. *J. Geophys. Res.*, *104*, 16 115–16 149, 1999.

Logan, J. A., M. J. Prather, S. C. Wofsy, and M. B. McElroy. Tropospheric chemistry: A global perspective. *J. Geophys. Res.*, *86*, 7210–7254, 1981.

Mahowald, N. M. *Developement of a 3-dimensional chemical transport model based on observed winds and use in inverse modeling of the source of CCl_3F*. Ph.D. thesis, Mass. Inst of Tech., Cambridge, 1996.

Mahowald, N. M., R. G. Prinn, and P. J. Rasch. Deducing CCl_3F emissions using an inverse method and chemical transport models with assimilated winds. *J. Geophys. Res.*, *102*, 28 153–28 168, 1997a.

Mahowald, N. M., P. J. Rasch, B. E. Eaton, S. Whittlestone, and R. G. Prinn. Transport of ^{222}radon to the remote troposphere using the Model of Atmospheric Transport and Chemistry and assimilated winds from ECMWF and the National Center for Environmental Prediction/NCAR. *J. Geophys. Res.*, *102*, 28 139–28 152, 1997b.

Malleson, A. M., H. M. Kellett, R. G. Myhill, and W. P. Sweetenham. FACSIMILE User Guide. Technical report, Harwell Laboratory, Oxfordshire OX11 0RA, 1990.

Manning, M. R., C. A. M. Brenninkmeijer, and W. Allan. Atmospheric carbon monoxide budget of the southern hemisphere: Implications of $^{13}C/^{12}C$ measurements. *J. Geophys. Res.*, *102*, 10 673–10 682, 1997.

Marenco, A., M. Macaigne, and S. Prieur. Meridional and vertical CO and CH_4 distributions in the background troposphere (70°N-60°S; 0–12km altitude) from scientific aircraft measurements during the STRATOZ III experiment (June 1984). *Atmos. Environ.*, *23*, 185–200, 1989.

Martinez, R. D., A. A. Buitrago, N. W. Howell, C. H. Hearn, and J. A. Joens. The near U.V. absoption spectra of several aliphatic aldehydes and ketones at 300 K. *Atmos. Environ.*, *26A*, 785–792, 1992.

Matson, P. NO_x emission from soils and its consequences for the atmosphere and biosphere: critical gaps and research directions for the future. *Nutrient Cycling in Agroecosystems*, *48*, 1–6, 1997.

McKee, D. J., editor. *Tropospheric Ozone, Human Health and Agricultural Impacts*. Lewis, Boca Raton, Fla., 1993.

McKeen, S. A., T. Gierczak, J. B. Burkholder, P. O. Wennberg, T. F. Hanisco, E. R. Keim, R.-S. Gao, S. C. Liu, A. R. Ravishankara, and D. W. Fahey. The photochemistry of acetone in the upper troposphere: A source of odd-hydrogen radicals. *Geophys. Res. Lett.*, *24*, 3177–3180, 1997.

McLinden, C. A., S. C. Olsen, B. Hannegan, O. Wild, M. J. Prather, and J. Sundet. Stratospheric ozone in 3-D models: A simple chemistry and the cross-tropopause flux. *J. Geophys. Res.*, *105*, 14 653–14 665, 2000.

McRae, G. J., W. R. Goodin, and J. H. Seinfeld. Numerical solution of the atmospheric diffusion equation for chemically reacting flows. *J. Comput. Phys.*, *45*, 1–42, 1982.

Meijer, E. W., P. F. J. van Velthoven, W. M. F. Wauben, J. P. Beck, and G. J. M. Velders. The effects of the conversion of nitrogen oxides in aircraft exhaust plumes in global models. *Geophys. Res. Lett.*, *24*, 3013–3016, 1997.

Meilinger, S. K., A. Tsias, V. Dreiling, M. Kuhn, C. Feigl, H. Ziereis, H. Schlager, J. Curtius, B. Sierau, F. Arnold, M. Zöger, C. Schiller, and T. Peter. HNO_3 Partitioning in Cirrus Clouds. *Geophys. Res. Lett.*, *26*, 2207–2210, 1999.

Meller, R., W. Raber, J. N. Crowley, M. E. Jenkin, and G. K. Moortgat. The UV-visible absorbtion-spectrum of methylglyoxal. *J. Photochem. Photobiol.*, *62*, 163–171, 1991.

Middleton, P., W. R. Stockwell, and W. P. L. Carter. Aggregation and analysis of volatile organic compound emissions for regional modeling. *Atmos. Environ.*, *24A*, 1107–1133, 1990.

Midgley, P. and A. McCulloch. The production and global distribution of emissions to the atmosphere of 1,1,1 trichlroethane (methyl chloroform). *Atmos. Environ.*, *29*, 1601–1608, 1995.

Miyoshi, A., S. Hatakeyama, and N. Washida. OH radical-initiated photooxidation of isoprene: An estimate of global CO production. *J. Geophys. Res.*, *99*, 18 779–18 787, 1994.

Monks, P. S. A review of the observations and origins of the spring ozone maximum. *Atmos. Environ.*, *34*, 3545–3561, 2000.

Monod, A., A. Chebbi, R. Durand-Jolibois, and P. Carlier. Oxidation of methanol by hydroxyl radicals in aqueous solution under simulated cloud droplet conditions. *Atmos. Environ.*, *34*, 5283–5294, 2000.

Montzka, S. A., C. M. Spivakovsky, J. H. Butler, J. W. Elkins, L. T. Lock, and D. J. Mondeel. New observational constraints for atmospheric hydroxyl on global and hemispheric scales. *Science*, *288*, 500–503, 2000.

Montzka, S. A., M. Trainer, P. D. Goldan, W. C. Kuster, and F. C. Fehsenfeld. Isoprene and its oxidation products, methyl vinyl ketone and methacrolein, in the rural troposphere. *J. Geophys. Res.*, *98*, 1101–1111, 1993.

Moxim, W. J., H. Levy, and P. S. Kasibhatla. Simulated global tropospheric PAN: Its transport and impact on NO_x. *J. Geophys. Res.*, *101*, 12 621–12 638, 1996.

Moxley, J. M. and J. N. Cape. Depletion of carbon monoxide from the nocturnal boundary layer. *J. Geophys. Res.*, *31*, 1147–1155, 1997.

Müller, J.-F. Geographical Distribution and Seasonal Variation of Surface Emissions and Deposition Velocities of Atmospheric Trace Gases. *J. Geophys. Res.*, *97*, 3787–3804, 1992.

Müller, J.-F. and G. Brasseur. IMAGES: A three-dimensional chemical transport model of the global troposphere. *J. Geophys. Res.*, *100*, 16 445–16 490, 1995.

Müller, J.-F. and G. Brasseur. Sources of upper tropospheric HO_x: A three-dimensional study. *J. Geophys. Res.*, *104*, 1705–1715, 1999.

Murphy, D. M. and D. W. Fahey. An estimate of the flux of stratospheric reactive nitrogen and ozone into the troposphere. *J. Geophys. Res.*, *99*, 5325–5332, 1994.

Murphy, D. M., D. W. Fahey, M. H. Proffitt, S. C. Liu, K. R. Chan, C. S. Euband, S. R. Kawa, and K. K. Kelly. Reactive nitrogen and its correlation with ozone in the lower stratosphere and upper troposphere. *J. Geophys. Res.*, *98*, 8751–8773, 1993.

Neeb, P. Structure-Reactivity Based Estimation of the Rate Constants for Hydroxyl Radical Reactions with Hydrocarbons. *J. Atmos. Chem.*, *35*, 295–315, 2000.

Neeb, P., O. Horie, and G. K. Moortgat. The Ethene-Ozone Reaction in the Gas Phase. *J. Phys. Chem. A*, *102*, 6778–6785, 1998.

Neeb, P. and G. K. Moortgat. Formation of OH Radicals in the Gas Phase Reaction of Propene, Isobutene, and Isoprene with O_3: Yields and Mechanistic Implications. *J. Phys. Chem. A*, *103*, 9003–9012, 1999.

Nesbitt, S. W., R. Zhang, and R. E. Orville. Seasonal and global NO_x production by lightning estimated from the Optical Transient Detector (OTD). *Tellus*, *52B*, 1206–1215, 2000.

Notholt, J., G. Toon, G. Stordal, S. Solberg, N. Schmidbauer, E. Becker, A. Meier, and B. Sen. Seasonal variations of atmospheric trace gases in the high Arctic at 79°N. *J. Geophys. Res.*, *102*, 12 855–12 861, 1997.

Novelli, P. C., K. A. Masarie, and P. M. Lang. Distribution and recent changes of carbon monoxide in the lower troposphere. *J. Geophys. Res.*, *103*, 19 015–19 033, 1998.

Odum, J., T. Hoffmann, F. Bowman, D. Collins, R. C. Flagan, and J. H. Seinfeld. Gas/Particle Partitioning and Secondary Organic Aerosol Yields. *Env. Sci. Tech.*, *30*, 2580–2585, 1996.

Olivier, J. G. J., J. P. J. Bloos, J. J. M. Berdowski, A. J. H. Visschedijk, and A. F. Bouwman. A 1990 global emission inventory of anthropogenic sources of carbon monoxide on $1° \times 1°$ developed in the framework of EDGAR/GEIA. *Chemosphere: Global Change Science*, *1*, 1–17, 1999.

Olivier, J. G. J., A. F. Bouwman, C. W. M. van der Maas, J. J. M. Berdowski, C. Veldt, J. P. J. Bloos, A. J. J. Visschedijk, P. Y. J. Zandveld, and J. L. Haverlag. Description of EDGAR Version 2.0: A set of global inventories of greenhouse gases and ozone-depleting substances for all anthrophogenic and most natural sources on a per country $1° \times 1°$ grid. RIVM Rep. 771060002, Rijksinstituut, Bilthoven, Netherlands, 1996.

Oltmans, S. J. and H. Levy. Surface ozone measurements from a global network. *Atmos. Environ.*, *28*, 9–24, 1994.

Orlando, J. J., B. Noziére, G. S. Tyndall, G. E. Orzechowska, S. E. Paulson, and Y. Rudich. Product studies of the OH- and ozone-initiated oxidation of some monoterpenes. *J. Geophys. Res.*, *105*, 11 561–11 572, 2000.

O'Sullivan, D. W., M. Lee, B. C. Noone, and B. G. Heikes. Henry's law constant determinations for hydrogen peroxide, methyl hydroperoxide, hydroxymethyl hydroperoxide, ethyl hydroperoxide, and peroxyacetic acid. *J. Phys. Chem.*, *100*, 3241–3247, 1996.

Parrish, D. D., M. Trainer, J. S. Holloway, J. E. Yee, M. S. Warshawsky, F. C. Fehsenfeld, G. L. Forbes, and J. L. Moody. Relationships between ozone and carbon monoxide at surface sites in the North Atlantic region. *J. Geophys. Res.*, *103*, 13 357–13 376, 1998.

Patton, E. G., K. J. Davis, M. C. Barth, and P. S. Sullivan. Decaying scalars emitted by a forest canopy: A numerical study. *in press to Bound. Lay. Met.*, 2001.

Paulson, S. E. and J. H. Seinfeld. Development and Evaluation of a Photooxidation Mechanism for Isoprene. *J. Geophys. Res.*, *97*, 20 703–20 715, 1992.

Penkett, S. A. and K. A. Brice. The spring maximum in photo-oxidants in the Northern Hemisphere troposphere. *Nature*, *319*, 655–657, 1986.

Pickering, K. E., A. M. Thompson, Y. Wang, W.-K. Tao, E. P. McNamara, V. W. J. J. Kichhoff, B. G. Heikes, G. W. SAchse, J. D. Bradshaw, G. L. Gregory, and D. R. Blake. Convective transport of biomass burning emissions over Brazil during TRACE A. *J. Geophys. Res.*, *101*, 23 993–24 012, 1996.

Plass-Dülmer, C., R. Koppmann, M. Ratte, and J. Rudolph. Light non-methane hydrocarbons in seawater. *Global Biogecles*, *9*, 79–100, 1995.

Poisson, N. *Impact des hydrocarbures non méthaniques sur la chimie troposphérique*. Ph.D. thesis, Université Paris, Paris, France, 1997.

Poisson, N., M. Kanakidou, and P. J. Crutzen. Impact of non-methane hydrocarbons on tropospheric chemistry and the oxidizing power of the global troposphere: 3-dimensional modelling results. *J. Atmos. Chem.*, *36*, 157–230, 2000.

Poppe, D., R. Koppmann, and J. Rudolph. Ozone formation in biomass burning plumes: Influence of atmospheric dilution. *Geophys. Res. Lett.*, *25*, 3823–3826, 1998.

Pöschl, U., M. G. Lawrence, R. von Kuhlmann, and P. J. Crutzen. Comment on "Methane photooxidation in the atmosphere: Contrast between two methods of analysis" by Harold Johnston and Douglas Kinnison. *J. Geophys. Res.*, *105*, 1431–1433, 2000a.

Pöschl, U., R. von Kuhlmann, N. Poisson, and P. J. Crutzen. Development and Intercomparison of Condensed Isoprene Oxidation Mechanisms for Global Atmospheric Modeling. *J. Atmos. Chem.*, *37*, 29–52, 2000b.

Pöschl, U., J. Williams, P. Hoor, H. Fischer, P. J. Crutzen, C. Warneke, R. Holzinger, A. Hansel, A. Jordan, W. Lindinger, H. A. Scheeren, W. Peters, and J. Lelieveld. High Acetone Concentration throughout the Troposphere over the Tropical Rainforest in Surinam. *J. Atmos. Chem.*, *38*, 115–132, 2001.

Prather, M. J. and D. J. Jacob. A persistent imbalance in HOx and NO_x photochemistry of the upper troposphere driven by deep convection. *Geophys. Res. Lett.*, *24*, 3189–3192, 1997.

Price, C., J. Penner, and M. Prather. NO_x from lightning: 1. Global distribution based on lightning physics. *J. Geophys. Res.*, *102*, 5929–5941, 1997a.

Price, C., J. Penner, and M. Prather. NO_x from lightning: 2. Constraints from the global atmospheric electric circuit. *J. Geophys. Res.*, *102*, 5942–5951, 1997b.

Price, C. and D. Rind. A simple lightning parameterization for calculating global lightning distributions. *J. Geophys. Res.*, *97*, 9919–9933, 1992.

Price, C. and D. Rind. Modeling global lightning distribution in a general circulation model. *Mon. Weather Rev.*, *122*, 1930–1939, 1994.

Prinn, R., D. Cunnold, P. Simmonds, F. Alyea, R. Boldi, A. Crawford, P. Fraser, D. Gutzler, H. D., R. Rosen, and R. R. Global average concentration and trend for hydroxyl radicals deduced from ALE/GAUGE trichloroethane (methyl chloroform) data for 1978-1990. *J. Geophys. Res.*, *97*, 2445–2461, 1992.

Prinn, R. G., J. Huang, R. F. Weiss, D. M. Cunnold, P. J. Fraser, P. G. Simmonds, A. McCulloch, C. Harth, P. Salameh, S. O'Doherty, R. J. J. Wang, L. Porter, and B. R. Miller. Evidence for substantial variations of atmospheric hydroxyl radicals in the past two decades. *Science*, *292*, 1882–1888, 2001.

Prinn, R. G., R. F. Weiss, B. R. Miller, J. Huang, F. N. Alya, D. M. Cunnold, P. J. Fraser, D. E. Hartley, and P. G. Simmonds. Atmospheric trends and lifetime of CH_3CCl_3 and global OH concentrations. *Science*, *269*, 187–190, 1995.

Quesada, J., D. G. E. Fernandez, J. Romero, E. Sanhueza, G. Moortgat, and P. J. Crutzen. Ground based gas phase measurements in Surinam during the LBA-Claire 98 experiment. *J. Atmos. Chem.*, *39*, 15–36, 2001.

Raper, J. L., M. M. Kleb, D. J. Jacob, D. D. Davis, R. E. Newell, H. E. Fuelberg, R. J. Bendura, J. M. Hoell, and R. J. McNeal. Pacific Exploratory Mission in the tropical Pacific: PEM-Tropics B, March-April 1999. *submitted to J. Geophys. Res.*, 2001.

Rasch, P. J. and J. E. Kristjánsson. A comparison of the CCM3 model climate using diagnosed and predicted condensate parameterizations. *J. Climate*, *11*, 1587–1614, 1998.

Rasch, P. J. and M. Lawrence. Recent Developement in Transport Methods at NCAR. In *MPI Workshop on conservative transport schemes*, number 265, pages 65–75. Max-Planck-Institute for Meteorology, Hamburg, Germany, 1998.

Rasch, P. J., N. M. Mahowald, and B. E. Eaton. Representations of transport, convection and the hydrologic cycle in chemical transport models: Implications for the modeling of short lived and soluble species. *J. Geophys. Res.*, *102*, 28 127–28 138, 1997.

Rasch, P. J. and D. L. Williamson. Computational aspects of moisture transport in global models of the atmosphere. *Q. J. R. Meteorol. Soc.*, *116*, 1071–1090, 1990.

Rasmussen, R. A. and M. A. K. Khalil. Isoprene over the Amazone basin. *J. Geophys. Res.*, *93*, 1417–1421, 1988.

Raupach, M. R. and A. S. Thom. Turbulence in and above plant canopies. *Ann. Rev. Fluid. Mech.*, *13*, 97–129, 1981.

Raynaud, D., J. C. nd J. M. Barnola, Y. S. Korotkevich, and C. Lorius. Vostok ice core reveals glacial-interglacial CH_4 change about 140 kyr ago: climatic and CH_4 cycle implications. *Nature*, *333*, 655–657, 1988.

Regener, V. H. Vertical flux of atmospheric ozone. *J. Geophys. Res.*, *62*, 221–228, 1957.

Regimbal, J. M. and M. Mozurkewich. Peroxynitric acid decay mechanisms and kinetics at low pH. *J. Phys. Chem. A*, *101*, 8822–8829, 1997.

Reissel, A., C. Harry, S. M. Aschmann, R. Atkinson, and J. Arey. Formation of acetone from the OH radical- and O_3-initiated reactions of a series of monoterpenes. *J. Geophys. Res.*, *104*, 113 869–13 879, 1999.

Rhee, T. S. *The process of air-water gas exchange and its application*. Ph.D. thesis, Texas A&M University, 2000.

Richter, A. *Absorptionsspecktroskopische Messungen stratosphärischer Spurengase über Bremen, 53°N*. Ph.D. thesis, University of Bremen, Bremen, Germany, 1997.

Richter, A. and J. P. Burrows. Tropospheric NO_2 from GOME measurements. *submitted to Advances in Space Research*, 2001.

Ridley, B., J. Walega, G. Hübler, D. Montzka, E. Atlas, D. Hauglustaine, F. Grahek, J. Lind, T. Campos, R. Norton, J. Greenberg, S. Schauffler, S. Oltmans, and S. Whittlestone. Measurements of NO_x and PAN and estimates of O_3 production over the season during Mauna Loa Observatory Photochemistry Experiment 2. *J. Geophys. Res.*, *103*, 8323–8339, 1998.

Rinsland, C. P., A. Goldman, F. J. Murcray, T. M. Stephen, N. S. Pougatchev, J. Fishman, S. J. David, R. D. Blatherwick, P. C. Novelli, N. B. Jones, and B. J. Connor. Infrared solar spectroscopic measurements of free tropospheric CO, C_2H_6, and HCN above Mauna Loa, Hawaii: Seasonal variations and evidence for enhanced emissions from the Southeas Asian tropical fires of 1997–1998. *J. Geophys. Res.*, *104*, 18 667–18 680, 1999.

Rinsland, C. P., N. B. Jones, B. J. Connor, J. A. Logan, N. S. Pougatchev, A. Goldman, F. J. Murcray, T. M. Stephen, A. S. Pine, R. Zander, E. Mahieu, and P. Demoulin. Nothern and southern hemisphere ground-based infrared spectroscopic measurements of tropospheric carbon monoxide and ethane. *J. Geophys. Res.*, *103*, 28 197– 28 217, 1998.

Rinsland, C. P., E. Mahieu, R. Zander, P. Demoulin, J. Forrer, and B. Buchmann. Free tropospheric CO, C_2H_6, and HCN above central Europe: Recent measurements from the Jungfraujoch station including the detection of elevated columns during 1998. *J. Geophys. Res.*, *105*, 24 235–24 249, 2000.

Roberts, J. M., D. D. Parrish, R. B. Norton, S. B. Bertman, J. S. Holloway, M. Trainer, F. C. Fehsenfeld, M. A. Caroll, G. M. Albercook, T. Wang, and G. Forbes. Episodic removal of NO_y species from the marine boundary layer over the North Atlantic. *J. Geophys. Res.*, *101*, 28 947–28 960, 1996.

Roelofs, G.-J. and J. Lelieveld. Distribution and budget of O_3 in the troposphere calculated with a chemistry general circulation model. *J. Geophys. Res.*, *100*, 20 983–20 998, 1995.

Roelofs, G.-J. and J. Lelieveld. Model study of the influence of cross-tropopause O_3 transport on tropospheric O_3 levels. *Tellus*, *49B*, 38–55, 1997.

Roelofs, G.-J. and J. Lelieveld. Tropospheric ozone simulation with a chemistry-general circulation model: Influence of higher hydrocarbon chemistry. *J. Geophys. Res.*, *105*, 22 697–22 712, 2000.

Roemer, M. *Trends of tropospheric ozone over Europe*. Ph.D. thesis, University of Utrecht, Utrecht, Netherlands, 1996.

Rogaski, C. A., D. M. Golden, and L. R. Williams. Reactive uptake and hydration experiments on amorphous carbon treated with NO_2, SO_2, O_3, HNO_3, H_2SO_4. *Geophys. Res. Lett.*, *24*, 381–385, 1997.

Rudolph, J. The tropospheric distribution and budget of ethane. *J. Geophys. Res.*, *100*, 11 369–11 381, 1995.

Rudolph, J. *Biogenic sources of atmopsheric alkenes and acetylene*, pages 53–65. SPB Academic Publishing bv, 1997.

Rudolph, J., A. Khedim, and E. Wagenbach. The Seasonal Variation of Light Non-methane Hydrocarbons in the Antarctic Troposphere. *J. Geophys. Res.*, *94*, 13 039–13 044, 1989.

Russel, J. The Halogen Occultation Experiment. *J. Geophys. Res.*, *98*, 10 777–10 798, 1993.

Salawitch, R. J., B. Sen, G. C. Toon, P. O. Wennberg, G. B. Osterman, and J. J. Margitan. Measurments of HNO_4: Implications for HO_x. *Geophys. Res. Abs.*, *3*, 5793, 2001.

Sander, R. and P. Crutzen. Modeling the chemistry of ozone, halogen compounds, and hydrocarbons in the arctic troposphere during sping. *Tellus, Ser. B, 49*, 522–532, 1996.

Sander, S. P., R. R. Friedl, W. B. DeMore, A. R. Ravishankara, D. M. Golden, C. E. Kolb, M. J. Kurylo, R. F. Hampson, R. E. Huie, M. J. Molina, and G. K. Moortgat. Chemical Kinetics and Photochemical Data for Use in Stratospheric Modeling — Supplement to Evaluation 12: Update of Key Reactions. Evaluation 13, 00-3, Jet Propulsion Laboratory, Pasadena, California, 2000.

Sandu, A., F. A. Potra, G. R. Carmichael, and V. Damian. Efficient implementation of fully implicit methods for atmospheric chemical kinetics. *J. Comput. Phys.*, *129*, 101–110, 1996.

Sandu, A., J. G. Verwer, J. G. Blom, E. J. Spee, and G. R. Carmichael. Benchmarking stiff ODE solvers for atmospheric chemistry problems II: Rosenbrock solvers. *Atmos. Environ.*, *31*, 3459–3472, 1997a.

Sandu, A., J. G. Verwer, M. van Loon, G. R. Carmichael, F. A. Porta, D. Dabdub, and J. H. Seinfeld. Benchmarking stiff ODE solvers for atmospheric chemistry problems I: implicit versus explicit. *Atmos. Environ.*, *31*, 3149–3164, 1997b.

Sanhueza, E. Impact of human activity on NO soil fluxes. *Nutrient Cycling in Agroecosystems*, *48*, 61–68, 1997.

Sanhueza, E., Y. Dong, D. Scharffe, J. M. Lobert, and P. J. Crutzen. Carbon monoxide uptake by temperate forest soils: The effects of leaves and humus layers. *Tellus*, *50 B*, 51–58, 1998.

Sanhueza, E., R. Holzinger, R. von Kuhlmann, B. Kleiss, L. Donoso, and P. J. Crutzen. Diurnal cycles and seasonal variation of isoprene and its oxidation products in the tropical savanna atmosphere. *submitted to Glob. Biogeochem. Cycles*, 2001.

Sanhueza, E., K. H. Octavio, and A. Arrocha. Surface ozone measurements in the Venezuelan tropical savannah. *J. Atmos. Chem.*, *2*, 377–385, 1985.

Saunders, S. M., M. E. Jenkin, R. G. Derwent, and M. J. Pilling. Development of a Master Chemical Mechanism for Use in Tropospheric Chemistry Models. EUROTRAC Newsletter 18, 1997a.

Saunders, S. M., M. E. Jenkin, R. G. Derwent, and M. J. Pilling. World Wide Web site of a Master Chemical Mechanism (MCM) for use in tropospheric chemistry models. *Atmos. Environ.*, *31*, 1249, http://www.chem.leeds.ac.uk/Atmospheric/MCM/mcmproj.html, 1997b.

Sawada, S. and T. Tutsuka. Natural and anthropogenic sources of atmopsheric ethylene. *Atmos. Environ.*, *20*, 821–832, 1986.

Schade, G. W. and P. J. Crutzen. CO emissions from degrading plant matter (II). Estimate of a global source strength. *Tellus*, *51B*, 909–918, 1999.

Scheel, H. E., H. Areskoug, H. Geiss, B. Gomiscek, K. Granby, L. Haszpra, L. Klasinc, D. Kley, T. Laurila, A. Lindskog, M. Roemer, R. Schmitt, P. Simmonds, S. Solberg, and G. Toupance. On the Spatial Distribution and Seasonal Variation of Lower-Troposphere Ozone over Europe. *J. Atmos. Chem.*, *28*, 11–28, 1997.

Schmitt, R. and A. Volz-Thomas. Climatology of Ozone, PAN, CO, and NMHC in the Free Troposphere Over the Southern North Atlantic. *J. Geophys. Res.*, *28*, 245–262, 1997.

Schultz, M. G., D. J. Jacob, J. D. Bradshaw, S. T. Sandholm, J. E. Dibb, R. W. Talbot, and H. B. Singh. Chemical NO_x Budget in the Upper Troposphere over the Tropical South Pacific. *J. Geophys. Res.*, *105*, 6669–6679, 2000.

Schwartz, S. E. and W. H. White. Solubility equilibria of the nitrogen oxides and oxyacids in dilute aqueous solution. In J. R. Pfafflin and E. N. Ziegler, editors, *Advances in Environmental Science and Engineering*, volume 4, pages 1–45. Gordon and Breach Science Publishers, NY, 1981.

Shallcross, D. E. and P. S. Monks. New Directions: A role for isoprene in biosphere-climate-chemistry feedbacks. *Atmos. Environ.*, *34*, 1659–1660, 2000.

Shaw, R. W. J., A. L. Crittenden, R. K. Stevens, D. R. Cronn, and V. S. Titov. Ambient Concentrations of Hydrocarbons from Conifers in Atmopsheric Gases and Aerosol Particles Measured in Soviet Georgia. *Env. Sci. Tech.*, *17*, 389–395, 1983.

Shepson, P. B., E. Mackay, and K. Muthuramu. Henry's law constants and removal processes for several atmospheric β-hydroxy alkyl nitrates. *Env. Sci. Tech.*, *30*, 3618–3623, 1996.

Sillman, S., J. A. Logan, and S. C. Wofsy. A Regional Scale Model for Ozone in the United States With Subgrid Representation of Urban and Power Plant Plumes. *J. Geophys. Res.*, *95*, 5731–5748, 1990.

Singh, H., Y. Chen, A. Tabazadeh, Y. Fukui, I. Bey, R. Yantosca, D. Jacob, F. Arnold, K. Wohlfrom, D. Atlas, F. Flocke, D. Blake, N. Blake, B. Heikes, J. Snow, R. Talbot, G. Gregory, G. Sachse, S. Vay, and Y. Kondo. Distribution and fate of selected oxygenated organic species in the troposphere and lower stratosphere over the Atlantic. *J. Geophys. Res.*, *105*, 3795–3805, 2000.

Singh, H. B., Y. Chen, A. C. Staudt, D. J. Jacob, D. R. Blake, B. G. Heikes, and J. Snow. Evidence from the Pacific troposphere for large global sources of oxygenated organic compounds. *Nature*, *410*, 1078–1081, 2001.

Singh, H. B. and P. L. Hanst. Peroxyacetyl nitrate (PAN) in the unpolluted atmosphere: An important reservoir for nitrogen oxides. *Geophys. Res. Lett.*, *8*, 941–944, 1981.

Singh, H. B., D. HJerlth, D. O'Hara, L. Salas, A. L. Torres, G. L. Gregory, G. W. Sachse, and J. F. Kasting. Atmospheric peroxyacetyl nitrate measurements over the Brazilian Amazon during the wet season: Relationships with Nitrogen oxides and ozone. *J. Geophys. Res.*, *95*, 16 945–16 954, 1990.

Singh, H. B. and D. J. Jacob. Future Directions: Satellite obeservations of tropospheric chemistry. *Atmos. Environ.*, *34*, 4399–4401, 2000.

Singh, H. B., M. Kanakidou, P. J. Crutzen, and D. J. Jacob. High concentrations and photochemical fate of oxygenated hydrocarbons in the global troposphere. *Nature*, *378*, 50–54, 1995.

Singh, H. B., D. O'Hara, D. Herlth, J. D. Bradshaw, S. T. Sandholm, G. L. Gregory, G. W. Sachse, D. R. Blake, P. J. Crutzen, and M. Kanakidou. Atmospheric measurements of peroxy acetyl nitrate and other organic nitrates at high latitudes: possible sources and sinks. *J. Geophys. Res.*, *97*, 16 511–16 522, 1992.

Singh, H. B., D. O'Hara, D. Herlth, W. Sachse, D. R. Blake, J. D. Bradshaw, M. Kanakidou, and P. J. Crutzen. Acetone in the atmosphere: Distribution, source, and sinks. *J. Geophys. Res.*, *99*, 1805–1819, 1994.

Singh, H. B., A. M. Thompson, and H. Schlager. SONEX airborne mission and coordinated POLINAT-2 activity: overview and accomplishments. *J. Geophys. Res.*, *104*, 3053–3056, 1999.

Singh, H. B. et al. Relationship between peroxyacetyl nitrate (PAN) and nitrogen oxides in the clean troposphere. *Nature*, *318*, 347–349, 1985.

Sinha, A. and R. Toumi. Trposperic ozone, lightning, and climate change. *J. Geophys. Res.*, *102*, 10 667–10 672, 1997.

Slingo, J. M. The development and verification of a cloud prediction scheme for the ECMWF model. *Q. J. R. Meteorol. Soc.*, *113*, 899–927, 1987.

Snider, J. R. and G. A. Dawson. Tropospheric light alcohols, carbonyls, and acetonitrile: Concentrations in the southwestern United States and Henry's law data. *J. Geophys. Res.*, *90D*, 3797–3805, 1985.

Solberg, S., C. Dye, N. Schmidbauer, A. Herzog, and R. Gehrig. Carbonyls and nonmethane hydrocarbons at rural European sites from the Mediterranean to the Arctic. *J. Atmos. Chem.*, *25*, 33–66, 1996.

Spivakovsky, C. M., J. A. Logan, S. A. Montzka, Y. J. Balkanski, M. Foreman-Fowler, D. B. A. Jones, L. W. Horowitz, A. C. Fusco, C. A. M. Brenninkmeijer, M. J. Prather, S. C. Wofsy, and M. B. McElroy. Three-dimensional climatological distribution of tropospheric OH: Update and evaluation. *J. Geophys. Res.*, *105*, 8931–8980, 2000.

Staffelbach, T. A., G. L. Kok, B. G. Heikes, B. McCuilly, G. I. Mackay, D. R. Karecki, and H. I. Schiff. Comparison of hydroperoxide measurements made during the Mauna Loa Observatory Experiment. *J. Geophys. Res.*, *23*, 33–66, 1996.

Staudinger, J. and P. V. Roberts. A critical review of Henry's law constants for environmental applications. *Crit. Rev. Environ. Sci. Technol.*, *26*, 205–297, 1996.

Stauffer, B., E. Lochbronner, H. Oescher, and J. Schwader. Methane concentration in the glacial atmosphere was half that of pre-industrial holocene. *Nature*, *332*, 812–814, 1988.

Sunwoo, Y., G. R. Carmichael, and H. Ueda. Charachteristics of background surface ozone in Japan. *Atmos. Environ.*, *28*, 25–27, 1994.

Tabazadeh, A., M. Z. Jacobson, H. B. Singh, O. B. Toon, J. S. Lin, R. B. Chatfield, A. N. Thakur, R. W. Talbot, and J. E. Dibb. Nitric acid scavenging by mineral and biomasss burning aerosols. *Geophys. Res. Lett.*, *25*, 4185–4188, 1998.

Talbot, R. W., J. D. Bradshaw, S. T. Sandholm, S. Smyth, D. R. Blake, N. R. Blake, G. W. Sachse, J. E. Collins, B. G. Heikes, B. E. Anderson, G. L. Gregory, H. B. Singh, B. L. Lefer, and A. S. Bachmeier. Chemical characteristics of continental outflow over the tropical South Atlantic Ocean from Brazil and Africa. *J. Geophys. Res.*, *101*, 24 187–24 202, 1996.

Taylor, J. P., P. Zimmerman, and D. Erickson. A 3-D modelling study of the sources and sinks of atmospheric carbon monoxide. CRES Work. Pap. 1990/3, Aust. Nat. Univ., Canberra, Australia, 1990.

Thakur, A. N., H. B. Singh, P. Mariani, Y. Chen, Y. Wang, D. J. Jacob, G. Brasseur, J.-F. Müller, and M. Lawrence. Distribution of reactive nitrogen species in the remote free troposphere: data and model comparisons. *Atmos. Environ.*, *33*, 1403–1422, 1999.

Tie, X. X. and P. Hess. Ozone mass exchange between the stratopshere and troposphere for background and volcanic sulfate aerosol conditions. *J. Geophys. Res.*, *102*, 25 487–25 500, 1997.

Tie, X. X., C. Y. J. Kao, and E. J. Mroz. Net yield of OH, CO and O_3 from the oxidation of atmospheric methane. *Atmos. Environ.*, *26A*, 125–136, 1992.

Torres, A. L. and H. Buchan. Tropospheric Nitric Oxide Measurements Over the Amazone Basin. *J. Geophys. Res.*, *93*, 1396–1406, 1988.

Touaty, M., B. Bonsang, M. Kanakidou, and N. Poisson. Monitoring and model comparison of the seasonal variation of tropospheric light hydrocarbons at Amsterdam Island. In *Proceeding of the EUROTRAC Symposium 1996*, pages 613–619. Computational Mechanism Publications, Southampton, 1996.

Toumi, R., J. D. Haigh, and K. S. Law. A tropospheric ozone-lightning climate feedback. *Geophys. Res. Lett.*, *23*, 1037–1040, 1996.

Treves, K., L. Shragina, and Y. Rudich. Henry's law constants of some β, γ and δ hydroxy alkyl nitrates of atmospheric interest. *Env. Sci. Tech.*, *34*, 1197–1203, 2000.

Tyndall, G. S., R. A. Cox, C. Granier, R. Lesclaux, G. K. Moortgat, M. J. Pilling, A. R. Ravishankara, and T. J. Wallington. The atmospheric chemistry of small organic peroxy radicals. *J. Geophys. Res.*, *106*, 12 157–12 182, 2001.

Tyndall, G. S., T. A. Staffelbach, J. J. Orlando, and J. G. Calvert. Rate coefficients for the reactions of OH radicals with methylglyoxal and acetaldehyde. *Int. J. Chem. Kinet.*, *27*, 1009–1020, 1995.

Umweltbundesamt. Jahresbericht 1999 aus dem Messnetz des Umweltbundesamtes. Technical Report 58/00, Umwelbundesamt, Berlin, Germany, 2000.

Verwer, J. G., W. H. Hundsdorfer, and J. G. Blom. Numerical time integration for air pollution models. MAS-R9825, Centrum voor Wiskunde en Informatica, Amsterdam, 1998.

Verwer, J. G., E. J. Spee, J. G. Blom, and W. H. Hundsdorfer. A second order Rosenbrock method applied to photochemical dispersion problems. MAS-R9717, Centrum voor Wiskunde en Informatica, Amsterdam, 1997.

Verwer, J. G., E. J. Spee, J. G. Blom, and W. H. Hundsdorfer. A second order Rosenbrock method applied to photochemical dispersion problems. *SIAM J. Sci. Computt.*, *20*, 1456–1480, 1999.

Villalta, P. W., E. R. Lovejoy, and D. R. Hanson. Reaction probability of peroxyacetyl radical on aqueous surfaces. *Geophys. Res. Lett.*, *23*, 1765–1768, 1996.

Villenave, E. and R. Lesclaux. Kinetic of the cross reaction of CH_3 and $C_2H_5O_2$ radicals with selected peroxy radicals. *J. Phys. Chem.*, *100*, 14 372–14 382, 1996.

Volz, A. and D. Kley. Evaluation of the Montsouris series of ozone measurements made in the 19th-century. *Nature*, *332*, 240–242, 1988.

Wahner, A., T. F. Mentel, and M. Sohn. Gas-phase reaction of N_2O_5 with water vapor: Importance of heterogeneous hydrolysis of N_2O_5 and surface desorption of HNO_3 in a large teflon chamber. *Geophys. Res. Lett.*, *25*, 2169–217, 1998.

Walmsley, J. L. and M. L. Wesely. Modification of coded parameterizations of surface resistances to gaseous dry deposition. *Atmos. Environ.*, *30*, 1181–1188, 1996.

Wang, Y., D. J. Jacob, and J. A. Logan. Global simulation of tropospheric O_3-NO_x-hydrocarbon chemistry, 1. Model formulation. *J. Geophys. Res.*, *103*, 10 713, 1998a.

Wang, Y., D. J. Jacob, and J. A. Logan. Global simulation of tropospheric O_3-NO_x-hydrocarbon chemistry, 3. Origin of tropospheric ozone and effects of non-methane hydrocarbons. *J. Geophys. Res.*, *103*, 10 757–10 767, 1998b.

Wang, Y., J. A. Logan, and D. J. Jacob. Global simulation of tropospheric O_3-NO_x-hydrocarbon chemistry, 2. Model evaluation and global ozone budget. *J. Geophys. Res.*, *103*, 10 727–10 755, 1998c.

Warneck, P. *Chemistry of the Natural Atmosphere*. Academic Press, 1988.

Warneke, C., R. Holzinger, A. Hansel, A. Jordan, W. Lindinger, U. Pöschl, J. Williams, P. Hoor, H. Fischer, P. J. Crutzen, H. A. Scheeren, and J. Lelieveld. Isoprene and Its Oxidation Products Methyl Vinyl Ketone, Methacrolein, and Isoprene Related Peroxides Measured Online over the Tropical Rain Forest of Surinam in March 1998. *J. Atmos. Chem.*, *38*, 167–185, 2001.

Warneke, C., T. Karl, H. Judmaier, A. Hansel, A. Jordan, and W. Lindinger. Acetone, methanol, and other partially oxidized volatile organic emissions from dead plant matter by abiological processes: Significance for atmospheric HO_x chemistry. *Global Biogecles*, *13*, 9–17, 1999.

Weller, R., O. Schrems, A. Boddenberg, S. Gäb, and M. Gautrois. Meridional distribution of hydroperoxide and formaldehyde in the marine boundary layer of the Atlantic (48°N-35°S) measured during the Albatross campaign. *J. Geophys. Res.*, *105*, 14 401–14 412, 2001.

Wesely, M. L. Parameterization of surface resistances to gaseous dry deposition in regional-scale numerical models. *Atmos. Environ.*, *23*, 1293–1304, 1989.

Wesely, M. L. and B. B. Hicks. A review of the current status of knowledge on dry deposition. *Atmos. Environ.*, *34*, 2261–2282, 2000.

Wildt, J., D. Kley, A. Rockel, P. Rockel, and H. J. Segschneider. Emission of NO from several higher plant species. *J. Geophys. Res.*, *102*, 5919–5927, 1997.

Williams, J., U. Pöschl, P. J. Crutzen, A. Hansel, R. Holzinger, C. Warneke, W. Lindinger, and J. Lelieveld. An Atmospheric Chemistry Interpretation of Mass Scans Obtained from a Proton Transfer Mass Spectrometer Flown over the Tropical Rainforest of Surinam. *J. Atmos. Chem.*, *38*, 133–166, 2001.

Williams, J., J. M. Roberts, F. C. Fehsenfeld, S. B. Bertman, M. P. Buhr, P. D. Goldan, G. Hübler, W. C. Kuster, T. B. Ryerson, M. Trainer, and V. Young. Regional ozone from biogenic hydrocarbons deduced from airborne measurements of PAN, PPN, and MPAN. *Geophys. Res. Lett.*, *24*, 1099–1102, 1997.

Williamson, D. L. and P. J. Rasch. Two-dimensional semi-Lagrangian transport with shape-preserving interpolation. *Mon. Weather Rev.*, *117*, 102–129, 1989.

WMO. International Meteorological Vocabulary. Technical Report No. 180, WMO, Geneva, 1992.

Wohlfrom, K.-H., T. Hauler, F. Arnold, and H. Singh. Acetone in the free troposphere and lower stratosphere: Aircraft-based CIMS and GC measurements over the North Atlantic and a first comparison. *Geophys. Res. Lett.*, *26*, 2849–2853, 1999.

Wollenhaupt, M., S. A. Carl, A. Horowitz, and J. N. Crowley. Rate Coefficients for Reaction of OH with Acetone between 202 and 395 K. *J. Phys. Chem.*, *104*, 2695–2705, 2000.

Wollenhaupt, M. and J. N. Crowley. Kinetic studies of the reactions $CH_3 + NO_2 \longrightarrow$ products, $CH_3O + NO_2 \longrightarrow$ products, and $OH + CH_3C(O)CH_3 \longrightarrow CH_3C(O)OH + CH_3$, over a range of temperature and pressure. *J. Phys. Chem.*, *104*, 6429–6438, 2000.

Wurzler, S. The scavenging of nitrogen compounds by clouds and precipitation: Part II. The effects of cloud microphysical parameterization on model predictions of nitric acid scavenging by clouds. *Atmos. Res.*, *48*, 219–233, 1998.

Yienger, J. J. and H. Levy. Empirical model of global soil-biogenic NO_x emissions. *J. Geophys. Res.*, *100*, 11 447–11 464, 1995.

Yokouchi, Y. Seasonal and diurnal variation of isoprene and its reaction products in a semi-rural area. *Atmos. Environ.*, *28*, 2651–2658, 1994.

Yokouchi, Y., H.-J. Li, T. Machida, S. Aoki, and H. Akimoto. Isoprene in the marine boundary layer (Southeast Asian Sea, eastern Indian Ocean, and Southern Ocean): Comparison with dimethyl sulfide and bromoform. *J. Geophys. Res.*, *104*, 8067–8076, 1999.

Zaveri, R. A. and L. K. Peters. A new lumped structure photochemical mechanism for large-scale applications. *J. Geophys. Res.*, *104*, 30 387–30 415, 1999.

Zdunkowski, W. G., R. M. Welch, and G. Korb. An investigation of the structure of typical two-stream-methods for the calculation of solar fluxes and heating rates in clouds. *Beitr. Phys. Atmosph.*, *53*, 147–166, 1980.

Zhang, G. J. and N. A. McFarlane. Sensitivity of Climate Simulations to the Parameterization of Cumulus Convection in the Canadian Climate Centre General Circulation Model. *Atmos. Ocean*, *33*, 407–446, 1995.

Zhang, H., C. M. Roehl, S. P. Sander, and P. O. Wennberg. Intensity of the second and third OH overtones of H_2O_2, HNO_3, and HO_2NO_2. *J. Geophys. Res.*, *105*, 14 593–14 598, 2000.

Zhao, Y., Y. Kondo, F. J. Murcray, X. Liu, M. Koike, K. Kita, H. Nakajima, I. Murata, and K. Suzuki. Carbon monoxide column abundances and tropospheric concentrations retrieved from high resolution ground based infrared solar spectra at 43.5°N over Japan. *J. Geophys. Res.*, *102*, 23 403–23 411, 1997.

Zhou, X., Y.-N. Lee, L. Newman, X. Chen, and K. Mopper. Tropospheric formaldehyde concentration at the Mauna Loa Observatory during the Mauna Loa Observatory Experiment 2. *J. Geophys. Res.*, *101*, 14 711–14 719, 1996.

Zhou, X. and K. Mopper. Photochemical production of low-molecular-weight carbonyl compounds in seawater and surface microlayer and their air-sea exchange. *Mar. Chem.*, *56*, 201–213, 1997.

Zimmerman, P. R., R. B. Chatfield, J. Fishman, P. J. Crutzen, and P. L. Hanst. Estimation of the production of CO and H_2 from the oxidation of hydrocarbon emissions from vegetation. *Geophys. Res. Lett.*, *5*, 679–682, 1978.

Zimmerman, P. R., J. P. Greenberg, and C. E. Westberg. Measurements of atmospheric hydrocarbons and biogenic emission fluxes in the Amazon boundary layer. *J. Geophys. Res.*, *93*, 1407–1416, 1988.

Zondlo, M. A., S. B. Barone, and M. A. Tolbert. Uptake of HNO3 on ice under upper tropospheric conditions. *Geophys. Res. Lett.*, *24*, 1391–1394, 1997.